Potential Impact of Underwater Released Exhaust Gas from Innovative Ships on the Marine Ecosystem Yuzhu Wei

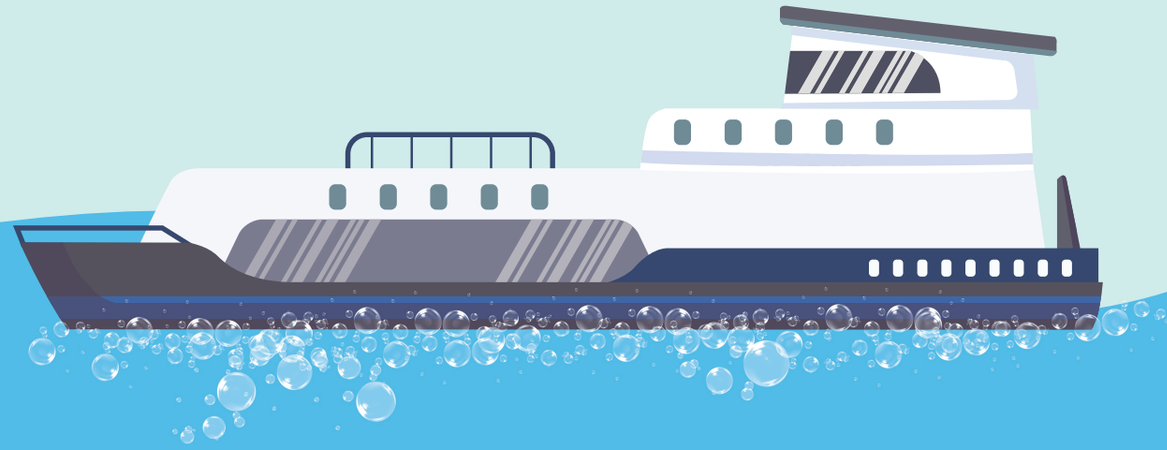

POTENTIAL IMPACT OF UNDERWATER RELEASED exhaust gas FROM INNOVATIVE SHIPS ON THE MARINE ECOSYSTEM

Yuzhu Wei

Propositions:

1. Exhaust gas becomes invisible when released underwater, but its impact cannot be hidden.
(this thesis)

2. CO_2 is not always the "culprit" to the environment as long as you identify and utilise it in a positive way.
(this thesis)

3. An environmental impact study is only valuable when input on local conditions is updated on a regular basis.

4. What brings us closer to the fact/truth is the discussion of a scientific article, not the results or conclusion.

5. A PhD program is more about self-cultivation than about becoming an academic specialist.

6. The impact of quarantine on working efficiency follows the same trend as the impact of elevated CO_2 concentrations on microalgae growth.

7. Assumptions are useful in scientific studies, but harmful in human interaction.

Propositions belonging to the thesis, entitled
'The potential impact of underwater released exhaust gas from innovative ships on the marine ecosystem'.

Yuzhu Wei
Wageningen, 20 January 2021.

Potential impact of underwater released exhaust gas from innovative ships on the marine ecosystem

Yuzhu Wei

Thesis committee
Promoter
Prof. Dr A.J. Murk
Professor of Marine Animal Ecology
Wageningen University & Research

Co-promoter
Dr E.M. Foekema
Senior Researcher, Marine Animal Ecology Group
Wageningen University & Research

Other members
Prof. Dr C. Kroeze, Wageningen University & Research
Prof. Dr G.J. Reichart, Utrecht University
Prof. Dr P.J. van den Brink, Wageningen University & Research
Dr L. van Biert, Delft University of Technology

The research was conducted under the auspices of the Graduate School for Socio-Economic and Natural Sciences of the Environment (SENSE)

Potential impact of underwater released exhaust gas from innovative ships on the marine ecosystem

Yuzhu Wei

Thesis
Submitted in fulfilment of the requirements for the degree of doctor
at Wageningen University
by the authority of the Rector Magnificus,
Prof. Dr A.P.J. Mol,
In the presence of the
Thesis Committee appointed by the Academic Board
to be defended in public
on Wednesday 20 January 2021
at 4:00 p.m. in the Aula.

Yuzhu Wei
Potential impact of underwater released exhaust gas from innovative ships on the marine ecosystem, 170 pages

PhD thesis, Wageningen University, Wageningen, the Netherlands (2021)
With references, with summary in English

ISBN: 978-94-6395-574-4
DOI: https://doi.org/10.18174/532404

To my love Richard Boter,
who made this book and the author better.

Table of Content

CHAPTER 1

General introduction

1.1 Air pollution by ship traffic

Maritime transportation, as one of the cheapest ways of moving large volumes of cargo over long distances, is the backbone of international trade (Christiansen et al., 2007). More than 80% of global trade by volume and over 70% by value is carried by ships (UNCTAD, 2018). In line with developments in the world economic recovery, population growth and elimination of trade barriers, the total volume of global seaborne transportation reached 10.7 billion tons in 2017 (UNCTAD, 2018) . This volume is expected to be continued to rise at an annual growth rate of 3.8% between 2018 and 2023 (UNCTAD, 2018). With increasing numbers of ship operations and the, in general, low quality of operated marine fuel, the stresses on the human and environmental health became a well-known concern (J Chen et al., 2019; Nunes et al., 2017; Williams et al., 2015). The maritime emission accounts for about 15%, 4 – 9% and 3% of the global anthropogenic emission of NO_x, SO_x and Green House Gas (GHG), respectively (Nunes et al., 2017; Song, 2014) (J Chen et al., 2019; Psaraftis &Kontovas, 2013). The released pollutants can cause severe health issues, such as lung cancer, cardiovascular and asthma (Nunes et al., 2017). Thus, eco-efficiency of marine transportation becomes more urgent, especially in risk characterization and management of marine emission.

1.1.1 Marine exhaust gas

The most widely adopted ship propulsion system is the heavy fuel oil powered main diesel engine, which generates large amount of pollutants in the emission (Nunes et al., 2017). The composition of maritime exhaust gas is very complex, which includes, but is not limited to, polycyclic aromatic hydrocarbons (PAHs), fine particles, NO_x, SO_x, O_2, CH_4, CO and CO_2 (M Anderson et al., 2015; Sippula et al., 2014). In addition, the amount and composition of the emission vary based on multiple factors, such as the size and load of the ship and the type and power of the engine. Typically, the exhaust gas consists of 1 - 10% v/v CO_2, 50 - 700 ppm CO, 200 - 1500 ppm NO, 20 - 1000 ppm SO_2, and 50 - 400 ppm volatile organic compounds (in which PAH is about 1%) (EPA, 2000).

The emitted pollutants from maritime transportation accelerate climate change and adversely affect environmental health even at low concentrations in several ways (Corbett et al., 2007; Fuglestvedt et al., 2009). In the short-term, the present-day shipping already impacted local areas with busy shipping intensity. For instance, local maritime traffic increased the ozone and, particulate matter (e.g. $PM_{2.5}$) levels along the Norwegian coast and is contributing to Arctic warming (Law et al., 2017). As early as 2012, the international shipping emitted an estimated 796 million tonnes of CO_2, which accounts for about 2.2% of the total global anthropogenic CO_2 mission (IMO, 2015). The amount of emitted CO_2 in 2020 was estimated to be around 870 million tonnes (Sofiev et al., 2018). This substantial amount of CO_2 is likely to lead to long-term consequences, such as ocean acidification and global warming (Mathesius et al., 2015) (Section 1.4 and 1.5). Under the pressure from maritime emission to both human and environmental health, numerous strict international regulations on marine fuel and emission are in place to date.

1.1.2 IMO regulations for maritime transportation

The regulations of marine fuel and emission from an environmental and public health perspective are issued by the International Maritime Organization (IMO), which was formally established in 1948 in Geneva. IMO is a united nation specialized global standard-setting authority for developing international shipping in all aspects including safety, security, efficiency and environmental performance (IMO, 2019). In the past decades, IMO authorized and adopted several regulations, which guide and support the maritime operation towards more efficiency and environmental friendliness. Regarding fuel regulations, IMO decided the sulphur content in marine fuel had to be reduced to 0.5% m/m (mass/mass) in January 2020 against current global limits of 3.5% m/m (IMO, 2016a). The implementation of this landmark decision forced a stop of using non – desulfurized heavy fuel oil in the shipping industry. In addition, IMO adopted new requirements in October 2016 for collecting fuel consumption data of 5000 gross tonnage and above ships, which account for about 85% of CO_2 emissions from international shipping (IMO, 2016b). This collected data will provide important insights on ship energy efficiency and GHG emission management for the authorities. This is not the first time that IMO regulates maritime emissions. The limits for nitrogen oxides (NO_x) and sulphur oxides (SO_x), the latter regulated via sulphur content in marine fuel oil emission, were started as early as 1997. The NO_x emission standards are commonly referred to as Tier I, II and III standards, which targeted ships that were constructed after 2000, 2011 and 2016 respectively (IMO, 1997a). In those standards, a stricter limit of NO_x was applied to high-speed engines than low-speed ones.

Besides the emission regulations, Emission Control Areas (ECA) were designated by IMO to protect vulnerable areas from maritime emission. The selection of ECAs follows multiple criteria, such as population and environmental risk, critical habitats, water characterization and economic impact (Okada, 2019). Within these ECAs (Baltic sea, North sea, the north American area and the Unites states Caribbean sea), stricter emission rules are applied compared to other areas (Fagerholt et al., 2015). For example, in sulphur ECAs, only 0.1% m/m sulphur content in fuel is allowed from January 2020, while a maximum of 0.5% m/m sulphur content in fuel is applied outside those areas (IMO, 1997b). Current ECAs focus on NO_X and SO_X emissions and are designed under MARPOL (Stand for Marine Pollutions, which refers to the international convention for the prevention of pollution from ships) Annex VI (Zhen et al., 2018). Besides environmental benefits, these regulations also bring economic benefits, e.g. from positive health impact due to cleaner air. Nitrogen ECAs in Baltic and North Sea are estimated to be on average € 1007 million/year benefits against € 230 million/year cost for conforming these regulations in 2030 (Åström et al., 2018).

1.2 Marine fuels

1.2.1 Fuel oils

Crude oil is refined via a complex boiling process called distillation into two basic types of marine fuels: distillate oil and residual oil (Figure 1.1) (Kołwzan &Narewski, 2012).

Distillate fuel oil has a low viscosity and flashpoint. Marine Gas Oil (MGO) and Marine Diesel Oil (MDO) belong to this group (Figure 1.1) (Latarche, 2017). It is generally cleaner and thus produces fewer polluting emissions than Residual Fuel Oil (RFO). Distillate fuel oil

is commonly applied in high and medium-speed engines, such as city buses and private vehicles, but little applied in marine transportation due to the high cost (Winnes &Fridell, 2009) (EIA; Latarche, 2017). Residual Fuel Oil (RFO) is a general classification for the heavier oil (Figure 1.1). It is the remained mixture after refinery consisting of heavy hydrocarbons and metals in oil-soluble form (Ali & Abbas, 2006; EIA, 2019). Heavy Fuel Oil (HFO), also known as Marine Fuel Oil (MFO), is pure or nearly pure residual oil and consists of more pollutants from the crude oil than the DFO does. In the exhaust gas, usually, a higher amount of SO_2 and NO_x is produced from HFO powered ships than DFO powered ships (Table 1.1). HFO is more famous in the maritime field as 'Bunker C fuel oil' and 'NO.6 fuel oil', since commonly used in cargo shipping and the cruise line industry (EIA, 2019). Although Marine Diesel Oil (MDO) belongs to DFO, it contains some HFO. Therefore, the exhaust gas from MDO combustion showed higher pollutant factors (e.g. SO_2) comparing with MGO (Table 1.1). In order to reduce harmful exhaust gas emission and meet regulations, a possible alternative resource is Liquified Natural Gas (LNG) (M Anderson et al., 2015; Burel et al., 2013).

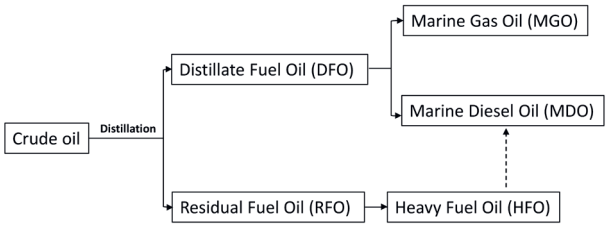

Figure 1.1 A scheme of fuel types for marine use. Marine Diesel Oil (MDO) is a mixture of Distillate Fuel oil (DFO) and Heavy Fuel Oil (HFO). Thus, a dash line was added from HFO to MDO.

Table 1.1 Emission factors for NO_x, CO, CO_2 and SO_2 for different marine fuels at 90% of maximum continuous rating (MCR) load from measured exhaust gas (Winnes &Fridell, 2009). Exhaust gas was generated via a four-stroke main engine tanker (11,000 tones deadweight) IMOZ with 4500 kw installed power.

Fuel Type	NO_x (g/kWh)	CO (g/kWh)	CO_2 (g/kWh)	SO_2 (g/kWh)
MGO	9.6	0.3	607	0.1
MDO	9.6	0.3	645	1- 4.1
HFO	10.7	0.3	607	4.6

1.2.1 Liquified Natural Gas

Natural gas contains many different compounds, with the largest component being methane (CH_4, 87 - 99 mol %) (M Anderson et al., 2015). For easier shipping and storage, natural gas is cooled to a liquid state and it becomes Liquefied Natural Gas (LNG) (EIA, 2018). The emission of LNG powered ships holds significantly lower amounts of NO_x, PM and SO_2 compared with marine fuel oil powered ships. Following the sulphur content regulation and other emission management by IMO, an increasing number of newly constructed vessels are operated by natural gas. Especially with the growth in natural gas infrastructure and with the

price of conventional marine fuels rising, while the regional price of natural gas declines (Fullenbaum et al., 2013; Schinas & Butler, 2016). The number of LNG powered ships, however, is only slowly increasing.

Globally, there are 125 ships using LNG with between 400 - 600 expected to be delivered by 2020 (Saul & Chestney, 2018). In comparison with over 60,000 commercial ships in the world, the transition towards LNG seems slow. This is likely due to the unsolved challenges of this less pollutant energy source operation. For example, for the same energy content, LNG takes about twice the volume of space compared to diesel oil. This large space requirement not only reduces the carrying ability of a cargo ship but also brings up a safety challenge for LNG tank installation (Burel et al., 2013). Additionally, the environmental concern of unburnt methane is addressed in multiple expert forums, since methane has a much higher global warming potential than CO_2 (Commission, 2016). A novel high-efficiency gas engine ship which breakthrough those LNG operation challenges is required to apply this energy source further in maritime shipping. The GasDrive project aims to develop such an innovative LNG powered ship.

1.3 GasDrive project

The NWO funded GasDrive project aims to develop LNG powered ships with more than 50% reduced fuel consumption by using a new generation of fuel cells in combination with turbocharged gas engines. In addition, it is planned that this innovative ship releases exhaust gas under water along the ship's hull as air lubrication to reduce the water resistance of the vessel. In this way, the total emission of GasDrive ships is expected to be significantly less compared to the present ships.

1.3.1 Air lubrication and underwater released exhaust gas

Air lubrication is one of the commercially available technologies in drag reduction of ships, which is categorized in Bubble Drag Reduction (BDR) and Air Layer Drag Reduction (ALDR) (S H Park & Lee, 2018). Bubble Drag Reduction (BDR) initially was reported in 1973 (McCORMICK &Bhattacharyya, 1973). The injected air forms bubbles near the liquid turbulent boundary layer beneath the flow surface, which leads to approximately 10 - 15% of total resistance reduction of ships (Ceccio, 2010). This method was further developed by increasing the injected gas flux, which results in the bubble coalescence of a thin air layer. It is estimated that this air layer could be able to steeply increase drag reduction up to over 80% (S H Park & Lee, 2018). However, optimization of the distribution and stability of the air layer in drag reduction of ships is currently still under research (Ceccio, 2010; S H Park & Lee, 2018).

Different from the traditional air lubrication technologies, GasDrive proposes to inject exhaust gas instead of pumping air along the ship's hull. The advantage of this change is not only improving the air quality of the deck by zero direct releasing exhaust gas to the atmosphere, but also saving 3 - 10% of the total energy that consumed by air bubble generator (Kumagai et al., 2015). Moreover, studies suggested that the drag reduction decreases in traditional air lubrication technologies, due to the discharge of gas bubbles from the boundary layer (Elbing et al., 2008; Kumagai et al., 2015). To overcome this challenge, GasDrive learned from emperor's penguin, who dive with air in their plumage. The trapped air is

released as fine bubbles over their bodies to form a smooth air layer, which reduces the drag force from water and increases their swim speed (Davenport et al., 2011). In GasDrive, a nanostructured ship's hull is designed to capture the released exhaust gas bubbles and form a smooth air layer around the ship with reducing 20% water resistance in theory. Because of the low water resistance, the total fuel/LNG consumption will decrease as well, which is followed by a reduction in **overall** exhaust gas emission, especially at global level. On the other hand, the nano laminate increased the dissolving time for the captured exhaust gas, charged with CO_2, NO_x, SO_x, etc., in water and its impact on the **local** marine ecosystem is unknown. Therefore, the GasDrive proposal includes the work package of studying the environmental impact of underwater release exhaust gas, which is also the aim of the presented PhD project.

1.4 Potential environmental consequences of sub-surface released exhaust gas

Several components in the maritime exhaust gas can impact marine ecosystems although they are less water-soluble compare with CO_2, for instance, PAHs and SO_x. PAHs are ubiquitously introduced to the environment by human activities, as they are present in petroleum and incomplete combustion products, e.g. exhaust gas. PAHs are nonpolar and lipophilic, thus hard to dissolve in water. However, they still have been detected in marine water (Hylland, 2006) and even drinking water (Karyab et al., 2013). PAHs are taken up by organisms via water and especially diet. They accumulate in fat tissue of the organisms due to their lipophilic properties and when high concentrations are reached it can affect the immune system and inhibit development, although varied responses between species were observed (Hylland, 2006; Nørregaard et al., 2015). SO_x, another compound of exhaust gas with low solubility may impact the marine ecosystem. SO_x can cause "acid rain", which in turn acidifies both marine and freshwater systems (Jägerbrand et al., 2019). The emitted SO_x usually form into H_2SO_4 in the atmosphere before dissolving in water (Hunter et al., 2011). It means SO_x emission causes ocean acidification by directly adding H^+ ions to the water, decreasing the ocean alkalinity with negative impact on calcifying organisms (Hunter et al., 2011; Jägerbrand et al., 2019).

CO_2 is the most dissolvable gas compared with other components in the exhaust gas. The biological impact of elevated CO_2 concentrations on marine organisms has been well studied in the past decades due to climate change concerns and related ocean acidification. However, most available studies only address the expected future atmospheric CO_2 levels (Currie et al., 2017; Vaqué et al., 2019). While the underwater released CO_2 may rapidly lead to exceed estimated future global CO_2 levels around the ship's hull, and its impact is still unclear. Therefore, the environmental impact of underwater released exhaust CO_2 remains the primary concern in the presented thesis. Although other components in the exhaust gas are less soluble in water compare with CO_2, it is still important to check whether they have an additional impact on marine organisms by discharging to the water beside the impact caused by CO_2 alone.

1.4.1 Ocean carbonate system and acidification

Approximately one-third of the anthropogenic emission of CO_2 is absorbed by the ocean (Sabine et al., 2004). The amount of dissolved CO_2 gas in aquatic (aq.) follows Henry's law (eq 1) with K_0 representing the proportionality factor between the aquatic and its particle

pressure above the liquid, in this case, the atmosphere (at.) (eq. 1). The proportionality factor, also called the solubility coefficient, is constant when the temperature, total pressure and salinity of the aquatic remain stable (Markou et al., 2014). With increasing water temperature or salinity, the CO_2 solubility in water decreases. While, more CO_2 dissolves in water with higher total pressure (Markou et al., 2014).

$$CO_{2\,(at.)} \overset{K_0}{\leftrightarrow} CO_{2\,(aq.)} \qquad \text{(eq. 1)}$$

After CO_2 gas dissolves in water, it follows a series of chemical reactions (eq 2): CO_2 reacts with water and forms H_2CO_3, which further dissociates into HCO_3^- and H^+. The free hydrogen ion can decrease not only the pH of the seawater but also the concentration of carbonate (CO_3^{2-}) by forming bicarbonate (HCO_3^-) due to the high affinity between H^+ and CO_3^{2-} ions (eq. 2) (Zeebe & Wolf-Gladrow, 2001). Therefore, additional dissolved CO_2 in water will eventually result in a low pH, low free CO_3^{2-} ions and high HCO_3^- condition (Figure 1.2). In normal situation (pH 8.2, 35‰ salinity, 25 ˚C and 1 atmosphere pressure), the average surface ocean carbonate system consists of 86.5% bicarbonate (HCO_3^-), 13% carbonate (CO_3^{2-}) and 0.5% dissolved CO_2) (Zeebe & Wolf-Gladrow, 2001). The inorganic carbon sources can directly be used by photosynthetic organisms such as microalgae as nutrients (mainly in form of CO_2), and calcifying organisms as skeleton ingredients (mainly in form of CO_3^{2-}, HCO_3^- as alternative). The consumption of CO_2 during photosynthesis forces equation 2 to move toward the left side, which means less free H^+ ions are available and results in a pH (pH = -log10[H^+]) increase.

$$CO_2 + H_2O \leftrightarrow H_2CO_3 \leftrightarrow HCO_3^- + H^+ \leftrightarrow CO_3^{2-} + 2H^+ \qquad \text{(eq. 2)}$$

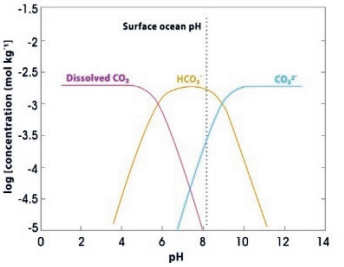

Figure 1.2 The composition of carbonate species, CO_2 (pink line), HCO_3^- (yellow line) and CO_3^{2-} (blue line), in water under different pH levels (35‰ salinity, 25 ˚C and 1 atmosphere pressure). The dash line represents the average surface ocean pH condition, pH 8.2. Figure is based on Zeebe and Wolf-Gladrow (2001).

Additional dissolved CO_2 in the water will shift equation 2 towards the right side and lead to a decrease in pH level and interfere with the ocean carbonate system by decreasing CO_3^{2-} availability and increasing HCO_3^- concentration. This ongoing process is known as ocean acidification (OA) (Doney et al., 2009). It is usually a long-term process due to the slow transfer of CO_2 from gas phase/the atmosphere to the liquid phase (Markou et al., 2014; Zeebe & Wolf-Gladrow, 2001). In the past decades, the increase in anthropogenic CO_2 emission has exacerbated the concentration difference between gas and liquid phases. It, in turn, accelerates the transfer velocity of CO_2 toward the water (Markou et al., 2014). It is estimated

that the pCO_2 in the atmosphere will reach 760 ppm in 2100 (while currently around 410 ppm in 2020) with 0.3 - 0.4 units of ocean pH decrease, if the annual anthropogenic CO_2 emission remains as the present amount (IPCC, 2007).

The GasDrive project aims to reduce the overall CO_2 emission from shipping and thus to reduce the global ocean acidification. However, in the GasDrive concept the remaining CO_2 will be emitted under water along the ship's hull which results in suddenly, but locally elevated CO_2 concentrations in the water column.

1.4.2 Comparison underwater released exhaust CO_2 with traditional ocean acidification

There are several differences between the exposure of underwater released exhaust CO_2 and traditional OA, including the path, time, area and dose (Table 1.2). In general, underwater released exhaust CO_2 from ships can be expected to be an acute and high dose exposure process for a limited part of a local marine ecosystem. Conversely, traditional OA usually represents a long term ongoing absorbing CO_2 via atmosphere at global level. The extended time period of exposure of traditional OA may provide an adjusting period for the organisms to the additional CO_2 condition. It has been shown that certain organisms, such as mussels (*Mytilus edulis*), that have been pre-exposed to elevated CO_2 concentrations are able to tolerate higher concentrations than organisms that miss this pre-exposure history (Thomsen et al., 2010). In the case of underwater released exhaust CO_2, the organisms will not experience any pre-exposure, but will be directly exposed to high CO_2 concentrations. Thus "shock" effects resulting from acute exposure are necessary to be included when evaluating the impact of underwater released exhaust gas. Due to these differences in exposure characterization, available studies that concern ecological impact and risk assessment of traditional OA may not be able to represent the potential impact of underwater released exhaust CO_2 from the ship's hull. It is important to choose experimental exposure regimes that match exposure conditions that will occur with under water exhausted CO_2.

Table 1.2 Different exposure characterization (path, time, area and dose) of OA and underwater exhaust CO_2.

	OA	Underwater exhaust CO_2
Exposure path	Uptake from atmosphere	Directly injected from ship's hull
Exposure time	Continuously for decades	Interruptedly (when GasDrive ship passing by)
Exposure area	Globally, the entire ocean	Locally, near the shipping lanes
Exposure dose	Equivalent with atmosphere, Estimation: around 760 ppm pCO_2 in 2100 (IPCC, 2007)	Can (temporarily) exceed the atmospheric equivalent

1.5 Potential ecological consequences of underwater exhaust CO_2

Transforming inorganic carbon (e.g. CO_2, HCO_3^- and CO_3^{2-}) to organic matters using light (photosynthesis) or chemical energy is an essential reaction for all organisms on earth (Cole, 2012). Changes in the amount of available carbon sources can have severe ecological

consequences. For example, CO_2 is an essential nutrient that can stimulate algal development, while elevated CO_2 concentration caused acidification negatively affects calcifying organisms.

The direct impact of additional CO_2, pH, light intensity, temperature and salinity on marine invertebrates vary between species (Ries et al., 2009; M K Thomas et al., 2012). In many cases, such as bivalve responses to salinity levels, the vulnerability even can be life stage-specific (Peteiro et al., 2018). The differences in vulnerabilities lead to a series of consequences, such as a shift in community composition followed by a decrease in biodiversity and indirectly impacting other species via the food web. A good example is given by a mesocosm experiment of elevated CO_2 concentration (approximately 760 µatm pCO_2) treated plankton communities from Taucher et al. (2017). They found nanophytoplankton blooms to results from additional CO_2 stimulation (direct impact) together with top-down control of large copepods on their feed competitor microphytoplankton (indirect impact). This bloom in nanophytoplankton further bottom-up (indirect impact) stimulated an increase of the density of small (not large) copepods due to the higher feed availability. Moreover, a continuous development of large copepods was absent, because the bloomed nanophytoplankton was too small for large copepods to keep sufficiently nourish (indirect impact) (Taucher et al., 2017).

Besides species specific, local condition is another factor that impact on the ecological consequences of underwater released exhaust CO_2. For instance, different local areas are expected to be exposed to different concentrations of CO_2, due to varied shipping intensity. Therefore, when carrying out the risk assessment of underwater released exhaust CO_2 from marine shipping, it is important to consider the local conditions, specifically nutrients level, alkalinity and shipping intensity of the ecosystem.

1.5.1 Photosynthetic organisms

Photosynthetic organisms, like microalgae, use solar energy and convert inorganic carbon into biomass and produce oxygen. CO_2 is the main form of carbon during photosynthesis, and therefore an essential nutrient for primary production. Some organisms are able to use the alternative source of HCO_3^- as well (Hussner et al., 2016).

Around 45% of photosynthesis on earth occurs in the aquatic environment and it plays a critical role in shaping the entire ecosystem and biogeochemistry on earth (Falkowski &Raven, 2013). The consumption of CO_2 for photosynthesis leads to an increase in pH of water surrounding those photosynthetic organisms (Section 1.4.1). The development of submerged aquatic photosynthetic organisms can be limited by CO_2 availability, due to the low diffusivity of dissolved CO_2 in water (Markou et al., 2014). The situation of being CO_2 limited likely occurs in algae bloom areas, where the algae consume CO_2 in water at a faster rate than the CO_2 transfer velocity from the atmosphere into the water (Hussner et al., 2016). During such CO_2 limited condition, underwater released CO_2 can overcome the carbon shortage and stimulate further development of the algae, which may trigger a long period of algae blooms or even harmful algae blooms. On the other hand, if the development of algae is limited by other factors (e.g. other nutrients or light intensity) instead of carbon availability, then additional CO_2 injection will not impact the growth of algae. Therefore, the stimulation

of underwater released exhaust CO_2 on photosynthetic organisms is dependent on local environmental conditions.

1.5.2 Calcifying organisms

Marine calcifying organisms are animals, such as molluscs, coccolithophores and crustaceans the excrete calcium carbonate ($CaCO_3$) skeletons (rigid structures or shell) via extracellular calcifying fluid (Fassbender et al., 2016). This physiologically controlled $CaCO_3$ production is known as biogenic calcification (eq. 3). The mechanism behind this complex process is still not fully understood (Cyronak et al., 2015).

$$Ca^{2+} + CO_3^{2-} \leftrightarrow CaCO_3 \qquad \text{(eq. 3)}$$

The stability of $CaCO_3$ minerals in water is indicated by the saturation state of carbonate minerals (Ω) (eq. 4), where K_{sp} is the soluble product of $CaCO_3$ minerals (Brockmann &Janse, 2008). Therefore, the precipitation of $CaCO_3$ is likely occurring in high Ω condition ($\Omega > 1$) and dissolution occurs when $\Omega < 1$ (Zeebe & Wolf-Gladrow, 2001).

$$\Omega = \frac{[Ca^{2+}][CO_3^{2-}]}{K_{sp}} \qquad \text{(eq. 4)}$$

There are two polymorphs of $CaCO_3$, aragonite and calcite. In general, aragonite is more soluble in water than calcite. Therefore, calcifying organisms with aragonite shells, e.g. clam and conch, are more vulnerable for $\Omega < 1$ conditions than calcite organisms, e.g. oyster and barnacles (Ries et al., 2009). The formation of these two types was traditionally believed to be controlled by the ratio of Mg : Ca in the surrounding water and water temperature (Morse et al., 2007). However, the following studies suggested that the number of influencing factors of the formation process are underestimated (Bots et al., 2011; C E Miller, 2018). Especially global warming and ocean acidification (OA), may become more and more dominant impactors on $CaCO_3$ formation than the ratio of Mg : Ca (C E Miller, 2018). Every year, CO_3^{2-} concentration in the ocean measurably decrease due to OA, which may inhibit biogenic calcification and threaten the life of calcifying organisms (Albright et al., 2016). However, it is acknowledged that HCO_3^- can be a resource in calcification as well (Bertucci et al., 2013; Herfort et al., 2008) (eq. 5).

$$Ca^{2+} + HCO_3^- \leftrightarrow CaCO_3 + H^+ \qquad \text{(eq. 5)}$$

Thus, CO_3^{2-} f is unlikely to be the only stressor for calcifying organisms in elevated CO_2 concentrations. Indeed, the high hydrogen ion (H^+) in the seawater is suggested to be the main threat (Cyronak et al., 2015). During acidification, the calcifying organisms up-regulate the pH level of calcifying fluid for carbonate equilibrium composition shifting in favour of CO_3^{2-} (McCulloch et al., 2012). To maintain intracellular pH level, H^+ is actively removed from calcifying fluid towards the external water column. Therefore, more energy is required for the pH up-regulation when H^+ concentration in the water column is higher (Cyronak et al., 2015). Energy limitation may occur during long periods of high energy demand (the critical period duration depends on the species), and likely will inhibit calcification. On the other hand, this theory also suggests that acidification may stimulate calcification, if the organism is able to increase energy production and continuously transport H^+ out of the

calcifying fluid (H L Wood et al., 2008) e.g. via increasing temperature (Navarro et al., 2016). However, Clements and Darrow (2018) found that multiple marine calcifying invertebrates experienced a decreased feeding rate and low energy under elevated CO_2 conditions. Both up-regulation pH and energy gain (e.g. feeding rate) regulation are species specific (H L Wood et al., 2008).

Some water conditions have a higher capacity to resist changes in pH than others. The ability of such resistance is indicated by alkalinity. Alkalinity is derived from titration with a strong acid, thus also known as titration alkalinity (TA) (Millero et al., 1993). It tracks the charge balance of water (eq 6) and indicates the capacity of water to resist changes in pH (Zeebe & Wolf-Gladrow, 2001). The higher the alkalinity, the higher the resistance of the water is to change in pH level.

$$TA = [HCO_3^-] + 2\,[CO_3^{2-}] + (B(OH)_4^-) + [OH^-] - [H^+]_F + \text{minor components} \quad \text{(eq 6)}$$

Where, $(B(OH)_4^-)$ is boric acid and $[H^+]_F$ is the free concentration of hydrogen ion. The CO_3^{2-} is counted twice due to its double negative charge.

The calculated global annual ocean average TA was 2298.9 ± 200 μmol/kg (based on SST = 12.5 ± 15 ºC and SSS = 34.6 ± 5) in 2014 (Rana A Fine et al., 2017).

Adding CO_2 to the seawater itself will not change the alkalinity level, because the reaction (eq. 2) produces equivalent amount of positively (H^+) and negatively charged ions (HCO_3^- and/or CO_3^{2-}). However, $CaCO_3$ formation, such as biogenic calcification (eq 3), will result in alkalinity decrease for 2 units, because of the usage of double negative change ion (CO_3^2) (Zeebe & Wolf-Gladrow, 2001). The other way around, decalcification will lead to an increase in alkalinity. Therefore, injecting CO_2, e.g. via GasDrive ships, in a high-density area of calcifying organisms is expected to indirectly increase local alkalinity by decalcification.

1.5.3 Sessile organisms

Sessile animals, such as barnacles and sessile algae attach and grow on a solid substrate, like rock and seabed. They rely on water flow and turbulence to bring nutrients and carry off their wastes and offspring (Koehl, 1982). Thus, very little energy is required for food collection and digestion, and a high energy budget can be used for growth and reproduction (Haris, 1990; Koehl, 1982). This sessile lifestyle leads to a relatively simple body structure compare with mobile animals (Haris, 1990). Their tissues are usually directly in contact with water, thus being additionally vulnerable to specific water conditions as they cannot avoid exposure by relocation, except some species that temporarily avoid exposure by closing their valves (Haris, 1990).For example, the shell thickness and feeding rate of mussel (*Mytilus edulis*) are reduced in elevated CO_2 concentration (2100 pCO_2) (Sadler et al., 2018), and the negative impact was accelerated when combined with hypoxia condition (Sui et al., 2016).

“Biofouling” is commonly defined as sessile animals attaching and growing on artificial substructures and may result in harmful consequences (Benson et al., 1973). The biofouling process starts from organic material accumulating on submerged surfaces in the sea, which further develop into bacterial colonization and attracts other marine invertebrates (Armstrong

et al., 2000; Callow & Callow, 2002). Biofouling can occur on ship hulls and lead to high frictional drag of the ship and increase as much as 40% fuel consumption (Champ, 2000). In GasDrive, the attached sessile organisms on ship's hull will be the first organisms to be exposed to underwater released exhaust gas and surrounding exhaust gas enriched water. Therefore, it is essential to include these organisms in the presented study for evaluating the environmental impact of the underwater releasing exhaust system (Chapter 3).

Besides the environmental perspective, the impact of exhaust gas on fouling organisms may also be an additional property of the GasDrive ships toward energy efficiency via an antifouling aspect. Antifouling has been a non-stop "battle" between human and fouling organisms in the past decades. The most common antifouling strategy is applying biocides in antifouling coatings. Unfortunately, most available antifouling coatings are harmful to non-target marine species as well (Amara et al., 2018). Therefore, developing an efficient and eco-friendly antifouling solution remains a challenge (Cyronak et al., 2015). The potential of applying underwater released exhaust CO_2 as an antifouling strategy is therefore proposed and studied in Chapter 3. On one hand, the presented thesis evaluates the environmental risk of underwater released exhaust gas on local marine ecosystem. On the other hand, it addressed the eco-friendly property, e.g. anti-fouling, of GasDrive ships as well. These contradicting properties are further evaluated and discussed in Chapter 6 and based on which the use of GasDrive is predicted.

1.6 Aim and outline of this thesis

This thesis aims to assess the potential environmental impact of underwater released exhaust gas and evaluate safe application strategies of this technique based on local environmental conditions.

The thesis has four main research questions:

1. What is the no-effect concentration of CO_2 to marine organisms?

2. Is CO_2 the main environmental impact driver in the exhaust gas of maritime shipping?

3. Where are vulnerable areas to underwater released CO_2 from maritime shipping located based on environmental conditions?

4. Could underwater exhaust system be applied safely from an environmental perspective?

Chapter 2 describes the impact of a wide range of CO_2 concentrations (pH 8.6 – pH 5.8), which may result from the underwater released exhaust CO_2, on marine invertebrate communities in a mesocosm. This acute exposure study included not only the direct impact of additional CO_2 but also indirect impact on varied species via food chain.

Chapter 3 addresses the biological impact of additional CO_2 on sessile microorganisms (biofilm) and barnacles. Biofilm formation is one of the initial steps of the biofouling process. Barnacles are common fouling organisms and the final step of the biofouling process. Therefore, it is important to evaluate the impact of elevated CO_2 on the development of

biofilm and the growth of barnacle for judging the potential of applying CO_2 as an antifouling strategy.

Chapter 4 includes the impact of actual exhaust gas from a diesel engine on a simple plankton community consisting of an microalgae and a rotifer species. To observe the additional impact of other components in the exhaust gas, elevated CO_2 concentrations were used as a comparison group in this study.

A preliminary risk assessment of global underwater released exhaust CO_2 is presented in **Chapter 5**. Relative risks between 262 marine ecoregions were characterized by plotting their increased DIC levels, causing by maritime shipping emitted CO_2, against vulnerability scores.

Finally, **Chapter 6** presents the summary of results from chapter 2 to chapter 5 and further discusses CO_2 and exhaust gas impacts on marine ecosystems. Here, the crucial question 'Could underwater exhaust system be applied safely from an environmental perspective?' is discussed. Future perspectives for applying GasDrive ships globally are addressed.

CHAPTER 2

2

The potential impact of underwater exhausted CO_2 from innovative ships on invertebrate communities

Yuzhu Wei[a], Lara Plath[b], Anne Penning[a], Maartje van der Linden[a], Albertinka J. Murk[a], Edwin M. Foekema[a, b]

[a.] Marine Animal Ecology group, Wageningen University, P.O. box 338, 6700 AH Wageningen, The Netherlands
[b.] Wageningen Marine Research, P.O. Box 57, 1780 AB Den Helder, The Netherlands

International Journal of Environmental Research (2019) 13 (4): 669 – 678

Abstract

Liquefied Natural Gas (LNG) powered ships equipped with an underwater exhaust system to reduce the ship's water resistance, could form a future generation of energy efficient ships. The potential consequences of the underwater exhaust gas to the local ecosystems are still unknown. Especially the CO_2 levels will locally exceed estimated future global levels, therefore higher exposures than that were included. The response of a marine community to a wide range of CO_2 dosages resulting in pH 8.6 - 5.8 was studied for 49 days. The zooplankton and benthic community were adversely affected by high CO_2 exposure levels. Between pH 6.6 and pH 7.1, polychaetes dominated the benthic community and their larvae became the dominant zooplankton group. Due to the reduced grazing pressure and the flux of nutrients from decaying organic material phytoplankton stared blooming at the highest exposure level. The periphyton community was not able to take advantage under these conditions. Periwinkles' shell damage and high mortality were observed at pH < 6.6. However, the growth of the surviving periwinkles was not directly related with pH, but was positively correlated with the availability of periphyton and negatively correlated with the polychaete density that most likely also used the periphyton as food source. The impact of underwater exhaust gasses depends on various factors including local biological and abiotic conditions. Future research of this subject will assess the boundaries, where the advantages of underwater exhaust gasses as ship hull lubricant can be applied with minimum impact on the marine ecosystem.

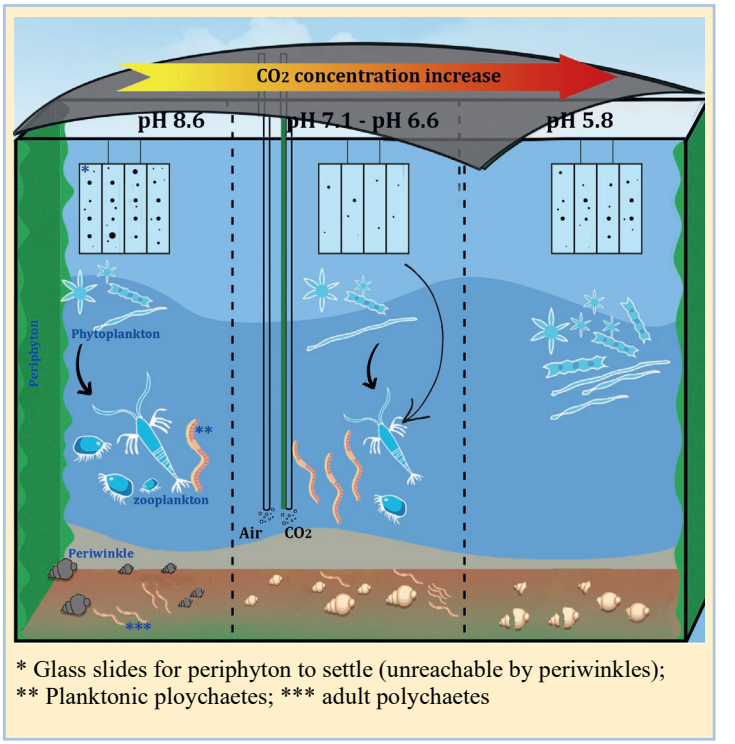

* Glass slides for periphyton to settle (unreachable by periwinkles); ** Planktonic ploychaetes; *** adult polychaetes

2.1 Introduction

The marine transport sector has been a fast-growing sector of the global economy and it contributes significantly to anthropogenic air pollution. In the period of 2007 to 2012, on average, shipping emission accounted for about 2.8% of annual greenhouse gas emission (IMO, 2014). The emitted air pollution contributes to climate change and adverse impacts on human and environmental health in several ways (Corbett et al., 2007; Fuglestvedt et al., 2009). The International Maritime Organization (IMO) thus implemented several regulations

to reduce the Sulfur oxides (SO_x) content in the fuel and nitrogen oxides (NO_x) emissions from shipping operations to the air (IMO, 1997a; b). The European Commission's white paper 2011 "Roadmap to a Single European Transport Area" described the goal of reducing shipping carbon emissions by 40% by 2050 in the European Union area (Commission, 2011).

To comply with the regulations of reducing NO_x, SO_x and CO_2 emissions all together, the interest in using Liquefied Natural Gas (LNG) engines in ships has been rising (Semin, 2008). LNG consists mainly of methane, which seems promising to meet the gas emissions limits (except carbon), and also reduce fuel consumption up to 15% (Burel et al., 2013). Besides shifting to LNG powered ships, in order to lower the direct emissions to the atmosphere, the maritime industries tend to apply underwater exhaust systems to minimize pollution on working decks (H Sapra et al., 2017; Van Biert et al., 2016). However, the impact of underwater exhaust gas from LNG powered ship on the marine ecosystems is largely unknown. Apart from inert nitrogen gas, hydrocarbons and nanoparticles, exhaust gas from LNG powered engines contains substantial amounts of CO_2 (M Anderson et al., 2015).

The underwater CO_2 emission may significantly increase the locally dissolved CO_2 level and could exacerbate local ocean acidification. Ocean acidification is predicted to have both direct and indirect effects on habitat-forming organisms, which in turn mediate biodiversity shifts, such as lower the species diversity in coral reefs, mussel beds and some macroalgal habitats (Sunday et al., 2017).

The majority of biogenic carbonate precipitation is carried out by planktonic microorganisms (Milliman, 1993). Several studies have focused on the direct effects of CO_2 on plankton (Kurihara et al., 2004; Rost et al., 2003). A recent study showed that elevated CO_2 concentrations (up to 1,296 µatm pCO_2) has no significant effects on the nutritional composition of dinoflagellates, and in turn has minimal impact on the fecundity and hatching success of the calanoid copepods that feed on them (Isari et al., 2016). While Taucher et al. (2017) found that the biomass of copepods increased with 30-40% in high CO_2 concentrations (up to 760 µatm pCO_2) as a result of increased primary production. These test concentrations, however, are lower than the potential local levels reached with underwater exhausted CO_2.

Most available studies only concern the effects of expected future atmosphere CO_2 levels may have on the marine ecosystem (de Vries et al., 2013; Fabry et al., 2008; Wittmann & Pörtner, 2013). Unfortunately, these studies often were limited to one or two elevated CO_2 concentrations, which makes it hard to quantify a (no) effect level (de Vries et al., 2013; Wittmann & Pörtner, 2013). Therefore, more information about the direct and indirect responses of marine communities to a wider range of CO_2 levels is needed to assess the risks of locally highly elevated CO_2 for marine organisms.

Here, we present a mesocosm study including plankton and benthic communities under a wide range of CO_2 dosages resulting in a pH range of 8.6 – 5.8. The lowest pH level that can be reached by directly injecting CO_2 into seawater in our mesocosms.

2.2 Material and Method

2.2.1 Experimental Set-up

Fourteen mesocosms were provided with fixed CO_2 fluxes resulting in seven pH levels ranging from 8.6 to 5.8 (Table 2.1) for 49 days (June 12th to July 31st 2017). The mesocosms (600 l) were filled with about 8 cm natural sandy sediment that was collected from the coastal North Sea and natural seawater collected from the Eastern Scheldt, the Netherlands. This site is often used as a reference site in marine ecotoxicological studies in the Netherlands (e.g. (Foekema et al., 2012; Kuiper et al., 2007)). After installation, the mesocosms were allowed 28 days to stabilize while the water was circulated through all mesocosms until the start of the CO_2 exposure. Each mesocosm was covered with a transparent lid as a defense against rainfall, birds and litter. Evaporation losses were replenished with demi-water to maintain salinity at 32 ± 1‰ throughout the study.

Table 2.1 The mesocosm number with treated fixed CO_2 flow rate, the calculated pCO_2 values and the mean pH level of the treatments. The mean pH levels were used to define different treatments in the result figures.

Mesocosm nr.	**Fixed CO_2 flow rate (ml/min)**	**Mean pCO_2 (µatm)**	**Mean pH level**
M6 M13	0	114	8.6 (control)
M2 M14	1	1410	7.8
M5 M11	5	3032	7.4
M8 M10	10	6678	7.1
M1 M7	20	29653	6.6
M3 M12	73	79954	6.2
M4 M9	310	179013	5.8

Phyto- and zooplankton and small benthic invertebrate species were naturally introduced to the mesocosm with water and sediment. Additionally, from relatively pristine field locations, identical number of macro invertebrates, periwinkle (*Littorina littorea)*, mud snail (*Peringia ulvae)* and mud shrimp (*Corophium volutator)* were introduced into each mesocosm (Table 2.2) during the first days of the establishment phase. They were representatives from various taxonomic classes that are commonly present in shallow soft sediment coastal ecosystems. Of each macroinvertebrate species that was introduced a representative sub-sample was stored at -20 ˚C for determination of initial size and biomass at a later stage.

Table 2.2 Species and number of macro invertebrate introduced to each mesocosm.

Group	**species**	**Common name**	**Nr. per mesocosm**
Mollusc	*Littorina littorea*	Periwinkle	20
Mollusc	*Peringia ulvae*	Mud snail	40
Crustacean	*Corophium volutator*	Mud shrimp	300

2.2.2 CO_2-application

The water column of each mesocosm was continuously aerated with 1300 ml/min compressed air in the center of the mesocosm at about 10 cm above the sediment, to ensure gas exchange and sufficient mixing of the water column. At the start of the exposure phase, the treatments were created by additional bubbling of CO_2 (Foodgrade, supplier Linde Gas BV, Netherlands) from the same position at six different fixed flow rates (Table 2.1 and Figure 2.1). Subsequently, a range of pH in steps of about 0.4 could be attained in the water column from the lowest attainable pH of 5.8 to a natural pH level of 8.6. Treatments were assigned randomly over the mesocosms (Figure 2.1).

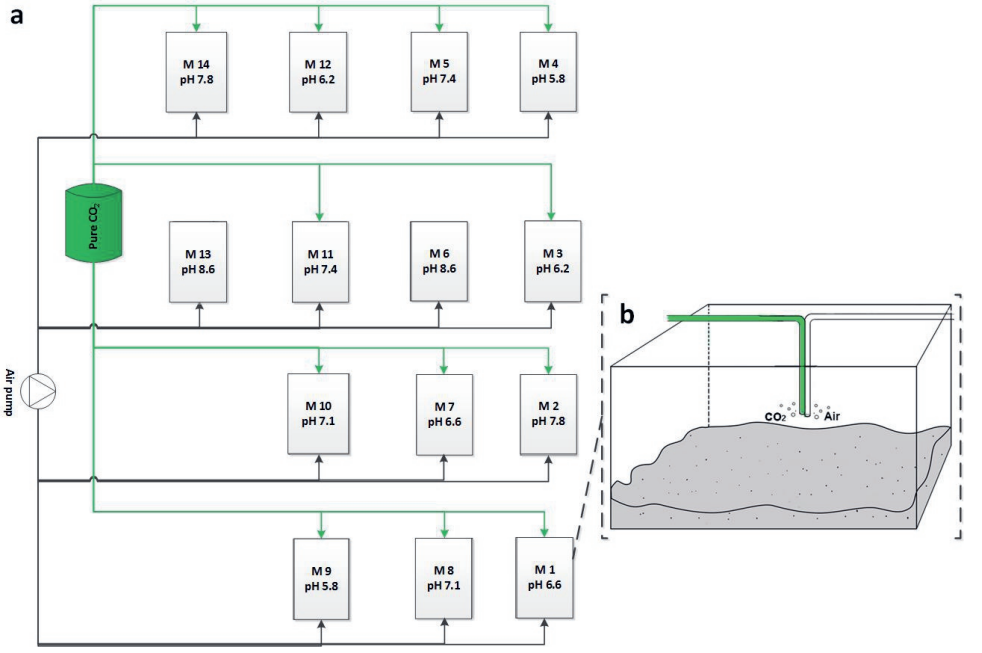

Figure 2.1 Schematic of the experiment setup. Fourteen mesocosms (M) are connected with both air pump and CO_2 tank (a). The treatment of each mesocosm is randomly selected. The mesocosms are filled with about 8 cm natural sandy sediment and natural seawater (b). Both CO_2 and compressed air are continuously injected in the center of the mesocosm at about 10 cm above the sediment.

2.2.3 Water Analysis

Water temperature, oxygen saturation level, salinity and alkalinity were measured weekly starting at 9 a.m. (local time) by submerging electrodes (Hach LDO101, LDO101 and CDC401 respectively) and alkalinity test kit (Hach model AL-DT). The pH level was measured daily by electrode pH meter (Hach PHC101) at 10 a.m. (local time) at half water depth. In the present study the so-called Seacarb package (Lavigne & Gattuso, 2010) in R (Team, 2013) was used to express all exposures as pCO_2 in micro atmosphere (µatm) based on alkalinity, pH, salinity and temperature values. On day 0 and 49 water samples were collected for analyzing nitrite, nitrate, ammonia, silicate and ortho-phosphate level by means

of a Aquakem Autoanalyzer with spectrophotometric detection, following Netherlands standard NEN-6604 (NEN, 2007).

2.2.4 Sampling and Analysis

Phytoplankton samples were taken on every Monday at 10 a.m. (local time) at approximately 30 cm below water surface. Phytoplankton biomass was measured in these samples as chlorophyll-a concentration by means of a 1Hz-kuvetten Fluorimeter (BBE-Moldaenke AlgaeLabAnalyser BG43000).

The development of sessile algae (periphyton) was monitored on four glass microscope slides (76 x 26 mm). These slides were introduced in vertical position facing south at ca.10 cm below the water surface in the mesocosm on the day the CO_2 application started. In order to avoid grazing by periwinkles the microscope slides were located about 3 cm away from the wall of the mesocosms. The chlorophyll - α fluorescence on these slides was measured during the experiment period, on day 2, 8, 17, 31, 43 and 49, by a microtiter plate reader (BioteK FLx800). As a proxy of the availability of periphyton throughout the study the area under the curve of the periphyton development was calculated.

For determination of the zooplankton community, a core sampler was used to collect 10 subsamples of 1 L each at 10 different positions in each mesocosm. From these sub-samples zooplankton was collected using a 55 µm-plankton net and the composite sample was preserved in a formaldehyde solution until visual microscopic analyses. This sampling was performed 4 times during the experiment period, on day 0, 7, 15 and 49.

In order to avoid disturbance of the systems, the introduced macroinvertebrates were only sampled on day 49. The alive and dead periwinkles were counted separately. Not all introduced periwinkles could be recovered from the mesocosms at the end of the study. Some individuals have climbed out of the mesocosms during the experiment period. Therefore, the mortality of the periwinkles was calculated based on the ratio of dead (empty shells) and total recovered periwinkles. The recovered periwinkles (both alive and dead) from each mesocosm were rinsed with demi water to wash away the sand, grouped and pictured to be able to compare the color and condition of the shells between treatments. The living periwinkles were dried overnight at 103 ˚C to determine the dry weight, and subsequently transferred to 450 ˚C oven for 4 hours to determine the ash weight. The flesh dry weight was calculated by subtracting the ash weight from the dry weight, while the ash weight was used as a proxy for shell weight.

The benthic invertebrates were sampled also on day 49. For this, two PVC tubes each with a surface of 0.07 m^2 (30 cm diameter) were pressed in the sediment surface before the water was fully pumped off. The sediment and water within each tube was collected and sieved (500 µm). The sediment sample on the sieve was preserved in a formaldehyde solution until further analysis.

The relation between treatment and abundance on day 49 of total zooplankton, adult polychaetes and planktonic polychaetes larvae were analyzed with a Generalized Additive Model (GAM, (S N Wood, 2006)). A GAM fits a smoothing function of potentially relevant explanatory variables (in this case, CO_2 enrichment causes pH reduction) to the density data

in order to describe the number of organisms in relation to the variables. All GAM analyses in our study were implemented using the Mixed GAM Computation Vehicle (mgcv) package (S N Wood, 2011) in R (Team, 2013).

GraphPad Prism 7 was used to draw graphs and perform statistical analysis using one-way or two-way ANOVA with Dunnett's multiple comparison post-test. The result was considered significant when $p < 0.05$.

2.3. Results and Discussion

During the 49 days with elevated CO_2 concentrations several effects were observed. In the highest CO_2 treatment, the invertebrate community collapsed and phytoplankton bloomed. In contrast to their planktonic equivalent, the sessile microalgae (periphyton) were not able to increase biomass. At lower concentrations of CO_2, more subtle changes were observed. In pH 7.1 and 6.6 treatments, high numbers of planktonic polychaete larvae appeared, corresponding with high numbers of sedentary adult polychaetes in these treatments. The periwinkles clearly suffered directly from the treatments as was illustrated by affected shells at pH 7.1 and below, and increasing mortality with higher CO_2 dosage. The development of their individual total biomass however was not directly related to the CO_2 treatment level, but more indirectly via the availability of their major food source, periphyton.

2.3.1 Water Parameters

The study was conducted during early summer (June 12th and July 31st 2017). Water temperatures in the mesocosms ranged between 16 ˚C at the start and 22 ˚C maximum. The pH in the untreated controls was 8.3 at the start and increased to over 9 at the end of the study. These values are relatively high compared to the global open ocean mean of pH 8.07 (in 2010) (Hofmann et al., 2011). In more shallow and productive areas, however, pH levels can increase to over 9 as well, as a result of primary production (Verspagen et al., 2014). The high pH in our controls can also be attributed to primary production. In the CO_2 treated mesocosms the pH rapidly decreased after the start of the CO_2 application, and then stabilized within the next 2 days at the target value (S 2.1a). The treatments followed a mean pH level gradient and were significantly different from each other: pH mean values of 8.6 (control), 7.8, 7.4, 7.1, 6.6, 6.2 and 5.8 (Table 2.1 and S 2.1b). The mean pH level of each treatment was used to define different treatments in the results. The salinity of all the mesocosms remained in the range of 31‰ – 34‰ (S 2.2). The alkalinity level increased along with the pH level decrease, from about 2.7 meq/l in the controls to the highest 6.4 meq/l in the pH 5.8 mesocosms (S 2.2).

The solubility of CO_2 is dependent on the temperature, pressure and the composition of the aqueous solution (Al-Anezi et al., 2008; Duan & Sun, 2003). Besides the widely studied and modelled CO_2 solubility in the CO_2 - H_2O system and in single or a mixed - salt aqueous system, CO_2 solubility in natural seawater is hard to predict due to the complicated chemical composition of the natural seawater (Duan & Sun, 2003; Zhao et al., 2015). Therefore, we could not calculate the exact solubility level of CO_2 in our mesocosms. In our study, the lowest pH level that could be reached by continuously adding CO_2 was pH 5.8. From this we assume that the maximum CO_2 saturation level was reached and maintained in our highest treatment level.

As the temperature, depth, pressure and composition of the seawater were identical in all mesocosms, the solubility of CO_2 and thus the maximum saturation level must have been similar as well. The CO_2 particle pressure in water (pCO_2 in µatm) was different between mesocosms due to the different CO_2 flow rates (Table 2.1). pCO_2 values were estimated based on pH, total alkalinity, salinity and temperature and were 114 µatm in the controls and extremely high (up to $1.7x10^5$ µatm) in the highest treatment groups. The low pCO_2 in the controls were in accordance with the high pH levels that increased during the study period from 8.6 to over 9, due to primary production, as can also be expected in shallow productive areas (Verspagen et al., 2014). The pCO_2 in seawater of global oceans is higher and varies seasonally about 60% below and above the current atmospheric pCO_2 level of about 360 µatm (Takahashi et al., 2002).

In presence of sufficient carbonate sources increasing CO_2 levels will result in increasing alkalinity. In the marine aquarium technology, a calcium reactor is used to raise alkalinity for coral cultivation (Brockmann & Janse, 2008). Our mesocosms contained calcium carbonate (shell fragments) rich sediments. This explains the rapid increase in alkalinity with elevated CO_2 concentration, resulting in a total alkalinity that was 1 to 5 times higher in the treated mesocosms than in the controls (S 2.2). This process was facilitated by the relatively high sediment surface-water volume ratio and lack of water replacement or exchange. These conditions represent a worst-case situation that could occur in isolated shallow water ecosystems. In a real situation where underwater release of exhaust gas is applied, CO_2 injection will appear near the water surface. This will probably lead to less harmful exposure conditions, especially in deeper water where only the upper part of the water column will be affected. On the other hand the mesocosms did not contain early life stages of calcifying species that are regarded most sensitive to elevated CO_2 concentrations (Kurihara, 2008).

The oxygen saturation level in the controls remained over 96% during the whole study. The lowest oxygen saturation level in all CO_2-treated mesocosms was observed in the replicated pH 5.8 treatments, namely 75% (S 2.2). This probably was related to high oxygen consumption by biodegradation of dead organisms (see next section). Other treatments remained above 85% (S 2.2). These values are all well above the levels where biological effects due to lack of oxygen will occur. Nutrient levels for P (PO_4) and N ($NO_3 + NH_4$) were not significantly different between treatments on the last day of the experiment, while SiO_2 levels were below detection limits (0.3 m/l) in all treated mesocosms, but around 0.8 mg/l in control groups (S 2.2).

2.3.2 Phytoplankton and Zooplankton

The chlorophyll-a concentration, a proxy for phytoplankton biomass in the controls remained below 20 µg/l during the whole experiment. The CO_2 treated groups showed similar development as the controls, except for the pH 5.8 treatment. The presence of planktonic grazers (e.g. zooplankton) at the moderate pH levels could explain why the chlorophyll - a concentrations in these mesocosms remained relatively low (Table 2.3). In the pH ≥ 7.1 mesocosms, the total abundance of zooplankton was increased at the beginning of the experiment. This increase was slightly slower in the CO_2 treated groups compared to the control (most cases > 500 ind./l) (Table 2.3). In addition, the development of chlorophyll-a concentration, could have been restricted by phosphorous availability, since the dissolved phosphorous concentrations in all our mesocosms were below the detection limit on day 49.

Although, the inorganic nutrients were limited, the chlorophyll-a concentration of the pH 5.8 mesocosms increased up to about 60 µg/l, which is more than 9 times higher than in the controls (Figure 2.2). Similarly, Bach et al. (2017) observed a positive CO_2 effect on chlorophyll-a build-up in their 50 m^3 mesocosms when the inorganic nutrient concentrations were close to the detection limit. This indicates that fluxes of inorganic nutrients that became available from decaying organic material were immediately used by developing phytoplankton, resulting in a continuously low nutrient concentration in the water column. In our pH 5.8 mesocosms, degradation of dead zooplankton and benthic organisms that did not survive the high CO_2 exposure, must have resulted in a flux of inorganic nutrients to the water column. For example, in pH 5.8, the total zooplankton abundance decreased from over 500 individuals per liter (ind./l) on day 0 to 3 ind./l on day 49 (Table 2.3). The high mortality amongst organisms (e.g. zooplankton) that feed on phytoplankton, subsequently reduced grazing pressure and provided inorganic nutrients, which resulted in the algae bloom that was observed in the pH 5.8 mesocosms.

The biodegradation of the organic material that become available in the high dosed mesocosms due to the increased mortality of invertebrates lead to higher oxygen consumption. This result in a concentration of dissolved oxygen in our pH 5.8 mesocosms that was about 15% lower than in the controls. The lowest observed oxygen concentration of 75% of the maximum saturation level is not that low as to have cause additional mortality among the organisms living in these mesocosms. The indications for reduced abundance or increased mortality of the zooplankton and benthic organisms in the mesocosms with higher treatment levels are therefore considered as a direct effect of the elevated CO_2 levels.

The high tolerance of phytoplankton to elevated CO_2 conditions may result from the utilization of different forms and amount of dissolved inorganic carbon. For example, microalgae are able to take up HCO_3^-, the dominant carbon form when pH is between 6.5 and 10, as well as free CO_2 and H_2CO_3, the predominant form when the pH is lower than 6.5 (Markou et al., 2014). Since the utilization of the carbon form is species specific (Camiro-Vargas et al., 2005), it is likely that there were different dominant microalgae species in the different treated mesocosms in our study. The fluorescent data indicated that green algae dominated the phytoplankton community throughout the whole study in each treatment (Figure 2.2 and S 2.3), but further identification of algae species was not performed.

At the start of the exposure the zooplankton community was already dominated by copepods, and the relative and absolute abundance of these crustaceans strongly increased during the first week application in all mesocosms with pH $\geq$ 7.1 (Table 2.3 and S 2.4). In these mesocosms the copepods remained the dominant zooplankton group until the end of the study on day 49. In mesocosms with pH 6.2 and pH 5.8, a strong decline of the copepod density was observed during the first week of CO_2 application, and the densities further declined until the end of the study. Such a clear decline was also observed in mesocosms with pH 6.6, although here the copepod population still showed some increase during the first week. It is clear from this data that the copepod community suffered directly from the elevated CO_2 concentrations. In our mesocosms it were thus not the copepods that took advantage of the elevated CO_2 concentrations as was described by Taucher et al. (2017), but it were the polychaete worms. The planktonic larvae of polychaete worms were almost absent in the control mesocosms, but reached high numbers and were the dominant zooplankton group in the pH 7.1 and 6.6 mesocosms at the end of the study (S 2.4). At the highest two treatment

levels, pH 6.2 and 5.6 even the polychaete could not maintain their position, and at the end of the study zooplankton was only present in extremely low numbers in these mesocosms.

The positive impact of the intermediate CO_2 levels on the development of the polychaete worms was also reflected by the numbers of adult worms, and affected other organisms, as will be discussed in the following sections.

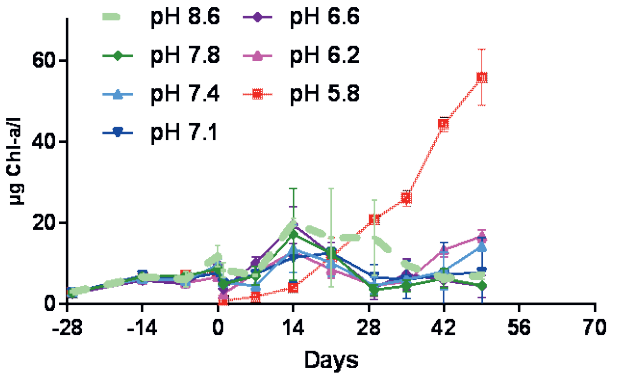

Figure 2.2 Development of phytoplankton under seven different pH conditions (pH 5.8- pH 8.6) from 28 days before starting the treatment to 49 days after. The result is expressed as chlorophyll-a concentration (µg Chl-a/l). Error bars represent the standard deviation of the 2 duplicate mesocosms. CO_2-application started on day 0.

Table 2.3 The average density of total zooplankton (ind./l) in the duplicate mesocosms under 7 different pH conditions (pH 5.8 - pH 8.6) on day 0, day 7, day 15 and day 49. CO_2-application started on day 0. The number in the bracket indicate the average density of copepod (ind./l). The average density of copepod was calculated by sum of the density of Nauplii, Calanoide, Harpacticoide and Cyclopoide in the mesocosms.

Ind./l	pH 8.6	pH 7.8	pH 7.4	pH 7.1	pH 6.6	pH 6.2	pH 5.8
day 0	111 (55)	372 (81)	102 (33)	105 (74)	177 (45)	59 (53)	517 (116)
day 7	702 (604)	396 (310)	507 (381)	432 (356)	86 (72)	14 (11)	12 (8)
day 15	733 (591)	427 (285)	754 (382)	288 (131)	43 (22)	17 (11)	11 (7)
day 49	208 (199)	264 (248)	185 (148)	237 (133)	177 (5)	6 (4)	3 (2)

2.3.3 Polychaetes and Periphyton

Development of sessile algae (periphyton) biomass on the glass slides that were introduced on day 0 was first detectable after 14 days. This time lag can be explained by the fact that the colonization of a new surface takes time since the algae adherence depends on the bacterial colonization and its secreted organic matrix which may take from days to weeks (Azim & Likens, 2009). After 14 days, a strong development of periphyton was observed in the control and most CO_2 treated groups, except at pH 6.6 and pH 5.8 (Figure 2.3a). In the pH 6.6

treatment, the chlorophyll-fluorescence, a proxy for periphyton biomass stayed below 300 units for the entire experiment period. It was similar to or lower than (e.g. on day 15) in the pH 5.8 treatment (Figure 2.3a). The integrated chlorophyll concentrations, a proxy for the general presence (availability) of periphyton biomass during the course of the study was lower in the pH 6.6 and pH 5.8 treatments than in the control. However, in the intermediate treatment (pH 6.2), the periphyton was able to develop and reached levels similar to the controls (Figure 2.3b). Thus, it is unlikely that the elevated CO_2 concentration on itself was responsible for the poor periphyton development in the pH 6.6 treatments. The main drivers in the development of periphyton biomass are growth (primary production) and grazing.

In our study, the glass slides that were used for the monitoring of the periphyton development were exposed out of reach of gastropods (periwinkles and mud snails) and the benthic invertebrates that all consume (benthic) periphyton. However, it cannot be excluded that planktonic polychaetes were able to colonise the glass slides as small juveniles and feed on the sessile algae. These planktonic polychaete larvae became especially abundant in the pH 6.6 mesocosms where the polychaete worms became the most dominant benthic group, reaching significantly ($p = 0.0194$) higher densities than in the controls on day 49 (Figure 2.4a). They produced substantial amounts of offspring as reflected by the significant ($p = 0.0299$) higher numbers of pelagic polychaete larvae in the plankton samples in pH 6.6 (Figure 2.4b). With decreasing pH the relative abundance of the polychaete larvae increased until it comprised over 85% of the total zooplankton community in treatments pH 7.1 and pH 6.6 (Figure 2.4b and S 2.4). The reduced periphyton biomass in the pH 6.6 mesocosms might thus be the result of additional grazing by larvae of polychaete worms.

This hypothesis is also corroborated with the finding of increasing biomass of periphyton in the pH 6.2 treatment, where the polychaetes were no longer able to take advantage and their larvae were only present in low numbers, as were the other primary consumers. As the glass slides were only analysed for fluorescence to determine periphyton biomass, no observations of other organisms were made that could test this hypothesis.

In the highest CO_2 treatment, pH 5.8, the development of periphyton was inhibited despite the virtual absence of polychaete larvae, and potential other grazers. These results indicate that sessile algae (periphyton) are less resilient to extreme CO_2 concentrations than planktonic algae (phytoplankton) that were able to bloom in the pH 5.8 mesocosms. The acidic condition may disturb the colonization process of bacteria and/or the attachment of the periphyton itself. Currently, little is still known about how exactly physical disturbance events in the environment influence periphyton attachment and development (Azim & Likens, 2009).

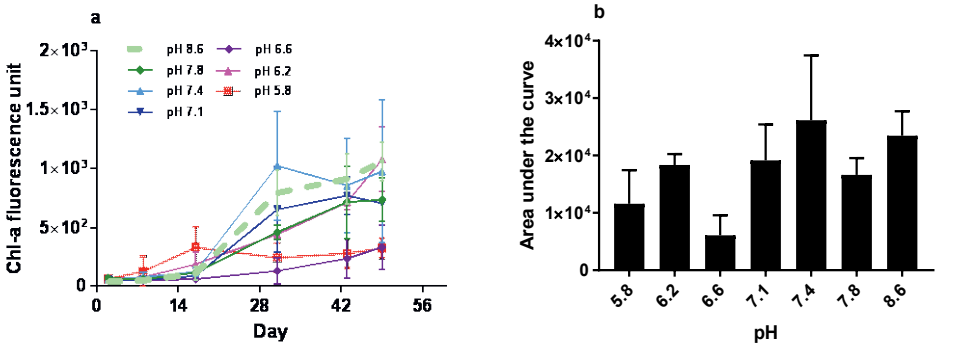

Figure 2.3 Development of periphyton on glass slides under 7 different pH conditions (pH 5.8- pH 8.6) in the mesocosms from day 0 to day 49, expressed as chlorophyll-a fluorescence units (a). CO_2-application started on day 0. The area under the curves of periphyton development in Figure 2.3a is calculated and represent the presence (availability) of periphyton biomass in the mesocosms under different pH conditions (b). Error bars represent the standard deviation of the 2 duplicate mesocosms.

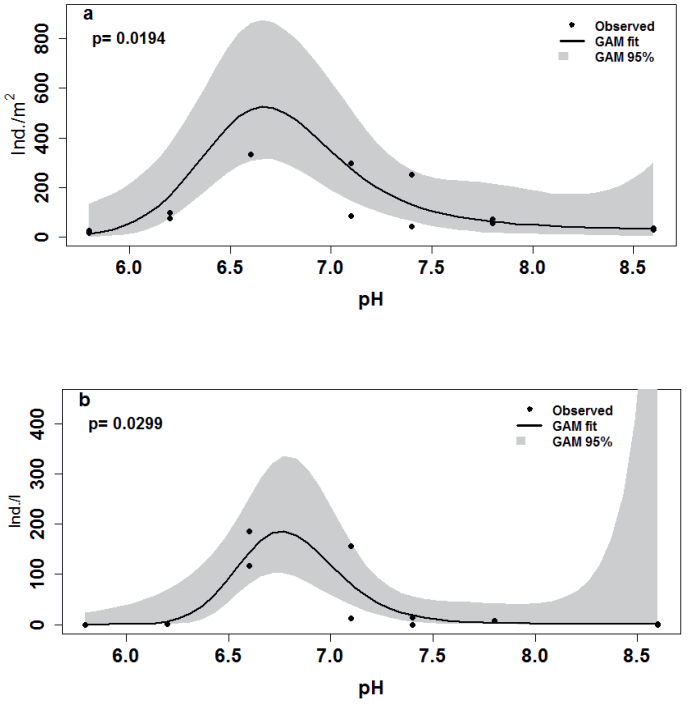

Figure 2.4 Generalized Additive Modelling results: the observed adult population (black dots) of polychaetes in sediment (ind./m^2) (a) and the observed density (black dots) of planktonic polychaetes (ind./l) (b) under 7 different pH conditions (pH 5.8- pH 8.6) on day 49 in all the mesocosms. CO_2-application started on day 0. The solid line represents a fit smoothing function of potentially relevant explanatory variables (in this case, enriched CO_2 caused pH reduction) to the observed density data. The grey area indicates the 95% confidence interval of the smooth function.

2.3.4 Periwinkles and Other Benthic Organisms

During the final sampling the *Peringia ulvae* (mud snail) and *Corophium volutator* (mud shrimps) numbers showed a high variation between duplicated mesocosms, which hampered the detection of subtle effects. None the less, it was clear that survival of both benthic species was strongly reduced to almost absent in treatments pH 6.2 and 5.8 (S 2.5).

The appearance of the periwinkle's shells showed the direct impact of the elevated CO_2 concentrations. A clear trend of the shell colour changing with increasing CO_2 concentration was observed. Starting from a normal dark shell (pH 8.6 - pH 7.4) via half shell dark and half shell bleached in the pH 7.1 treatments, to the entire shell bleached in the pH 6.6 treatment, eventually with shell damage (pH 6.2 - pH 5.8) (S 2.6). The shell calcification rate of periwinkles is reported to be negatively affected by elevated CO_2 concentrations (Ries et al., 2009). When the organisms are not able to compensate the dissolution rate of shells in acidic condition with a higher calcification rate, shell bleaching and damage occurs. Although the major part of the shell is covered by an external organic layer, the protection is not sufficient to fully protect against to elevated CO_2 (Ries et al., 2009). It is possible that the first bleaching indicates the erosion of the external organic layer.

Besides the color changes, the mortality of periwinkles also significantly increased ($p = 0.0011$ in pH 6.2; $p = 0.0007$ in pH 5.8) with increasing CO_2 concentrations. In pH 6.2 and pH 5.8 treatments, where the shell damage occurred, the mortality was as high as 85% (Figure 2.5 and S 2.7). However, the CO_2 induced pH decrease had no significant effect on the biomass of surviving periwinkles (Figure 2.6a). In comparison to the periwinkles at introduction, both flesh and inorganic weight (shell weight) in the control groups increased with 31% and 20%, respectively. While in the most extreme treatment, pH 5.8, the flesh and shell weight did not change relative to the initial weights (Figure 2.6a and S 2.7). In addition, both weights showed no direct relation with CO_2 concentration. The weights, however, showed a significant positive correlation with the total periphyton biomass available (Figure 2.6b), which forms the periwinkles main food source. As discussed above the development of the periphyton biomass was indirectly affected by the CO_2 concentration through the increasing abundance of polychaete larvae at intermediate CO_2 levels (pH 6.6), and directly affected by higher CO_2 levels. The periwinkles are thus indirectly affected by these complex interactions that consider their main food source.

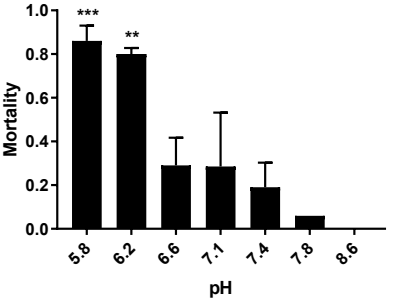

Figure 2.5 Mortality of recovered periwinkles under seven different pH conditions (pH 5.8- pH 8.6) in the mesocosms on day 49. Error bars represent the standard deviation of the mortality between the 2 duplicate mesocosms. Statistical difference between the CO_2 treated groups and control (pH 8.6): **, $p < 0.01$; ***, $p < 0.001$. CO_2 application start on day 0.

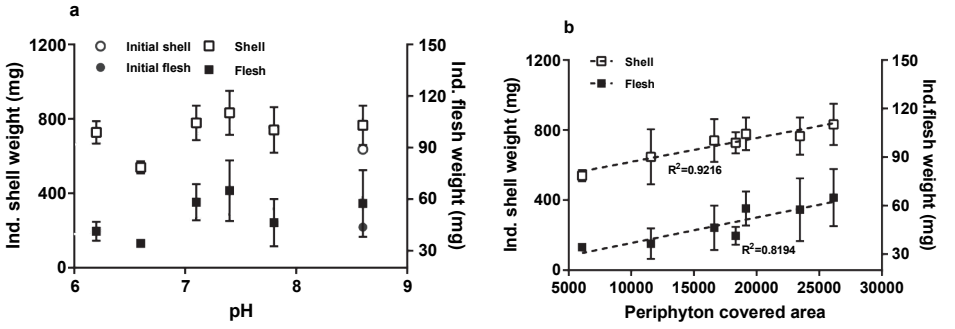

Figure 2.6 The average initial shell (empty blue circle) and flesh (solid blue dot) weights of periwinkle and the average shell (empty black square) and flesh (solid black square) weight of surviving periwinkles under seven different pH conditions on day 49 (a); the average shell (empty square) and flesh (solid square) weight of surviving periwinkles under different periphyton availabilities (b). Error bars represent the standard deviation of the mortality between the 2 duplicate mesocosms. CO_2 application start on day 0.

2.4 Conclusion

During the 49 days with elevated CO_2 concentrations several effects were observed. In the highest CO_2 treatment, the invertebrate community collapsed and phytoplankton bloomed. In contrast to their planktonic equivalent, the sessile microalgae (periphyton) were not able to increase biomass. At lower concentrations of CO_2, more subtle changes were observed. In pH 7.1 and 6.6 treatments, high numbers of planktonic polychaete larvae appeared, corresponding with high numbers of sedentary adult polychaetes in these treatments. The periwinkles clearly suffered directly from the treatments as was illustrated by affected shells at pH 7.1 and below, and increasing mortality with higher CO_2 dosage. The development of their individual total biomass however was not directly related to the CO_2 treatment level, but more indirectly via the availability of their major food source, periphyton. As the periwinkles shared this food source with the polychaete worms their biomass was affected by the increasing densities of these worms with increasing CO_2 levels. This mesocosm study shows the importance of species interactions in the response of an ecosystem to elevated CO_2 concentrations. It illustrates that the environmental impact of underwater release of exhaust gasses depends on various factors including the composition of the gas, the shipping intensity, the volume of the receiving water body, and local environmental conditions. The relative importance of these factors is subject of future research that will be used to assess the boundaries where the advantages of underwater release of exhaust gasses can be applied with minimum adverse impact on the local marine ecosystem.

Acknowledgment

This research was supported by the project “GasDrive: Minimizing emissions and energy losses at sea with LNG combined prime movers, underwater exhausts and nano hull materials” (project 14504) of the Netherlands Organization for Scientific Research, domain Applied and Engineering Sciences (TTW).

2.5 Supplementary Material for Chapter 2

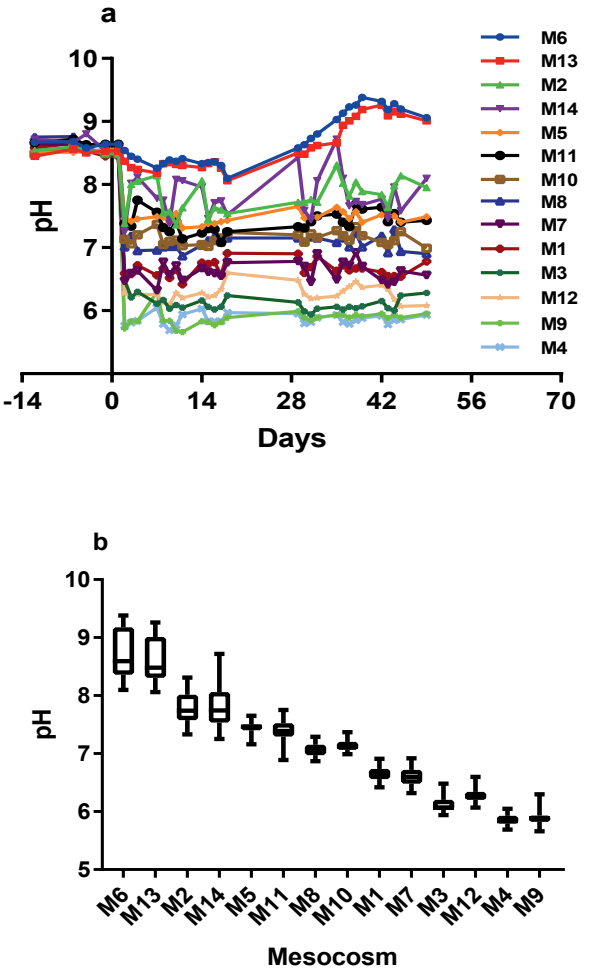

S 2.1 pH levels of mesocosms over the experiment period, 49 days (a), CO_2-application started on Day 0. Box & whiskers of measured pH in the mesocosms express CO_2 flux (b). The mesocosms were randomly chosen for expressing certain consistent CO_2 flux (duplicate study). CO_2-application started on Day 0.

S 2.2 Average values of water parameters measured in the water columns of the mesocosms and the nutrient level on day 49 of the experiment. Initial values were measured just before starting the treatment (averages of all mesocosms). For the treatment phase, the average values of the duplicated treatment are presented. The standard deviation between the duplicate groups is indicated by "±".

		pH 8.6	pH 8.6	pH 7.8	pH 7.8	pH 7.4	pH 7.4	pH 7.1	pH 7.1	pH 6.6	pH 6.6	pH 6.2	pH 6.2	pH 5.8	pH 5.8
	Initial	M6	M13	M2	M14	M5	M11	M8	M10	M1	M7	M3	M12	M4	M9
Temp. (˚C)	16.6 ± 0.3	20.0 ± 2.1	19.3 ± 2.1	20.0 ± 2.1	19.7 ± 2.2	19.8 ± 2.0	19.8 ± 2.0	19.6 ± 2.1	19.7 ± 2.1	19.9 ± 2.1	20.0 ± 2.1	19.9 ± 2.0	19.8 ± 2.1	19.5 ± 2.1	19.7 ± 2.0
Salinity (‰)	30.8 ± 0.6	32.05 ± 0.7	32.65 ± 0.9	33.34 ± 0.9	30.97 ± 1.1	32.86 ± 0.8	31.50 ± 0.9	32.42 ± 1.0	32.36 ± 0.8	32.25 ± 0.9	32.53 ± 0.9	32.52 ± 0.9	32.17 ± 1.0	32.40 ± 0.8	33.43 ± 1.2
Oxygen (%)	96.7 ± 0.6	97.7 ± 2.9	98.9 ± 2.8	98.5 ± 3.7	98.3 ± 2.8	99.0 ± 4.2	96.1 ± 3.1	95.0 ± 3.7	97.1 ± 2.5	95.4 ± 3.4	93.7 ± 4.4	85.8 ± 8.1	91.1 ± 6.0	76.8 ± 9.6	75.8 ± 8.9
Alkalinity (meq/l)	2.5 ± 0.1	2.6 ± 0.5	2.8 ± 0.4	3.0 ± 0.2	2.9 ± 0.3	2.9 ± 0.3	3.1 ± 0.4	3.4 ± 0.4	3.4 ± 0.5	5.1 ± 1.7	5.7 ± 1.7	5.8 ± 2.1	5.1 ± 1.4	5.3 ± 1.7	6.4 ± 1.8
NH_4 (mg N/l)	0.48	0.58	0.51	0.48	0.57	0.53	0.52	0.54	0.55	0.59	0.54	0.48	0.49	0.47	0.55
NO_3 (mg N/l)	0.2	< 0.2	< 0.2	< 0.2	< 0.2	< 0.2	< 0.2	< 0.2	< 0.2	< 0.2	< 0.2	< 0.2	< 0.2	< 0.2	< 0.2
PO_4 (mg P/l)	0.03	< 0.02	< 0.02	< 0.02	< 0.02	0.02	< 0.02	< 0.02	< 0.02	< 0.02	< 0.02	0.06	< 0.02	< 0.02	< 0.02
SiO_2 (mg Si/l)	2	0.9	0.8	< 0.3	< 0.3	< 0.3	< 0.3	< 0.3	< 0.3	< 0.3	< 0.3	< 0.3	< 0.3	< 0.3	< 0.3

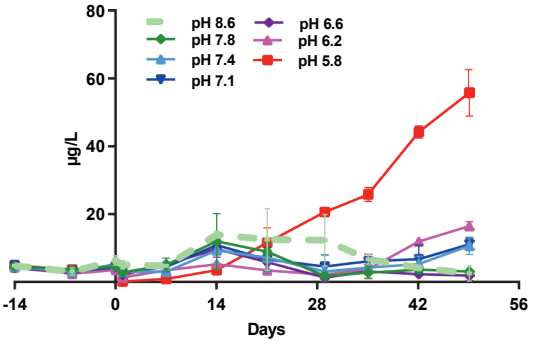

S 2.3 Development of green algae under seven different pH conditions (pH 5.8 - pH 8.6) from 28 days before starting the treatment to 49 days after. The result is expressed as chlorophyll-a concentration (µg/l). Error bars represent the standard deviation between the 2 duplicate mesocosms. CO_2-application started on day 0.

S 2.4 The density (ind./l) of total zooplankton and 9 different identified zooplankton species in individual mesocosms on day 49.

	pH 8.6	pH 8.6	pH 7.8	pH 7.8	pH 7.4	pH 7.4	pH 7.1	pH 7.1	pH 6.6	pH 6.6	pH 6.2	pH 6.2	pH 5.8	pH 5.8
Ind./l	M 6	M 13	M 2	M 14	M 5	M 11	M8	M10	M 1	M 7	M3	M 12	M4	M9
Total zooplankton	171	244	148	381	168	201	90	384	153	201	7	6	1	5
Nauplii	92	191	77	318	102	20	42	164	1	5	3	2	0	4
Harpacticoide	69	16	21	1	12	11	7	6	0	5	1	0	0	1
Calanoide	2	26	14	0	0	152	24	22	0	0	1	1	0	0
Cyclopoide	1	0	6	0	0	0	0	1	0	0	0	0	0	0
Rotifera	0	0	3	1	8	0	0	1	0	0	0	0	0	0
Gastropoda	0	4	17	1	4	5	4	4	34	1	0	0	0	0
Polychaeta	1	0	8	2	0	14	12	156	117	186	1	1	0	0
Bivalvia	3	5	0	0	2	0	0	0	0	0	0	0	0	0
Nematoda	3	2	1	0	5	0	0	0	0	4	1	2	0	0

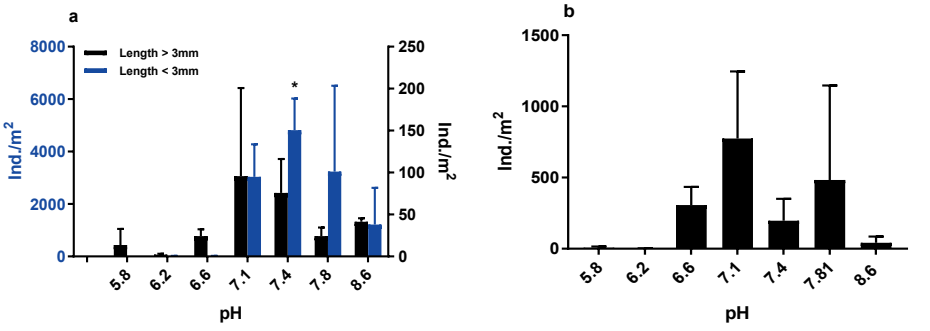

S 2.5 The population of benthic *Peringia ulvae* (a, separated in 2 groups: length > 3 mm (black bar) and length < 3 mm (blue bar)) and *Corophium volutator* (b) under seven different pH conditions on Day 49 in all the mesocosms. Error bars represent the standard deviation between the 2 duplicate mesocosms.CO_2-application started on day 0. * indicates statistically significant difference from control (pH 8.6) at $p < 0.05$. CO_2 application start on day 0.

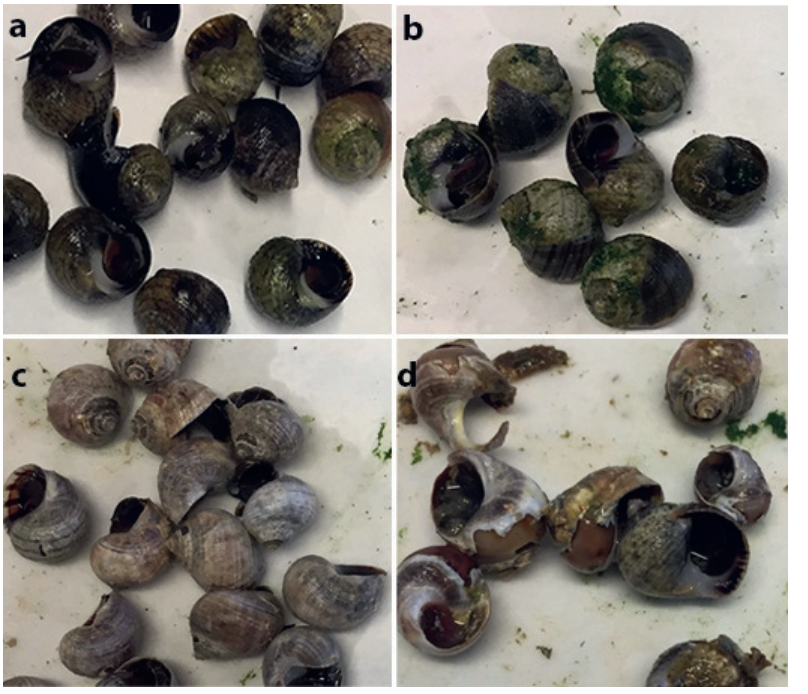

S 2.6 The pictures of periwinkles under four different pH conditions, pH 8.6 (a), pH 7.1 (b), pH 6.6 (c) and pH 5.8 (d) in the mesocosms on day 49. CO_2 application start on day 0. Starting from a normal dark shell (a, pH 8.6) via half shell dark and half shell bleached in pH 7.1 (b), to the entire shell bleached in pH 6.6 (c), eventually with shell damage (d, pH 5.8)

S 2.7. The periwinkle data per mesocosm and the initial two groups of 20 periwinkles that were stored in -20 ˚C fridge on day 0 as reference. The number of introduced and recovered periwinkles on day 0 and 49, respectively. The number of alive periwinkles on day 49. The total dry weight, shell and flesh weight of the initial periwinkles and the alive periwinkles on day 49.

	Initial	Initial	pH 8.6	pH 8.6	pH 7.8	pH 7.8	pH 7.4	pH 7.4	pH 7.1	pH 7.1	pH 6.6	pH 6.6	pH 6.2	pH 6.2	pH 5.8	pH 5.8
Replicate	1	2	M6	M13	M2	M14	M5	M11	M8	M10	M1	M7	M3	M12	M4	M9
Introduce Nr.	20	20	20	20	20	20	20	20	20	20	20	20	20	20	20	20
Recover Nr.	20	20	13	16	16	16	15	18	13	18	20	16	17	18	16	11
Alive Nr.	-	-	13	16	15	15	11	16	7	16	16	10	3	4	4	1
Total dry weight (alive periwinkles) (mg)	13773	13428	9538	14586	10358	13255	8815	15890	6374	12214	8817	5955	2420	2919	1698	802
Total shell weight (alive periwinkles) (mg)	12904	12548	8970	13448	9810	12414	8238	14650	5914	11401	8259	5619	2308	2738	1609	758
Total fresh weight (alive periwinkles) (mg)	869.6	879.1	568.4	1138.4	547.8	840.3	576.4	1239.3	459.3	812.8	557.1	336.3	112.1	180.6	89.2	43.1

CHAPTER 3

3

Environmental impact of underwater exhausted CO_2 from ships and its potential as antifouling strategy

Yuzhu Wei[a], Yuekai Xu[a], Luna M. van der Loos[a], Reindert Nijland[a], Albertinka J. Murk[a], Edwin M. Foekema[a,b]

[a.] Marine Animal Ecology group, Wageningen University, P.O. box 338, 6700 AH Wageningen, The Netherlands
[b.] Wageningen Marine Research, P.O. Box 57, 1780 AB Den Helder, The Netherlands

Submitted

Abstract

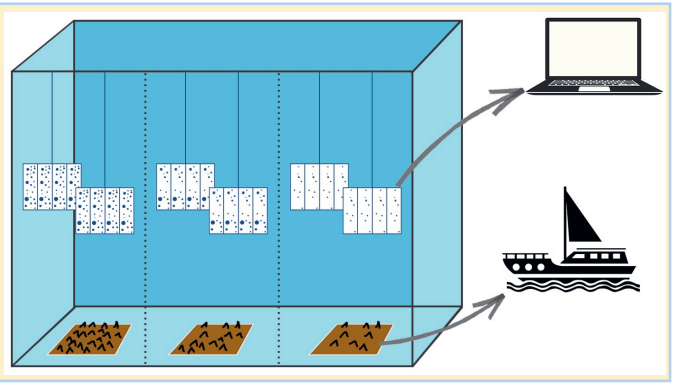

Several engineering projects have studied the application of underwater exhaust systems as air lubrication to reduce the water resistance of ships. The system would increase the energy efficiency and as such reduce ships emissions on a global scale. At local scale however, the underwater released exhaust gas, and especially the CO_2 in it, may significantly acidify the water with unknown impact. Most available biological impact studies reflect the expected chronic future ocean acidification, which does not represent the rapid and high dose of CO_2 from an underwater exhaust system. Therefore, we assessed the impact of high CO_2 concentrations (resulting in pH 7.8 to 6.3) on developing microbial biofilms and barnacles. With decreasing pH to 6.3, the development of biofilm biomass was significantly reduced and a shift in taxonomic composition occurred. The barnacles tolerated acidic conditions up to pH 6.8 for 25 days although their feeding activity and growth rate decreased, and high mortality occurred in the pH 6.3 group. Moreover, we found over 50% of the barnacles in the pH 6.3 group was removed by the water force generated by 12 km h^{-1} sailing for 15 min. This suggests that CO_2-induced acidic conditions around the ship's hull may increase the anti-fouling property, which could be an added benefit of underwater exhaust systems on ships.

3.1 Introduction

In an effort to reduce noise, harmful emission on working decks, and risk of hotspot detection for naval ships, maritime industries tend to release exhaust gas underwater (H Sapra et al., 2017). In addition, an underwater emission system could be used for air lubrication, which could reduction of ship's total resistance with approximately 10 - 15% (Ceccio, 2010). Several technical research projects were funded to focus on combining underwater exhaust systems with new generation fuel cells and turbocharged gas engines to further enhance fuel efficiency and decrease overall emission (H Sapra et al., 2017; H D Sapra et al., 2019; Van Biert et al., 2016; Van Biert et al., 2018). This development would increase the energy efficiency and so reduce the ship emissions on a global scale. Effects on a local scale, however, are yet unknown.

Releasing exhaust gas containing CO_2 may significantly acidify the surrounding water, creating a low pH condition around the ship's hull. Most available studies on biological impact of elevated CO_2 levels in seawater applied pH levels reflecting expected future atmosphere CO_2 concentrations, which are estimated to be around 936 ppm in 2100, and are thought to maximally represent a 0.5 unit decrease in global average ocean pH (Wittmann & Pörtner, 2013). This narrow range of elevated CO_2 concentration does not represent local conditions where the CO_2 from underwater released exhaust gas may cause a rapid decrease

of the pH to much lower levels. Therefore, more information about how marine organisms respond to a wider range of CO_2 levels is needed.

When an underwater exhaust system is applied, fouling organisms living on the ship's hull are acutely exposed to a high dose of exhaust gas. Biofouling initiates from a biofilm (an accumulation of organic material, bacterial colonisation and some unicellular algae) (Armstrong et al., 2000; Callow & Callow, 2002), which is followed by the settlement and development of sessile marine invertebrates (Chambers et al., 2006; Hadfield, 2011). Studies have shown that elevated CO_2 concentrations impact marine fouling animals, such as barnacles (Campanati et al., 2015; Findlay et al., 2010a). Campanati et al. (2015) suggested that early-life stages of barnacles developed less and/or weaker calcified structures under low pH (pH 7.6) and oxygen (3 mg/l) conditions.

Regardless to the protection of marine ecosystems, the battle between human and fouling organisms has continued for decades. Due to biofouling, fuel consumption is known to increase as much as 40% (Champ, 2000), as it increases hull roughness and wall shear stress, which in turn raises frictional drag. For example, a layer of calcareous fouling is able to increase the resistance penalty of a frigate from 34% to 86% (Schultz, 2007). Unfortunately, most commercial antifouling coatings contain biocides and these toxicants are harmful to non-target marine species as well (Dafforn et al., 2011; K Thomas & Brooks, 2010). Besides the environmental contamination risk, coating deterioration over time also decreases the shipping efficiency. Limited coating deterioration leading to an equivalent of only 100 µm height sand roughness, may already significantly increase the resistance penalty of a ship's hull with approximately 11% (Schultz, 2007). Therefore, antifouling paint requires frequent maintenance, which is costly and time consuming. A nontoxic silicone oil lubricant combined with a nanostructured wrinkled surface is developed to reduce the attachment of fouling organisms. However, the efficiency of this antifouling technology decreases too fast because the silicone oil depletes over time (Ware et al., 2018). Thus, there is still a need for an environmentally friendly yet also efficient antifouling strategy.

As far as we are aware of no studies to date have examined the application of elevated CO_2 concentrations for antifouling purposes. Therefore, besides understanding the impact of elevated CO_2 on fouling organisms, the presented study also addressed the potential of using underwater emission in anti-fouling.

Accordingly, the present study focused on the impact of a wide range of CO_2 dosages resulting in a pH range of 7.8 - 6.3 (equivalent to 784 - 23,189 µatm pCO_2) on the development of microbial biofilms and on previously settled barnacles, *Balanus crenatus*. In addition, the potential of underwater exhaust systems for antifouling purposes was evaluated by testing the resistance of the pre-treated barnacles against the water force generated by sailing at a relatively low speed of 12 km $h^{-1.}$

3.2 Materials and methods

3.2.1 Microcosm set-up

Fifteen glass microcosms (35 cm x 30 cm x 25 cm), each with individual water pumps for internal circulation, were installed in a temperature-controlled room (approximately 13.5 -

14 ˚C, Wageningen, the Netherlands) and filled with artificial seawater. The artificial seawater (Tropic Marin®, Zoo mix) was adjusted to an alkalinity level of 2.42 meq/l, which is in the same range as the water at the location where the PVC plates were exposed to collect the barnacles (see below). After the barnacles and the substrates for biofilm development (day 0, see details below) were introduced, all microcosms except 3 controls, were provided with CO_2 fluxes (day 0). The CO_2 flux, and hence the pH level was maintained in each microcosm via a pH controller (Milwaukee, MC125). The target pH level of each microcosm was reached within 3 hours after the CO_2 flux started (triplicate study) (Table 3.1). Half of the seawater was refreshed every 2 - 3 days, after which the target pH level was reached again within 1 hour.

Temperature, dissolved oxygen saturation level, salinity, alkalinity, NH_4^+ and NO_2^- concentrations of the seawater in the microcosms were measured before and after each water change. The pH level was measured twice a day with an electrode pH meter (Hach PHC101), around 10 am and 2 pm.

In the present study, the so-called Seacarb package (Lavigne & Gattuso, 2010) in R (Team, 2013) was used to express all exposures as pCO_2 in micro atmosphere (µatm) based on alkalinity, pH, salinity and temperature values. Conditions in the control groups mimicked the pH, salinity and alkalinity measured in the local seawater at the barnacle collection point.

Table 3.1 The microcosm number with the mean pH level of the treatments and the calculated pCO_2 value.

Microcosm number	Mean pH	Mean pCO_2 (µatm)
1, 10, 15	7.8	784
2, 12, 14	7.6	1104
4, 8, 13	7.2	2488
6, 9, 11	6.8	7445
3, 5, 7	6.3	23189

3.2.2 Biofilm biomass and biodiversity

The biomass development and taxonomic composition of the biofilm were monitored on 8 glass microscope slides (76 x 26 mm) per microcosm, which were hung in horizontal position at a water depth of approximately 20 cm in the centre of each microcosm. Two slides were taken out from each microcosm on day 10, 17 and 24 of the experiment. Of these two slides, one was used for biofilm quantification and the other was sampled for DNA analyses.

To quantify biofilm biomass, the slide was stained using 5 ml of 0.5% crystal violet (CV) solution for 20 min. Unbound CV stain was removed by rinsing the glass slide with artificial seawater until no more CV was observed to dissolve in the water. The glass slides were air dried. Subsequently, 5 ml of 96% ethanol containing 2% acetic acid (v/v) was used to dissolve the bound CV stain from the glass slide. Adsorption at 595 nm was measured using a Filter Max F5 multiple - mode microplate reader (Molecular Devices, USA), and the data was analysed in Microsoft Excel. The absorbance by the dissolved biofilm-bound CV was used to indicate the biofilm biomass.

To analyse bacterial taxonomic composition and biodiversity, the biofilm on the second slide was carefully collected with cotton swabs (COPA150C, VWR International B.V.) and stored in 2 ml Longmire's buffer (Longmire et al., 1997) at - 20 ˚C for later gene analysis.

Bacterial genomic DNA was extracted from the Longmire's preserved cotton swabs after thawing the samples at room temperature. Tweezers were used to carefully break off and remove the stick of the cotton swabs and return the tip of the swab to the Longmire buffer. The tube was vortexed vigorously for 30 seconds and 3 µl antifoam (Reagent DX, Qiagen) was added to each sample. The sample was sterilely transferred to a 15ml tube with approximately 200 µl of 100 µm zirconia beads and vortexed for 10 min. 50 µl Protease K was added, and samples were incubated at 56 ˚C for 20 min. Next, 3 ml Phenol/Chlorophorm/IAA (P/C/I, 24: 24: 1) was added to each sample, and samples were vortexed for 10 seconds and then rotated for 10 min. Tubes were centrifuged at 5000 rpm for 10 min before transferring the aqueous phase to clean 15 ml tubes. A second P/C/I clean up step was performed as above. 250 µl of 3 M NaAcetate and 5 ml of ice cold 100% ethanol were added to the final aqueous phase of the sample. The samples were inverted gently, placed on ice for 10 min and centrifuged for 10 min at 5000 rpm in 4 ˚C to precipitate and collect the DNA. The resulting DNA pellet was washed twice using 1 ml 70% ethanol. The pellet was air dried for 25 min and dissolved in 50 µl TE. DNA was quantified using a Nanodrop microvolume spectrophotometer (Thermo Fisher) and checked for size using agarose gel electrophoresis. An isolation control using a clean swab in buffer solution collected during original sampling was included.

The 16S rRNA genes of the extracted DNA sample were amplified by PCR using the 27F_BCtail-FW (TTTCTGTTGGTGCTGATATTGC_AGAGTTTGATCMTGGCTCAG) and 1492R_BCtail-RV (ACTTGCCTGTCGCTCTATCTTC_CGGTTACCTTGTTACGACTT) primers with added barcoding attachment sequences. 0.5 µl of isolated DNA was used as a template in a 20 µl PCR volume with the Thermo Scientific 2X Phire Tissue Direct PCR Master mix. For the thermocycling conditions see Table S 3.1. 1µl of PCR product from the first round of amplification was used a template in the barcoding PCR, using the PCR Barcoding expansion 1 - 96 Kit (EXP -PBC096) (Oxford Nanopore Technologies, Oxford, UK) according to manufacturer's instructions. Barcoded PCR products were sequenced according to the Ligation Sequencing Kit 1D (SQK-LSK108) (Oxford Nanopore Technologies, Oxford, UK) protocols. Negative PCR controls were included in the sequencing to check for contamination (the samples contained low levels of handling and/or kit contamination; those OTUs were removed from the dataset).

The Fastq 16S workflow revision 3.1.0 with the 16S classification version 2.1.1 were used on the Oxford Nanopore Epi2me platform (Metrichor, Oxford, UK) to classify raw sequences. A total of 264,722 reads were obtained, of which 253,153 reads were successfully classified and passed quality filtering (Q score threshold ≥ 8). A taxonomic hierarchy of all the classified taxa was obtained using the Entrez Taxonomy NCBI database and the taxize package in R (Chamberlain & Szöcs, 2013; Team, 2013), which was used to generate an OTU table on genus level. Data visualisation and statistical tests were performed using the vegan (Oksanen et al., 2018), ggplot2 (Wickham, 2016) and phyloseq (McMurdie & Holmes, 2013) packages. To test for differences in alpha diversity (within-sample diversity; observed OTU richness) between pH levels and days, a generalized linear mixed model was used with a random intercept for microcosm to correct for repeated measures. A Tukey post - hoc test

was performed for pair-wise contrasts. To asses differences in beta diversity (between-sample diversity) with pH levels and days, the weighted Unifrac (Lozupone et al., 2007) and Bray - Curtis (Bray & Curtis, 1957) dissimilarities were calculated. These metrics were then visualised with a Principal Coordinates Analysis (PCoA) plot and compared in a permutational analysis of variance (PERMANOVA) with 9,999 permutations (the permutations within the microcosms were constrained). The dataset passed the tests for the underlying assumption of a PERMANOVA, i.e. that the multivariate spread is equal among groups (M J Anderson, 2014). Genera that showed significant differences in abundance between pH treatments and days were determined using the DESeq2 package (Love et al., 2014) with Benjamini - Hochberg corrected p - values.

3.2.3 Barnacle collection and exposure

Balanus crenatus were collected by allowing them to naturally settle on 20 roughened PVC plates (7.5 cm x 7.5 cm) that were exposed for 25 days (28th May - 21st June 2018) at approximately 40 cm depth of seawater in the harbour of Den Helder, in the northwest of The Netherlands. The plates were checked weekly for barnacle settlement, and all other observable organism species were manually removed. On collection, the plates contained barnacles ranging from newly settled cyprids to 4 weeks old post-larvae. Water samples (500 ml) were taken from the same location for later water parameter analysis.

After transporting the PVC plates to the laboratory facilities in Wageningen, the Netherlands, the barnacles were allowed to acclimatise to the artificial seawater for 72 hours. The number of barnacles on each of the 20 PVC plates was counted and 15 plates that contained at least 450 individuals were selected. After the buoyant weight of these selected plates was determined, they were placed in one of the microcosms (1 plate per microcosm). During the exposure period that lasted 25 days, the barnacles were fed with a commercially available mixed microalgae diet (Isochrysis T-ISO (33%) / Nannochloropsis (31%) / Tetraselmis (18%) / Phaeodactylum (18%); Easybooster, Easyreefs) at 1 x 10^5 cells/ml, and approximately 100 *Artemia* nauplii per barnacle per day.

3.2.4 Barnacle growth and feeding activity

The buoyant weight of barnacles on each PVC plate was measured to calculate the biomass development of the barnacles. The density of the barnacle's soft tissue is expected to be almost similar to that of seawater, thus may not be included in the buoyant weight. Since the ratio of the weight of organics to the weight of shell is consistently less than 3% (Bourget, 1987), buoyant weight is a good approximation of the total biomass of barnacles.

Before barnacle collection, the 20 empty PVC plates (7.5 cm x 7.5 cm) were incubated for 2 days in artificial seawater in the experimental room (about 13.5 – 14 ˚C) to avoid possible water uptake caused by the material interfering the buoyant weight result of barnacles. All plates were brushed before the buoyant weight measurement to minimise the effects of biofouling on total weights. Buoyant weight was measured by the method as described by Schutter et al. (2008). The PVC plate was suspended on a hook in a defined volume of seawater at a constant depth. Seawater was maintained at 15 °C and 34‰ salinity. The hook was attached to an underweighting analytical balance (Kern&Sohn D - 72458 Albstadt, type 870 - 13) using a thin nylon string (Osinga et al., 1999).

The same conditions and procedures were followed to measure the buoyant weight of barnacles attached to the PVC plates on a weekly basis during the exposure in the microcosms. All buoyant weights were corrected for the original empty PVC plate weight. Changes in barnacle covered area on each plate were recorded weekly with a digital camera (Nikon, D5200). The photographs were analysed for percentage cover with software ImageJ.

On day 20, the feeding behaviour of the barnacles in the microcosms was recorded on video (Olympus Tg - 5). The recording started 1 minute after injecting 2ml *Artemia* nauplii (3,000 individual/ml) into the microcosm and stopped after 1.5 - 2 min of recording. Eight barnacles were randomly selected from each video, 30 feeding movements of individual barnacles were counted and the required time for these movements was recorded for feeding speed analysis. Each feeding movement was counted from the moment the barnacle extended its cirri from the shell until the cirri were completely back in the shell. Eventually, the average feeding speed of 8 barnacles in each microcosm was calculated as the average time required for one feeding movement.

3.2.5 Barnacle attachment strength

After 25 days of exposure in the microcosms, the PVC plates with barnacles were transported back to the harbour (Den Helder, the Netherlands). Here, first photos were taken of the individual plates which were subsequently fixed at the rear of a vessel (military Ops Landtdiep). The vessel sailed for 15 min at 12 km h^{-1}. After sailing, photos were taken from the individual plates for later determination of the barnacle cover percentage using ImageJ. The impact of faster sailing speed could not be tested due to limitations of the technical set up.

3.2.6 Barnacle data analysis

GraphPad Prism 7 (Graphpad Software Inc., CA, USA) was used to make the figures and perform statistical analyses. One-way or Two-way ANOVA (time and pH level) with Dunnett's multiple comparisons test were used to test the significant difference between the CO_2 treated groups and the control. P values < 0.05 were considered statistically significant in all the statistical analysis. All data presented here are expressed as means with standard deviation, unless stated otherwise.

3.3 Results

3.3.1 Water parameters

The pH of the seawater in the controls initially was 8.2 and stabilized after one day at an average pH of 7.8. In the treatment groups, pH rapidly decreased after the start of the CO_2 application, and then stabilized within one day at the target value (S 3.2a). The treatments followed a pH gradient with mean pH levels that were significantly different from each other ranging from 7.8 to 6.3 (lowest pH treatment) (Table 3.1). These mean pH levels are used here to indicate the different treatments. The corresponding pCO_2 levels of the groups are ranging from 784 µatm (control) to 23189 µatm (Table 3.1; S 3.2b; S 3.3).

The salinity, temperature and oxygen saturation level of all the groups remained at 33‰, 13˚C and over 90%, respectively (S 3.3). The alkalinity level slightly increased along with the pH level decrease, from about 2.4 meq/l in the controls to a maximum of 2.6 meq/l in the pH 6.3 treatments (S 3.3). Conversely, the NO_2^- concentration decreased with pH level decrease, and was below 1 mg/l for all experimental groups. The concentration of NH_4^+ remained 0.01 mg/l throughout the experimental period (S 3.3).

3.3.2 Biomass and biodiversity of the biofilm

The biomass of the biofilm increased from day 17 to day 24 in all the groups, with highest biomass in the control on day 24 (Figure 3.1). This increase over 1 week, however, was not statistically significant, and due to technical problems, no data were available for day 10. With decreasing pH, the biomass was significantly less relative to the controls (Figure 3.1).

The number of observed genera per biofilm sample ranged from 40 - 139. There were no differences in alpha diversity between the pH treatments on either day 10, 17 or 24. The alpha diversity of the biofilm was higher at day 24 at pH 6.8 ($p = 0.01$) and pH 7.6 ($p < 0.0001$) compared to day 10, and at pH 7.8 compared to day 17 ($p < 0.001$). The PCoA plots reflecting the PERMANOVA results (Bray - Curtis; Figure 3.2, Weighted UniFrac; Figure S 3.4) show that both day and pH had a significant effect on genus composition (Bray-Curtis; $p = 0.0001$, Weighted UniFrac; $p = 0.001$) and no interaction effect between day and pH was observed (Bray - Curtis; $p = 0.113$, Weighted UniFrac; $p = 0.131$). Post-hoc tests showed that the genus composition on day 10 significantly differed from the composition on day 17 and 24 (Bray - Curtis & Weighted UniFrac; $p = 0.003$, both comparisons). Additionally, genus composition at pH 6.3 was significantly different from pH 7.6 and 7.8 (Bray-Curtis; $p = 0.01$ for all comparisons, Weighted UniFrac; $p = 0.04$ for all comparisons), but not from pH 6.8 and 7.2 (Bray - Curtis; $p = 0.10$ and $p = 0.13$; Weighted UniFrac; $p = 0.49$ and $p = 0.79$) (Figure 3.2). Furthermore, 20 genera showed significant differential abundance between pH 7.8 (control) and pH 6.3. Of these, 9 genera were more abundant at high pH and 11 were more abundant at low pH (Figure 3.3). Raw sequence data and a list with the observed taxa have been uploaded and are publicly available in the European Nucleotide Archive, accession number PRJEB35703.

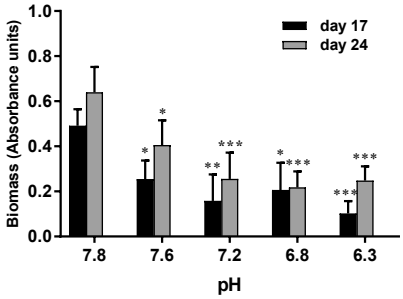

Figure 3.1 Biomass of biofilm (absorbance units) developed on microscope plates (n = 3) under pH 6.3 – 7.8 treatments on day 17 and day 24. The biomass was stained with crystal violet and quantified as Abs595 nm. Differences were assessed between the treated group and the control group on the same day only (*, $p < 0.05$; **, $p < 0.01$; ***, $p < 0.001$). CO_2 application start on day 0.

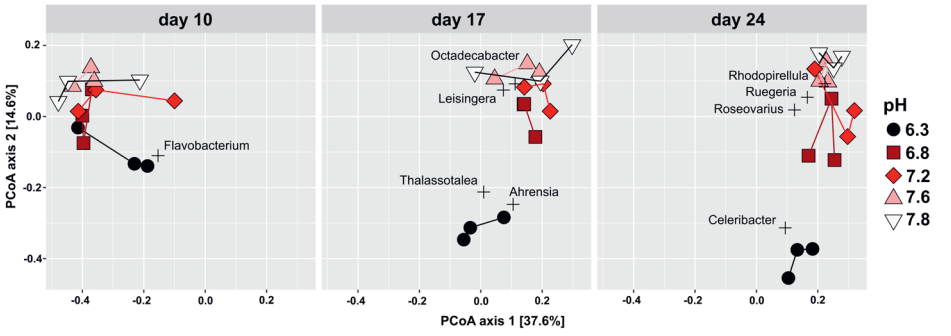

Figure 3.2 Biofilm genus composition on microscope slides incubated in artificial seawater of pH 6.3 – 7.8 on day 10, 17 and 24. Principal coordinates analysis (PCoA) plot is based on a Bray - Curtis dissimilarity index. The genera explaining most of the variability are labelled in each plot. CO_2 application start on day 0.

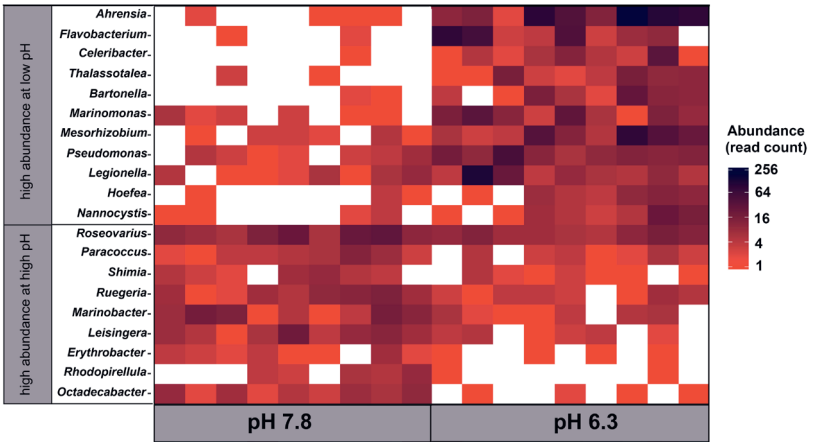

Figure 3.3 Heatmap of the twenty significantly differential abundant (read count) genera of biofilm on microscope slides incubated in artificial seawater of pH 6.3 and 7.8 on day 23. Each colored box represents the abundance of a single microcosm (triplicates of day 10, 17 and 24). The heatmap is based on Benjamini - Hochberg corrected p-values.

3.3.3 Mortality and feeding activity of barnacles

All barnacles in the controls survived until the end of the experiment, and mortality was less than 5% in all CO_2 treated groups except pH 6.3, where it was significantly higher (27%; Figure 3.4). Besides survival, the feeding activity was barely impacted by the elevated CO_2 in the pH ≥ 6.8 groups. At pH 6.3, the feeding movements of the barnacles were significantly slower with 0.5 - 1 s activity^{-1}, which is twice as long as for the other groups (Figure 3.5).

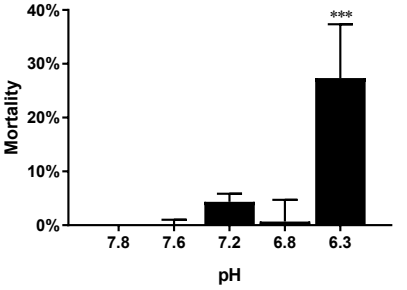

Figure 3.4 Mortality of barnacles (% of > 450 barnacles per plate, n = 3) after 23 days of exposure to pH 6.3 - 7.8 treatments. Differences were assessed between the treated group and the control group only (***, $p < 0.001$).

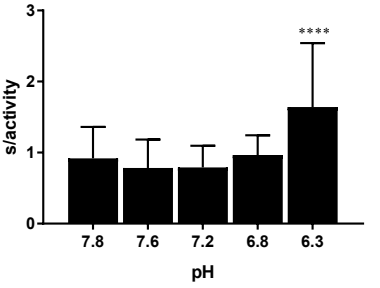

Figure 3.5 Time required for a barnacle per feeding movement (s activity^{-1}), 1min after injecting *Artemia* to the microcosm on day 20 (8 barnacles per plate, n = 3). Differences were assessed between the treated group and the control group only (****, $p < 0.0001$).

3.3.4 Growth of barnacles

The biomass of barnacles per plate linearly increased with time in all treatments with pH ≥ 6.8. On day 23 the biomass increase ranged from 120% (pH 6.8) to 200% (control) (Figure 3.6). With decreasing pH from 7.6 to 6.3, the growth rate (slope) reduced and it was significantly less in pH 6.3 relative to the control. Although the growth rate of the pH 6.8 groups was not statistically significant different from the controls for the duration of the whole experiment, significant differences developed from day 16 onwards. In the pH 6.3 groups this difference from the controls already started on day 9, and instead of increasing like the other groups, the biomass decreased with 20% since the start of the CO_2 exposure (Figure 3.6). Consistently, a trend of less biomass per barnacle with lower pH treatment was observed, although within the experimental period, significant differences with the controls were only reached in the pH 6.3 groups (S 3.5).

Similar to biomass changes, the area of the PVC plates that was covered with barnacles linearly increased with more than 50% over 23 days in the pH ≥ 6.8 groups (Figure 3.7). In these groups, the barnacle covered area increased more with decreasing pH level (slope = 2.66 ± 0.33 in control and slope = 4.23 ± 0.14 in pH 6.8). In pH 6.8, the increase of covered area was significantly higher than in the controls on day 16 and 23 (Figure 3.7). On those days, a significant decrease of the covered area was observed in the pH 6.3 groups (Figure 3.7; S 3.6).

The increase in barnacle biomass and covered area in the control group and decrease in number and size of barnacles in the pH 6.3 group were visible from the pictures from day 0 (Figure 3.8a) to day 25 (Figure 3.8b). The pictures of other experimental groups are given in Figure S 3.9.

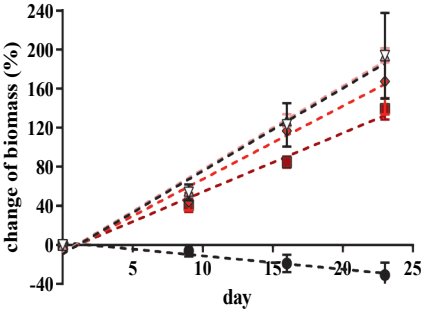

pH	Slope	95% CI of slope	R^2	Significance on ind. day	Significance of slope
6.3	-1.38	(-2.27, -0.48)	0.96	*** (9, 16, 23)	****
6.8	6.04	(3.66, 8.41)	0.98	*(16) ***(23)	ns
7.2	7.50	(4.24, 10.77)	0.98	ns	ns
7.6	8.55	(5.51, 11.58)	0.99	ns	ns
7.8	8.49	(5.14, 11.83)	0.98	ns	ns

Figure 3.6 Change in barnacle biomass (% compared to day 0) on day 0, 9, 16 and 23 under pH 6.3 - 7.8 treatments. Linear regression was showed as dash line. Differences were assessed between the treated group and the control group on the same day only (ns, no significance; *, $p < 0.05$; ***, $p < 0.001$; ****, $p < 0.0001$). CO_2 application start on day 0.

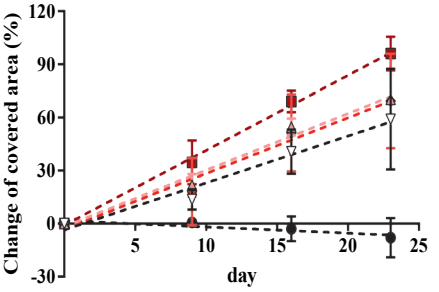

pH	Slope	95% CI of slope	R^2	Significance on ind. day	Significance of slope
6.3	-0.35	(-0.94, 0.23)	0.77	***(16) **** (23)	**
6.8	4.23	(3.61, 4.86)	0.99	*(16) **(23)	ns
7.2	3.15	(1.57, 4.73)	0.97	ns	ns
7.6	3.20	(1.80, 4.60)	0.98	ns	ns
7.8	2.66	(1.25, 4.07)	0.97	ns	ns

Figure 3.7 The change of barnacle covered area (% compared to day 0) on day 9, 16 and 23 under pH 6.3 - 7.8 treatments. Linear regression was showed as dash line. Differences were assessed between the treated group and the control group on the same day only (*, $p < 0.05$; **, $p < 0.01$; ***, $p < 0.001$; ****, $p < 0.0001$). The significance day was indicated in bracket.

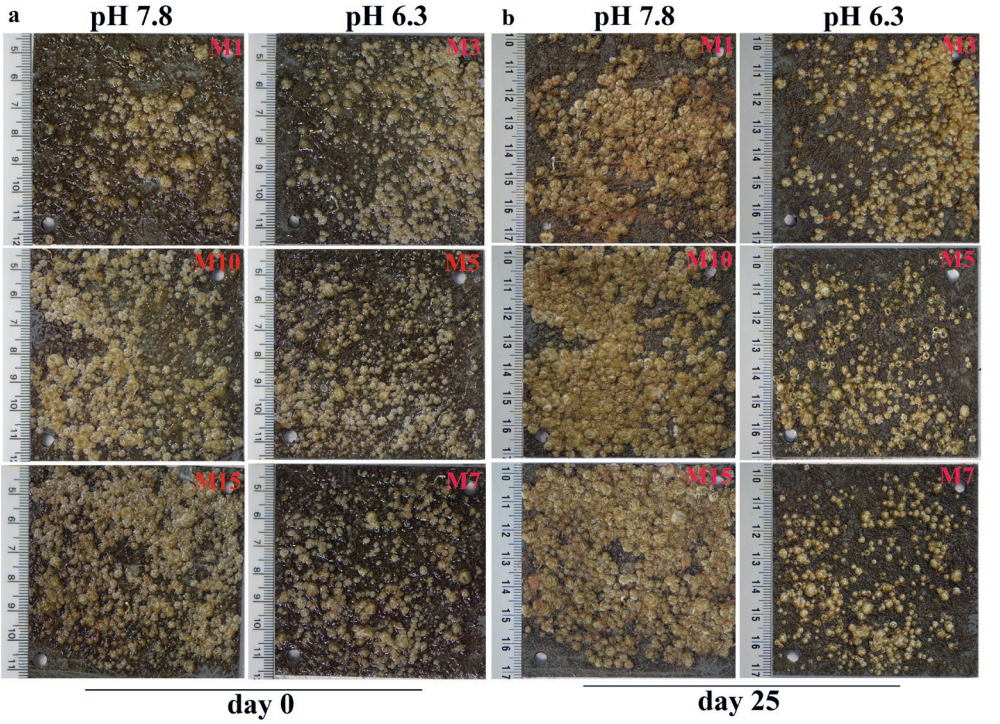

Figure 3.8 Pictures of plates with barnacles exposed to pH 7.8 (control) and pH 6.33 on day 0 (a) and day 25 (b).

3.5. Detachment of barnacle after sailing

The water force that was created by sailing for 15 min at 12 km/h was not sufficient to remove barnacles from the plates that had been exposed in the pH ≥ 6.8 groups (S 3.7). From the plates incubated at pH 6.3 however, more than 50% of the barnacles were removed during this sailing activity (S 3.7; S 3.8).

3.4 Discussion

This study investigated the impact of elevated CO_2 concentrations, resulting in a pH level range of 7.8 - 6.3, on biofilm formation and the growth and attachment strength of barnacles. Biofilms developed in all treatments, and the increase in biomass was significantly less with decreasing pH. The alpha diversity of the microbial community did not differ between pH levels, while the beta diversity at pH 6.3 distinctly differed from other exposure groups.

The barnacles were able to tolerate high acidic conditions as low as pH 6.8. However, at pH 6.3, the mortality was significantly higher and feeding activity and growth were significantly lower than in the other groups. In addition, 50% of the barnacles that had been kept at pH 6.3 for 25 days were not able to resist the water force created by sailing for 15 mins at 12 km/h.

3.4.1 Water parameters

The target pH levels were reached within one day in all the CO_2 treated groups. Therefore, limited time was provided for the barnacles to acclimate to the treatment. The dramatic decrease in pH level may have had a shock effect on the barnacles, especially for pH 6.8 and 6.3 treatments. Both of the CO_2 treatments' possible shock effect represent the actual condition that underwater exhaust gas may create to the sessile organisms, in this case the barnacles.

Although in the present study half of the water was refreshed with artificial seawater (about pH 8.1) every 2 - 3 days, the mean pH level in the control became lower than anticipated. The pH in controls was relatively low compared to the global open ocean mean pH of 8.07 (in 2010). The pCO_2 levels in this study calculated based on pH, total alkalinity, salinity and temperature, was 784 µatm in the control. The pCO_2 in seawater of global oceans varies seasonally about 60% below and above the current atmospheric pCO_2 level of about 415 µatm. The low pH level in the control is most likely caused by the respiration of the barnacles and the *Artemia* nauplii that were applied as food, and the absence of primary production or aeration. This is also reflected in the maximum 95% O_2 saturation levels in the microcosms (S 3.3). Although survival of barnacles in the controls was 100%, it cannot be excluded that the pH 7.8 in the control already affected the organisms thus reducing the difference with the exposure groups. However, as significant effects were only observed in the higher treatment levels, this seems unlikely.

3.4.2 Growth and taxonomic composition of biofilm

Elevated CO_2 concentrations inhibited the development of the biofilm. In addition to the total biofilm biomass, the bacterial genus composition was distinctly different between the lowest pH and the other treatments. For example, *Ahrensia, Celeribacter, Thalassotalea* and *Flavobacterium* dominated at low pH (6.3), while *Leisingera, Octadecabacter, Ruegeria* and *Roseovarius* were more common at higher pH levels. The genus composition likely reflects the tolerances of species to grow at low pH levels. For instance, *Leisingera methylohalidivorans* is known to have an optimum growth at pH 7.7, and rapidly decreases below pH 7.3 (Schaefer et al., 2002). On the other hand, *Ahrensia kielensis* has a wide tolerance to low pH level (pH 7.0) (J Liu et al., 2016). As the biofilm forms the initial phase of the succession process of fouling (Bressy & Lejars, 2014; Wahl, 1989), this impact on the biofilm development could affect the further development of biofouling.

The composition of the biofilm influences the settlement of larvae from marine organisms including barnacles, which can be an inhibiting effect (e.g. (Lau & Qian, 2000; Maki et al., 1988; Mary et al., 1993)) or a stimulating effect (e.g. (Qian et al., 2003; Thiyagarajan et al., 2006; Wieczorek et al., 1995)), e.g. through the production and release of signal molecules (Hadfield, 2011). The type of influence is highly connected to the taxa present in the biofilm: Holmström et al. (1992) found that certain bacterial isolates (designated D2 CCUG 26757) displayed non-pH-dependent inhibitory effects on settlement of larvae of the barnacle *Amphibalanus amphitrite*, whereas other taxa has been reported to promote cypris larval settlement of the barnacle *Amphibalanus improvisus* (Tait & Havenhand, 2013) through the production of N-acylhomoserine lactones (AHLs). In addition, some research suggests that the age and size of the biofilm may also play a role, although the results are not congruent.

Wieczorek et al. (1995) reported that barnacle larvae prefer older biofilm (in their case 18 days), while Olivier et al. (2000) suggested that other things than age, e.g. species composition, are more important in determining suitability of a particular settlement site for barnacle juveniles. A positive correlation between biofilm biomass and larval settlement has also been found for other invertebrate fouling species such as *Mytilus edulis* (Toupoint et al., 2012) and *Crassostrea virginica* (Campbell et al., 2011).

3.4.3 Mortality and growth of barnacles

The barnacles (*Balanus crenatus*) showed high tolerance to acidic conditions but mortality increased to nearly 30% when the pH level became as low as 6.3. This is in line with the findings by Findlay et al. (2010b), who reported that the survival rate of another barnacle species (*Semibalanus balanoides*) did not differ between juveniles grown at pH 7.3 and at the control level (pH 8.1). However, another study from Findlay et al. (2009) showed increased mortality of *S. balanoides* when exposed to pH 7.7 - 7.8. The different mortality results between studies may be attributed to the varied abilities of the barnacles to maintain their energetic balance. The energetic cost of calcification is suggested to increase with higher pCO_2 conditions (Clements &Darrow, 2018). Besides the increase in energy demand, multiple studies with bivalves have shown significantly reduced feeding rates at pH conditions < 7 (R Bamber, 1990; R N Bamber, 1987). The present study shows this is also the case for barnacles. Low feeding speed may lead to the inability to support energy demands, in turn negatively impacting core functions, such as survival, growth and immune response (Bouchard et al., 2014; Hernroth et al., 2012).

The reduced feeding speed must directly have inhibited the growth of the barnacles in the present study, as is reflected in the poor development of the biomass and covered area in pH 6.3 groups. However, the feeding speed seems not the only limiting factor for barnacle development, since a reduced growth rate was already found in higher pH conditions than pH 6.3, for which feeding speed was unaffected. This suggests that for the barnacles the energetic cost increase with increasing CO_2 concentrations. The extremely slow feeding speed also suggested that the barnacles in pH 6.8 treatment experienced energy exhaustion. Another, perhaps additional explanation is the suffocation effect on the organisms, as elevation of CO_2 in water reduces the outward diffusion of CO_2 from water-breathing animals (Ishimatsu et al., 2005). Another crustacean, the lobster *Homarus americanus*, showed increased susceptibility to diseases in high CO_2 conditions (pH 7.7), which significantly negatively affected its probability of survival (McLean et al., 2018).

Nardone et al. (2018) found a 20% increase of base plate area of the barnacle *Amphibalanus amphitrite* in their CO_2 treated groups (pH 7.78 and pH 7.40 compared to pH 8.01 in the controls). In addition, they claimed that neither the height or the thickness of the shell was affected by exposure to pH 7.5 for 13 weeks. Instead, the size of the calcite crystal of the barnacle shells was dramatically increased to nearly twice as large as in pH 8.01 (Nardone et al., 2018). Larger basal shell diameter also was observed in McDonald et al. (2009)'s study. They suggested the calcium carbonate production raised in lower pH levels cause the increase in basal shell diameters, which was proved by the higher basal shell ash level in low pH (pH 7.4) cultivation. Both two studies focused on *A. amphitrite* at 25 ˚C. None such alterations of the shape of the barnacles were observed in our study. The different species of barnacles (*B. crenatus,* in the present study) and culture conditions (13 ˚C, in the present study) may have

led to these different results. Especially raising the temperature 4 - 5 ˚C is suggested to reduce the net calcification rate of barnacles in elevated CO_2 concentration (Findlay et al., 2010a).

3.4.4 Attachment of barnacles

The adhesive system of the barnacles does not seem to be very sensitive to the pH of the seawater. Nardone et al. (2018), already concluded that the adhesive system of barnacles is not affected by seawater pH as low as 7.4, and in our study none of the barnacles that had been exposed to a pH as low as 6.8 were removed from the plates after sailing 12 km/h for 15 min. Only the barnacles from the pH 6.3 groups were not able to resist the water pressure related to this sailing speed.

3.4.5 Potential as anti-fouling strategy

The presented results suggest that if exhaust gas would be released underwater and is subsequently able to lower the water pH near the ship's hull to at least 6.3, attached barnacles could be removed from the ship's hull during sailing, thus cleaning the ship's hull. In practice it will most likely not be possible to maintain the pH around the ship's hull as low as 6.3 for 25 days, which hampers the direct application of the present findings for anti-fouling purposes. However, it opens some perspectives. Barnacles may be less vulnerable to acidification than other fouling organisms like molluscs, as the exoskeletal $CaCO_3$ of barnacles mostly consists of calcite, which is less soluble than the aragonite that is present in molluscs (Boßelmann et al., 2007; Whiteley, 2011). Additionally, the tested speed (12 km h^{-1}) in the present study is relatively low for commercial ships. With higher sailing speed, more water resistance will create a higher 'swapping' force to remove the attached barnacles and other fouling organisms. Finally, exhaust gas will have a higher temperature that may also strengthen the anti-fouling effect in practise.

Even when these factors are not sufficient to remove attached fouling organisms from the ship's hull, underwater released exhaust gas might be able to reduce the development of a biofilm. The presented results show that the development of the fouling microbial community is affected already at relatively low CO_2 concentrations. If this results in an unattractive biofilm composition for the larvae of larger fouling organisms deserves further study. In addition, underwater released gas may also directly prevent larvae to settle in the area, either because the pH is too far from the organisms optimum or the high CO_2 level affects the respiration.

3.5 Conclusion

The aim of this study was to assess the impact of CO_2 from underwater released exhaust gas on fouling organisms and perform a first evaluation of its anti-fouling property. The results clearly indicate that elevated CO_2 concentrations inhibit the development of a microbial biofilm, which could have implications for the settlement of fouling invertebrates like barnacles and mussels. Once settled, barnacles can tolerate relatively high CO_2 concentrations, but at the highest exposure condition (equivalent to pH = 6.3) feeding activity and growth were negatively affected and mortality increased. Our results indicate that the impact of underwater released CO_2 depends on various factors including the reduced pH level by the exhaust gas and the duration of such acidic conditions. The relative importance of

these factors is a subject for future research based on the composition of the gas, the shipping intensity and the local environmental conditions. The water force of 12 km h^{-1} sufficiently removed over 50% of the attached barnacles that had been exposed to the highest CO_2 concentrations (pH 6.3). Based on physiological features, it is to be expected that smaller animals, new larvae and fouling molluscs will be more sensitive. These findings suggest that CO_2 released along a ship's hull can negatively impact on fouling organisms and thus has potential as new anti-fouling strategy. It is interesting to further study the role of CO_2 in the anti-fouling mechanism in addition to acidification.

Acknowledgments

The authors wish to thank Dr. Job Klijnstra from Endures B.V. for helping with exposing the barnacle plates in the Den Helder Harbour and the Dutch Royal Navy for arranging and sailing the ship used in the test. Also, the authors want to express their appreciation for the technical support at research facility 'CARUS' of Wageningen University. This research was funded from the project 'GasDrive: Minimizing emissions and energy losses at sea with LNG combined prime movers, underwater exhausts and nano hull materials' (project 14504) of the Netherlands Organization for Scientific Research, domain Applied and Engineering Sciences (TTW).

3.6 Supplementary material for Chapter 3

S 3.1 Thermocycling conditions used for PCR amplification.

Cycle step	Temp.	Time	Cycles
Initial denaturation	98 ˚C	3 min	1
Denaturation	98 ˚C	8 sec	
Annealing	58 ˚C	8 sec	30
Extension	72 ˚C	30 sec	
Final extension	72 ˚C	3 min	1
Hold	12 ˚C		

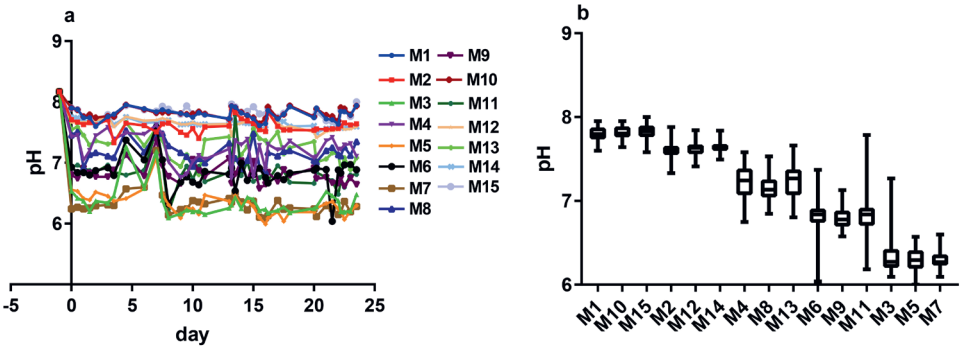

S 3.2 The pH levels of microcosms from day -1 to 25 (CO_2-application started on day 0) (a); Box & whiskers of measured pH in the microcosms (b). The microcosms were randomly chosen for reaching designed pH levels by expressing additional CO_2 (triplicate study).

S 3.3 Water parameter of the microcosms. Mean ± standard deviation (of the triplicate plates) are given for pH, pCO_2, temperature (˚C), salinity (‰) oxygen saturation level (%), NO_2^- concentration (mg/l) and NH_4^+ concentration (mg/l) in each microcosm.

	pH	pCO_2 (µatm)	Temp. (˚c)	Salinity (‰)	Alkalinity (meq/l)	Oxygen saturation level (%)	NO_2^- (mg/l)	NH_4^+ (mg/l)
M1	7.80 ± 0.09	807 ± 55	13.73 ± 0.31	33.29 ± 0.24	2.42 ± 0.16	94.80 ± 4.17	0.58 ± 0.18	0.01 ± 0.02
M10	7.82 ± 0.08	759 ± 57	13.69 ± 0.36	33.43 ± 0.36	2.40 ± 0.18	95.96 ± 2.75	0.34 ± 0.17	0.01 ± 0.02
M15	7.83 ± 0.09	787 ± 55	13.62 ± 0.27	33.35 ± 0.27	2.42 ± 0.17	94.49 ± 3.96	0.45 ± 0.16	0.01 ± 0.02
M2	7.61 ± 0.11	1220 ± 103	13.70 ± 0.29	33.31 ± 0.29	2.34 ± 0.20	91.98 ± 4.31	0.74 ± 0.38	0.06 ± 0.18
M12	7.62 ± 0.09	1074 ± 75	13.64 ± 0.23	33.45 ± 0.23	2.39 ± 0.17	92.73 ± 3.55	0.45 ± 0.22	0.06 ± 0.18
M14	7.65 ± 0.07	1019 ± 80	13.57 ± 0.25	33.28 ± 0.25	2.44 ± 0.19	92.28 ± 3.76	0.40 ± 0.19	0.06 ± 0.18
M4	7.22 ± 0.23	2292 ± 104	13.66 ± 0.25	33.33 ± 0.25	2.46 ± 0.11	90.95 ± 4.76	0.41 ± 0.18	0.06 ± 0.18
M8	7.17 ± 0.17	3216 ± 230	13.73 ± 0.17	33.41 ± 0.17	2.48 ± 0.18	92.06 ± 4.05	0.34 ± 0.18	0.06 ± 0.18
M13	7.24 ± 0.20	1958 ± 102	13.65 ± 0.31	33.30 ± 0.31	2.43 ± 0.13	92.31 ± 3.89	0.40 ± 0.16	0.06 ± 0.18
M6	6.83 ± 0.23	6900 ± 350	13.65 ± 0.28	33.42 ± 0.28	2.51 ± 0.13	93.25 ± 3.09	0.24 ± 0.11	0.06 ± 0.18
M9	6.82 ± 0.16	8097 ± 283	13.70 ± 0.19	33.35 ± 0.19	2.50 ± 0.09	92.75 ± 3.60	0.17 ± 0.06	0.06 ± 0.18
M11	6.84 ± 0.26	7338 ± 300	13.69 ± 0.24	33.42 ± 0.24	2.49 ± 0.10	93.98 ± 2.79	0.24 ± 0.12	0.06 ± 0.18
M3	6.35 ± 0.19	18976 ± 906	13.68 ± 0.27	33.28 ± 0.27	2.60 ± 0.12	91.34 ± 4.02	0.09 ± 0.03	0.06 ± 0.18
M5	6.32 ± 0.20	20927 ± 1181	13.70 ± 0.23	33.39 ± 0.23	2.61 ± 0.15	91.36 ± 4.03	0.08 ± 0.04	0.13 ± 0.23
M7	6.31 ± 0.19	29663 ± 1256	13.73 ± 0.25	33.31 ± 0.25	2.62 ± 0.12	91.06 ± 4.01	0.09 ± 0.05	0.13 ± 0.23

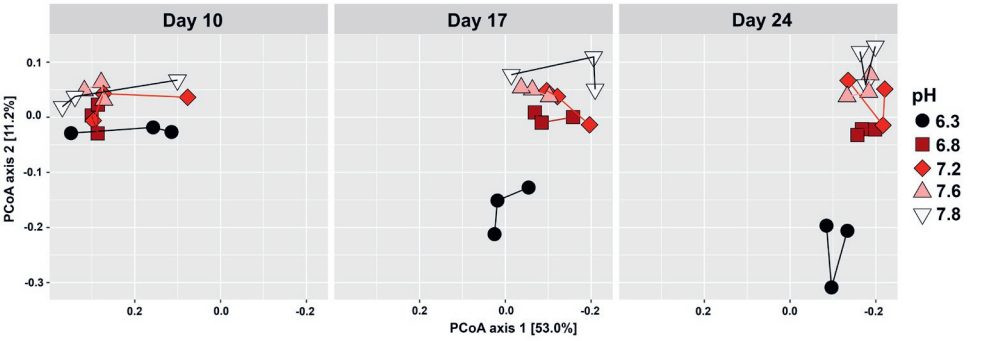

S 3.4 Biofilm genus composition on microscope slides incubated in artificial seawater of pH 6.3 – 7.8 on day 10, 17 and 24. Principal coordinates analysis (PCoA) plot based on a weighted Unifrac dissimilarity index. CO_2 application started on day 0.

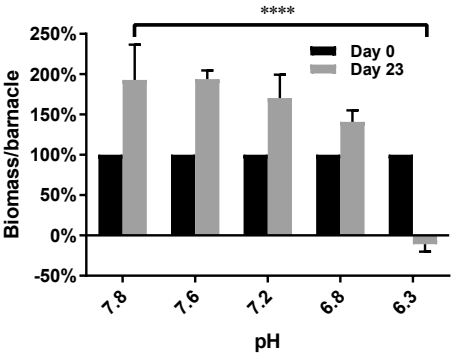

S 3.5 Biomass per barnacle (%) on day 0 and 23 under pH 6.3 – 7.8 treatments. The biomass on day 0 was set as 100%. Statistical difference (*, $p < 0.05$; ***, $p < 0.001$) were compared treated group with the control on day 23 only.

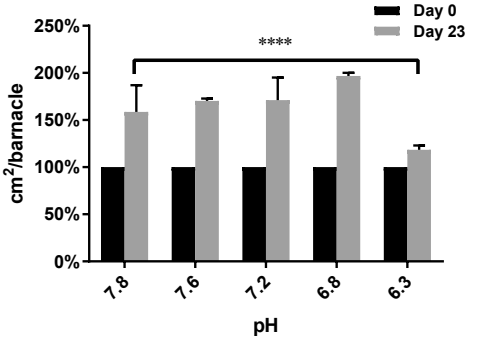

S 3.6 Cover area per barnacle (%) on day 0 and 23 under pH 6.3 – 7.8 treatments. The biomass on day 0 was set as 100%. Statistical difference (*, $p < 0.05$; ***, $p < 0.001$) were compared treated group with the control on day 23 only.

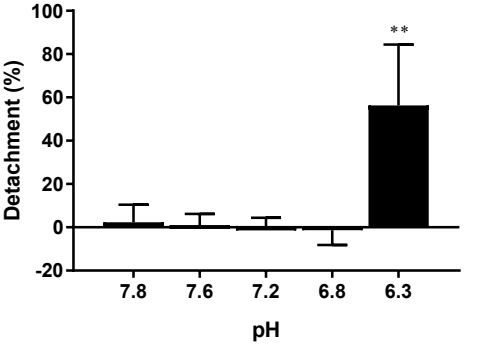

S 3.7 The average of detached barnacles on each plate (%) after 12 km/h sailing for 15min. These plates (n = 3) were cultured in pH 6.3 – 7.8 treatment for 23 days before sailing. Statistical difference (**, $p < 0.01$) were compared with the control group only.

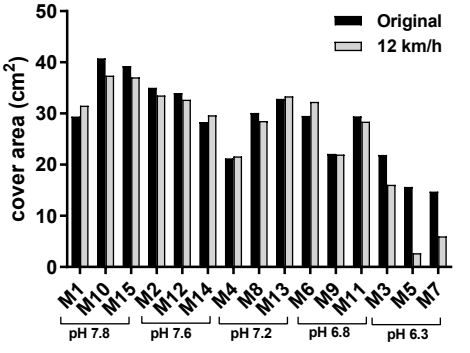

S 3.8 Cover area (cm^2) of barnacles on each plate before and after 12 km/h sailing for 15mins. These plates were cultured in pH 6.3 – 7.8 treatment for 23 days before sailing.

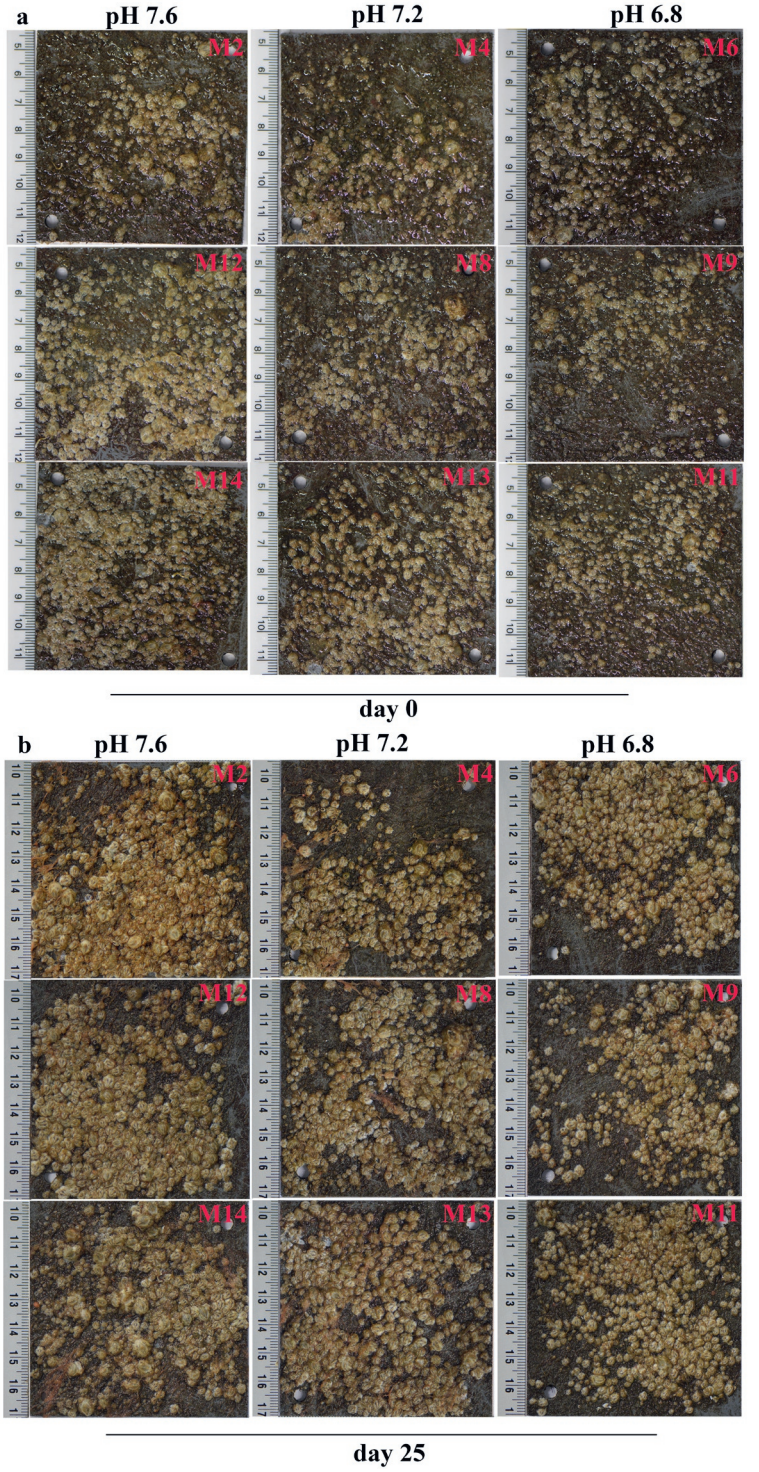

S 3.9 Pictures of plates with barnacles exposed to pH 6.8 – 7.6 treatment on day 0 (a) and day 25 (b)

CHAPTER 4

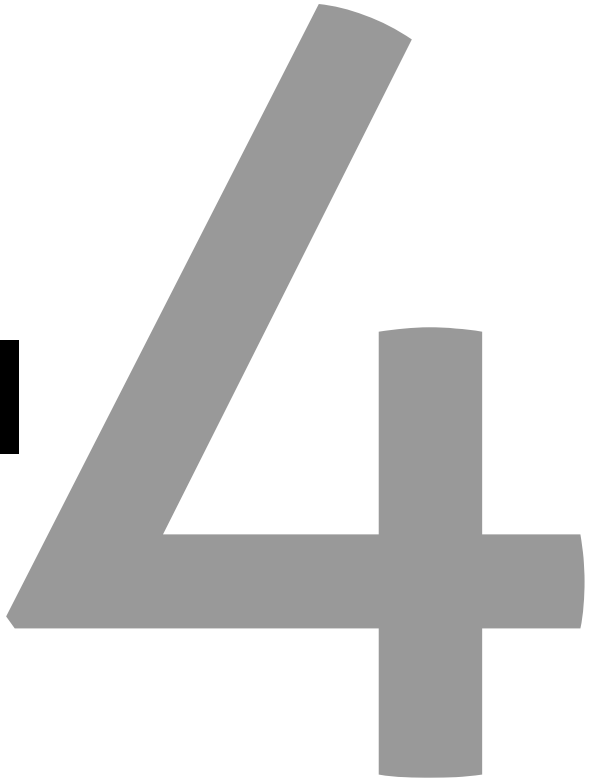

Impact of underwater released exhaust gas on a simple algae-rotifer plankton community

Yuzhu Wei[1], Pranchalee Duanyai[1], Marinus C. Keur[2], Bodil E. Boelens[1], Albertinka J. Murk[1], Edwin M. Foekema[1,2]

[1.] Marine Animal Ecology group, Wageningen University and Research, P.O. box 338, 6700 AH Wageningen, The Netherlands
[2.] Wageningen Marine Research, Wageningen University and Research, P.O. Box 57, 1780 AB Den Helder, The Netherlands

Submitted

Abstract

Submerged discharge of exhaust gas from ships is considered for its potential to reduce drag force. However, multiple compounds in the exhaust gas can negatively impact marine organisms, while on the other hand the CO_2 is an essential nutrient for photosynthetic organisms like microalgae. The combination of stimulated algal growth and negative effects on algal consumers could facilitate the development of algal blooms. To study this, experiments were performed in which the microalgae *Isochrysis galbana* alone or in combination with rotifers (*Brachionus plicatilis*) that feed on them, were exposed to seawater pre-treated with diesel engine exhaust gas and seawater pre-treated with pure CO_2. Since CO_2 concentrations in exhaust gas can vary, a wider range of CO_2 concentrations (resulting in pH 5 to 8) were tested in separate experiments with the same species combination, but also with *Dunaliella salina* as algal species that is more resistant to low pH levels. We found no indications that the mixture of compounds from underwater released exhaust gas stimulates the development of an algal bloom through a combination of negative impact of toxic compounds on zooplankton, and a stimulation of algal development by CO_2. All observed effects were caused by CO_2 only. The impact of other compounds like NO_x and PAHs was not evident. Repeated injection of CO_2, which might occur at busy shipping lanes when underwater gas release systems are becoming more popular could however locally extend the algal bloom period and induce a shift in plankton community composition.

4.1 Introduction

Maritime emissions contribute to approximately 2.2% CO_2, 15% NO_x and 5 - 8% SO_x of global anthropogenic emissions (Corbett et al., 2007; UNCTAD, 2018) which threatens both environmental and human health (Brandt et al., 2013). As one of the least regulated emission sources and with increasing ocean transportation, the weight of shipping emissions in total anthropogenic emissions is expected to rise further (EEA, 2013; UNCTAD, 2018). In an effort to reduce emissions, the International Maritime Organization (IMO) issued several regulations in the past two decades. For example, the global limit of sulphur in fuel oil used by board ships has to be reduced to 0.5% in 2020, while it was 4.5 % before 2012 (IMO, 1997b). More and more strict controls also applied to NO_x emissions, which were separated into Tier I, II and III regulations and came into effect in 2000, 2011 and 2016 respectively (IMO, 1997a). These regulations stimulated manufacturers to invest in techniques that improve energy efficiency and reduce emissions.

Applying underwater released exhaust systems as ‘air lubrication’ along the ship’s hull is proposed by maritime industries to reduce the water resistance and the related energy demand hence the total marine emission (H Sapra et al., 2017; Wei et al., 2019). Although this novel approach seems promising to reduce global emissions, an impact on the local marine ecosystem is to be expected but unknown. The composition of exhaust gas includes, but is not limited to, polycyclic aromatic hydrocarbons (PAHs), NO_x, SO_x, and CO_2 (M Anderson et al., 2015; Sippula et al., 2014). Carcinogenic PAHs are known to accumulate in sediment and biota, posing risks for long-term effects on ecosystems (Hylland, 2006). Both dissolved NO_x and SO_x can decrease the water’s total alkalinity (Doney et al., 2007; Hunter et al., 2011), and as such reduce the capability of water to resist changes in pH and become more vulnerable in the ocean acidification (Doney et al., 2007). CO_2 is one of the most water-soluble gases in the exhaust gas of combustion engines. Releasing CO_2 directly into the ocean

will decrease the pH and CO_3^{2-} level in seawater (Doney et al., 2007). Reduced pH and CO_3^{2-} concentrations will have a negative impact on the calcification rate of calcifying organisms, that need $CaCO_3$ to construct shells and skeletons (Ries et al., 2009). Long-term exposure, or acute exposure to a high dose of CO_2 will damage shells, reduce animal survival and can cause community shifts (Ries et al., 2009; Wei et al., 2019). In contrast to the adverse impact, CO_2 also is an essential nutrient for photosynthetic organisms including microalgae. A growth stimulating effect on microalgae combined with a negative effect on algae consumers could potentially result in algal blooms (Wei et al., 2019). To study this potential in a plankton community, experiments were conducted with microalgae and rotifers feeding on them. Microalgae and rotifers are popular model organisms for microscale aquatic toxicity tests due to their high sensitivity and cost-efficiency (Bautista-Chamizo et al., 2019; Seoane et al., 2017; P G Wells et al., 1997). Both groups are ecologically important as food source for other aquatic organisms, such as copepods and fish larvae, effects could thus influence the entire food web (Nagata et al., 2006; P G Wells et al., 1997).

The presented study aimed to study the effect on the simple plankton community of the complex mixture of compounds that dissolve in seawater when it is bubbled with diesel engine generated exhaust gas, and to compared this with the effect of seawater that is treated with pure CO_2 to reach the same initial pH level (6.8) as the exhaust gas enriched water.

The algae *Isochrysis galbana* alone and combined with the rotifer *Brachionus plicatilis* were exposed to the treatments for 7 days. Subsequently, a wide range of initial CO_2 concentrations (resulting in pH-8.0 – pH-5) was applied in a separate experiment to represent the varied CO_2 concentrations in the exhaust gas under different powered fuel types and operating conditions. For this study the more CO_2 resistant algae *Dunaliella salina* were used to better study potential algal blooms at pH < 6.

4.2 Materials and methods

4.2.1 Pre-cultivation of studied organisms

Marine algae, *Isochrysis galbana* (NIVA-4/91) and *Dunaliella salina* were purchased from NORCCA (The Norwegian Culture Collection of Algae, Norway). The algae were further cultivated in 250 ml Erlenmeyer flasks with 150 ml F2 medium (Guillard's Marine Water Enrichment solution, Sigma Aldrich) in artificial seawater (Tropic Marin®, Zoo mix). The initial pH, salinity and alkalinity of the culture were approximately 8.1, 31.5‰ and 2.2 meq/l, respectively (measured by pH meter Hach PHC101, electrode Hach CDC401 and Salifert alkalinity test kit, respectively). The algae were cultured in a 20 °C climate room with approximately 2916 lux light density (16/8 h, light/dark cycle) without shaking. Approximately 10 ml of algae culture was transferred to a new medium weekly to maintain an exponential growth phase. The same culture conditions, seawater and equipment were used in all experiments in this study unless stated otherwise.

Mixed-age rotifers*, Brachionus plicatilis,* were kindly provided by CARUS (Wageningen University, the Netherlands). The rotifers were allowed to adjust to feeding on the algae species for 7 days, before used in the experiments. Algae densities were *D. salina*, ~1.0 x 10^4 cells/ml or *I. galbana*, ~ 1.0 x 10^6 cells/ml before the experiments started. The culture

conditions for the rotifers were the same as for the algae, except that F2 medium was excluded from the culture.

4.2.2 Enrichment and analysis of 'Gas-enriched-seawater' and 'CO2-enriched-seawater'

The exhaust gas was generated with a diesel engine (MAN, 4-stroke-4L20/27 engine) in the laboratory of the Dutch Royal Navy (Den Helder, the Netherlands). Exhaust gas was collected from the main flow and injected with 6 l/min into 30 l artificial seawater stored in a stainless steel container. The composition of the exhaust gas was measured semi-continuously and was on average 5.6 vol % CO_2, 14.6 vol % O_2, 0.14 mg/l CO, 2.77 mg/l NO_x and 0.14 mg/l SO_2. In the meantime, the pH, temperature and O_2 level of the seawater were measured with a submerging electrode Hach LDO 101 (Online Resource 1). When the monitored parameters stabilized after about 1.5 h, it was assumed that the saturation level of dissolving exhaust gas in the seawater was reached and the injection was terminated. The stainless steel container with the 'gas-enriched-seawater' was then closed airtight and transported to the laboratory of Wageningen Marine Research (Den Helder, the Netherlands) for further analysis and experimenting.

In the laboratory, about 2.5 l of gas-enriched-seawater was forced through a C18 column (Sep-Pak® Vac 6cc, Waters, USA) to extract dissolved compounds. The extracted compounds were then collected in 5 ml methanol by washing the column. This 5 ml methanol sample was stored in a dark glass vial at 4 ˚C for later analyze of PAH concentrations. This whole extraction procedure was performed three times to obtain independent triplicate samples. Similar extractions were performed with 'control-seawater' not treated with exhaust gas. The nitrite (NO_2), nitrate (NO_3), ammonium (NH_4^+) and phosphate (PO_4^{3-}) concentration of the gas-enriched seawater and the control-seawater were measured with test kits (Hach Model NI-11, NI-12, NI-SA and PO-23).

4.2.3 Experimental set-up

Thirty-six identical 250 ml Erlenmeyer flasks were prepared to create three conditions: control-seawater, gas-enriched-seawater and CO2-enriched-seawater. All flask were filled with 139 ml control-seawater or gas-enriched-seawater with F2 medium. Subsequently, the 1.5 l of the *I. galbana* culture was concentrated by centrifugation (Allegra® X – 12 Centrifuge, Beckman Coulter, USA) at 1500 rpm for 3 min into a 20 ml concentrated algal sample. A 1 ml of the concentrated algae sample was transferred to each flask resulting in a final density of ± 1.2 x 10^6 cells/ml (*Bürker* hemocytometer, Thermo Fisher Scientific, US) in each flask.

In half of the flasks, the 'algae + rotifer group' approximately 150 individuals of the rotifer *B. plicatilis* were introduced with 10 ml of control-seawater, after quantification under a light microscope (ZEISS, Germany) using Sedgewick Rafter Counting Chambers (Pyser - SGI Limited, the UK). The other flasks formed the 'algae alone' group, and received 10 ml of control-seawater without rotifers. Therefore, the final volume of the culture in each flask was about 150 ml.

At the start of the experiment (day 0) the pH of the gas-enriched-seawater in each flask was 6.8. The same pH was created in all CO_2-enriched-seawater flasks by injecting pure CO_2

(Linde gas, the Netherlands) directly into the Erlenmeyer flasks. The initial pH, oxygen saturation level and salinity of each flask were measured after introducing the organisms and applying treatment. Then, half of the flasks (open) were covered with cotton to allow air exchange, while the rest (closed) were covered with parafilm and aluminum foil to minimize air exchange. All flasks were placed randomly on a table in the climate room with the conditions as described in 2.1. The flask locations were randomly shifted every day to avoid structural variation in light intensity between the flasks.

Table 4.1 Experimental set-up for comparing the impact of exhaust gas-enriched with pure CO_2-enriched seawater on *Isochrysis galbana* (algae) and *Brachionus plicatilis* (rotifer). Control: only artificial seawater with F2 medium. Open: air exchange was possible; the flask was only covered with cotton wool; Closed: the flask was closed with parafilm and aluminum film to minimize air exchange.

Flask Nr.	Condition	Organisms	Initial pH	Open/closed
1 - 3	Control	Algae alone	8.1	Open
4 - 6	Control	Algae alone	8.2	Closed
7 - 9	Exhaust gas	Algae alone	6.8	Open
10 - 12	Exhaust gas	Algae alone	6.8	Closed
13 - 15	CO_2	Algae alone	6.8	Open
16 - 18	CO_2	Algae alone	6.8	Closed
19 - 21	Control	Algae + Rotifer	8.1	Open
22 - 24	Control	Algae + Rotifer	8.1	Closed
25 - 27	Exhaust gas	Algae + Rotifer	6.8	Open
38 - 30	Exhaust gas	Algae + Rotifer	6.8	Closed
31 - 33	CO_2	Algae + Rotifer	6.8	Open
34 - 36	CO_2	Algae + Rotifer	6.8	Closed

4.2.4 Sampling and analysis

The experiment lasted for 7 days in total. The salinity of all experimental groups remained in a range of 29.5 - 31.5‰ during the study period. The water pH and oxygen saturation levels were measured on day 0 - 5 and day 7. On the same days, a 10 ml sample was taken from each flask after gently mixing the culture. The living and dead rotifers were visually counted under a microscope. Individuals were classified as dead if no movement was observed within 5 seconds. The counted samples were filtered through a 10 µm-plankton sieve to remove the rotifers from the sample before performing algae analysis. For algae biomass analysis of all groups, the chlorophyll-a concentration was measured with a 1Hz-cuvette Fluorimeter (BBE-Moldaenke AlgaeLabAnalyser BG43000). After that, the samples were preserved in a 5% lugol solution for later visual counting under a microscope.

4.2.5 Testing a wide range of CO_2 concentrations

To test the dose-related impact of CO_2 in the exhaust gas on the plankton community, *I.galbana* alone or *I. galbana* with *B.plicatilis* were exposed to a wide range of initial pH levels: 5.0 - 8.0 (control) (Table 4.2) induced by pure CO_2 injection as described above (Section 4.3) and only closed flasks were used in this experiment (Table 4.2). Furthermore,

the water parameters (pH and O_2) were measured and samples were taken daily in the same way as described in 2.3. The salinity and alkalinity of each flask were measured on the first and last day of the test, and remained 32‰ and 2.2 meq/l respectively. For algae biomass analysis, only the chlorophyll-a concentration was measured in this test.

To test the impact of a more extreme CO_2 concentration on the plankton community, the more CO_2 resistant algae *D. salina* was used to replace *I.galbana*. *D. salina* alone and in combination with *B.plicatilis* were exposed to an initial pH-8 (control) or CO_2 induced initial pH-6 (Table 4.3). Only duplicate closed flasks were used in this 5 days study. The experimental set-up was the same as described in 2.3 with the exception of a lower starting density (on day 0) of *D. salina* (~2 x10^5 cell/ml, measured with a coulter counter, Beckman Coulter ® Inc., USA) because of its higher growth rate. The pH level of each flask was measured daily. A 2 ml sample was taken every day for measuring the algae chlorophyll-a concentration using the fluorimeter (in *I. galbana* experiment) or algae cell counting via the coulter counter (in *D. salina* experiment). A 7 ml sample was taken on day 2,4 and 5 for rotifer counting under a microscope. The oxygen saturation level was not measured, and the salinity and alkalinity were measured on days 0 and 5. The salinity and alkalinity of each flask were 31.5‰ and 2.4 meq/l respectively, both on the first as well as the last day of the experiment.

Table 4.2 Experimental set-up of the impact of CO_2-enriched artificial seawater with F2 medium, with exposure resulting in pH 5.0 - 8.0). Organisms exposed were *Isochrysis galbana* (algae) and *Brachionus plicatilis* (rotifer). Control: only artificial seawater with F2 medium. All flasks were closed with parafilm and aluminum film to minimum air exchange.

Flask Nr.	Initial pH	Organisms
1 - 3	8.0 (Control)	Algae alone
4 - 6	7.0	Algae alone
7 - 9	6.0	Algae alone
10 - 12	5.0	Algae alone
13 - 15	8.0 (Control)	Algae + Rotifer
16 - 18	7.0	Algae + Rotifer
19 - 21	6.0	Algae + Rotifer
22 - 24	5.0	Algae + Rotifer

Table 4.3 Experimental set-up of an extreme CO_2-enriched (pH 6.0) impact study with *Dunaliella salina* (algae) and *Brachionus plicatilis* (rotifer). Control: only artificial seawater with F2 medium. All flasks were closed with parafilm and aluminum film to minimum air exchange.

Flask Nr.	Initial pH	Organisms
1 - 2	8.0 (Control)	Algae alone
3 - 4	6.0	Algae alone
5 - 6	8.0 (Control)	Algae + Rotifer
7 - 8	6.0	Algae + Rotifer

4.2.6 Data analysis

GraphPad Prism 8 (Graphpad Software Inc., CA, USA) was used to draw graphs and perform statistical analysis. Two-way ANOVA (time and treatment) with a Tukey multiple comparison post-hoc test was used for testing the significant difference between 1) the CO_2, exhaust gas treated groups and the control and 2) the elevated CO_2 concentrations treated groups and the control. Multiple t-test was used for testing the significant difference between algae alone and algae with rotifer at the same sampling time and with the same treatment. The results were considered significant when $p < 0.05$. All data presented here are expressed as means with standard deviation unless stated otherwise.

4.3. Results

4.3.1 Exhaust gas vs. pure CO_2

Impact of exhaust gas on water chemistry

During the injection of exhaust gas into 30 l seawater, the water temperature remained at 20˚C, while the oxygen saturation level and pH dropped from approximately 95% and 8.5 to 62% and 6.5 respectively and stabilized at these levels (S 4.1). On the experiment starting day (day 0), the dissolved oxygen was about 100% of saturation and pH had increased to 6.8 (Table 4.1 and S 4.2). The fluorene and phenanthrene levels in control-seawater were 1.12 ± 0.16 ng/l and 2.37 ± 0.24 ng/l respectively, the rest of PAHs were < 0.87 ng/l (Table 4.4). Concentrations of most measured PAHs in the gas-enriched-seawater were below the limit of quantification, except phenanthrene (4.25 ± 0.47 ng/l), fluoranthene (1.66 ± 0.59 ng/l), pyrene (2.25 ± 0.89 ng/l) and benzo(a)anthracene (1.18 ± 0.40 ng/l) (Table 4.4). Higher Nitrite (4.66 ± 0.031 mg/L) and Nitrate (15.80 ± 0.26 mg/l) concentrations were detected in the gas-enriched-seawater compared to the control-seawater (0.32 mg/l and 5.75 mg/l respectively) (Table 4.4).

Table 4.4 The composition of exhaust gas enriched seawater (EGES) and unexposed artificial seawater with F2 medium (Control). The concentration of nitrite, nitrate, ammonium are in mg/l and of the 14 PAHs in ng/l. The EGES was sampled and measured 3 times, while the artificial seawater alone was sampled and measured twice. The standard deviation between the triplicate/duplicate groups is indicated by " ± ".

		EGES	Normal seawater
Nitrite (mg/l)	NO_2	4.66 ± 0.031	0.32 ± 0.01
Nitrate (mg/l)	NO_3	15.80 ± 0.26	5.75 ± 0.02
Ammonium (mg/l)	NH_4^+	0.06 ± 0.00	Not detected
Phosphate (mg/l)	PO_4^{3-}	0.09 ± 0.00	Not detected
Acenafteen (ng/l)	$C_{12}H_{10}$	< 1.36	< 0.87
Fluorene (ng/l)	$C_{13}H_{10}$	< 0.98	1.12 ± 0.16
phenanthrene (ng/l)	$C_{14}H_{10}$	4.25 ± 0.47	2.37 ± 0.24
Anthraceen (ng/l)	$C_{14}H_{10}$	< 0.98	< 0.87
Fluoranthene (ng/l)	$C_{16}H_{10}$	1.66 ± 0.59	< 0.87
Pyrene (ng/l)	$C_{16}H_{10}$	2.25 ± 0.89	< 0.87
Benzo(a)anthraceen (ng/l)	$C_{18}H_{12}$	1.18 ± 0.40	< 0.87
Chryseen (ng/l)	$C_{18}H_{12}$	< 1.36	< 0.87
Benzo(b)fluoranteen (ng/l)	$C_{20}H_{12}$	< 1.36	< 0.87
Benzo(k)fluoranteen (ng/l)	$C_{20}H_{12}$	< 1.36	< 0.87
Benzo(a)pyreen (ng/l)	$C_{20}H_{12}$	< 1.36	< 0.87
Dibenz(a,h)anthracee (ng/l)	$C_{22}H_{14}$	< 1.36	< 0.87
Benzo(g,h,i)peryleen (ng/l)	$C_{22}H_{12}$	< 1.36	< 0.87
Indeno(1,2,3-cd)pyre (ng/l)	$C_{22}H_{12}$	< 1.36	< 0.87

Water parameters during the test

The initial pH was 6.8 for all treatments. In all open flasks pH values increased to 9.5 during the first 3 days and remained at that level until the end of the experiment (Figure 4.1a and Figure 4.1c). A similar pH increase was observed in the closed flasks but here stabilization took place at a higher pH level of 9.8 (Figure 4.1b and Figure 4.1d). These maximum pH values were only affected by the 'open' or 'closed' condition, but showed no differences between Controls, CO_2-enriched-seawater or Gas-enriched seawater.

The dissolved oxygen concentrations continued to increase during the entire experimental period in all open flasks (S 4.2e and S 4.2g). In the closed flasks however, the oxygen concentrations only increased until day 1 in the Controls and until day 2 in the CO_2-enriched-seawater or the Gas-enriched seawater. Maximum oxygen concentration in both enriched groups were similar and higher than in the Controls (S 4.2f and S 4.2h). After reaching the highest level, the oxygen in all closed flasks started to decrease and stabilized at 100 % on day 4 (S 4.2f and S 4.2h).

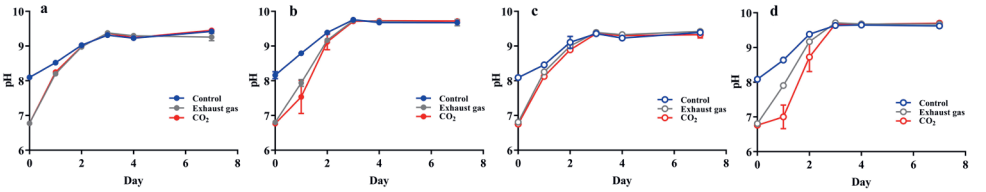

Figure 4.1 The pH of the control, exhaust gas- and CO_2- treated flasks during the 7 days experimental period with algae (*I. galbana*) alone or in combination with rotifers (*B. plicatilis*). Four conditions are included in this figure: an algae alone open flask; b algae alone closed flask; c algae with rotifer open flask and d algae with rotifer closed flask

Impact on plankton

With air exchange (open flasks), the density of *I. galbana* increased during the entire experiment and in the flasks without rotifers the final algal density was between 6 x 10^6 and 8 x 10^6 cell/ml. In presence of rotifers the development of the algal density slowed down after day 4 resulting in a final density of 4 x 10^6 cell/ml on day 7 (Figure 4.2a and Figure 4.2b). No statistically significant difference was observed between the algae development in CO_2 and exhaust gas treated groups. In the (closed) flasks with minimum air exchange, the algae did not reach higher densities than 3.1 x 10^6 cell/ml regardless of the presence of rotifers (Figure 4.3a and Figure 4.3b). In both CO_2 and exhaust gas exposed flasks, algal densities at the end of the test were significantly higher than in the controls. In absence of rotifers this difference was more pronounced in the exhaust gas groups than with the CO_2 groups.

Rotifer densities increased in all conditions, which especially became clear after day 4 (Figure 4.4a and Figure 4.4b). In the closed flasks the rotifer population was significantly smaller at the end of the test (day 7) in CO_2 -enriched-seawater than in the Controls and the Gas-enriched-seawater (Figure 4.4b). In the open flasks these differences were not significant (Figure 4.4a). The mortality of rotifers remained under 10% in all conditions (S 4.3). The presence of rotifers reduced the chlorophyll-a concentrations in all conditions (Figure 4.5), although this was not significant in the CO_2 treated open flasks (Figure 4.5c, $p = 0.073$) probably due to the relatively large variation between replicates in the algae-rotifer group. On an absolute scale, the impact of the rotifers on the algal density was more pronounced in the open than in the closed flasks.

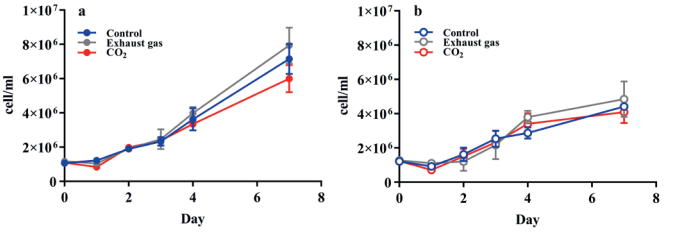

a	day 1
Control vs. CO_2	*

Figure 4.2 The density of algae (cell/ml) in the control, exhaust gas- and CO_2- treated flasks (starting pH 6.8) with air exchange during the 7 days experiment with algae (*I. galbana*) alone or with rotifers (*B. plicatilis*). an algae alone and b algae with rotifers. Differences between groups were assessed on the same day only and listed in the inserted table (*: $p < 0.05$).

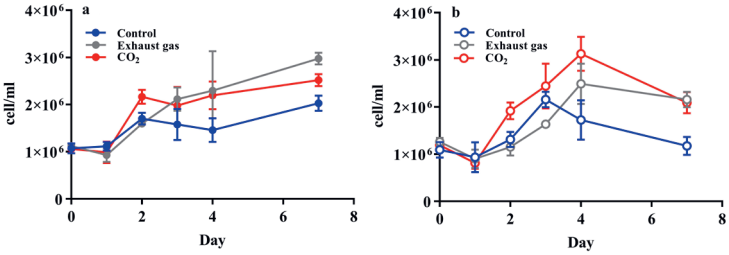

a Algae alone	day 2	day 7
Control vs. CO_2	*	*
Control vs. exhaust gas	ns	**
Exhaust gas vs. CO_2	*	*

b Algae + Rotifers	day 2	day 4	day 7
Control vs. CO_2	*	*	**
Control vs. exhaust gas	ns	ns	**
Exhaust gas vs. CO_2	*	ns	ns

Figure 4.3 The density of algae (cell/ml) in the control, exhaust gas- and CO_2- treated flasks when minimum air exchange during the 7 days experiment with algae (*I. galbana*) alone or with rotifers (*B. plicatilis*). an algae alone and b algae with rotifers. Differences between groups were assessed on the same day only and listed in the inserted table (ns, not significant, *: $p < 0.05$; **: $p < 0.01$).

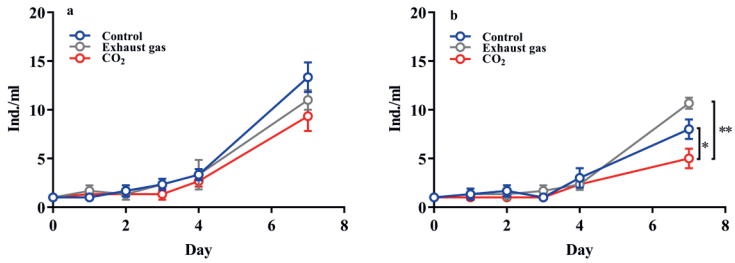

Figure 4.4 The density of rotifers (Ind./ml) in the control, exhaust gas- and CO_2- treated flasks during the 7 days experiment with algae (*I. galbana*) alone or with rotifers (*B. plicatilis*). an algae with rotifers open flask and b algae with rotifers closed flasks. Differences between groups were assessed on the same day only and listed in the table (*: $p < 0.05$; **: $p < 0.01$).

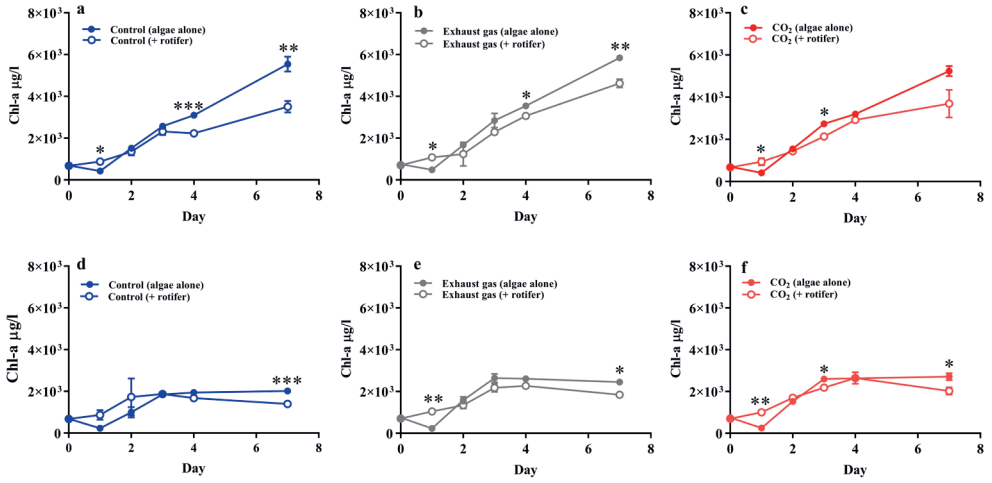

Figure 4.5 Development of chlorophyll-a concentration in the control (a, b), exhaust gas- (b, e) and CO_2- (c, f) treated flasks during the 7 days experiment with algae (*I. galbana*) alone or with rotifers (*B. plicatilis*). a - c open flasks and d - f closed flasks. Differences between groups were assessed on the same day only (*: $p < 0.05$; **: $p < 0.01$; ***: $p < 0.001$).

4.3.2 Testing a wide range of CO_2 concentrations using Isochrysis galbana

Water parameters

The pH of all control and pH-7 groups increased in the first 3 days to around pH 9.6 and overlapped from day 2 on (Figure 4.6a and Figure 4.6b). The pH of the pH-6 and pH-5 groups increased during the entire experimental period and reached the same pH as the controls and pH-7 groups on day 14. In the algae alone group, the development of the pH in pH-5 and pH-6 hardly differed (Figure 4.6a), while, in the presences of rotifers, the pH of the pH-6 group remained significantly higher than that of the pH-5 group (Figure 4.6b). The dissolved oxygen level of all Control and pH-7 groups increased on the first day to about 150% of saturation, then returned to about 100% for the rest of the experiment (Figure 4.6c and Figure 4.6d). The dissolved oxygen level in pH-5 flasks decreased to about 50% of saturation on day 1, and returned to around 100% on day 4. In the pH-6 group it only changed in the presence of rotifers, and the pattern resembled more the Control and pH-7 group, but with one day delay.

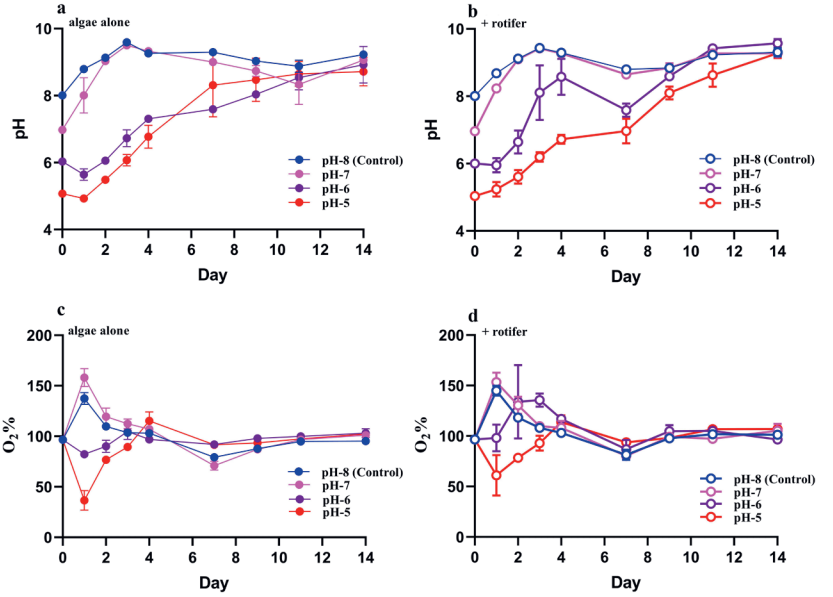

Figure 4.6 Development of pH and oxygen saturation in closed flasks with four different initial CO_2 treatments: pH-5 - 8 (control) over 14 days (triplicate study). Two conditions are included: algae alone (a, c) and algae with rotifer (b, d). All flasks are closed. The studied algae is *I. galbana* alone and studied rotifer is *B. plicatilis*.

Impact on plankton

Without rotifers, the chlorophyll-a concentrations sharply increased during the first 4 days in the control and pH-7 groups (Figure 4.7a). Maximum concentrations for these groups were roughly between 1500 and 2000 µg/L with the highest values in the pH-7 treatments. In the pH-6 and pH-5 groups the algal densities declined from the start of the test. After day 4, a strong decline was also observed in the Control and pH-7 groups, resulting in an almost

complete absence of chlorophyll in all flasks without rotifers on day 9. This situation more or less continued, although some indications of a slight recovery of the algal community were observed at the end of the test on day 14, especially in the pH-7 groups.

In the presence of rotifers the development of the chlorophyll concentration in the Control and pH-7 groups was topped off after day 2 at concentrations below 1500 µg/L, before it collapsed after day 4 (Figure 4.7b). In the pH-5 group the chlorophyll concentrations declined from the start of the test, similar as in the situation without rotifers. The chlorophyll concentration in the pH-6 group with rotifers showed on average an increase until day 4, however with a very large variation between replicates. After day 4, the chlorophyll-a concentration decreased in all groups followed by a slight increase after day 9, except in the rotifer pH-5 flasks.

Similar to the algal development, the rotifer density in the control and pH-7 groups overlapped (Figure 4.8), increasing until day 7 after which it dropped to zero individuals on day 9. The rotifer density in the pH 5 group decreased to zero at day 4, and the numbers in the pH-6 groups were in between the control (and pH-7) and the pH-5 groups**.**

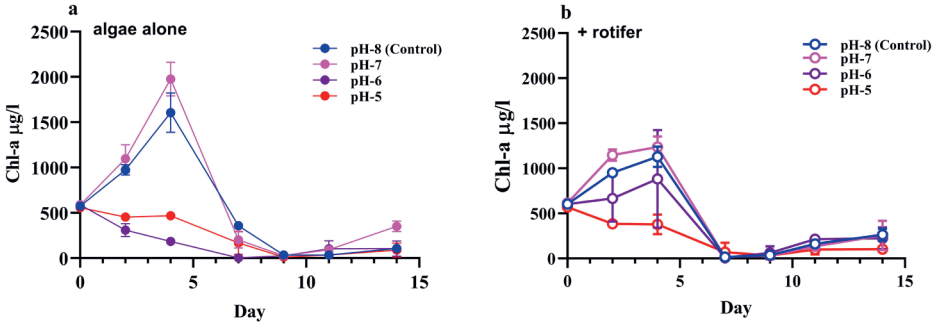

Figure 4.7 The development of chlorophyll-a concentration of algae (*I. galbana*) alone or with rotifers (*B. plicatilis*) under four different initial pHs (pH-5 - 8 (control)) over the 14 days experimental period (triplicate study). Two conditions are included: an algae alone and b algae with rotifer. All flasks are closed.

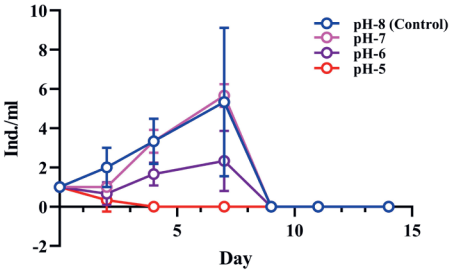

Figure 4.8 The development of rotifer density (individuals/ml) under four different initial pH treatments (pH-5 - 8 (control)) over the 14 days experimental period (triplicate study). All flasks were closed. The studied algae is *I. galbana* and the studied rotifer is *B. plicatilis*.

Testing an extreme CO_2 concentration using Dunaliella salina

Regardless of the initial pH of 6 or 8 (controls) the pH rapidly increased in all flasks during the first 2 days. From then on it more or less stabilized at pH 9.8 and pH 9.0 for flasks without and with rotifers respectively (Figure 4.9).
Without rotifers the population density of the algae *Dunaliella salina* increased during the first 2 days and then more or less stabilized at 8 x 10^5 cell/ml in pH-8 (control) and at a significantly higher level of 1.5 x 10^6 cell/ml in pH-6 (Figure 4.10a). In the presence of rotifers, the maximum algal densities were significantly lower, but also here, significantly higher algal densities were observed in the pH-6 groups compared to the pH-8 groups. In contrast to the flasks without rotifers, the algal densities were not maintained until the end of the test in presence of rotifers, but gradually became depleted towards the end of the test.
The densities of rotifers in both pH levels increased from 1 to on average 5 (in pH-6) or 6 (in pH-8) individuals/ml until day 4. During the final sampling on day 5 rotifer densities were significantly lower than on the day before ($p = 0.038$) in the pH-8 group, and more or less stable in the pH-6 group (Figure 4.10b).

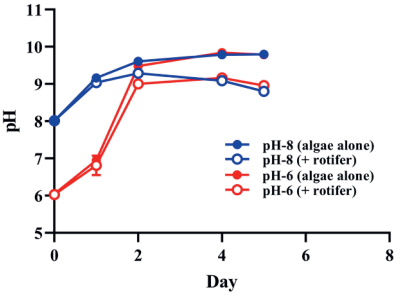

Figure 4.9 The pH development of initial pH-8 (control) and CO_2 induced initial pH-6 groups, containing algae (*D. salina*) with or without rotifers (*B. plicatilis*). The flasks were closed during the 5 days experimental period.

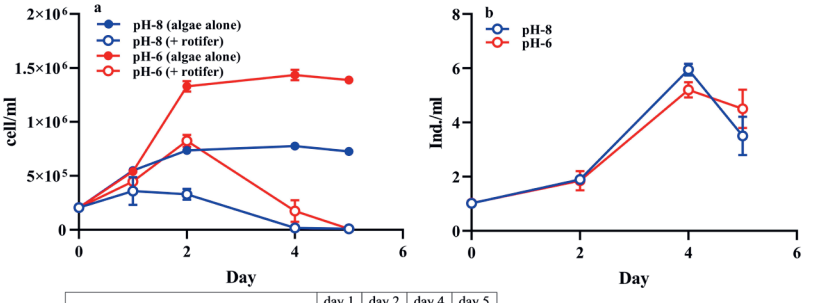

	day 1	day 2	day 4	day 5
pH-8 (algae alone) vs. pH-6 (algae alone)	ns	*	*	***
pH-8 (+ rotifer) vs. pH-6 (+ rotifer)	ns	*	ns	ns
pH-8 (algae alone) vs. pH-8 (+rotifer)	ns	*	*	**
pH-6 (algae alone) vs. pH-6 (+rotifer)	ns	*	*	*

Figure 4.10 The development of algae (*D. salina*) (cells/ml) (a) and rotifer (*B. plicatilis*) (individuals/ml) (b) density in the control (pH-8) and CO_2- treated groups (pH-6) for 5 days. Error bars represent the standard deviation between the duplicate flasks. Differences between groups in (a) were assessed on the same day only and listed in the inserted table (ns, not significant, *, $p < 0.05$; **, $p < 0.01$; ***, $p < 0.001$). There is no significant difference in (b).

4.4 Discussion

The main aim of this study was to compare the impact a mixture of compounds from underwater released exhaust gas, with that of one of the main components, CO_2 on a simple community of marine algae and their consumers (rotifers). In both cases the pH of the water was substantially lowered by the treatments, which is a well-known effect of CO_2 addition. In our experiments additional CO_2 was rapidly taken up by the developing algae, resulting in CO_2 depletion within a few days. Direct and indirect effects on rotifer and algae became apparent below pH 6, and the pH sensitivity differed among the used two algal species. Additional effects of other compounds from the exhaust gas on the plankton community were not found.

4.4.1 Representativeness of the exhaust gas treated water

After the seawater had been injected with exhaust gas, it took for practical reasons about 6 days before the experiment was started. Although the water was stored in a closed stainless steel container placed in a cool room, oxygen concentration and pH increased during storage, most likely caused by the O_2 and CO_2 exchange between the air-liquid interface within the 30 l tank (Zeebe & Wolf-Gladrow, 2001). Thus, the initial pH of the treatment groups in this experiment was 6.8 instead of 6.5, as it was directly after gas injection. The effect of the 0.3 difference in exposure on the outcome of the experiment is probably ignorable, since due to primary production the pH of all experimental groups increased to about 9.0 in already 2 days (Figure 4.1).

Given the storage conditions and the fact that artificial seawater without notable biological activity was used, it seems unlikely that substantial changes occurred with the compounds that were absorbed from the exhaust gas. We therefore believe that the treated water we used for our tests formed a good representative for the actual water quality that could occur when exhaust gas from a diesel engine is released sub-surface in sea.

4.4.2 Potential impact of compounds in exhaust gas, other than CO_2

Exhaust gas of combustion engines always contains CO_2 among many other compounds. We found elevated levels of PAHs, nitrite and nitrate in our gas-enriched-seawater (Table 4.4) but observed no differences between the impact of this seawater on the studied plankton community compared with seawater treated with CO_2 only. Therefore, we conclude that CO_2 was the main impactor in the exhaust gas in our experiments.

This is in line with the fact that all detected PAHs in the gas-enriched-seawater were significantly lower than their reported no-observed-effect-concentration (NOEC) for aquatic ecosystems. For instance, as NOECs of Pyrene and Phenanthrene 1,670 ng/l and 32,000 ng/l are indicated respectively (Wang et al., 2014; Wu et al., 2011), while only 2.25 ng/l of Pyrene and 4.25 ng/l of Phenanthrene was present in our gas-enriched-seawater. Thus, it is also logical that no impact of dissolved PAHs on the studied plankton community was found.

Nitrogen concentrations in the form of nitrite and nitrate were substantially elevated in the gas-enriched-seawater. Algae can use both forms as a nitrogen source and also excrete nitrite during nitrate assimilation (Malerba et al., 2012). In our study, the development of algae in

the gas-enriched-seawater was not stimulated by the additional nitrogen compared to the control-seawater or CO_2-enriched-seawater groups. This was because nitrogen was never depleted in any of the flasks. Instead, carbon shortage already occurred between day 2 and day 3, as indicated by the maximum pH that is then reached (Figure 4.1).

Nitrite is known to be toxic at higher concentrations for aquatic animals. Rotifers, however seem not particularly sensitive. W Chen et al. (2011) reported a NOEC for reproduction and growth of freshwater rotifers of 19.7 mg/l NO_2, being four times higher than the initial level in the gas-enriched-seawater. Fish are much more sensitive to high nitrite concentrations, that can result in a large variety of physiological disturbances (Kroupova et al., 2005). Usually a significant impact was caused by > 20 mg/l NO_2 to adult freshwater fish (Kroupova et al., 2005; Martinez & Souza, 2002) and > 40 mg/l to adult marine fish (Grosell & Jensen, 2000). Thus, the NO_2 concentration in our gas-enriched-seawater was still too low to cause such effects. However, nitrite can also be accumulated in the body fluids of fish. Longer exposure to concentrations above 0.5 mg/l NO_2 can in this way result in negative effects (Kocour Kroupová et al., 2018). Therefore, the impact of nitrite in exhaust gas enriched water on fish cannot be ruled out.

4.4.3 Responses of the algae and rotifers to the elevated CO_2 concentrations

Due to the algae development and related CO_2 consumption, the pH levels rapidly increased in all groups in the first 3 days of the experiments until reaching the highest level above 9, that was maintained for the remaining experimental period. In the closed flasks without rotifers also the algal density stabilised after day 3, apparently limited by the depleted CO_2. In the open flasks in-flux of additional CO_2 facilitated further development of the algal density after the pH reached its maximum value. The stabilized pH level after day 3 suggests that the algal development was limited by the CO_2 transfer velocity between air - liquid interface (Esters et al., 2017; Markou et al., 2014). Our observations are also in line with Verspagen et al. (2014) who showed that a dense algal concentration (algal bloom) can deplete the dissolved CO_2 concentration in water and raise the pH level sometimes even over 10, after which the algal growth is inhibited by carbon limitation. They also state that the potential of carbon limitation strongly depends on the water alkalinity. Owing to the high inorganic carbon availability in high alkalinity water (> 3 meq/l), carbon limitation is unlikely to occur during algal development (Verspagen et al., 2014). In the presented study, the alkalinity was stabilized at 2.4 meq/l in the entire experiment, and carbon limitation caused algae growth termination was observed on day 2.

Although some air exchange could not be avoided during sampling, the carbon source for algal development in the closed flasks mainly consisted of the initial CO_2 level of the water. Significantly higher algal densities than in the controls were expected in the CO_2 and exhaust gas treated closed flasks due to the higher initial carbon concentrations. The dissolved oxygen concentrations that reached higher concentrations in the flasks enriched with CO_2 and exhaust gas than in the controls indeed suggest a higher primary production. This was however not reflected by significantly higher algal densities in the treated flasks. Apparently, the absolute amount of additional CO_2 that was present in the closed flasks in the experiment with exhaust gas to reach the initial pH value of 6.8 was too low to result in a noticeable increase of the density of the algal species *I. galbana*. Higher initial CO_2 concentrations resulting in pH 6 or below turned out to have a negative impact on this algal species. In the final experiment when

D. salina, an algal species that is more tolerant to low pH levels was used, the positive impact of an elevated initial CO_2 concentration resulting in pH-6 was demonstrated.

An initial pH level of 5 caused rotifer mortality from day 1 onwards in our test, but the organisms survived pH levels as low as 6.0. Arnold et al. (2010) already reported that pH 6.8 does not significantly impact the mortality of *B plicatilis*, and our results indicate that this species can still reproduce at that pH level.

4.4.4 Plankton community response to underwater released exhaust gas

The aim of our study was to test the hypothesis that the mixture of compounds that is absorbed from sub-surface released exhaust gas has a strong potency to cause algal blooms, due to negative effects of toxic compounds on organisms that feed on phytoplankton in combination with a stimulating effect of CO_2 on algal growth rates.

Although water concentrations of some potentially toxic compounds were indeed elevated after exposure to exhaust gas, the concentrations were too low to cause toxic effects during the test. All observed effects could be attributed to the elevated CO_2 concentrations only. As the rotifer we used were capable of coping with high CO_2 concentrations, situations where negative impact on rotifers were combined with positive effect on algal growth rates were never reached. In general, the algal species *I. galbana* showed higher sensitivity to low pH levels than the rotifers. As long as the initial pH was 6.0 or higher the rotifers were able to increase in numbers and their grazing clearly reduced the algal density. At lower initial pH levels *I. galbana* did not survive, and the rotifers died either from the low pH or from starvation.

In our experiment with the more CO_2 resistant algal species *D. salina*, the impact of CO_2 propagated up the food web was observed. The stimulated algal density in pH-6 was almost depleted by the growing rotifer population on day 4 and the development of rotifers followed the trend of algal development Taucher et al. (2017). and Algueró-Muñiz et al. (2019) also reported that the increased abundance of zooplankton under high CO_2 concentration occurred as a response to the phytoplankton bloom (Taucher et al., 2017). also found that the dominant zooplankton species mainly depended on the size of blooming algae in the high CO_2 treatment (~ 760 µatm pCO_2, ~pH 7.4), since different zooplankton species have different suitable feed size and nutrients. Such interaction between species was not included in the presented study, since our experiments focused on a single phytoplankton species-rotifer community. It would be interesting to study the impact of additional CO_2 exposure on the species developments in more diverse plankton communities with different sizes as they occur in real-world situations.

In a previous mesocosm study, a complex plankton community (in combination with a benthic community) was exposed to continuously elevated CO_2 concentrations (resulting in a range of pH values from 8.6 to 5.8) for 49 days (Wei et al., 2019). At the end of the study zooplankton was almost absent in both pH 6.2 and pH 5.8 treatments, while an algal bloom occurred. This indicated that the collapse of the zooplankton population was directly caused by the high CO_2 concentration, and that at least some of the algal species present were able to take advantage of the new situation, with low predation pressure and high CO_2 availability. Such a strong response was not found in the present flask study. Besides species-specific

responses to elevated CO_2 concentrations, the different results can be attributed to the fact that the rotifers in the flask experiments only experienced the elevated CO_2 concentration for a short period, since the high algal growth rate raised the pH rapidly when the CO_2 became depleted. This rapid CO_2 depletion also limited the possibility for algal development in our flask experiments. To overcome this, future experiments should be performed with repeated CO_2 application to extend the exposure period and so to mimic the situation in frequently used shipping lanes. In addition, a more complex plankton community should be involved, so that the potential of underwater released exhaust gas to induce a plankton community shift can be predicted.

4.5 Conclusions

We found no indications that the mixture of compounds from underwater released exhaust gas stimulates the development of an algal bloom through a combination of negative impact of toxic compounds on zooplankton, and a stimulation of algal development by CO_2. All observed effects were caused by CO_2 only. The impact of other compounds like NO_x and PAHs on the studied marine plankton was not evident. Repeated injection of CO_2, which might occur at busy shipping lanes when underwater gas release systems are becoming more popular could however still stimulate the primary production locally and induce a shift in plankton community composition.

4.6 Supplementary materials for Chapter 4

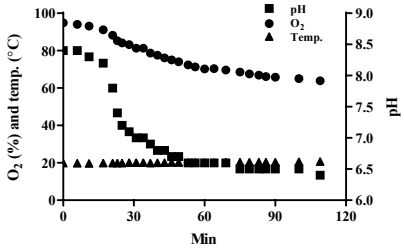

S 4.1 The development of pH, temperature and oxygen saturation level of 30 l artificial seawater during 1.5 hours of exhaust gas injection.

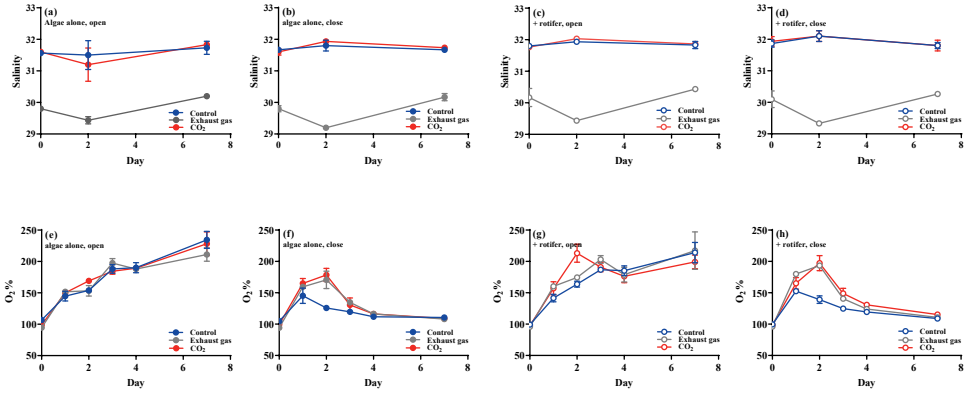

S 4.2 The development of salinity (‰, a - d) and oxygen saturation level (%, e - h) of the control, exhaust gas- and CO_2- treated flasks during the 7 days experimental period with algae (*I. galbana*) alone or in combination with rotifers (*B. plicatilis*). Control: only artificial seawater with F2 medium. (a and e) algae alone open flask; (b and f) algae alone closed flask; (c and g) algae with rotifer open flask and (d and h) algae with rotifer closed flask.

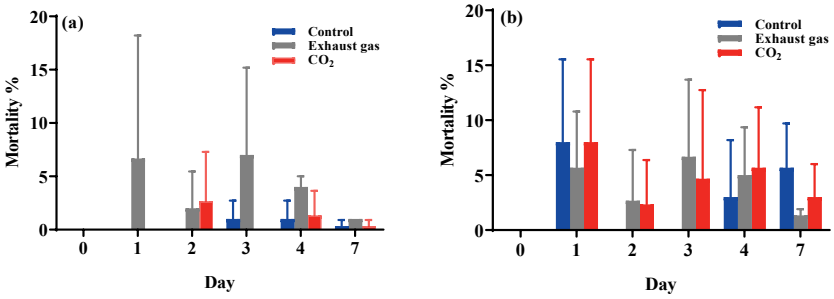

S 4.3 The mortality of rotifers (%) in the control, exhaust gas- and CO_2- treated flasks during the 7 days experimental period with algae (*I. galbana*) alone or in combination with rotifers (*B. plicatilis*). Control: only artificial seawater with F2 medium. The initial pH of the exhaust gas- and CO_2- treated flasks is 6.8. (a) open flasks with algae and rotifer and (b) closed flasks with algae and rotifers.

CHAPTER 5

5

Relative risk assessment of ecological areas with the highest potential impact of underwater released exhaust CO_2 from innovative ships

Yuzhu Wei[a], Michel Kroeze[c], Csilla Vámos[c], Edwin M. Foekema[a,b], Ron van Lammeren[c] and Albertinka J. Murk[a]

[a.] Marine Animal Ecology group, Wageningen University and Research, P.O. box 338, 6700 AH Wageningen, The Netherlands
[b.] Wageningen Marine Research, Wageningen University and Research, P.O. Box 57, 1780 AB Den Helder, The Netherlands
[c.] Laboratory of Geo-Information Science and Remote Sensing, Wageningen University and Research, P.O. Box 8130, 6700 EW Wageningen, The Netherlands

Submitted

Abstract

Applying underwater released exhaust gas as 'air lubrication' along the ship's hull to reduce the energy consumption is under development. However, this direct emission to the water could pose a risk to the local marine environment, especially in shipping-dense areas. Specifically, CO_2, a dominant component in the exhaust gas, has the potency to enhance algal blooms and cause acidification. This study provides the first relative risk assessment of ships with underwater release exhaust gas systems on a global scale, taking into account local water conditions and shipping intensity. Risk was characterized for 262 marine ecoregions by plotting the expected CO_2 emission from ships to water against the estimated vulnerability to acidification and algal blooms. The vulnerability of each ecoregion was assessed based on background dissolved inorganic carbon (DIC) level, chlorophyll-a concentrations and total alkalinity. The results reveal that areas with relatively high vulnerability are mainly located above 30° N latitude. The Yellow Sea, Southern China Sea, and North Sea come out as relatively high-risk areas. Looking in more detail to European high-risk ecoregions, the highest risk levels are found in areas with dense shipping lanes and maritime chokepoints, e.g. the Strait of Dover and the Strait of Gibraltar. This was the first attempt to make such a risk assessment and the outcome is only indicative. In a next phase additional parameters, such as water currents and biological composition of the ecosystem should be included.

5.1 Introduction

Underwater released exhaust gas systems as 'air-lubrication' of ship hulls are under development and expected to reduce the drag force, in turn reducing the fuel consumption and total emission of global shipping activities (H Sapra et al., 2017; Van Biert et al., 2016). Additionally, it improves the air quality on working decks (H Sapra et al., 2017). These advantages make the system attractive, especially under the more strict maritime emission regulation (H Sapra et al., 2017; Van Biert et al., 2016), e.g. the nitrogen oxides (NO_x) emissions control (IMO, 1997a). However, such an application implies concentrated input of exhaust gas in the local marine ecosystem and may pose a serious risk, especially in the case of intensively used shipping lanes. Specifically, CO_2, one of the main components in the exhaust gas (M Anderson et al., 2015), could enhance algal bloom and cause acidification, depending on the local environmental conditions.

For photosynthetic organisms, dissolved CO_2 is one of the essential nutrients (together with N, P, Fe, etc.). CO_2 is continuously exchanged between the atmosphere and seawater phases, which provides carbon nutrients to these aquatic primary producers, like microalgae (Markou et al., 2014; Zeebe & Wolf-Gladrow, 2001). In the case of high algal densities, the mass transfer of CO_2 from the atmosphere to the liquid state can be slower than the algal uptake rate (Markou et al., 2014; Zeebe & Wolf-Gladrow, 2001). As long as other nutrients are still available, CO_2 availability will then become the factor determining further algal growth (Markou et al., 2014). In such conditions, underwater released exhaust CO_2 may relieve this carbon resource limitation and stimulate further development of algae densities potentially resulting in an algal bloom or extending the blooming period.

After release, CO_2 dissolves in water and increases the Dissolved Inorganic Carbon (DIC) level (Zeebe &Wolf-Gladrow, 2001). With increasing DIC levels, the seawater becomes acidified, as indicated by a reduction of the pH value. This acidification may e.g. inhibit the

calcification process of organisms such as corals and mussels (Kurihara, 2008; Sunday et al., 2017). The inhibition of the calcification process hampers the organism's ability to form calcium carbonate ($CaCO_3$) structures like skeletons and shells (Fassbender et al., 2016) with negative impact on growth and survival (Kurihara, 2008; Wei et al., 2019). The capacity of seawater to resist a decrease in pH with increasing CO_2 concentrations mainly depends on the amount of anions present (e.g. CO_3^{2-} and HCO_3^-) (Zeebe & Wolf-Gladrow, 2001) and is indicated by Total Alkalinity (TAlk). Waters with a higher TAlk have stronger acid-neutralizing capacity and can absorb larger amounts of CO_2 before the water pH drops (Omernik &Powers, 1983). The sensitivity of marine regions for enhanced CO_2 exposure therefore will depend on the local TAlk level and nutrient levels, information that can be derived from data described for global marine ecoregions (Spalding et al., 2007) and can be used in ArcGIS to combine different conditions.

Both, stimulation of the algae density growth and inhibition of the growth of calcifying organisms, can be devastating for local marine ecosystems. Of course, the intensity of the CO_2 exposure as well as the sensitivity of the receiving marine ecosystem will determine the eventual risk for adverse effects to develop. The present study aims to assess for ecoregions the relative risk that projected underwater released exhaust CO_2 will cause algal blooms or acidification.

5.2 Materials and Methods

To be able to assess the risk of underwater exhausted CO_2 for the local marine environment, both the exposure, as well as the vulnerability to CO_2 needed to be quantified and compared for each ecoregion (Figure 5.1) (Section 5.2.4). The exposure level was assessed from the reported CO_2 emission from maritime traffic in 2018 in combination with the assumed saturation level of DIC in seawater (Section 5.2.2). Quantification of the vulnerability to CO_2 was based on two indicators: 1) TAlk level as a measure of resistance to acidification, and 2) chlorophyll-a concentration as a measure of eutrophication (Section 5.2.3).

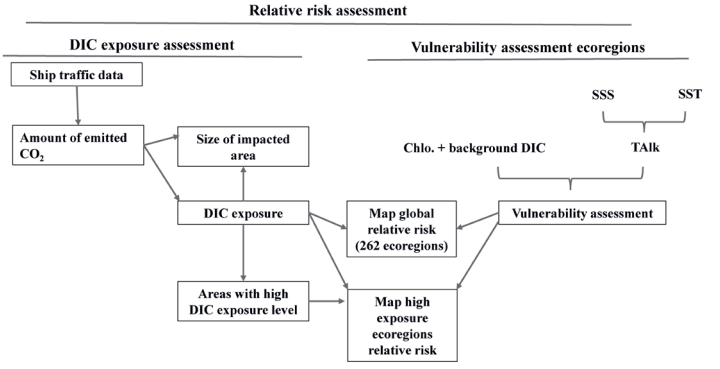

Figure 5.1 Workflow diagram of the relative risk assessment of underwater released exhaust CO_2 from maritime shipping for global and local ecoregions. Dissolved inorganic carbon (DIC) exposure assessment of CO_2 emitted from maritime shipping and vulnerability assessment of algal bloom (indicated as Chlo. + original DIC level) and acidification (indicated as TAlk level) were considered in risk characterization for global and local ecoregions to CO_2 emitted by underwater exhausts. SSS: seawater surface salinity; SST: seawater surface temperature; Chlo.: chlorophyll-a; TAlk: Total Alkalinity.

5.2.1 Data collection, representation and projection

All pre-processing and spatial analyses were performed in ESRI ArcGIS 10.6.1 unless described otherwise. All datasets were converted to the Compact Miller projection prior to further analyses.

Global ocean map data collection

The coastlines of the global map were created using the land-sea mask dataset and methods as described by Halpern et al. (2008). The land-based data that in reference to this data mask occurred within the ocean, or ocean based data that occurred on land were clipped and removed to ensure consistency across all data used in our analysis (Halpern et al., 2008). All data were represented at 1 km^2 resolution. For the collected data that was only available at a coarser native resolution, it was assumed that the coarse-scale value was evenly distributed across all 1 km^2 cells within that region (Halpern et al., 2015). This essentially maintains the coarse-scale pattern while the finer resolution information is preserved when it is available. For the gaps in datasets, the null values were filled with a 5 x 5 focal mean filter (Sharma et al., 2010; Tomlin, 2016). I**t** was specified that only cells containing values were used to find the focal mean of the target cell. This means that a null value will be ignored when it exists within the neighbourhood of the focal mean filter. Thus, this process removed gaps while minimizing unjustified smoothing effects of missing data on the dataset (Sharma et al., 2010; Tomlin, 2016). The filter was run multiple times from the edge of each gap until all encapsulated null values were filled (i.e. null values surrounded by values). Very large data gaps occurred in areas with sea ice. These data gaps were not filled due to their large size. Instead, ice masks were created to indicate where scores are less certain. Ice masks were created to indicate where scores are less certain. To indicate which areas are counted as sea ice, the daily fractional ice cover data from 2012 were obtained via the Advanced Very High Resolution Radiometer (AVHRR) Pathfinder Version 5.2 (Casey et al., 2011). The daily fractional ice cover data were then averaged by meteorological season and converted to binary terms: either the cell has ice, or the cell has no ice. Grid cells that contained an average sea ice fraction greater than 0.15 were considered to have ice, and were thus included in the ice masks.

Ecoregions

The global ocean was divided into 262 ecoregions by taking two steps: 1) the coastal and shelf waters shallower than 200m were divided into 232 ecoregions based on biogeographic patterns (Spalding et al., 2007), and 2) all remaining open oceans were divided into 30 ecoregions following similar classifications as the coastal and shelf water areas (Spalding et al., 2012). Each ecoregion consists of relatively homogeneous species composition that is distinct from adjacent areas (Spalding et al., 2007). The datasets were collected via the Nature Conservancy's Geospatial Conservation Atlas (Atlas, 2019) and UNEP's Ocean data viewer (Conservancy, 2012).

As Europe was later indicated to be continent that experiences the highest DIC exposure, the 15 marine ecoregions around Europe (S 5.1a) were subdivided into ecologically relevant classes based on ocean floor depth (Waller, 1996): the epipelagic zone (0 – 200 m), the mesopelagic zone (200 – 1,000 m), the bathypelagic zone (1,000 – 2,250 m), the

abyssopelagic zone (2,250 – 4,500 m), and the hadopelagic zone (4,500 – 11,500 m). To show variation in risk level between coastlines and open seas, the epipelagic zone was arbitrarily sub-divided into five depth classes, resulting in a total of 9 depth classes (S 5.1b). Dividing the 15 European ecoregions by depth class resulted in a total of 114 European sub-ecoregions that were labelled according to the ecoregion code (same as the global ocean code) and depth class.

Chlorophyll-a concentration and DIC

Nutrient concentrations in seawater are regularly measured on a local scale, but a dataset with global coverage that met our needs was not available. As an alternative, the chlorophyll-a concentration was used as an indicator for algal biomass, since the chance that additional DIC will promote further algal development is greater at higher algal density. The chlorophyll-a dataset was collected from NASA's Aqua-MODIS satellite (NASA Goddard Space Flight Center, 2018) for each calendar month of 2018 and aggregated to seasonal means (December - February, March - May, June - August, and September - November). The yearly average DIC concentrations of the ocean were collected from the GLODAPv2 dataset (Lauvset et al., 2016; Olsen et al., 2016).

Talk

As the vulnerability indicator for acidification, TAlk was calculated based on sea surface temperature (SST) and sea surface salinity (SSS) by following the equation described by Lee et al. (2006). The SSS and SST data for each calendar month of 2018 were collected from NASA's JPL SMAP satellite (Nasa/Jpl, 2019) and NOAA's Coral Reef Watch satellites (Watch, 2018, updated daily) respectively.

5.2.2 DIC exposure assessment

Maritime CO_2 emission

To assess the DIC exposure level caused by underwater released exhaust CO_2, the amount of maritime emitted CO_2 has to be estimated. For this, a 2013 shipping intensity dataset was collected from the Knowledge Network for Biocomplexity (Halpern et al., 2015). This dataset contains the registered number of ships in each 1 km^2 grid cell (X) in a $\log[X + 1]$ transformed and rescaled (between 0 and 1, with the highest per-pixel transformed value = 1) form. The emission factors for each ship class were collected from the literature (ECTA, 2011; McKinnon & Piecyk, 2010; Otten et al., 2017).

Shipping intensity and the amount of emitted CO_2

To calculate the number of ships in each grid cell (X), the rescaling of the collected shipping intensity dataset (occurring in a rescaled $\log[X + 1]$ form) was reversed first using the following formula (eq.1):

$$Y = Y'(X_{max} - X_{min}) + X_{min} \qquad \text{(eq.1)}$$

Here Y' is the log [X+1] transformed data, Y is the collected data and X_{min} and X_{max} are the minimum and the maximum number of registered ships in each grid cell. The collected dataset contains zero, which is the result of 'log 1'. Thus, X_{min} is zero. The unknown X_{max} was estimated by $\log[X+1]$ transforming the raw ship traffic dataset from Halpern et al. (2015)'s study. This raw dataset contains the number of ships in each grid cell, but also includes invalid and cross land routes. Finally, the number of registered ships in a grid cell (X) of 2013 was calculated by the exponential of the log transformed data (eq.2).

$$X = Exp(Y) - 1 \qquad \text{(eq.2)}$$

Next, the calculated data were multiplied with the 8.16% growth rate (from 2013 to 2018) in the global merchant fleet to project the ship traffic intensity for 2018 (UNCTAD, 2018). The presented study focused on maritime shipping in 2018, because that was the most recent and reliable maritime shipping information available from the United Nations annual review of maritime transportation, when this study was carried out. This adaption also created a worst-case-scenario as it assumes that all vessels are merchant ships.

Finally, the total amount of emitted CO_2 per ship per grid cell (E_T) is quantified by multiplying the proportional share (P_i) of each $i \ldots m$ vessel class, the amount of emitted CO_2 per km (K_i) of each $i \ldots m$ vessel class, and the average travel distance of a ship to pass a 1 km^2 grid cell: 0.7 km (S 5.2) (eq.3). To consider the worst-case-scenario, K_i was determined based on the highest emission factors in Table 1. An emission factor of the 'other ships' class was not available because of the broad definition of this class (including all liquefied petroleum gas tankers, ferries, cruises, etc.) by UNCTAD (2018). Therefore, the emission factor of 'other ships' was assumed to be in the same range as 'general cargo', since both classes share a similar average deadweight tonnage (dwt) and short-sea shipping function (Table 5.1).

$$E_T = \sum_{i=1}^{m} P_i \times K_i \times 0.7 \quad \text{(eq.3)}$$

Table 5.1 The number of global maritime merchant ships in each purpose class (nr. ship), the mean deadweight tonnage (dwt) of each ship in 2018 (UNCTAD, 2018), the corresponding CO_2 emission factors (ECTA, 2011; McKinnon & Piecyk, 2010; Otten et al., 2017), as well as the mean kg CO_2 emitted per traveled km per ship.

Merchant ship class	Nr. ship	Mean dwt/ship (tonnes)	Emission factors (lower and upper levels) (g CO_2 /ton/km[a])	kg CO_2 emitted/km/ship[d]
Oil tankers	10,420	53,839	10.3 - 15	807.6
Bulk carriers	11,125	73,618	7 - 11.9	876.1
Container ships	5,164	48,993	8.4 – 12[b]	587.9
General cargo	19,613	3,773	13.9 - 21	79.2
Other vessels	47,847	4,535	13.9 - 21[c]	95.2

[a]Unit defining transport performance. An output of one is reached when one ton is transported one km.
[b]Emission factors of container ships based on twenty-foot equivalent units (TEU's) instead of dwt.
[c]Emission factors are assumed to be the same as for 'general cargo' due to their similar mean dwt and short-sea shipping function.
[d]Calculated as: (mean dwt per ship x emission factor) / 1000.

Emitted CO_2 induced DIC exposure

For the risk assessment, we assumed that all CO_2 produced by the ships is emitted underwater. The water DIC level is determined by the amount of dissolved CO_2 instead of the total emitted CO_2 (Figure 5.1). Potentially, all CO_2 can dissolve in water and change the carbon composition in water. However, when the saturation of DIC is reached (depending on e.g. temperature, salinity and pressure), additional CO_2 will not dissolve in the water anymore (Zeebe & Wolf-Gladrow, 2001) and will "escape" to the atmosphere. In addition, the dissolved CO_2 continually exchanges with the CO_2 gas in the atmosphere, which eventually leads to an equilibrium. Due to the saturation of DIC in water and the equilibrium of CO_2 concentrations between water and atmosphere, increasing the amount of injected CO_2 in DIC saturated water does not raise the exposure of the local marine ecosystem further. Therefore, the saturation level of DIC and the equilibrium of CO_2 concentrations in water and atmosphere phases determine the maximum exposure level caused by underwater released exhaust CO_2.

Determination of the DIC saturation level

We determined the maximum saturation level of DIC in seawater and the time required to reach this in a laboratory experiment. For this, a flow of air (flow rate 148 ml/min) with 5% CO_2 was continuously injected into 150ml of artificial seawater (sea salt Marine Zoomix®; temperature 20 ˚C; salinity 31.7‰; alkalinity 2.07 mmol/l and background pH 8.1). The uptake of CO_2 in the water was reflected by the lowering of the pH. The injection was terminated when the water pH level did not further decrease indicating that the maximum saturation was reached. After terminating the CO_2 supply, the water pH level started increasing as the surplus CO_2 from the water escaped to the atmosphere. The water pH was continually measured until the pH was stable, and the equilibrium of CO_2 in the water and atmosphere was re-established. The DIC concentrations in the water were calculated based on temperature, salinity and pH level of the water using the *Seacarb* package in R (Team, 2013). The DIC data was plotted against time.

Based on the outcome of the experiment, the increased average DIC level was calculated for the number of ships passing a 1x1 km grid during 24 hours. In this model, we assumed 1) all CO_2 produced by a ship is emitted underwater and immediately dissolves; 2) the background and saturated DIC levels of the local water are the same as in the laboratory test, 2.07 mmol/l and 3.97 mmol/l respectively; 3) the temperature condition is the same as in the laboratory test, 20 ℃, and 4) after a ship passed, the DIC concentration returns to the atmospheric equilibrium in the same time as in the laboratory test. The relationship between the average increased DIC and the number of ships in 24 hours was applied to the ship traffic dataset for creating a global DIC exposure map.

In the actual shipping condition, the CO_2 will be injected along the ship's hull instead of in the entire grid cell (1 km x 1 km). Therefore, the actual size of the exposure area was estimated by assuming 1) the injected CO_2 impacts a 5m depth of water column, and 2) the DIC saturation level (3.97 mmol/l) has to be reached before additional CO_2 could impacts a larger waterbody. Finally, the impacted surface area (DIC saturated area) of a grid cell was calculated by dividing the DIC saturated water volume by the impacted depth (5 m).

5.2.3 Vulnerability assessments of ecoregions

Vulnerability for CO_2 induced algal blooms

From the collected chlorophyll-a concentration dataset, 5000 random data points were plotted against their background DIC levels (Figure 5.2). The plot shows no relation between DIC and chlorophyll-a at DIC levels above 1840 µmol/kg. At lower DIC levels, the lower limits of the plot show a negative correlation between DIC and chlorophyll-a. This suggests depletion of DIC by primary production, thus a situation where additional CO_2 can facilitate further algal development. As 1 mg/m^3 chlorophyll-a is considered as the low limit of a "productive area" for microalgae (Demarcq et al., 2007; Nixon & Thomas, 2001), situations with < 1 mg chlorophyll-a /m3, that only occur at DIC > 1840 µmol/kg are unlikely to be limited by DIC. This condition was therefore assigned as having low vulnerability for CO_2-induced algal blooms (score 0 - 0.2) (Table 5.2). In order to derive a relative vulnerability score for situations with Chlorophyll-a > 1 mg/m3, the background DIC levels of the 5000 random data points (Figure 5.2) were divided into 4 ranges with DIC = 1840 µmol/kg as median value. Vulnerability scores for chlorophyll-a > 1 mg/m^3 situations were then defined as '0.2 - 0.4', '0.4 – 0.6'. '0.6 – 0.8' and '0.8 – 1', when 1060 < DIC < 1460 µmol/kg, 1460 < DIC < 1840 µmol/kg, 1840 < DIC < 2100 µmol/kg and 2100 < DIC < 2347 µmol/kg, respectively (Table 5.2). Here, a range of vulnerability scores was given instead of a categorical score, because continuous values of vulnerability generate a map with gradual changes, which better represents reality. Within each vulnerability range, a high vulnerability score was given to the place with a relatively low background DIC level as a relatively small addition could be enough to facilitate an algal bloom in a situation with enough nutrients.

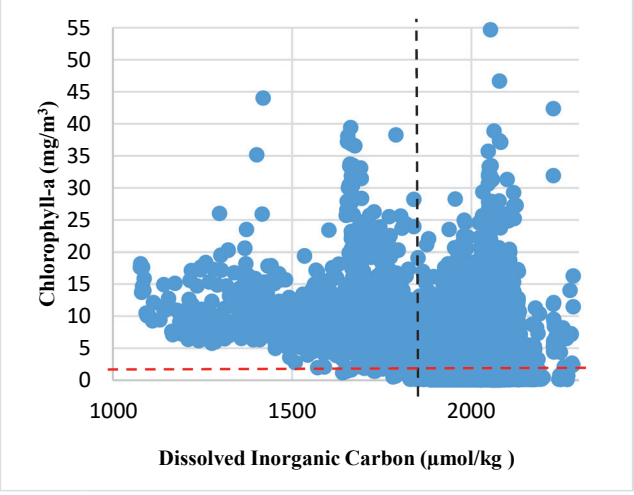

Figure 5.2 Chlorophyll-a concentration (mg/m^3) and the yearly average DIC level (µmol/kg) of 5,000 random sample points of the NASA's Aqua-MODIS satellite dataset in 2018 (NASA Goddard Space Flight Center, 2018). Sample points with 1 mg chlorophyll-a/m^3 and DIC with 1840 µmol/kg are indicated as red and black dash line, respectively. 1 mg/m^3 chlorophyll-a was reported as the threshold value to define the low limits of a "productive area" for microalgae (Demarcq et al., 2007; Nixon &Thomas, 2001). The linear correlation between chlorophyll-a concentration and DIC level is not observed when DIC > 1840 µmol/kg in this figure.

Table 5.2 Relative vulnerability classes for elevated CO_2 concentrations assigned to local water conditions indicating sensitivity for CO_2 induced algal bloom or acidification. The criteria include the chlorophyll-a concentration (mg/m^3) as a measure for nutrient availability, dissolved inorganic carbon (DIC) concentration (µmol/kg), and Total Alkalinity (TAlk) levels (µmol/kg).

	Vulnerability range and conditions				
	0 - 0.2	**0.2 - 0.4**	**0.4 - 0.6**	**0.6 - 0.8**	**0.8 - 1**
Chlorophyll-a (mg /m^3) & DIC (µmol/kg)	<1 & 1,840 – 2,347	>1 & 2,100 – 2,347	> 1 & 1,840 – 2,100	> 1 & 1,460 – 1,840	> 1 & 1,060 – 1,460
TAlk (µmol/kg)	2,450 – 2,400	2,400 – 2,350	2,350 – 2,300	2,300 – 2,250	2,250 – 2,200

Vulnerability to acidification

The derived monthly TAlk values were aggregated to seasonal mean (same season as chlorophyll-a concentration) levels. A TAlk level around the global mean, 2,300 – 2,350 µmol/kg, was classified as 'medium' vulnerability to acidification with a score range '0.4 – 0.6'. TAlk values below this range have a lower acid-neutralizing capacity and therefore the vulnerability score increased with increments of 50 µmol/kg to a maximum score of 1.0 at TAlk 2,200 µmol/kg. The same approach was followed in the opposite direction, where the vulnerability score was reduced with increments of 50 µmol/kg to a minimum vulnerability score of 0 at 2,450 µmol/kg (Table 5.2).

Vulnerability assessment

The vulnerability to algal bloom (chlorophyll-a and DIC) and acidification (TAlk level) were given equal weights (0.5). The final per-pixel (1x1 km) vulnerability score (*Overall Vuln*) could be computed by summation of the weight (*0.5*) of each indicator (TAlk and Chlorophyll combined with background DIC level (Chlo. _DIC)) multiplied by the vulnerability score (*S*) of each indicator, as (eq.4):

$$Overall\ Vuln = S(TAlk) \times 0.5 + S(Chlo.\_DIC) \times 0.5 \qquad \text{(eq.4)}$$

5.2.4 Relative risk assessment

The relative risk level of each ecoregion to acidification and algal bloom was characterized by plotting the DIC exposure level via maritime shipping against the vulnerability score. The ecoregions with relatively high increased DIC concentrations and higher vulnerability scores are considered as higher risk than the ecoregions with lower increased DIC concentrations and vulnerability scores.

The 262 global ecoregions and 144 European sub-ecoregions were mapped and assigned with code numbers. On this map, the layer with the average DIC exposure level via maritime shipping and the average seasonal vulnerability to algal bloom and acidification of each region were mapped. Also, the specific DIC exposure level and vulnerability scores for algal bloom and acidification of individual ecoregion can be found via their code numbers.

5.3. Results

5.3.1 Ship intensity and emitted CO_2

The worldwide total CO_2 emission via marine transportation in 2018 was estimated at 1,389 million tonnes under a worst-case-scenario (based on the upper emission factor from Table 5.1) (Figure 5.3). The emissions per grid cell were relatively low in the open sea due to the high dispersion of shipping lanes. Contrastingly, high emissions per grid cell were found at dense shipping lanes in coastal areas. Between 1,549 and 12,734 tonnes of CO_2 were emitted per grid cell in the top 5% busiest ship areas (Figure 5.3). The highest CO_2 emission per grid cell was estimated for the Strait of Gibraltar at 12,734 tonnes, closely followed by other maritime chokepoints such as the Panama Canal, the Malacca Strait, the Strait of Hormuz and the Danish Straits (Figure 5.3).

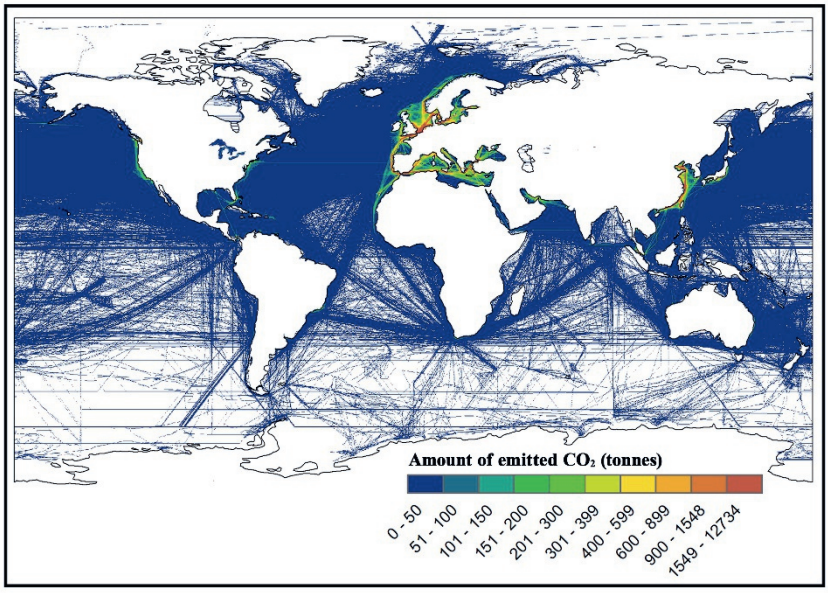

Figure 5.3 The estimated total amount of CO_2 (tonnes) emitted from shipping in 2018. The estimation was based on a worst-case-scenario by using the upper emission factors from Table 5.1. Colours indicate the estimated CO_2 amount emitted in each 1 km^2 grid cell.

5.3.2 DIC exposure assessment

The background and saturated DIC concentrations in this study were set at 2.07 mmol/l and 3.97 mmol/l respectively and the temperature was set at 20 °C. Thus, a maximum of 1.90 mmol/l DIC can be added via CO_2 exposure. The estimated added DIC concentration steeply went up with increasing number of ships per 24 hours until after the ninth ship the concentration reached 1.61 mmol/l, so still below the maximum level of 1.90 mmol/l) (Figure 5.4). From then on, the added DIC concentration levelled off at around 1.61 - 1.90 mmol/l regardless of the shipping frequency. Therefore, we assumed that after 9 ships, more volume of water started to experience an increase in the DIC level. With less than 9 ships passing by,

the volume of impact water remained ≤ 17 m^2 of the grid cell (Table 5.3). In the highest shipping intensity grid cell (134 ships/24 hours), 228 m^2 water of the 1 km^2 grid cell (0.023% of the grid cell) reached a saturated DIC level.

Approximately 70% of the grid cells (with registered ships) in the open sea experienced a DIC increase between 0.15 - 0.22 mmol/l, corresponding to less than one ship per 24 hours, since 1 ship/24 hour already can increase 0.51 mmol/l DIC level (Figure 5.5). High average DIC exposure (0.52 – 1.9 mmol/l, were located along with European, Chinese and North American coastlines. Eventually, ecoregions along European coastlines were selected to run a zoomed-in local relative risk assessment (Section 5.3.4).

Table 5.3 The relationship between the number of ships (nr. ships) passing through a 1km^2 grid cell during 24 hours and the part (total m^2 and %) of the 1 km^2 grid cell that will be completely DIC saturated. The total impacted area will be larger (not fully DIC saturated).

Ships nr.	≤ 9	10	20	30	60	90	120	134
DIC saturated area (m^2)	≤ 17	19	34	51	102	153	204	228
% of 1 km^2 grid cell	0.002	0.002	0.003	0.005	0.010	0.015	0.020	0.023

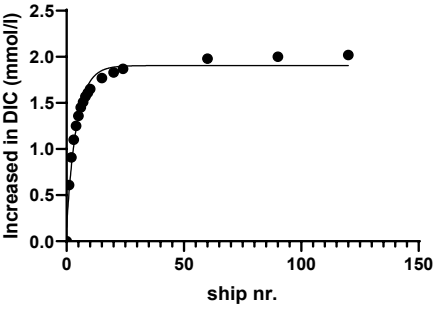

Figure 5.4 The correlation of increased in DIC level (mmol/l) and the number of ships (ship nr.) passing through a 1 km^2 grid cell during 24 hours. Assumptions: 1) all CO_2 produced by the ship(s) is emitted underwater and immediately dissolves and 2) the background and saturation DIC levels of the local water are 2.07 mmol/l and 3.97 mmol/l, respectively, therefore the maximum increase in DIC level is 1.90 mmol/l.

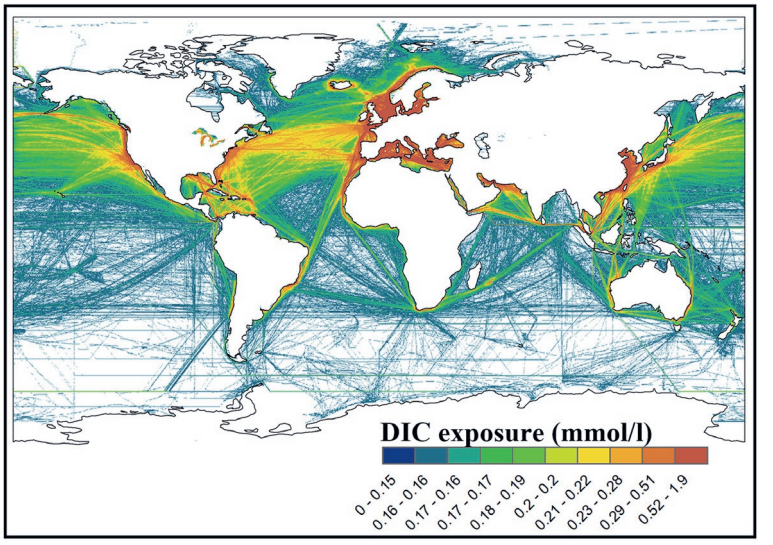

Figure 5.5 Estimated dissolved inorganic carbon (DIC) exposure (mmol/l) per 24 hours from global shipping, assuming 100% underwater exhaust emission. The scale maximum is restricted by the maximum dissolved CO_2 saturation level. Colours indicate DIC exposure level in each 1 km^2 grid cell.

5.3.3 Vulnerability assessment

The spatial distribution of global ocean vulnerability to algal blooms in 2018 was studied based on chlorophyll-a concentration with the background DIC level, and its vulnerability to acidification was evaluated based on the TAlk level. For the 'chlorophyll-a and background DIC', almost all vulnerability score ≥ 0.5 areas were located around the coastal lines of the Northern Hemisphere (S 5.3 and S 5.4). Contrastingly, almost the entire Southern Hemisphere showed a vulnerability score ≤ 0.2, except the coastline along with Argentine with scores between 0.5 - 0.6 (S 5.3 and S 5.4). For the TAlk level, areas with > 2,500 µmol/kg TAlk were found in the Atlantic Ocean (S 5.5). While the Pacific Ocean, especially along its coastlines, showed a lower TAlk level (higher vulnerability) compared with other oceans. More seasonal variation seems to occur in the Northern Hemisphere than it does in the South.

After combining all the vulnerability scores, the high vulnerability areas to both acidification and algal blooms were mainly found in coastal areas and above 30° N latitude till the ice edge (Figure 5.6). The sea ice areas (polar zone) are not being considered in discussion and conclusion due to the missing data in the input datasets (Figure 5.6). A seasonal impact on the results was observed within the same region, with higher vulnerability scores in the warm season than for the cold season (Figure 5.6 and S 5.6).

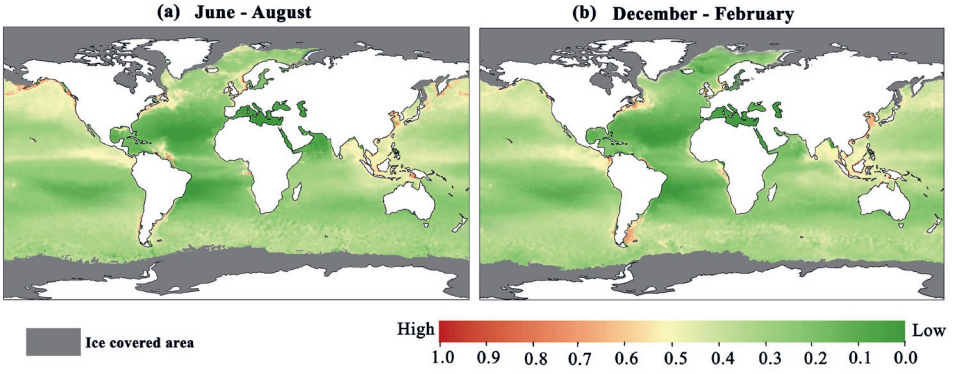

Figure 5.6 Spatial distribution of vulnerability to algal blooms and acidification in surface layers of the global oceans in June – August (a), and December - February (b) of 2018. Colours show gridded values based on a merge of three vulnerability indicators, chlorophyll-a & DIC and TAlk as presented in Table 5.2.

5.3.4 Relative risk assessment

Over 90% of the global ecoregions showed a DIC exposure level < 0.48 mmol/l and a vulnerability score to acidification and algal blooms < 0.5 (Figure 5.7). The Yellow Sea and Southern China Sea showed relatively higher risk than other areas in all seasons (Figure 5.7, S 5.7, S 5.8 and S 5.9). Next in line is the North Sea, which is exposed to over 0.95 mmol/l DIC by maritime emissions, and a relatively highly vulnerable score close to 0.5 especially during June – August. Seasonal variation in shipping intensity was not included in this study. Therefore, the DIC exposure level of each region was consistent over the year. The seasonal variation of global risk was therefore only influenced by the seasonal vulnerability score (Figure 5.6 and Figure 5.7).

When looking at a more detailed level to Europe, it becomes clear that the relatively high risk that was predicted for this ecoregion only concerns areas with dense shipping lanes and maritime chokepoints, such as the Strait of Dover and the Strait of Gibraltar (Figure 5.8). The biggest seasonal increase in the relative risk could be observed in coastal areas of the Celtic Seas, the Saharan Upwelling, and the South European Atlantic Shelf in spring and summer (Figure 5.8, S 5.10, S 5.11 and S 5.12).

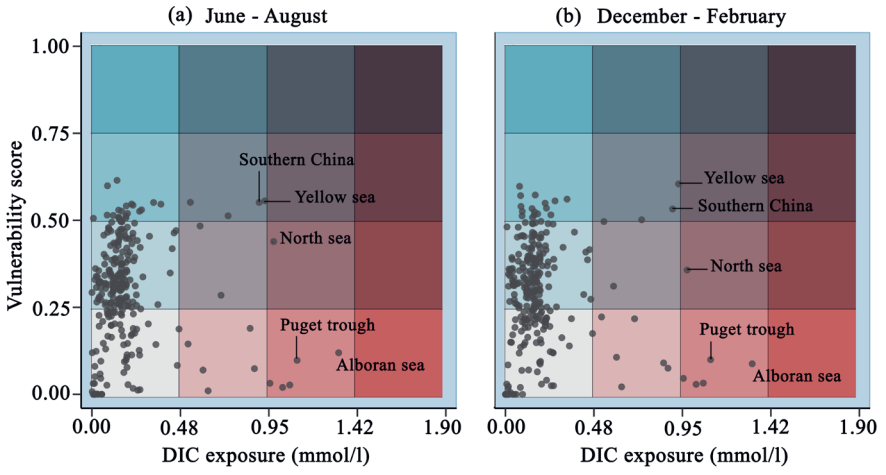

Figure 5.7 Plot of the vulnerability scores of 262 global maritime ecoregions to algal blooms and acidification and the estimated DIC exposure (mmol/l) by shipping in June - August (a) and December – February (b). Assumption: all ships would be equipped with underwater exhaust systems. The colour intensity indicates the vulnerability score (blue) and increase in DIC level (red) combined into a relative risk level from low (light grey) to high (blue/red).

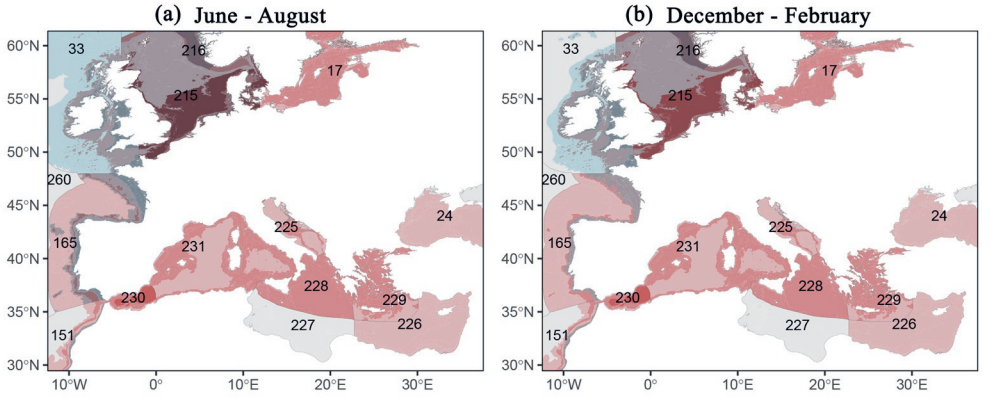

Figure 5.8 Spatial distribution of the relative risk for algal blooms and acidification in the 15 European marine ecoregions (global ecological codes: 17, 24, 33, 151, 165, 215, 216, 225, 226, 227, 228, 229, 230, 231, and 260 (Spalding et al., 2007) in June – August (a), and December – February (b). Colours show gridded values from plotting vulnerability scores against DIC exposure caused by maritime shipping emitting CO_2 underwater. The vulnerability score and DIC exposure level of each ecoregion are presented in the separate table (S 5.12). The colours in this map are corresponding with the colours in Figure 5.7. Thus, the colour intensity indicates the vulnerability score (blue) and increase in DIC level (red) combined into a relative risk level from low (light grey) to high (blue/red).

5.4. Discussion

In the presented study an assessment was made of the relative risk that a local marine environment is negatively impacted by the application of underwater released exhaust gas as 'air lubrication' along the ship's hull. High nutrient availability potentially inducing algal blooms or low buffering capacity potentially resulting in acidification were used as indicators of environmental vulnerability. Following a worst-case exposure scenario, it is assumed that all ships will be equipped with underwater exhaust systems and that all emitted CO_2 is absorbed by the water. Based on this a first-tier risk environmental assessment was performed for 262 ecoregions.

5.4.1 Shipping emitted CO_2 and DIC exposure

The worldwide CO_2 emission from marine shipping was extrapolated from data of 2013 to be 1,389 million tonnes in 2018. This number can be considered as the worst case, as current developments suggest a lower growth of CO_2 emission. IMO predicted the CO_2 emission to grow 50% - 250% (to 1,194 – 2,786 million tonnes) by 2050, but estimated that emission < 900 million tonnes CO_2 in 2018 (IMO, 2015). In our study, we also used the upper emission factors from Table 1 which also contribute to a worst-case-scenario of the emitted CO_2 amount. If the amount of shipping emitted CO_2 would continue to increase in the future as predicted, the DIC exposure (concentration and surface size) via underwater exhaust gas will increase as well. For the amount of emitted CO_2 in an individual grid cell, our calculation used the average travel distance in that cell (0.7 km). This was not according to a worst-case-scenario, since the longest travel distance to pass a 1 x 1 km grid cell is over its full diagonal, so 1.41 km. Using the average travel distance in the calculation leads to the amount of CO_2 emission per grid cell closer to the real conditions, especially from the ecoregion perspective, which consists of many grid cells.

In this study, we excluded the effect of water currents, and thus the transport and dilution of the dissolved CO_2 that result from that. It can therefore be assumed that our calculations overestimate the volumes of water where the maximum area DIC saturation level will be reached while we underestimate the volume of water that is exposed to lower (diluted) CO_2 concentrations. We also assumed that all emitted CO_2 will be completely dissolved in the water, whereas in reality it may be expected that some will escape to the atmosphere. The maximum DIC exposure levels calculated here are worst-case estimations. These and several other aspects need to be taken into account in further refinement of the exposure assessment for areas where the DIC levels are indicated to become a potential problem. Especially the size of the impacted area with water currents, the ship's speed, the water mixing depth (here set at 5 m depth) and the extent to which the underwater released exhaust CO_2 is likely to fully dissolve in the water or will partially immediately escape to the atmosphere with gas bubbles. The dissolving of CO_2 gas in water phases involves a series of reactions (Zeebe & Wolf-Gladrow, 2001) , which takes time and has a saturation level assuming a static situation.

For refining the exposure assessment, also the assumed DIC saturation level should be further fine-tuned. The current exposure assessment is based on a single water condition (20 ˚C, 31.7‰ salinity and 2.07 mmol/l alkalinity) without primary production. The background and saturation level of DIC, however, are influenced by the water conditions, such as temperature, salinity, and algal productivity (Markou et al., 2014; Zeebe &Wolf-Gladrow, 2001). If a

specific water condition is known, a prediction of the DIC exposure level can be made based on the presented approach. For example, between July - August, Chukchi Sea shelves experience relatively high-water temperature (-1.5 to + 7 ℃) and phytoplankton production. Thus, it is expected that the background DIC level in this area is lower than in the cold season and also than the background DIC level assumed in this study. Indeed, the reported background DIC level in part of this area is even below 0.6 mmol/l DIC in July – August (Bates et al., 2005).

5.4.2 Vulnerability assessment

Areas vulnerable to acidification and algal blooms are mostly the subtropical ecotypes, especially near coastal regions and in warm seasons (e.g. East China seas in June - August and south coastline of Argentina in December – February). This distribution can mostly be attributed to the high vulnerability for algal blooms around nutrient rich nearshore areas (S 5.3). Algal blooms are shown to exacerbate in eutrophic areas during seasonal warming (Lee et al., 2006; J K Moore & Abbott, 2000). Anthropogenic nutrients input along the coastline and at large river mouths, e.g. from aquaculture, runoff, sewage and other point-source pollution, is the main driver to create those eutrophic conditions (Halpern et al., 2015).

Other areas with high vulnerability scores (> 0.7) are mainly located above 30°N latitude. L Q Jiang et al. (2015) reported similar results when they identified the vulnerability of the global oceans to acidification via aragonite saturation state, which decreased toward higher latitude after 40°. They attribute this latitudinal gradient to the water temperature influenced change in TAlk/DIC ratio. In our study, the overall high vulnerability scores above 40° latitudes are mainly caused by the low TAlk level in those regions, thus high vulnerability to acidification as well. TAlk is mainly reflected by SSS (sea surface salinity) changes instead of SST (sea surface temperature) (Lee et al., 2006). Low TAlk usually results from low large influxes of freshwater through ice melting (sea ice edge) and through river outflows (e.g. the Amazon, the Congo River and the Bay of Bengal), or where precipitation exceeds evaporation (Buis et al., 2011). Therefore, TAlk levels generally are lower at higher altitudes and usually show high seasonal variation. Another seasonal variable in TAlk was found in the Northern Hemisphere more than in the Southern Oceans (Rana A. Fine et al., 2015), namely due to high salinity variability and active water currents that resulted in upwelling of water enriched in alkalinity during winter and autumn (Z P Jiang et al., 2014). Such a difference in seasonal impact between north and south was not found in the overall vulnerability distribution map that combines the TAlk with ‘chlorophyll -a and background DIC’ indicators.

It is important to be aware that the vulnerability of areas may change with time due to changes in anthropogenic activities and also due to climate change, especially towards the current ice-covered areas. Halpern et al. (2015) reported that a significant amount of ice was lost over the 5 years period of their study of the human impact on the world’s oceans, demonstrating that the water conditions near the polar zone are rapidly changing with time. Likewise, the estimation of vulnerable areas in the present study will be influenced by such large scale changes.

5.4.3 Potential impact assessment of underwater released exhaust CO_2

Ecoregions with a high estimated DIC exposure and vulnerability to algal blooms and acidification would be at risk according to our tier 1 relative risk assessment when all ships would be equipped with underwater exhaust systems. Globally, the Yellow Sea and the Southern China Sea were identified as the ecoregions with the relatively highest risk (relatively high exposure and vulnerability) in those 262 ecoregions, closely followed by the North Sea. There clearly would be hotspots of exposure in the busiest shipping traffic grid cell (134 ships/24 hours) in the Yellow Sea, Southern China Sea and the North Sea.). Based on this first tier potential impact assessment it cannot yet be concluded whether there will be a relatively small area with very high exposure or a larger area with a lower exposure but a greater total DIC increase. But in general terms, it is clear that in these ecoregions the relative risk via high exposure concentration and vulnerability score is high.

The European marine ecoregion risk assessment revealed high local exposure conditions. The result supports the conclusion of the global relative risk assessment that especially dense shipping lanes and maritime chokepoints determine the potential impact of the entire ecoregion. In the more detailed relative risk assessment, seasonal variation in risk was more apparent than in the global assessment. The seasonal variation in the European ecoregions can be attributed to the increased algal density during the warming period (March-August) (Lee et al., 2006; J K Moore & Abbott, 2000), as well as elevated TAlk concentrations in the North Sea and the Celtic Seas from February through May. The result suggests that risk assessment on smaller ecoregions can reveal specific local conditions that would be unnoticed at the global ecoregions level.

Further fine-tuning still can be achieved for the vulnerability assessment and potential impact assessment. For example, both global and local risk assessments in this study assume a linear response of the ecosystem to increased exposure level and vulnerability scores. However, most marine ecosystems exhibit synergistic and antagonistic responses to stressors instead of additive (Crain et al., 2008), which creates a nonlinear relationship of risk to exposure and vulnerability level. Also, the biological composition of each ecoregion would be relevant to consider, something we did not include in this study. Some nearshore locations dominated by coral reefs, such as the Australian Great Barrier reef, scored low on vulnerability or risk in this study but are quite vulnerable for elevated CO_2 concentrations (Ainsworth et al., 2016). Therefore, it is recommended to perform local risk assessments for specific ecoregions, also including the unique biological composition and water conditions of the studied regions to identify specific exposure-response relationships.

5.5. Conclusions

In this study, we carried out a first-tier relative risk assessment of potential future underwater released exhaust CO_2 from merchant ships on marine ecosystems. The relative risk of 262 marine ecoregions for enhanced algal blooms and acidification based on specific water conditions was combined with the predicted additional DIC exposure level for each ecoregion from the extra CO_2 exposure. Globally, relatively high-risk ecoregions were mainly located in the Northern Hemisphere, especially along coastlines, such as in the North Sea and Southern China sea. Those regions combine high shipping frequencies with high vulnerability to CO_2 induced algal blooms and acidification. In this study, worst-case

exposure-scenarios were applied, that need to be refined to better assess the impacted water volume and area and the maximum DIC level that could be reached. Furthermore, this study paves the path for ongoing risk assessment of underwater released exhaust CO_2 when more information becomes available. In addition, this approach could be used for sensitivity assessment of ecoregions for future elevated CO_2 levels, and can be further refined by including additional important parameters, such as the biological composition of the ecosystem and the magnitude and influence of water mixing. For sure it already indicates areas that deserve further attention.

Acknowledgments

This research was funded from the project 'GasDrive: Minimizing emissions and energy losses at sea with LNG combined prime movers, underwater exhausts and nano hull materials' (project 14504) of the Netherlands Organization for Scientific Research, domain Applied and Engineering Sciences (TTW). The authors wish to thank Mr. Achmad Sahri (MSc) for technical support in using the ArcGIS program.

Data Availability Statement

The datasets of 232 Marine Ecoregions of the World were collected from The Nature Conservancy's Geospatial Conservation Atlas via link: https://geospatial.tnc.org/datasets/ed2be4cf8b7a451f84fd093c2e7660e3_0?geometry=58.359%2C-89.110%2C-58.359%2C87.258. The 30 Marine Ecoregions and Pelagic Provinces of the World were collected from UNEP's Ocean Data Viewer: https://data.unep-wcmc.org/datasets/38. Chlorophyll-a data were collected from NASA's Aqua-MODIS satellite for each calendar month of 2018 via link:https://oceancolor.gsfc.nasa.gov/data/10.5067/AQUA/MODIS/L3M/CHL/2018/. Sea Surface Salinity (SSS) data were collected from NASA's JPL SMAP satellite (https://doi.org/10.5067/SMP42-3TMCS). Sea Surface Temperature (SST) data were collected from NOAA's Coral Reef Watch satellites for each calendar month of 2018 (https://data.nodc.noaa.gov/cgi-bin/iso?id=gov.noaa.nodc:AVHRR_Pathfinder-NODC-L3C-v5.2;view=html). A ship traffic intensity map developed by Halpern et al. (2015) was collected from the Knowledge Network for Biocomplexity (https://knb.ecoinformatics.org/view/doi:10.5063/F19Z92TW).

5.6 Supplementary material for Chapter 5

S 5.1 The 15 marine ecoregions of Europe (a) and their bathymetry depth classes (b).

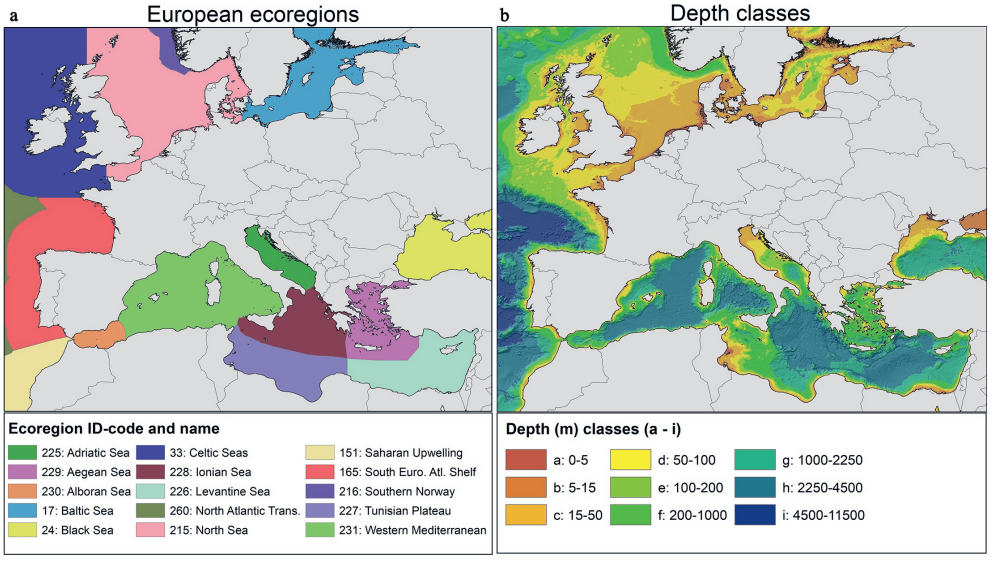

S 5.2 The average travel distance of a ship through a 1 km^2 grid cell

Given the large distances that ships travel and the assumption that mariners prefer great circle distances (Halpern et al., 2015), it was assumed that ship routes were straight from their entry point in a grid cell to their exit point in that grid cell. With straight routes, the maximum distance a ship could travel to pass through a grid cell (1 km x 1 km) is the maximum diagonal distance, so about 1.4 km. A random float number between 0 and 1.4 was generated for each vessel (94169 total). The mean of the randomly generated numbers is 0.7, which represented the average distance a ship travels to pass through a grid cell.

S 5.3 Distribution of global chlorophyll-a concentration (mg/m^3) in four seasons. Colours indicate the values of the chlorophyll-a concentration in each 1 km^2 grid cell.

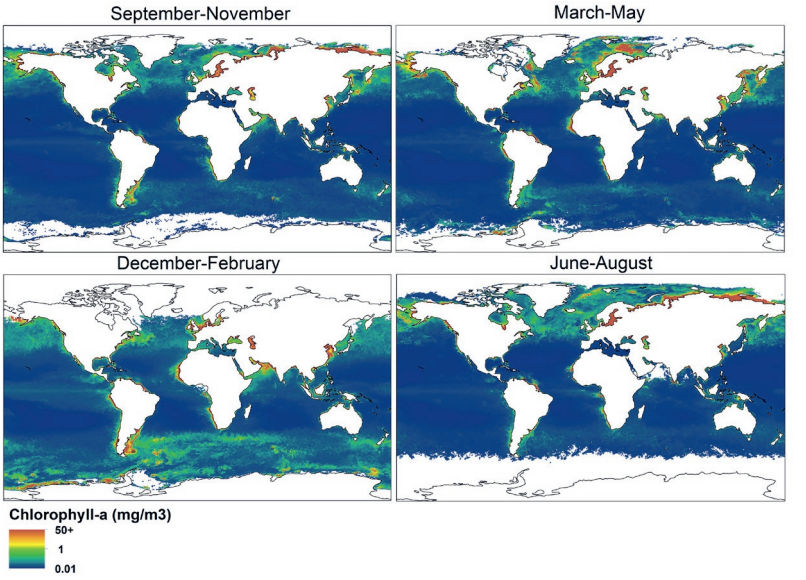

S 5.4 The global yearly average dissolved inorganic carbon (DIC) background concentration (µmol/kg) indicated with colours per 1 km^2 grid cell.

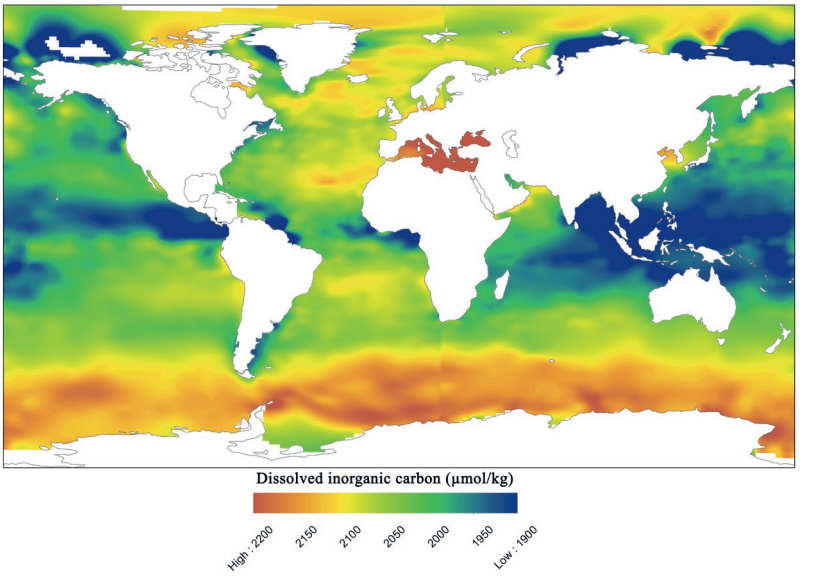

5.5 Distribution of the global total alkalinity (TAlk) level (µmol/kg) in four seasons, indicated with colours per 1 km^2 grid cell.

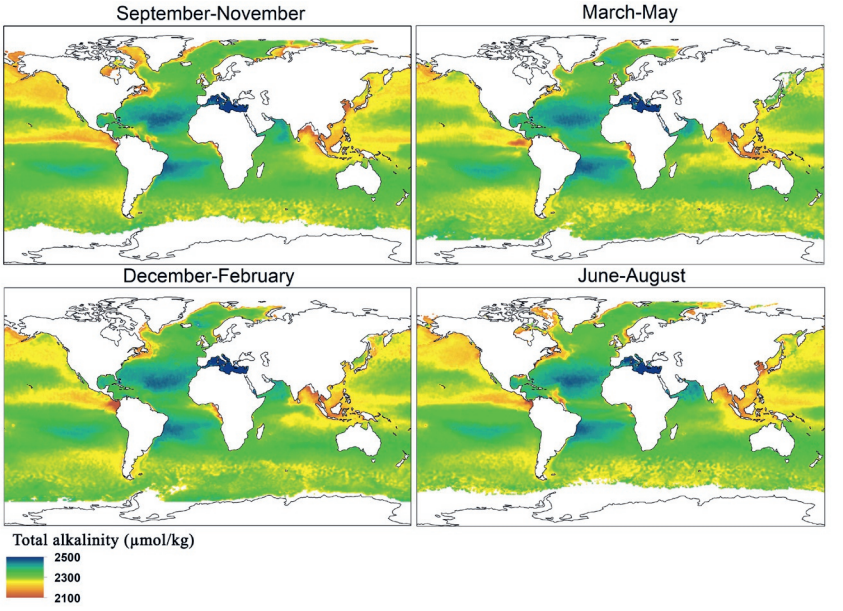

S 5.6 Global distribution of vulnerability to algal blooms and acidification in four seasons. Colours show gridded values based on a merge of three vulnerability indicators, chlorophyll-a & background DIC and TAlk.

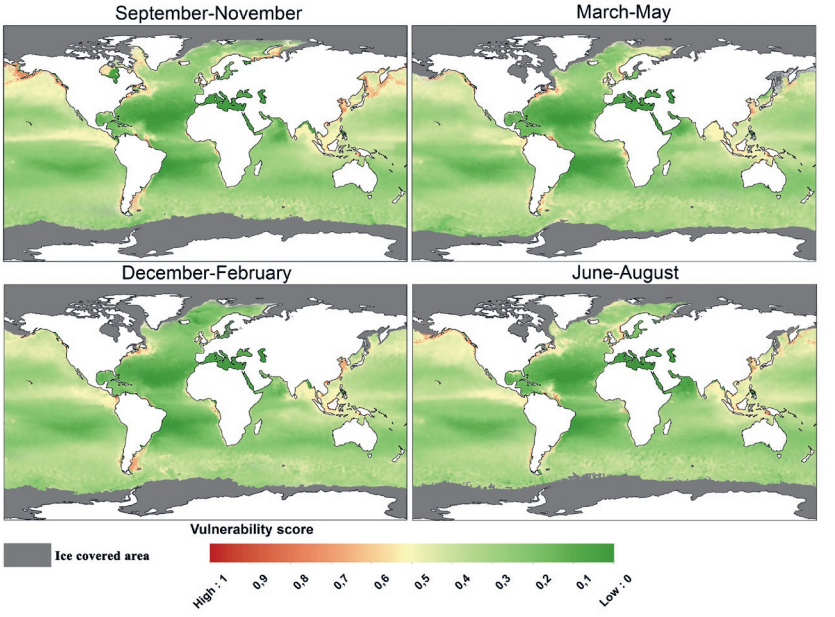

S 5.7 Plot of the vulnerability of 262 global ecoregions for algal blooms and acidification following predicted extra DIC exposure (mmol/l) from maritime shipping with underwater released CO_2, in four seasons. The colour intensity indicates the vulnerability score (blue) and increase in DIC level (red) and risk from low (light grey) to high (blue/red). The data underlying these plots can be found in Table S 5.9.

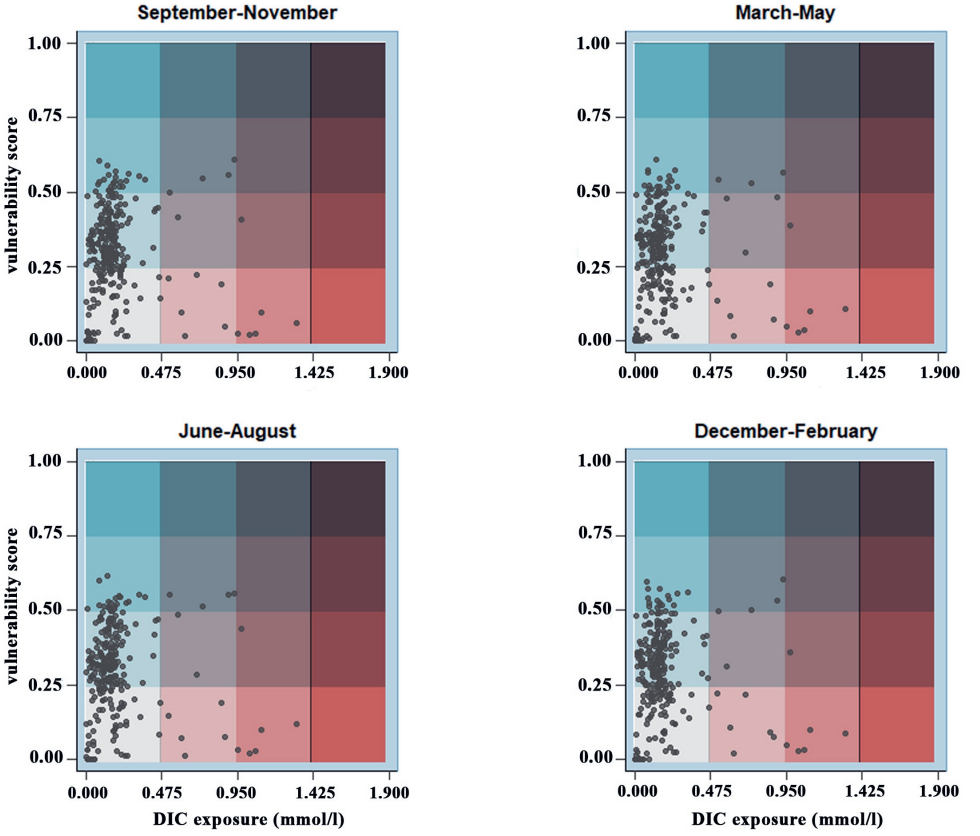

S 5.8 Map of the vulnerability of 262 global ecoregions for algal blooms and acidification following predicted extra DIC exposure (mmol/l) from maritime shipping with underwater released CO_2, in four seasons.

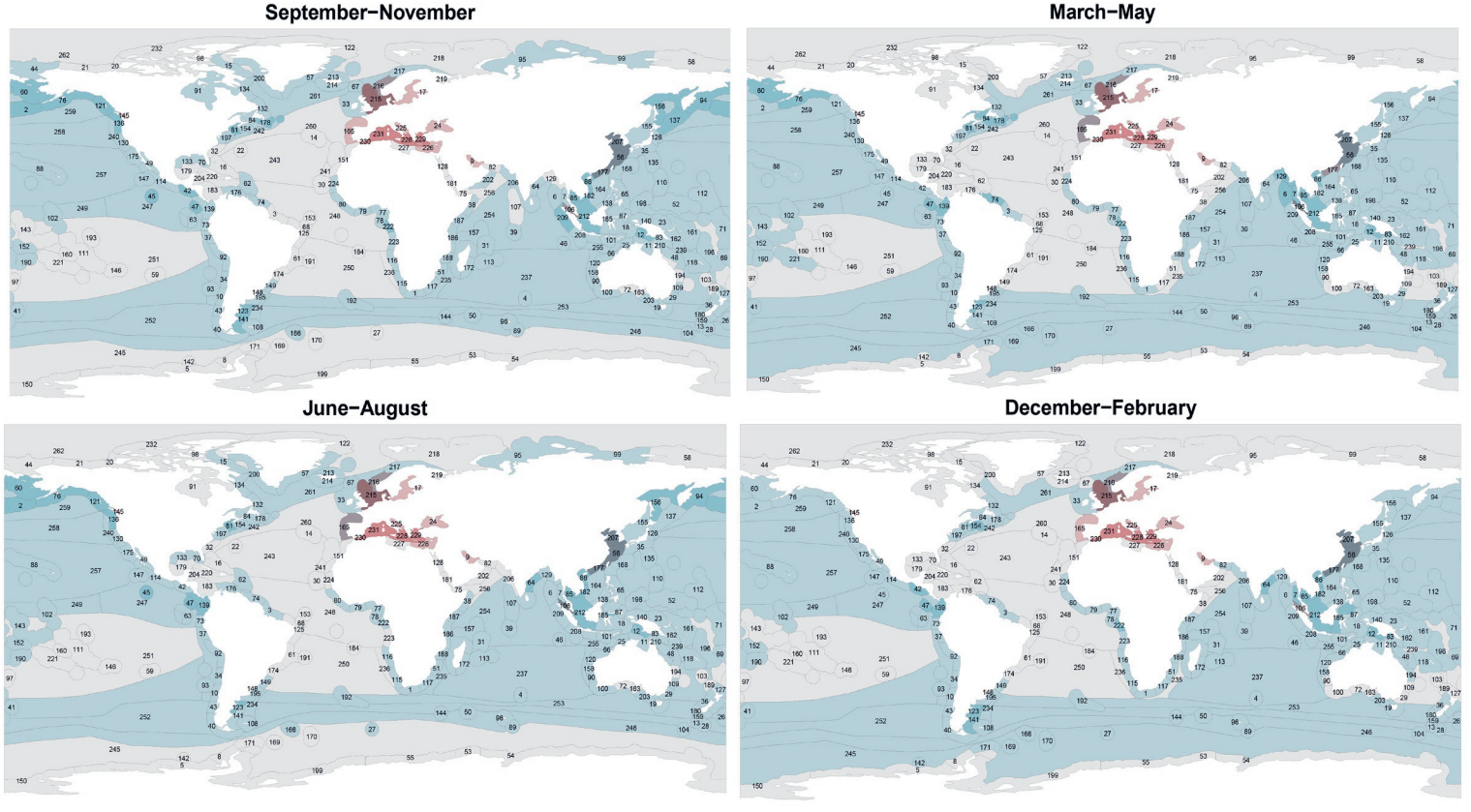

S 5.9 Predicted extra DIC Exposure level and vulnerability scores of the 262 global ecoregions in four seasons. The risk for adverse effects from maritime shipping with underwater released CO_2, as also presented in Figures S 5.7 and S 5.8, can be calculated by multiplying exposure with vulnerability.

Code	Ecoregion	DIC exposure (mmol/l)	Vulnerability to algal blooms and acidification			
			Sep. - Nov.	Mar. - May	Jun. - Aug.	Dec. - Feb.
1	Agulhas Bank	0.1821	0.3371	0.2977	0.3153	0.3023
2	Aleutian Islands	0.1822	0.5338	0.4626	0.5124	0.4496
3	Amazonia	0.1607	0.2385	0.2768	0.2710	0.2574
4	Amsterdam-St Paul	0.0479	0.2730	0.2635	0.2713	0.2721
5	Amundsen/Bellingshausen Sea	0.0135	0.0018	0.0407	0.0000	0.0845
6	Andaman and Nicobar Islands	0.1063	0.4714	0.5086	0.4944	0.4935
7	Andaman Sea Coral Coast	0.0904	0.3930	0.5202	0.4756	0.5254
8	Antarctic Peninsula	0.0509	0.0249	0.1829	0.0003	0.1921
9	Arabian (Persian) Gulf	0.5160	0.2117	0.1340	0.1447	0.2223
10	Araucanian	0.1559	0.4964	0.4960	0.4959	0.4587
11	Arnhem Coast to Gulf of Carpenteria	0.1249	0.3701	0.4866	0.4317	0.4188
12	Arafura Sea	0.0834	0.5334	0.5745	0.5992	0.5399
13	Auckland Island	0.0384	0.3289	0.3472	0.3231	0.3534
14	Azores Canaries Madeira	0.2562	0.0992	0.1385	0.1127	0.1190
15	Baffin Bay - Davis Strait	0.0920	0.4000	0.0000	0.3560	0.0000
16	Bahamian	0.2534	0.1301	0.1156	0.1264	0.1200
17	Baltic Sea	0.8491	0.1896	0.1898	0.1895	0.0902
18	Banda Sea	0.4112	0.4112	0.4880	0.4734	0.4563
19	Bassian	0.1018	0.3106	0.3046	0.2880	0.3065
20	Beaufort-Amundsen-Viscount Melville-Queen Maud	0.0069	0.0294	0.0000	0.0310	0.0000
21	Beaufort Sea - continental coast and shelf	0.0154	0.0886	0.0000	0.0804	0.0000
22	Bermuda	0.0884	0.0884	0.0909	0.1054	0.0872
23	Bismarck Sea	0.1321	0.3997	0.3935	0.3802	0.4005
24	Black Sea	0.5963	0.0943	0.0833	0.0697	0.1065
25	Bonaparte Coast	0.1399	0.4064	0.4955	0.4658	0.4534
26	Bounty and Antipodes Island	0.0372	0.3239	0.3525	0.3209	0.3618
27	Bouvet Island	0.0403	0.1693	0.3241	0.2800	0.3135
28	Campbell Island	0.0746	0.3289	0.3554	0.3159	0.3553
29	Cape Howe	0.1921	0.2928	0.2544	0.2680	0.2492
30	Cape Verde	0.1703	0.1513	0.1790	0.1423	0.1759

31	Cargados Carajos/Tromelin Island	0.1156	0.2912	0.3451	0.3191	0.3061
32	Carolinian	0.3027	0.1873	0.1712	0.2023	0.1627
33	Celtic Seas	0.4201	0.3115	0.3670	0.3486	0.2867
34	Central Chile	0.1759	0.3623	0.3383	0.3482	0.3521
35	Central Kuroshio Current	0.4310	0.4358	0.3927	0.4185	0.4087
36	Central New Zealand	0.1420	0.3565	0.3430	0.3286	0.3351
37	Central Peru	0.1455	0.2887	0.3447	0.2605	0.3286
38	Central Somali Coast	0.1026	0.2598	0.2395	0.2633	0.2143
39	Chagos	0.1192	0.3260	0.3569	0.2993	0.3846
40	Channels and Fjords of Southern Chile	0.0688	0.3861	0.3580	0.3418	0.3827
41	Chatham Island	0.0732	0.3236	0.3261	0.3039	0.3208
42	Chiapas-Nicaragua	0.1734	0.5314	0.4300	0.4679	0.5185
43	Chiloense	0.0834	0.4856	0.4680	0.4651	0.4549
44	Chukchi Sea	0.0383	0.3632	0.0671	0.2267	0.0000
45	Clipperton	0.1474	0.5073	0.4388	0.5031	0.4900
46	Cocos-Keeling/Christmas Island	0.1290	0.3859	0.4050	0.4144	0.3964
47	Cocos Islands	0.1449	0.5076	0.5170	0.5073	0.5079
48	Coral Sea	0.1628	0.2519	0.2919	0.2667	0.2989
49	Cortezian	0.1180	0.3426	0.3424	0.3335	0.3864
50	Crozet Islands	0.0300	0.3561	0.3545	0.3374	0.3590
51	Delagoa	0.1529	0.2772	0.2334	0.2645	0.2555
52	East Caroline Islands	0.1175	0.4292	0.3890	0.4347	0.3888
53	East Antarctic Enderby Land	0.0533	0.0005	0.2073	0.0000	0.2144
54	East Antarctic Wilkes Land	0.0278	0.0084	0.1167	0.0010	0.1498
55	East Antarctic Dronning Maud Land	0.0323	0.0012	0.1449	0.0000	0.1490
56	East China Sea	0.7312	0.5451	0.5287	0.5127	0.5014
57	East Greenland Shelf	0.0985	0.3614	0.1594	0.2622	0.1413
58	East Siberian Sea	0.0017	0.1319	0.0000	0.1196	0.0000
59	Easter Island	0.0388	0.1959	0.1695	0.1957	0.1710
60	Eastern Bering sea	0.1348	0.5900	0.6094	0.6147	0.3546
61	Eastern Brazil	0.1935	0.0233	0.0271	0.0278	0.0292
62	Eastern Caribbean	0.2043	0.3217	0.1996	0.3285	0.1866
63	Eastern Galapagos Islands	0.1394	0.3635	0.3806	0.3386	0.4215
64	Eastern India	0.1430	0.4471	0.4882	0.5083	0.5336
65	Eastern Philippines	0.1541	0.3707	0.3796	0.3923	0.3913
66	Exmouth to Broome	0.1850	0.3473	0.3492	0.3574	0.3480

67	Faroe Plateau	0.1880	0.2715	0.2754	0.3527	0.1573
68	Fernando de Naronha and Atoll das Rocas	0.1655	0.1481	0.1759	0.1676	0.1483
69	Fiji Islands	0.1243	0.3076	0.3297	0.3122	0.3200
70	Floridian	0.3541	0.2605	0.1796	0.2577	0.2173
71	Gilbert/Ellis Islands	0.0473	0.3058	0.3121	0.3056	0.3122
72	Great Australian Bight	0.1041	0.2474	0.2174	0.2246	0.2186
73	Guayaquil	0.3737	0.3737	0.4469	0.3464	0.4546
74	Guianan	0.1583	0.4361	0.5010	0.4980	0.3460
75	Gulf of Aden	0.2138	0.2213	0.1442	0.1133	0.1965
76	Gulf of Alaska	0.1847	0.5476	0.5039	0.5413	0.4218
77	Gulf of Guinea Central	0.1834	0.3949	0.4054	0.3792	0.3123
78	Gulf of Guinea Islands	0.1543	0.3520	0.4159	0.3745	0.4616
79	Gulf of Guinea Upwelling	0.1766	0.3451	0.3464	0.3290	0.3400
80	Gulf of Guinea West	0.1851	0.3676	0.3081	0.3143	0.3961
81	Gulf of Maine/Bay of Fundy	0.2555	0.5379	0.5717	0.5259	0.4889
82	Gulf of Oman	0.4581	0.2150	0.2379	0.0831	0.2731
83	Gulf of Papua	0.0891	0.4640	0.5081	0.4790	0.5125
84	Gulf of St. Lawrence - Eastern Scotian Shelf	0.2148	0.4359	0.5541	0.4328	0.4267
85	Gulf of Thailan	0.5160	0.5160	0.5347	0.5467	0.5491
86	Gulf of Tonkin	0.2662	0.5603	0.5166	0.5300	0.5556
87	Halmahera	0.1424	0.3969	0.4526	0.4375	0.4406
88	Hawaii	0.1539	0.3114	0.3180	0.3175	0.2978
89	Heard and Macdonald Islands	0.0189	0.3411	0.3524	0.3612	0.3600
90	Houtman	0.1941	0.2546	0.2466	0.2541	0.2364
91	Hudson Complex	0.0580	0.3013	0.0087	0.2095	0.0001
92	Humboldtian	0.1533	0.2826	0.2824	0.2766	0.2937
93	Juan Fernandez and Desventuradas	0.0972	0.3460	0.3307	0.3495	0.3373
94	Kamchatka Shelf and Coast	0.1430	0.5569	0.4477	0.5293	0.3902
95	Kara Sea	0.0262	0.2701	0.0011	0.2652	0.0055
96	Kerguelen Islands	0.0365	0.3729	0.3737	0.3554	0.3875
97	Kermadec Island	0.1160	0.2247	0.2252	0.2364	0.2142
98	Lancaster Sound	0.0472	0.0287	0.0000	0.0458	0.0000
99	Laptev Sea	0.0000	0.2569	0.0000	0.2925	0.0000
100	Leeuwin	0.1495	0.2590	0.2432	0.2582	0.2461
101	Lesser Sunda	0.1533	0.4258	0.4551	0.4738	0.4303
102	Line Islands	0.1117	0.3052	0.2761	0.2928	0.2784

103	Lord Howe and Norfolk Islands	0.1597	0.2247	0.2214	0.2272	0.2156
104	Macquarie Island	0.0234	0.3023	0.3433	0.3071	0.3407
105	Magdalena Transition	0.1981	0.3782	0.4161	0.4472	0.3691
106	Malacca Strait	0.5285	0.4980	0.5413	0.5516	0.4962
107	Maldives	0.1525	0.2336	0.3262	0.2699	0.3208
108	Malvinas/Falklands	0.0685	0.4532	0.4164	0.3739	0.4801
109	Manning-Hawkesbury	0.2400	0.2537	0.2481	0.2555	0.2399
110	Mariana Islands	0.1626	0.3584	0.3432	0.3746	0.3380
111	Tuamotus	0.0852	0.1726	0.1775	0.1671	0.1812
112	Marshall Islands	0.1065	0.3973	0.3576	0.3856	0.3545
113	Mascarene Islands	0.1466	0.2876	0.3117	0.3060	0.2912
114	Mexican Tropical Pacific	0.2025	0.4304	0.3716	0.4086	0.4048
115	Namaqua	0.1701	0.3355	0.3076	0.3102	0.3221
116	Namib	0.1506	0.3507	0.3308	0.3490	0.3237
117	Natal	0.1859	0.2927	0.2490	0.2808	0.2656
118	New Caledonia	0.1459	0.2652	0.2900	0.2720	0.2810
119	Nicoya	0.1910	0.4508	0.4955	0.5197	0.4967
120	Ningaloo	0.1815	0.3047	0.3035	0.3081	0.2862
121	North American Pacific Fijordland	0.1828	0.5195	0.4615	0.5067	0.4046
122	North Greenland	0.0161	0.0287	0.0000	0.0509	0.0000
123	North Patagonian Gulfs	0.0815	0.6040	0.5640	0.5149	0.5707
124	Northeast Sulawesi	0.0082	0.4875	0.4912	0.5056	0.4810
125	Northeastern Brazil	0.1884	0.1015	0.1053	0.1137	0.0947
126	Northeastern Honshu	0.3092	0.4799	0.4601	0.4540	0.4223
127	Northeastern New Zealand	0.1439	0.2699	0.2538	0.2734	0.2416
128	Northern and Central Red Sea	0.2581	0.0164	0.0163	0.0134	0.0248
129	Northern Bay of Bengal	0.0648	0.2385	0.5231	0.4022	0.3177
130	Northern California	0.4516	0.4463	0.4319	0.4704	0.4158
131	Northern Galapagos Islands	0.1441	0.4640	0.4985	0.4434	0.4907
132	Northern Grand Banks	0.1619	0.4840	0.3574	0.4958	0.3898
133	Northern Gulf of Mexico	0.2384	0.2707	0.2302	0.2857	0.1951
134	Northern Labrador	0.1244	0.4523	0.0625	0.3905	0.0699
135	Ogasawara Islands	0.1653	0.3399	0.3111	0.3332	0.3261
136	Oregon Washintgon Vancouver Coast and Shelf	0.3703	0.5406	0.4868	0.5462	0.4660
137	Oyashio Current	0.1903	0.5696	0.4664	0.4803	0.4498
138	Palawan/North Borneo	0.1622	0.4968	0.4542	0.4750	0.4931

139	Panama Bight	0.1600	0.3804	0.5450	0.5263	0.5725
140	Papua	0.1001	0.4221	0.4221	0.4272	0.4248
141	Patagonian Shelf	0.0758	0.5259	0.4936	0.3936	0.5975
142	Peter the First Island	0.0169	0.0160	0.2466	0.0000	0.3105
143	Phoenix/Tokelau/Northern Cape	0.0716	0.2487	0.2648	0.2570	0.2484
144	Prince Edward Islands	0.0465	0.3541	0.3349	0.3226	0.3345
145	Puget Trough/Georgia Basin	1.1013	0.0973	0.0982	0.0977	0.0995
146	Rapa-Pitcairn	0.1041	0.2003	0.1877	0.1979	0.1913
147	Revillagigedos	0.1637	0.3931	0.3656	0.3746	0.3814
148	Rio de la Plata	0.3433	0.1422	0.1403	0.1432	0.1390
149	Rio Grande	0.1624	0.3256	0.2299	0.3183	0.2506
150	Ross Sea	0.0069	0.0017	0.0017	0.0000	0.0294
151	Saharan Upwelling	0.4674	0.1421	0.1892	0.1876	0.1746
152	Samoa Islands	0.1026	0.2999	0.3562	0.3397	0.3154
153	Sao Pedro and Sao Paulo Islands	0.1588	0.1903	0.1873	0.1841	0.2013
154	Scotian Shelf	0.2438	0.4584	0.4484	0.4417	0.5156
155	Sea of Japan/East Sea	0.1837	0.4930	0.3637	0.4476	0.3813
156	Sea of Okhotsk	0.1144	0.5408	0.3191	0.5139	0.2535
157	Seychelles	0.1127	0.2797	0.3017	0.2952	0.2940
158	Shark Bay	0.1806	0.2755	0.2876	0.2781	0.2610
159	Snares Island	0.0913	0.3428	0.3424	0.3150	0.3744
160	Society Islands	0.1031	0.1706	0.2339	0.1983	0.2044
161	Solomon Archipelago	0.0937	0.3671	0.3637	0.3574	0.3637
162	Solomon Sea	0.1581	0.3626	0.3845	0.3621	0.3748
163	South Australian Gulfs	0.1508	0.2470	0.2035	0.2005	0.2264
164	South China Sea Oceanic Island	0.2200	0.4808	0.4346	0.4628	0.4653
165	South European Atlantic Shelf	0.6932	0.2229	0.2965	0.2846	0.2171
166	South Georgia	0.0346	0.3372	0.4031	0.2744	0.3929
167	South India and Sri Lanka	0.1928	0.4184	0.4073	0.4003	0.4602
168	South Kuroshio	0.2244	0.3870	0.3539	0.3837	0.3691
169	South Orkney Islands	0.0438	0.1402	0.2871	0.0587	0.3225
170	South Sandwich Islands	0.0477	0.1153	0.3360	0.0953	0.2868
171	South Shetland Islands	0.0610	0.1716	0.3206	0.1466	0.2586
172	Southeast Madagascar	0.1510	0.2997	0.3134	0.3118	0.3041
173	Southeast Papua New Guinea	0.1577	0.3053	0.3704	0.3004	0.3681
174	Southeast Brazil	0.2403	0.1997	0.1206	0.1871	0.1225

175	Southern California Bright	0.2591	0.3945	0.4115	0.4219	0.3880
176	Southern Caribbean	0.2203	0.2906	0.1959	0.2653	0.2201
177	Southern China	0.8974	0.5569	0.4838	0.5514	0.5324
178	Southern Grand Banks	0.2290	0.5193	0.5361	0.4918	0.4902
179	Southern Gulf of Mexico	0.1914	0.1518	0.1404	0.1462	0.1475
180	South New Zealand	0.1266	0.3665	0.3587	0.3207	0.3787
181	Southern Red Sea	0.2207	0.0370	0.0363	0.0173	0.0407
182	Southern Vietnam	0.3308	0.5541	0.4933	0.5511	0.5607
183	Southwestern Caribbean	0.2162	0.2148	0.1618	0.1728	0.2076
184	St. Helena and Ascension Islands	0.0738	0.1270	0.0988	0.1302	0.1184
185	Sulawesi Sea/Makassar Strait	0.1540	0.4311	0.4998	0.4525	0.5148
186	East African Coral Coast	0.1156	0.2852	0.3197	0.3101	0.2986
187	Northern Monsoon Current Coast	0.0522	0.2739	0.2601	0.2877	0.2616
188	Bight of Sofala/Swamp Coast	0.1309	0.3060	0.3123	0.3130	0.2930
189	Three Kings-North Cape	0.1636	0.2354	0.2241	0.2421	0.2249
190	Tonga Islands	0.1148	0.2655	0.2982	0.2768	0.2879
191	Trindade and Martin Vaz Island	0.0801	0.0288	0.0172	0.0263	0.0198
192	Tristan Gough	0.0444	0.3067	0.3202	0.3239	0.3197
193	Marquesas	0.0901	0.2183	0.2163	0.2225	0.2081
194	Tweed-Moreton	0.2222	0.2374	0.2417	0.2309	0.2508
195	Uruguay-Buenos Aires Shelf	0.1451	0.4856	0.4240	0.4580	0.4654
196	Vanuatu	0.1134	0.3181	0.3378	0.3258	0.3299
197	Virginian	0.4408	0.4426	0.4325	0.4637	0.3864
198	West Caroline Islands	0.1409	0.4132	0.4139	0.4273	0.4166
199	Weddell Sea	0.0160	0.0008	0.0175	0.0000	0.0226
200	West Greenland Shelf	0.1195	0.4379	0.1908	0.3746	0.1640
201	Western and Northern Madagascar	0.1159	0.2877	0.3194	0.3118	0.3006
202	Western Arabian Sea	0.1883	0.2842	0.1323	0.0775	0.2306
203	Western Bassian	0.1217	0.2797	0.2692	0.2550	0.2765
204	Western Caribbean	0.2107	0.1813	0.1706	0.1691	0.2066
205	Western Galapagos Islands	0.1343	0.3413	0.3432	0.3161	0.3467
206	Western India	0.2298	0.2548	0.3089	0.1754	0.3452
207	Yellow Sea	0.9293	0.6075	0.5659	0.5557	0.6045
208	Southern Java	0.1017	0.4624	0.4656	0.4692	0.4533
209	Western Sumatra	0.0637	0.5010	0.4485	0.4572	0.4515

210	Torres Strait Northern Great Barrier Reef	0.1501	0.2896	0.3837	0.3000	0.3676
211	Central and Southern Great Barrier Reef	0.1869	0.2431	0.3183	0.2551	0.2980
212	Sunda Shelf/Java Sea	0.2201	0.5326	0.5150	0.5434	0.5348
213	North and East Iceland	0.1364	0.3119	0.3014	0.3413	0.2061
214	South and West Iceland	0.1960	0.3213	0.2834	0.3857	0.2129
215	North Sea	0.9756	0.4092	0.3882	0.4389	0.3571
216	Southern Norway	0.5805	0.4161	0.4794	0.4837	0.3107
217	Northern Norway and Finnmark	0.2736	0.4113	0.3883	0.3373	0.2512
218	North and East Barents Sea	0.0816	0.1974	0.1901	0.2404	0.1353
219	White Sea	0.0878	0.2347	0.0975	0.2334	0.0688
220	Greater Antilles	0.2214	0.2431	0.1697	0.1892	0.2185
221	Southern Cook/Austral Islands	0.0992	0.2199	0.2672	0.2470	0.2372
222	Gulf of Guinea South	0.1561	0.5170	0.5192	0.4972	0.5240
223	Angolan	0.1557	0.2669	0.4565	0.2315	0.3824
224	Sahelian Upwelling	0.2621	0.2824	0.3818	0.2454	0.3641
225	Adriatic Sea	0.8724	0.0499	0.0718	0.7386	0.0751
226	Levantine Sea	0.6236	0.0162	0.0170	0.0101	0.0214
227	Tunisian Plateau/Gulf of Sidra	0.2461	0.0167	0.0169	0.0118	0.0247
228	Ionian Sea	1.0237	0.0207	0.0267	0.0199	0.0288
229	Aegean Sea	1.0622	0.0236	0.0354	0.0268	0.0322
230	Alboran Sea	1.3245	0.0619	0.1068	0.1194	0.0877
231	Western Mediterranean	0.9553	0.0234	0.0479	0.0319	0.0457
232	High Arctic Archipelago	0.0013	0.0003	0.0001	0.0077	0.0000
233	Humboldt Current	0.1148	0.3112	0.2839	0.3048	0.3010
234	Malvinas Current	0.0708	0.3684	0.3991	0.3192	0.4024
235	Agulhas Current	0.1305	0.2635	0.2373	0.2637	0.2378
236	Benguela Current	0.1242	0.2470	0.2030	0.2350	0.2194
237	Indian Ocean Gyre	0.0744	0.2599	0.2532	0.2636	0.2542
238	Leeuwin Current	0.1522	0.2964	0.2773	0.2979	0.2727
239	Non-gyral Southwest Pacific	0.1540	0.2571	0.2458	0.2548	0.2440
240	California Current	0.2180	0.4597	0.3943	0.4514	0.4149
241	Canary Current	0.1831	0.0850	0.0920	0.0977	0.0917
242	Gulf Stream	0.2325	0.3089	0.3155	0.3115	0.3088
243	North Central Atlantic Gyre	0.1711	0.0632	0.0647	0.0627	0.0645
244	Kuroshio	0.4222	0.4222	0.3590	0.3937	0.3807
245	Antarctic	0.0224	0.1120	0.2570	0.1236	0.2667

246	Antarctic Polar Front	0.0169	0.3239	0.3427	0.3295	0.3454
247	Eastern Tropical Pacific	0.1207	0.4073	0.3874	0.3884	0.3973
248	Equatorial Atlantic	0.1218	0.2036	0.1853	0.2027	0.1924
249	Equatorial Pacific	0.1015	0.3628	0.3286	0.3463	0.3329
250	South Central Atlantic Gyre	0.1050	0.1642	0.1443	0.1639	0.1483
251	South Central Pacific Gyre	0.0830	0.2255	0.2282	0.2309	0.2227
252	Subantarctic	0.0227	0.3359	0.3565	0.3392	0.3560
253	Subtropical Convergence	0.0379	0.3157	0.3230	0.3194	0.3269
254	Indian Ocean Monsoon Gyre	0.1269	0.3101	0.3415	0.3112	0.3194
255	Indonesian Through-Flow	0.1646	0.3888	0.3787	0.4091	0.3739
256	Somali Current	0.1741	0.1943	0.1401	0.0939	0.2172
257	North Central Pacific Gyre	0.1555	0.34739 ;0	0.3346	0.3431	0.3326
258	North Pacific Transitional	0.1868	0.4211	0.3898	0.4204	0.3891
259	Subarctic Pacific	0.1784	0.4813	0.4128	0.4551	0.4299
260	North Atlantic Transitional	0.2134	0.2296	0.2379	0.2498	0.2125
261	Subarctic Atlantic	0.1579	0.3132	0.3044	0.3479	0.2738
262	Arctic	0.0134	0.0306	0.0225	0.0313	0.0156

S 5.10. Plot of the vulnerability of 115 European sub-ecoregions for algal blooms and acidification following predicted extra DIC exposure (mmol/l) from maritime shipping with underwater released CO_2, in four seasons. The colour intensity indicates the vulnerability score (blue) and increase in DIC level (red) and risk from low (light grey) to high (blue/red). The data underlying these plots can be found in Table S 5.12.

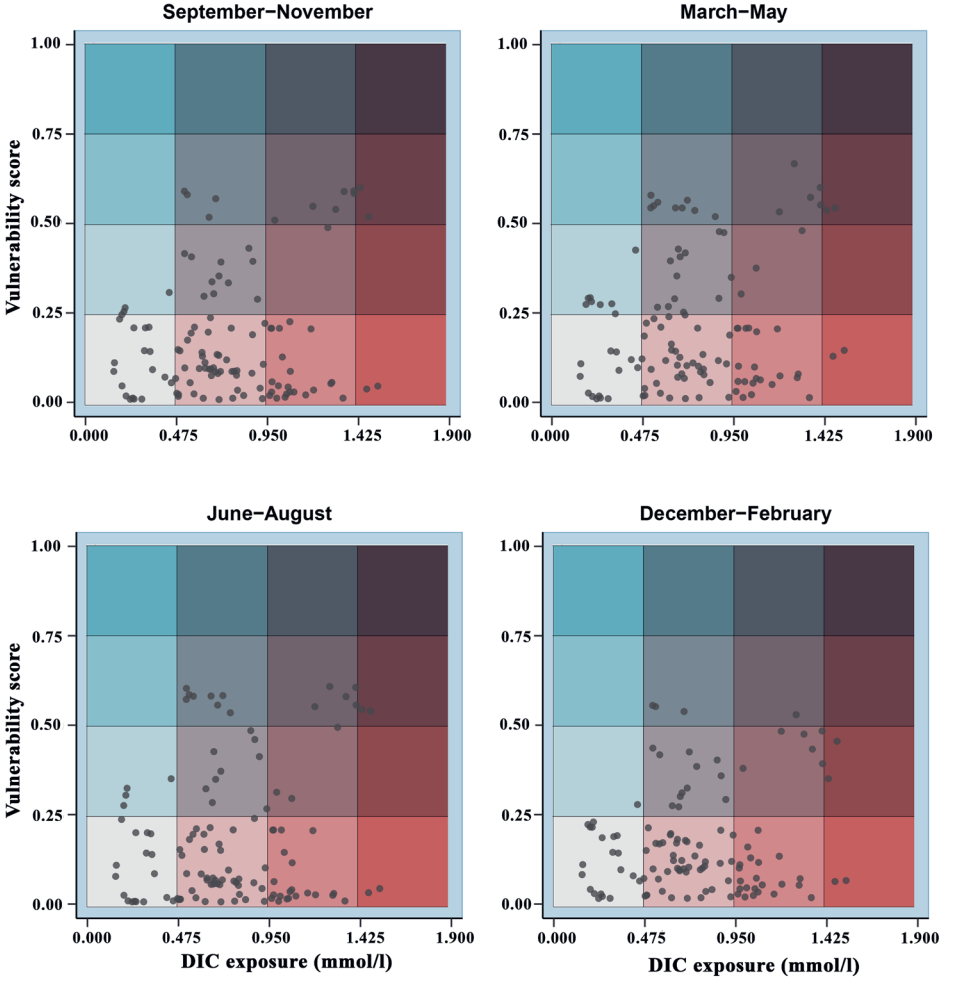

S 5.11. Map of the vulnerability of European sub-ecoregions for algal blooms and acidification following predicted extra DIC exposure (mmol/l) from maritime shipping with underwater released CO_2, in four seasons.

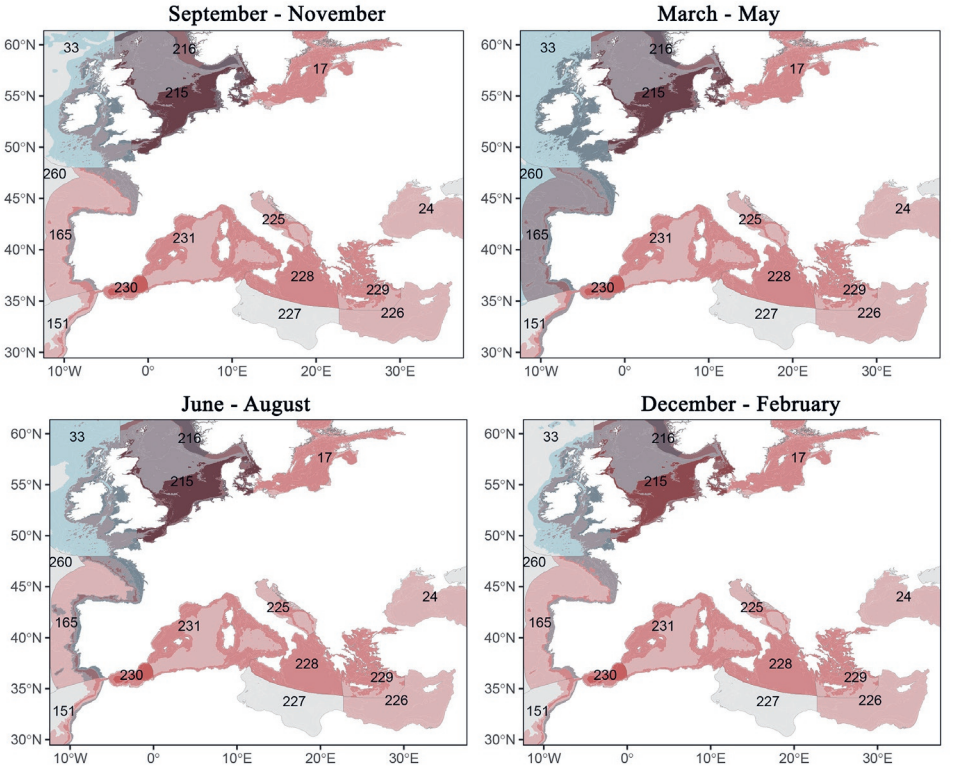

S 5.12 Predicted extra DIC exposure level and vulnerability scores of the 15 marine ecoregions around Europe (Ecological code: 17, 24, 33, 151, 165, 215, 216, 225, 226, 227, 228, 229, 230, 231, and 260) in four seasons (Dec.- Feb., Mar. – May, Jun. – Aug, and Sep. – Nov.). The ecoregions were subdivided into 9 classes based on ocean floor depth (Waller 1996) : 0 – 5m (a), 5 – 15m (b), 15 – 50 m (c), 50 – 100m (d), 100- 200m (e), 200 - 1000 m (f), 1000 – 2250 m (g), 2250 - 4500 m (h), 4500 – 11500 m (i). The risk for adverse effects from maritime shipping with underwater released CO_2, as also presented in Figures S10 and S11, can be calculated by multiplying exposure with vulnerability.

Code	Ecoregion	DIC exposure (mmol/l)	Vulnerability to algal blooms and acidification			
			Sep. - Nov.	Mar. - May	Jun. - Aug.	Dec. - Feb.
17a	Baltic Sea	0.5686	0.2103	0.2103	0.2103	0.1715
17b	Baltic Sea	0.7604	0.2073	0.2074	0.2074	0.1643
17c	Baltic Sea	1.0122	0.2070	0.2070	0.2070	0.1594
17d	Baltic Sea	1.1768	0.2052	0.2052	0.2052	0.1335
17e	Baltic Sea	0.9710	0.2069	0.2069	0.2069	0.1100
17f	Baltic Sea	0.9676	0.2069	0.2070	0.2070	0.1005
24a	Black Sea	0.3366	0.1420	0.1408	0.1384	0.1423
24b	Black Sea	0.3075	0.1443	0.1435	0.1424	0.1445
24c	Black Sea	0.7363	0.1187	0.1100	0.0948	0.1342
24d	Black Sea	0.7907	0.0885	0.0929	0.0700	0.1181
24e	Black Sea	0.7757	0.0868	0.0849	0.0600	0.1001
24f	Black Sea	0.6776	0.0854	0.0797	0.0567	0.0984
24g	Black Sea	0.6907	0.0805	0.0670	0.0540	0.0895
24h	Black Sea	0.6567	0.0745	0.0701	0.0558	0.0929
33a	Celtic Seas	0.5310	0.5806	0.5497	0.5852	0.5519
33b	Celtic Seas	0.5159	0.5902	0.5437	0.5721	0.5553
33c	Celtic Seas	0.6796	0.5692	0.5434	0.5560	0.5382
33d	Celtic Seas	0.8525	0.4307	0.5191	0.4849	0.4026
33e	Celtic Seas	0.4368	0.3071	0.4256	0.3503	0.2781
33f	Celtic Seas	0.2003	0.2540	0.2924	0.3041	0.2147
33g	Celtic Seas	0.1894	0.2450	0.2909	0.2754	0.2153
33h	Celtic Seas	0.1778	0.2326	0.2737	0.2364	0.2221
151a	Saharan Upwelling	0.6182	0.2965	0.3955	0.3221	0.2748
151b	Saharan Upwelling	0.6963	0.3532	0.4178	0.3712	0.3243
151c	Saharan Upwelling	0.6693	0.3035	0.4069	0.3486	0.3110
151d	Saharan Upwelling	0.6519	0.2364	0.3533	0.2837	0.2717
151e	Saharan Upwelling	0.8715	0.1889	0.2909	0.2391	0.2063
151f	Saharan Upwelling	1.0273	0.1267	0.2077	0.1444	0.1290
151g	Saharan Upwelling	0.6455	0.0929	0.1426	0.0549	0.0996

151h	Saharan Upwelling	0.4143	0.0704	0.1194	0.0182	0.0789
151i	Saharan Upwelling	0.4479	0.0546	0.0970	0.0089	0.0644
165a	South European Atlantic Shelf	0.5167	0.4159	0.5790	0.6029	0.4359
165b	South European Atlantic Shelf	0.5528	0.4067	0.5594	0.5808	0.4171
165c	South European Atlantic Shelf	0.7069	0.3921	0.5650	0.5827	0.4252
165d	South European Atlantic Shelf	0.7457	0.3340	0.5364	0.5346	0.3846
165e	South European Atlantic Shelf	0.8975	0.2882	0.4745	0.4121	0.2922
165f	South European Atlantic Shelf	1.0662	0.2254	0.3754	0.2951	0.2062
165g	South European Atlantic Shelf	0.9359	0.2207	0.3493	0.2663	0.1927
165h	South European Atlantic Shelf	0.6404	0.1963	0.2895	0.2135	0.1705
165i	South European Atlantic Shelf	0.5510	0.1936	0.2659	0.1948	0.1681
215a	North Sea	1.1871	0.5481	0.5327	0.5520	0.4830
215b	North Sea	1.3058	0.5394	0.4800	0.4938	0.4750
215c	North Sea	1.4780	0.5190	0.5431	0.5397	0.4551
215d	North Sea	0.8734	0.3942	0.4773	0.4599	0.3584
215e	North Sea	0.6599	0.3369	0.4284	0.4262	0.3007
215f	North Sea	0.9876	0.5090	0.3029	0.3125	0.3793
215g	North Sea	0.2067	0.2643	0.2814	0.3237	0.2294
216a	Southern Norway	0.6450	0.5174	0.5436	0.5814	0.1808
216b	Southern Norway	1.4329	0.6003	0.5370	0.5439	0.3504
216c	Southern Norway	1.4025	0.5841	0.5519	0.5564	0.3923
216d	Southern Norway	1.3496	0.5894	0.5731	0.5799	0.4330
216e	Southern Norway	1.4006	0.5909	0.6005	0.6059	0.4840
216f	Southern Norway	1.2649	0.4884	0.6671	0.6082	0.5294
225a	Adriatic Sea	0.5324	0.1739	0.2338	0.1805	0.1696
225b	Adriatic Sea	0.4821	0.1472	0.1853	0.1521	0.1496
225c	Adriatic Sea	0.9278	0.1062	0.1879	0.1010	0.1191
225d	Adriatic Sea	0.9112	0.0394	0.1075	0.0435	0.0651
225e	Adriatic Sea	0.9713	0.0286	0.0585	0.0257	0.0424
225f	Adriatic Sea	0.7934	0.0340	0.0771	0.0271	0.0351
225g	Adriatic Sea	0.4840	0.0168	0.0389	0.0131	0.0243
226a	Levantine Sea	0.3497	0.0915	0.0896	0.0848	0.0958
226b	Levantine Sea	0.5179	0.0961	0.0923	0.0851	0.0980
226c	Levantine Sea	0.5458	0.0549	0.0532	0.0373	0.0697

226d	Levantine Sea	0.5660	0.0235	0.0253	0.0173	0.0355
226e	Levantine Sea	0.4854	0.0216	0.0194	0.0134	0.0251
226f	Levantine Sea	0.4763	0.0251	0.0180	0.0125	0.0222
226g	Levantine Sea	0.6144	0.0114	0.0121	0.0068	0.0175
226h	Levantine Sea	0.6968	0.0078	0.0105	0.0060	0.0160
227a	Tunisian Plateau/Gulf of Sidra	0.1508	0.1106	0.1078	0.1084	0.1103
227b	Tunisian Plateau/Gulf of Sidra	0.1475	0.0863	0.0726	0.0773	0.0823
227c	Tunisian Plateau/Gulf of Sidra	0.1903	0.0458	0.0259	0.0245	0.0410
227d	Tunisian Plateau/Gulf of Sidra	0.2116	0.0178	0.0163	0.0090	0.0291
227e	Tunisian Plateau/Gulf of Sidra	0.2461	0.0118	0.0176	0.0076	0.0282
227f	Tunisian Plateau/Gulf of Sidra	0.2531	0.0093	0.0122	0.0067	0.0212
227g	Tunisian Plateau/Gulf of Sidra	0.2337	0.0086	0.0099	0.0060	0.0157
227h	Tunisian Plateau/Gulf of Sidra	0.2936	0.0090	0.0102	0.0062	0.0159
228a	Ionian Sea	0.7042	0.0862	0.1026	0.0676	0.1030
228b	Ionian Sea	0.6675	0.0966	0.1258	0.0666	0.1217
228c	Ionian Sea	0.8685	0.0814	0.1167	0.0594	0.1138
228d	Ionian Sea	1.2857	0.0557	0.0793	0.0296	0.0709
228e	Ionian Sea	1.2804	0.0524	0.0690	0.0244	0.0528
228f	Ionian Sea	1.0064	0.0462	0.0578	0.0220	0.0454
228g	Ionian Sea	0.9611	0.0191	0.0304	0.0156	0.0280
228h	Ionian Sea	0.9978	0.0116	0.0137	0.0079	0.0196
228i	Ionian Sea	1.3439	0.0118	0.0132	0.0085	0.0177
229a	Aegean Sea	0.5938	0.0945	0.1169	0.0840	0.0908
229b	Aegean Sea	0.6549	0.0929	0.1038	0.0728	0.0959
229c	Aegean Sea	0.7644	0.0862	0.1009	0.0642	0.0959
229d	Aegean Sea	0.9736	0.0573	0.1011	0.0626	0.0643
229e	Aegean Sea	1.0665	0.0288	0.0666	0.0399	0.0337
229f	Aegean Sea	1.1492	0.0206	0.0499	0.0307	0.0279
229g	Aegean Sea	1.0416	0.0145	0.0214	0.0142	0.0237
229h	Aegean Sea	0.9234	0.0103	0.0140	0.0076	0.0201
229i	Aegean Sea	0.7683	0.0115	0.0132	0.0080	0.0176
230a	Alboran Sea	0.4930	0.1440	0.2215	0.1360	0.2130
230b	Alboran Sea	0.6102	0.1289	0.2395	0.1526	0.1969
230c	Alboran Sea	0.6950	0.1313	0.2442	0.1500	0.1742

230d	Alboran Sea	0.6868	0.1337	0.2520	0.1675	0.1777
230e	Alboran Sea	0.6078	0.1394	0.2677	0.1951	0.1934
230f	Alboran Sea	1.0687	0.0865	0.1973	0.1153	0.1162
230g	Alboran Sea	1.5256	0.0454	0.1452	0.0432	0.0657
230h	Alboran Sea	1.4675	0.0371	0.1289	0.0316	0.0630
231a	Western Mediterranean	0.6245	0.0956	0.1463	0.0668	0.1216
231b	Western Mediterranean	0.6234	0.1112	0.1628	0.0728	0.1361
231c	Western Mediterranean	0.7880	0.0757	0.1338	0.0520	0.1060
231d	Western Mediterranean	1.0573	0.0427	0.0987	0.0348	0.0722
231e	Western Mediterranean	1.1905	0.0344	0.0739	0.0258	0.0553
231f	Western Mediterranean	1.0880	0.0288	0.0627	0.0223	0.0534
231g	Western Mediterranean	1.0495	0.0232	0.0537	0.0158	0.0427
231h	Western Mediterranean	0.8253	0.0192	0.0553	0.0123	0.0405
260f	Atlantic Transitional	0.4701	0.0664	0.1215	0.0153	0.0715
260g	North Atlantic Transitional	0.3309	0.2101	0.2475	0.1963	0.1913
260h	North Atlantic Transitional	0.3125	0.2081	0.2755	0.1994	0.1884
260i	Atlantic Transitional	0.2523	0.2081	0.2732	0.1995	0.1854

CHAPTER 6

6

General Discussion

6.1 Introduction

GasDrive technology applied to ships is expected to reduce more than 50% fuel consumption. This high efficiency is attributed to a new generation of fuel cells and gas engines, and to the innovative design of the underwater release exhaust gas system. The released exhaust gas bubbles fill into the nanostructures of the ship's hull and form an air layer that reduces the water resistance, which in turn increases the shipping efficiency. This will thus reduce the total amount of propulsion-related maritime emissions. However, the impact of the underwater released exhaust gas on the local marine ecosystem is unknown (Figure 6.1).

This thesis is the first to focus on the impact of acute exposure of marine ecosystems to CO_2, one of the most water dissolvable components of exhaust gas. The effects on marine phytoplankton, zooplankton and benthic invertebrates are studied.

Marine plankton and benthic communities were introduced to mesocosms and exposed for 49 days to a wide range of CO_2 dosages, resulting in pH values ranging from 8.6 (control) to 5.8 (high CO_2 dosage) **(Chapter 2)**. This mesocosm study showed both communities were directly and indirectly (via the food chain) affected by high CO_2 exposure (< pH 7.1). For example, periwinkles directly suffered from the extreme CO_2 treatment (pH ≤ 6.6) indicated by shell erosion and high mortality. The individual weight of the survivors was positively correlated with the availability of their main food source, periphyton, and not with the treatments. The highest CO_2 dosage, resulting in pH 5.8, caused massive mortality of the invertebrates present and induced an algal bloom.

A second microcosm study **(Chapter 3)** focused on sessile organisms that can live on the ship's hull, barnacles and microbial biofilm. This experiment also addressed the potential of using underwater exhausted CO_2 for anti-fouling purposes. Attached barnacles showed high tolerance to elevated CO_2 concentrations with a limited response of growth and feeding activity at pH levels as low as 6.8. However, at pH 6.3, about 30% of the population died and over 50% of the attached barnacles could not resist the water force during 15 km/h sailing for 15 minutes. The development of the microbial biofilm was significantly inhibited with increasing CO_2 concentrations from pH 7.6 on and a shift in taxa was observed.

Although CO_2 is one of the most soluble components in the exhaust gas, other substances that can be expected in exhaust gas may impact marine organisms as well, such as SO_x, NO_x and PAHs. Therefore, the impact of underwater released real exhaust gas from a diesel engine on a plankton community was compared with the impact of pure CO_2 treatments **(Chapter 4)**. In these experiments, algae (I. *galbana*) and zooplankton (*Brachionus plicatilis,* a rotifer) were exposed for 7 days to seawater that had been bubbled with exhaust gas, or with CO_2 to reach the same pH level of 6.8. During the exposure, no significantly different effects were found between these two treatments. Thus, CO_2 is the main impactor in the exhaust gas on the studied plankton community, regardless of other dissolved components.

In higher CO_2 concentration exposure (pH as low as 5), *I. galbana* collapsed in initial pH ≤ 6 treatments, while the development of *D. salina* (an algal species more resistant to low pH values) was stimulated at pH 6. It suggests that the CO_2 from underwater released exhaust gas can stimulate blooming of algae that can resist a temporary pH drop to 6, under conditions of unlimited nutrient availability. The rotifers that were used for these experiments were able

to resists the low initial pH levels as well. Therefore, no levels of CO_2 could be indicated that in theory pose the highest risk for algal blooms by a combination of stimulated algal development and reduced grazing by zooplankton.

The conclusions from Chapters 2 – 4 can be summarized as acute exposure to the main impactor in the exhaust gas, CO_2, could have a significant impact on multiple marine invertebrates at relatively high dosages (Figure 6.2). To investigate if this indicates that local marine environments can become at risk when underwater exhaust systems on ships are becoming popular, a risk assessment was performed. The shipping related potential increase of the dissolved inorganic carbon (DIC) level was plotted against the estimated vulnerability of 262 marine ecoregions **(Chapter 5)**. The vulnerability of each region was assessed by merging three indicators: DIC, chlorophyll-a and total alkalinity. The results suggest regardless of the season that the ecoregions with relatively high vulnerability are mainly located above 30° N latitude. In addition, only limited volume of water in dense shipping lanes and maritime chokepoints were under risk instead of the entire ecoregion.

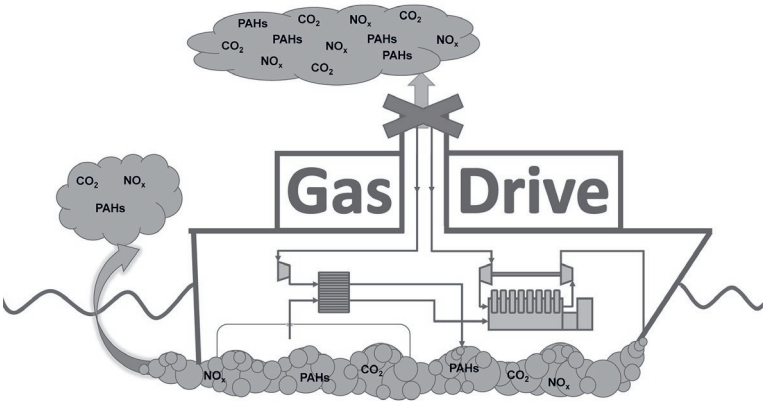

Figure 6.1 A GasDrive ship will not emit exhaust gas directly to the atmosphere. Due to its high efficiency the energy consumption and thus total volume of exhaust gas produced will be reduced. Part of the components of the exhaust gas that is released along the ship's hull will dissolve in the water and some will (re-)escape to the atmosphere.

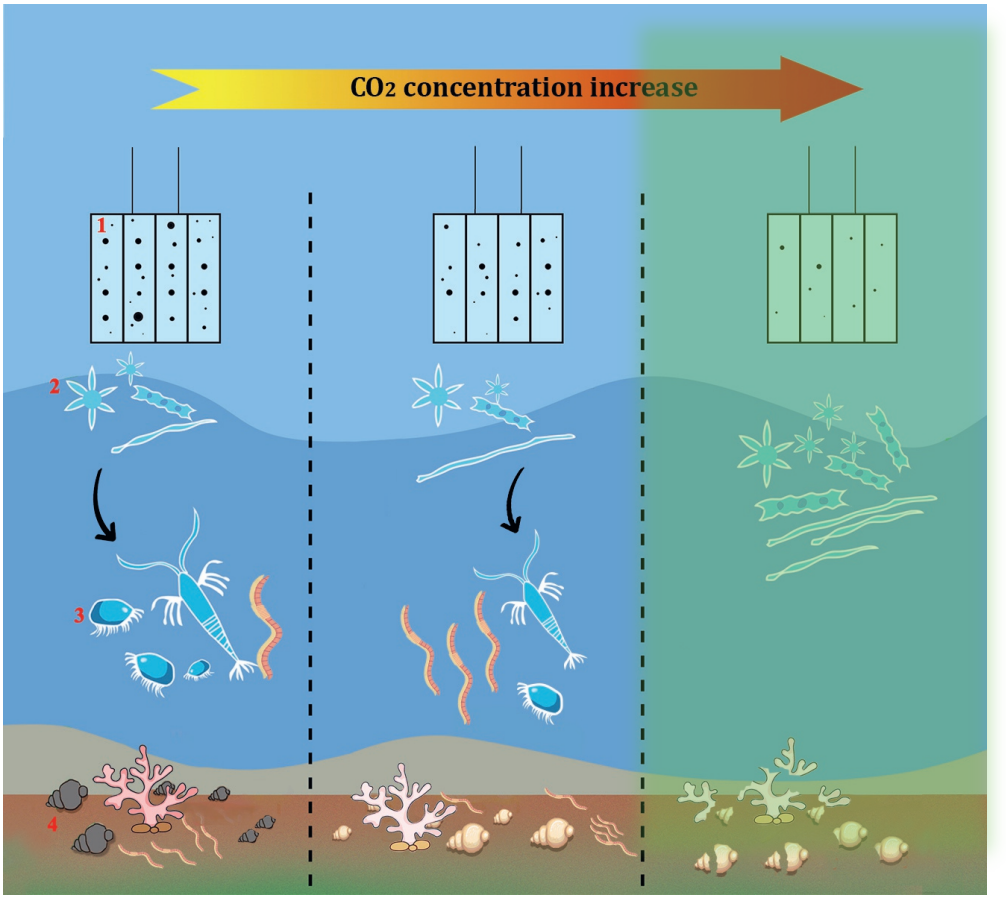

Figure 6.2 Schematic overview of the impact of elevated CO_2 concentration on marine organisms. 1. Biofilm development was inhibited and shifted in taxonomic composition; 2. Phytoplankton: CO_2 resistant microalgae bloomed by taking advantage of high CO_2 availability and reduced grazing pressure; 3. Zooplankton: relatively CO_2 resistant zooplankton profits of the increased food availability at intermediate CO_2 concentrations, but cannot survive high CO_2 concentrations; 4. Benthic organisms: Calcifying benthic organisms with shell structures directly suffer from the increasing acidification observed as shell bleaching and erosion. Noncalcifying benthic organisms such as polychaetes are more CO_2 tolerant and profit at intermediate CO_2 concentrations.

6.2 What is the no-effect concentration of CO_2 for marine organisms?

CO_2 as a carbon nutrient is crucial for the development of marine species, such as microalgae and calcifying organisms (Cole, 2012; Fassbender et al., 2016). Insufficient CO_2 levels in the water may lead to carbon starvation and inhibit the growth of autotrophic organisms (Markou et al., 2014). On the other hand, elevated CO_2 concentrations can cause ocean acidification, which is also a threat to marine invertebrates (Doney et al., 2009). Therefore, the dose-response curves for CO_2 will have a highest and a lowest no-effect level, making risk assessment challenging as it is for other micronutrients. A few years ago, de Vries et al. (2013) conducted a marine ecological risk assessment of elevated CO_2 levels using a dataset of 67

species in a Species Sensitivity Distribution. They found that most available studies used only one or two exposure concentrations next to the controls (de Vries et al., 2013). Thus, neither No Observed Effect Concentrations (NOECs) nor median effect concentrations (LC_{50} or EC_{50}) could be derived in those studies that lacked a full dose-response relationship. Unfortunately, this information gap remains unfilled. Still, only very few published studies include a full dose-response curve of CO_2 to marine organisms. Studies with acute high dose exposure which can represent situations that can be expected due to underwater released exhaust gas are even more rare.

6.2.1 Impact of CO_2 on marine autotrophic organisms

To determine the impact of elevated CO_2 concentrations on autotrophic organisms, in the mesocosm study described in Chapter 2, phytoplankton (algae) and zooplankton (grazers) communities were exposed to seven CO_2 concentrations (114 µatm pCO_2 – 179,013 µatm pCO_2, resulting in pH 8.6 – pH 5.8) for 49 days. No negative impact on growth was observed in any of the treatments. Instead, in the highest CO_2 concentrations (resulting in pH 5.8) the chlorophyll-a concentrations, a proxy for algal biomass, continued to develop during the entire experimental period and reached 60 µg/l chlorophyll-a on day 49 (Figure 2.2). This algal bloom is likely to be the result from the combined effects of reduced grazing pressure due to the high animal mortality caused by the low pH, and the high nutrients availability (flux of nutrients from decaying organic material and injected CO_2). The carbon source can be unlimited in such a continuous CO_2 injection set-up. In natural situations, however, carbon shortage can be one of the causes that terminate algal blooms (Markou et al., 2014). In the algae-rotifer community experiments in Chapter 4, the development of algae (without rotifer) was terminated by the CO_2 limitation at pH > 9.0 (Figure 4.1 and Figure 4.8). The result suggests that as long as the CO_2 injection keeps the pH below 9, it can support primary production. This is relevant information in a field situation because it means that underwater released exhaust gas possibly causes a strong impact in high algae density areas, such as estuarine and coastal environments, where eutrophication occurs by anthropogenic activities (Heil et al., 2005; D Liu et al., 2009). Of course, high primary production does not necessarily lead to algal blooms when sufficient algal consumers (e.g. zooplankton and filter feeders) are present. In such condition, an increase in the development of primary consumers will occur instead of an algal bloom. The algae-rotifer community in Chapter 4 further showed that some algae species are better in coping with low pH than others (*D. Salina* showed more low pH resistance than *I. galbana* in this case). Therefore, the bloom in the mesocosms at high CO_2 levels (pH 5.8) in the study in Chapter 2 must have been caused by specific species that could tolerate and take advantage of the low pH. As the phytoplankton community was not identified, we do not know which species were able to benefit from the CO_2 rich situation, with low grazing pressure.

With the development of algae continuously without control, Harmful Algal Blooms (HABs) can occur (Amara et al., 2018), which threatens human and environmental health (Dolah et al., 2001). Harmful algae release toxins, e.g. saxitoxins and brevetoxins, that can cause shellfish poisoning and further pass the toxins on along the food chain causing illness or death if consumed by humans or other organisms (Dolah et al., 2001). Some non-toxic HABs remain as high biomass which significantly reduces the light intensity in the water column and the dissolved oxygen level for aerobic organisms in the nighttime (S K Moore et al., 2008). It was reported that the development of a globally wide distributed toxic algae,

Vicicitus globosus, significantly increased in 800 µatm CO_2 concentration and inhibited the development of other phytoplankton species (Riebesell et al., 2018). Such effect level can be reached by underwater released exhaust gas (Chapter 5, 8,357 µatm CO_2, pH 6.8). It suggests that underwater exhaust gas could pose an emergent threat to areas where harmful algae are already present but not yet dominant, although the response of HA to additional CO_2 varies among different taxa. It is important to realize that the underwater released exhaust gas is likely to result in a much higher CO_2 concentration (7,970 µatm, pH 6.8, Chapter 4) than in Riebesell et al. (2018)'s study. On the other hand, the volume of CO_2 enriched water by the underwater released exhaust gas might be too small to impact the algae before it is diluted by the surrounding water (Chapter 5). There is limited knowledge of the direct impact of extremely high CO_2 concentrations on the blooming and development of toxicity of HA, but it is certainly species-specific (M L Wells et al., 2015). The most common marine HA are dinoflagellates and diatoms (S K Moore et al., 2008). It was predicted that in warmer marine waters with enhanced ocean stratification in the future, mobile dinoflagellates are favored over non-mobile phytoplankton (S K Moore et al., 2008), because dinoflagellates can reach deeper nutrient rich water layers that other phytoplankton cannot access. However, such prediction may not hold when underwater released exhaust gas is applied. The released exhaust gas bubbles along the ship hulls will mix the water column in the shipping lanes. These bubbles can bring deeper nutrients, although not as deep as the ocean stratification, to the surface, and accelerate O_2 and CO_2 exchange between the air-liquid interface. In that case, the NOEC of CO_2 is not the only "red line" that requires attention for algal bloom control, but also the increased nutrient availability. Therefore, the nutrient level indicator, chlorophyll-a concentration, was one of the vulnerability indicators for ecological areas with the potential impact of underwater exhausted CO_2 in Chapter 5.

In the study in Chapter 3, bacterial biofilms were exposed to elevated CO_2 concentrations for 24 days, which reduced their biomass (Figure 3.1). Also, a clear shift in taxonomic composition was observed with a decreasing pH level from 7.8 to 6.3 (Figure 3.2). Unfortunately, it was not studied whether those bacteria were autotropic or heterotrophic since the study in Chapter 3 aimed to test the potential of applying additional CO_2 in anti-fouling in general (the anti-fouling property is further discussed in Section 6.6.) In literature, the growth and nitrogen fixation of the marine autotrophic cyanobacteria *Trichodesmium* was enhanced by around 900 µatm CO_2 exposure (Levitan et al., 2007) and the cell division rate of *Cyanobacteria Cylindrospermopsis* increased in 1,300 µatm CO_2 treatment (Pierangelini et al., 2014). In addition, those autotropic bacteria can live in an environment with a 10-fold seasonal variation of dissolved CO_2 concentrations (Pierangelini et al., 2014). Thus, we hypothesize that such a cyanobacteria will survive and take advantage of acute exposure to high CO_2 concentrations caused by underwater released exhaust gas. Then the enhanced nitrogen fixation may drive other inorganic sources into shortage, such as phosphorus (Barcelos e Ramos et al., 2007).

In summary, CO_2 is an essential carbon source for the survival and growth of autotrophic species. On the other hand, not all algae species are able to cope with high CO_2 levels. The elevated CO_2 concentrations (e.g. at pH 5.8) can shift the composition of algae communities and stimulate the surviving species, that can include cyanobacteria to bloom. This could develop into a harmful algal bloom, which can release toxins or deplete the dissolved oxygen, consequently threatening the entire food chain.

6.2.2 Impact of CO_2 on marine invertebrates

The impact of elevated CO_2 concentrations on marine invertebrates varies between taxonomic groups. Molluscs form one of the most sensitive invertebrate groups, while Crustaceans are relatively less sensitive (de Vries et al., 2013). In the study presented in Chapter 2, two mollusc species, one crustacean species and other small benthic invertebrates that are naturally present in a shallow marine ecosystem were exposed to a wide range of CO_2 concentrations in the mesocosms. A significant impact was found in the pH ≤ 7.1 (≥ 6,678 µatm CO_2) mesocosms. The communities shifted toward polychaetes dominance between pH 6.6 - 7.1. Shell damage and high mortality of periwinkles (Molluscs) occurred in pH < 6.6 (> 29,653 µatm CO_2). Although a quite high variation in the response of mud snail (Molluscs) and mud shrimp (Crustacean) was found between the duplicate mesocosms, high mortality of both species was evident in the pH ≤ 6.2 treatment.

Overall, these results implied that a significant impact only occurred at pH ≤ 7.1 treatments. Thus, the NOEC of CO_2 for the studied marine invertebrate communities is pH 7.4 (3,032 µatm pCO_2). Since the NOEC is highly dependent on the selected exposure concentrations in the experiment, the LC_{50} for the periwinkles in the mesocosms was derived as well, which was about 60,000 µatm pCO_2 (pH 6.36, Figure 2.5). The effect levels were much higher than what was concluded from many other studies. For instance, both 600 µatm (low-end prediction for 2050) and 760 µatm pCO_2 (low-end prediction for 2100) have been reported to cause significant impact on multiple marine invertebrates, including periwinkles (Clements &Darrow, 2018; Currie et al., 2017; de Vries et al., 2013; Ries et al., 2009). The differences in pCO2 effects concentrations between studies could be attributed to factors such as: species and life-stage specific physiological characteristics, temperature, size of the animals, food availability, exposure period and differences in alkalinity.

As mentioned above, species-specific responses were shown in the mesocosm study described in Chapter 2, but life-stage specific negative responses were not found. The polychaetes dominated the benthic community between pH 6.6 – pH 7.1, and their larvae dominated the zooplankton group at the same conditions (Chapter 2). However, due the high variation between the duplicated mesocosms, the observed effects on both adult and larvae of *Peringia ulvae* and *Corophium volutator* were not statistically significant (Chapter 2). Thus, no life-stage specific response was found in these two species either. In literature, veliger stage bivalves were reported to be more vulnerable than prediveliger stage ones to elevated CO_2 concentrations (Gobler &Talmage, 2013). Besides marine invertebrates, marine fish also showed juvenile stages were more susceptible than the flexion stages (Ishimatsu et al., 2004). This could be related to the smaller body size as well as the developmental processes taking place in the younger life stages.

Although Ocean Acidification (OA) has been studied for decades, the mechanisms of interference with biogenic calcification remains unclear (Cyronak et al., 2015; Ries et al., 2009). These unclear mechanisms lead to unstandardized test protocols. Although the 'Guide to best practices for ocean acidification research and data reporting' much improved the quality of OA studies, the downside is that it strictly standardized the chemical methods of manipulating seawater instead of the experimental design (Cornwall &Hurd, 2016). As a result the experimental set-up differs between studies to mimic specific local conditions (wind, water current and human activities). This plus the different study endpoints and

inappropriate replication contribute to different "safety levels" of CO_2 resulting from the studies. As addressed in the introduction (Section 1.4.2), underwater released exhaust gas to the marine ecosystem may locally cause acute exposure instead of the global chronic exposure that is caused by traditional OA condition. Therefore, the studies in the presented thesis logically did not follow the 'Guide to best practices for ocean acidification research and data reporting'. In reverse, the reported effect concentrations from traditional OA and climate change studies are not applicable to determine the NOEC level for the GasDrive ships' condition. However, as hardly any other studies were conducted with similar exposure conditions with underwater exhausted CO_2, findings in Chapters 2 - 4 were compared and discussed with results from OA articles to get an impression of the order of magnitude of the effects, but with the awareness of the limitations of such comparisons.

The 96-h acute toxicity test of additional CO_2 on marine shrimp from Furtado et al. (2017) is one of the few studies that are comparable to the underwater released CO_2 condition. They derived an LC_{50} of only 59 mg/l (around 30,000 µatm pCO_2), and with 23.5 mg/l (around 12,000 µatm) as NOEC concentration for mortality (Furtado et al., 2017). The NOEC in Chapter 2 was 10 times lower, 3,032 µatm, and this difference could be attributed to the difference in experimental conditions (indoor aquaculture of outdoor mesocosm) and exposure period (96 hours or 49 days). However, the suggested NOEC of CO_2 is more meaningful in shrimp cultivation than protecting the natural environment, because of the excluded complex biological composition in fields and the unstable outdoor physical conditions. In comparison, the NOEC, 3,032 µatm pCO_2 (pH 7.4), that was determined in the mesocosm study in Chapter 2 seems more representative in the GasDrive ship's situation, although the 49 days exposure time is long. It indicated a worst-case-scenario that may occur in isolated shallow-water ecosystems with busy shipping lanes. It is necessary to highlight that our studied organisms in the experiment that is described in Chapter 2 were collected from shallow water areas. Thus, they are probably tolerant to anthropogenic stressors (e.g. addition nutrients input including CO_2 concentration). Therefore, the determined NOEC, 3,032 µatm pCO_2, in this worst-case-scenario study, may underestimate the response of more sensitive communities, such as organisms that occur in the open sea, where less human impact occurs and with large amount of water volume.

It was noticed that the pCO_2 levels in the mesocosms study in Chapter 2 are higher than most other studies which report the pCO_2 levels at the same pHs. This is due to the fact that elevated CO_2 concentration caused decalcification, which increased the water alkalinity in our mesocosm study. Thus, a higher amount of dissolved CO_2 is required to drop the same level of pH than it does in low alkalinity water. Such a change in water chemistry can further change the entire CO_2 impact conclusion.

6.2.3 Impact of CO_2 when alkalinity increased

The alkalinity level of mesocosms described in Chapter 2 significantly increased with higher CO_2 exposure. While in the microcosm experiments without sediment described in Chapter 3, the alkalinity remined stable with increasing CO_2 concentrations. Although it is likely that part of the shells of barnacles (especially the dead barnacles) decalcified at higher CO_2 levels, the CO_2 level (lowest pH 6.3) was apparently not enough to significantly increase the alkalinity of 30 liters of water. These results suggest that underwater released exhausted gas

is unlikely to increase the alkalinity level in the open ocean, while it may do so in shallow areas where the shell fragments in the sediment can be dissolved.

Increase of alkalinity is not commonly addressed or measured in ocean acidification studies. This may be because adding CO_2 to water will not directly change the alkalinity level especially when shells are absent (Section 1.5.2). Furthermore, most ocean acidification studies only cover pH ranges higher than where the significant decalcification was observed ($pH \leq 7.1$, Chapter 2). Some studies included $pH < 7.0$ treatments (Furtado et al., 2017; Preziosi et al., 2017), but no sediments were involved in the experimental set-up. Therefore, no significant increase in alkalinity was to be expected. One may assume that, decalcification of shell fragments will occur already in much less acidic conditions than pH 7.1, but the change in alkalinity was not detected in the experiment of Chapter 2, probably because the method we used to measure alkalinity was not sensitive enough to register small changes. Tribollet et al. (2019) used microscopy analysis on the dead coral blocks in enriched CO_2 conditions and calculated that the decalcification of coral caused an increase in alkalinity at 920 µatm pCO_2 (pH 7.7) already.

High alkalinity indicates high resistance of water pH changing against CO_2 uptake and this favors $CaCO_3$ precipitation (calcification), while calcification continuously reduces the alkalinity level of the water (Section 1.5.2). Thus, if the change in alkalinity is not considered in OA studies, the environmental impact of elevated CO_2 concentration may be underestimated, especially in shallow areas that are in contact with calcium carbonate rich sediments. Since high alkalinity water can uptake more CO_2 than low alkalinity water to drop the same level of pH, artificial ocean alkalization (AOA) has been proposed and investigated as a method to store CO_2 in the ocean and mitigate ocean acidification. Well- known methods for alkalinity enhancement include using alkalizing agents, olivine and limestone powder, calcium carbonate (Ferrer-Gonzalez &Ilyina, 2015). Both experimental and modeling studies showed that AOA can mitigate regional ocean acidification and protect local organisms, such as coral reefs (Feng et al., 2016) and red calcifying algae (Gore et al., 2018). However, in practice, the regionally enhanced alkaline water is expected to exchange fast with untreated water from outside the region, and subsequently decreases the alkalinity level again (Feng et al., 2016). In the meantime, applying AOA at a global level is a technical and financial challenge. Importantly, the effects of increasing alkalinity on other organisms besides calcifiers and on the ocean carbon cycle are still unknown, thus more research is required in these fields.

Overall, it is concluded that due to the impact of the shell fragments in the sediment, the NOEC of CO_2 for marine invertebrate is around 3,000 µatm (Section 6.2.2). While, in areas without sediment, the NOEC level will be < 3,000 µatm.

6.3 Is CO_2 the main environmental impact driver in the exhaust gas from maritime shipping?

6.3.1 From CO_2 alone to exhaust gas in general

The impact of diesel engine produced exhaust gas on a planktonic community was compared with pure CO_2 in the experiment described in Chapter 4. No significant different effects were found between these two treatments. It was concluded that CO_2 is the main impactor in the

exhaust gas to the studied organisms. Due to the continuous gas exchange at the air-liquid interface, the exposure time may have been too short for the relatively less water-soluble components (such as NO_x and PAHs) in the exhaust gas to cause additional impact than CO_2 alone. In fact, even for relatively high soluble CO_2, the one-time injection induced exposure time is not sufficient to cause biological impact (Chapter 4). The planktonic communities in the study in Chapter 4 were dead from carbon shortage instead of showing effects from addition CO_2 treatment. Thus, a repeated exhaust gas application is suggested to further study the impact of exhaust gas. Nevertheless, the potential impact of some typical components in the exhaust gas on the marine ecosystem can be predicted based on their toxicity, fate and bioaccumulation ability.

Besides CO_2, the well-known components in the exhaust gas are carbon monoxide (CO), sulfur oxides (SOx), nitrogen oxides (NOx), hydrocarbons (especially in LNG powered ships emissions), particulate matters (PM), oxygen (O_2), water vapor (H_2O) and nitrogen (N_2) (M Anderson et al., 2015; Winnes & Fridell, 2009).

Carbon monoxide

CO is primarily produced by incomplete combustion of carbonaceous fossil fuel (Kao & Nanagas, 2006). Thus, all types of marine fuel are expected to form CO in their exhaust gas. CO is produced more during low engine load and low engine temperature (Winnes & Fridell, 2009). Low engine temperature results in relatively higher CO content in the exhaust gas of LNG powered ships than that of present marine fuel oils (M Anderson et al., 2015). Besides operating conditions, the amount of oxygen that flows into the engine also forms a factor in the CO formation. A low ratio of air/fuel mixture in the combustion chamber will directly lead to high production of flammable CO, in turn resulting in inefficient operation (Er, 2002). CO is a highly toxic gas that can cause direct cell toxicity after inhalation. The impact of emitted CO is mainly concerned as air pollutant via inhalation and related with occupational safety. Due to its low solubility in water (27.6 mg/l at 25 °C) (Kao & Nanagas, 2006), the CO in the underwater released exhaust gas is most likely diffusing back to the atmosphere and eventually further oxidized to CO_2 by hydroxyl radicals and microorganisms (Wilbur et al., 2012). Before it is oxidized, the terrestrial organisms and humans may be exposed to the exhausted CO and cause health issues, but such impact is out of the scope of the present marine environmental impact study.

Sulfur oxides and nitrogen oxides

SO_x and NO_x emitted via shipping traffic are a significant source for air pollution, which contributes approximately for 15% to global NO_x emissions and for 4 - 9% to the SO_2 emissions (Seddiek & Elgohary, 2014). The main environmental concern of both emitted SO_x and NO_x is acidification via formed H_2SO_4 and HNO_3. Different from CO_2 induced acidification, dissolved SO_x and NO_x can directly reduce the alkalinity level of the water and inhibit biogenic calcification (Jägerbrand et al., 2019; Omstedt et al., 2015). SO_x in the exhaust gas mainly consists of SO_2 and SO_3, typically in a ratio of 15:1 (Er, 2002). Due to technical difficulties, the concentration of dissolved SO_x could not be measured in the experiment in Chapter 4. Considering the measured SO_2 in the diesel engine produced exhaust gas was 54 ppm, the total amount of SO_x is calculated to be 58 ppm (approximately 0.15 mg/l, assuming SO_2: SO_3 = 15:1). Due to the high solubility of SO_2 and SO_3, it is assumed

that all SO_x were dissolved in water. No significant impact from the dissolved 58 ppm SO_x on water alkalinity or studied organisms was observed in this experiment. Similarly, the dissolved NO_2 and NO_3 (1.42 mg/l and 3.57 mg/l respectively) did not cause a significant impact on studied algae or rotifers either (Chapter 4). But NO_2 (even < 1 mg/L) can be actively taken up across the gill epithelium and disrupt multiple physiological functions of aquatic organisms (Jensen, 2003; Kroupova et al., 2005). Furthermore, nitrite can accumulate in the body fluids of the fish and its concentration in blood plasma may reach 10 times the concentration in the surrounding water (Lewis Jr & Morris, 1986). Thus, the impact of nitrite in exhaust gas enriched water (measured as 4.66 mg/L in the study in Chapter 4) on fish cannot be ruled out and exposing fish to exhaust gas enriched water is recommended for future studies. This is particularly important for mariculture, the farming of marine organisms for food around the world's coastlines, since it overlaps with most busy shipping lanes (Chapter 5) and the high exposure to NO_2 may have a negative impact on the production of the marine fish farming. Besides the negative impact, NO_x is known to contribute to water eutrophication as a nitrogen source (Glibert et al., 2018). For example, the intensive sailing activities in 2008 Olympic in China was proven to be the "supplier" of N source for several local "green tides" (Glibert et al., 2018; D Liu & Zhou, 2018). Thus, releasing exhaust gas underwater in busy shipping lanes is likely to contribute to algal blooms, at least via inorganic nitrogen supply.

Hydrocarbons

Depending on the types of fuel and the combustion characteristics, different amounts and types of hydrocarbons will be formed because of incomplete combustion. The most common hydrocarbons are methane (CH_4) and PAHs. Especially in LNG powered ships, CH_4 leakage is still one of the unsolved challenges for widely applying this energy source in maritime traffic (Pavlenko et al., 2020). CH_4 is a greenhouse gas that is toxic to both humans and the environment but is less of a concern in the aquatic environment due to its low water solubility (22.7 mg/l) (Fugiel et al., 2017; Pavlenko et al., 2020).

PAHs are a class of multiphase organic compounds in the exhaust gas from combustion of fossil fuels and are always found as a mixture of compounds (Guo et al., 2011). In the experiment in Chapter 4, the concentrations of the measured ten PAHs in exhaust gas enriched water were lower than the NOECs, and no impact on the growth of studied algae and rotifers was observed. However, many of the hydrophobic PAHs are well-known to be rather resistant to biodegradation, and can bioaccumulate from water in animal tissue, which represents a long-term threat to human and environmental health (Guo et al., 2011). Although the PAHs concentrations were not measured in the exhaust gas (Chapter 4), most released PAHs were expected to exchange back to the atmosphere, due to the properties of being hard to dissolve and easily lost by volatilization. The PAHs that exchanged back to the atmosphere can be widespread in the air by bonding to particulate matters (Plaza-Bolaños et al., 2010). The PAHs that dissolve and become absorbed to submerged substances, can be taken up by aquatic organisms. Especially phenanthrene and fluoranthene, which toxicities were enhanced by fluorescent light, can pose a hazard for mussels and sea-urchins (Bellas et al., 2008; Honda & Suzuki, 2020). Planktonic communities, especially copepods and microzooplankton, are able to accumulate PAHs from the water and play an important role in PAHs cycling in the ocean, likely as distributors (Almeda et al., 2013). But for the dissolved underwater released exhaust PAHs, the bioaccumulation and distribution are negligible, due to their extremely low concentrations (> 800 times lower than the no-

observed-effect-levels, Chapter 4). Besides bioaccumulation to organisms, the PAHs may eventually reach and bound to sediment and cause a direct impact on benthic organisms. The sediment bounded PAHs are most likely exposed to insufficient ultraviolet radiation, thus the risk of photoactivated toxicity of PAHs is low (Diamond et al., 2003). Overall, low priority was given to the concern of underwater released PAHs from shipping on the marine benthic ecosystem.

Particulate matter

The Particulate Matter (PMs) in exhaust gas consists of small particles that can suspend in the air and cause toxic impact after inhalation (M Park et al., 2018). For example, $PM_{2.5}$ and black carbon are both commonly known PMs in exhaust gas. Most PMs showed a limited toxic impact on aquatic organisms, although 10 µg/l nano-sized black carbon is reported to induce inflammatory processes in some aquatic invertebrates (Canesi et al., 2008). PAHs also present in the exhaust gas can adsorb to PMs and be transported in the air or sink to the sediment in the ocean. In general, limited impact caused by PM itself on the aquatic organisms is expected, and the potential effects are more considered as a distributor of the attached PAHs in the ocean. In the GasDrive case, the released PMs can be a technical challenge, because it may damage the nanostructure of the ships' hull by blocking those artificial nano "holes". If that happens, the ship's efficiency can be significantly reduced due to the loss of air lubrication.

Overall, multiple components in the exhaust gas of maritime shipping could significantly modify the impact on the marine ecosystem. Some of the components are of relatively less concern than others. For example, CO and CH_4 (low solubility), PAHs (high volatilization and low exposure concentration), and PMs (low toxicity to aquatic organisms). In comparison, CO_2, SO_x and NO_x are the "red flag" components. Fortunately, IMO has issued several regulations and announced emission control areas that focus on maritime traffic released SO_x and NO_x (IMO, 1997a). Additionally, there are commercially available exhaust gas cleaning systems and techniques on the market. It is expected that the amount of SO_x and NO_x in the exhaust gas from maritime shipping will be lower than the current level and cause less and less impact on the marine environment. Therefore, the main concern of causing significant impact on the marine ecosystem from the underwater released exhaust gas is CO_2.

6.3.2 From a simple plankton community to complex marine ecosystems

To assess the impact of underwater released exhaust gas on marine ecosystems, multiple communities should be studied. However, for practical reasons, only a simple plankton community was used to work with actual exhaust gas (Figure 6.3), and other experiments presented in this thesis were carried out on invertebrates exposed to CO_2 alone. This paragraph discusses if such an approach is sufficient to address a complex marine ecosystem response to the underwater released exhaust gas.

Chapter 4 describes experiments that aim to identify the additional impact from other components besides CO_2 in the exhaust gas. Therefore, a planktonic community was used to indicate the potential effects of both stimulation (on algae) and inhibition (on rotifers) by CO_2 exposure, and all experimental groups started at the same pH level. On the other hand, some organisms that are more sensitive to other components in the exhaust gas than and rotifers

may not be included. For instance, like mentioned in Section 6.3.1, fish are more relevant animal models for studying the impact of released NO_X, while sea urchins and daphnia are more suitable species in PAHs toxicity studies (Honda & Suzuki, 2020). Such a selection in the animal model and experimental design could shield off the impact of other components in the experiments and contribute to the conclusion that CO_2 is the main impact factor. But the toxicity data and physicochemical properties of the other major components in the exhaust gas (Section 6.3.1) also indicate that CO_2 is the major concern. Therefore, the conclusion is considered valid although it was determined via a simple plankton community.

Of course, a simple plankton community is not sufficient to show the response of the entire marine ecosystem to the underwater exhausted CO_2. An experimental set-up with complex communities that meets the natural conditions as much as possible (e.g. mesocosm or field study) is preferred. The mesocosm study in Chapter 2 clearly showed the interaction between communities under outdoor conditions. For example, the growth of periwinkles was not directly related to the pH level in the experiment but positively correlated with the availability of its food, periphyton. The availability of periphyton depends on the densities of its predators, such as polychaetes, that are directly inhibited at $pH < 7.1$. This series of interactions within the food chain shows that although some species are not vulnerable to elevated CO_2 or other pollutant concentrations, the negative impact can be spread to those species as well indirectly.

In the present thesis, such indirect impact via the food chain was only addressed for phytoplankton and invertebrates, while vertebrates were not included in the studies. For studying the ecotoxicological impact of the pollutants in the exhaust gas, using invertebrates is an appropriate approach. Because in invertebrate studies it is technically relatively easy to include higher biological organizations (e.g. populations and communities), while they are easily accepted from an animal welfare perspective (Lagadic & Caquet, 1998). Furthermore, the reproductive and developmental responses of invertebrates are commonly accepted to be an early warning of acute impact at the population/community level (Lagadic &Caquet, 1998). Here, to protect the entire marine ecosystem, the basic knowledge of metabolic and physiological pattern of CO_2 in the organisms is essential to derive the response of vertebrates from invertebrates. For ocean acidification, a large amount of researches has been done on marine invertebrates and fish. Thus, the metabolic and physiological patterns are relatively clear. The main challenges of translating the impact from invertebrates to vertebrates, and/or the entire marine ecosystem are the variable local conditions, which can highly influence the exposure concentration (Section 6.4), and the increased threshold sensitivity under combined stressor effects (e.g. thermal stress, Section 6.5).

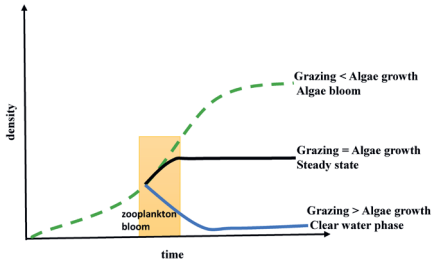

Figure 6.3 A scheme of the impact of toxic compounds on a simple plankton community. Zooplankton blooms (yellow area) after sufficient food is available (the density of microalgae). If the zooplankton is more sensitive to the exposure than the algae, then the grazing pressure will be lower than the growth rate of algae, algal bloom occurs (green line). If the algae are more sensitive to the exposure than the algae, then its density will decrease, and the zooplankton will not survive either due to starvation (blue line). If the algae and zooplankton have similar sensitivity to the exposure, then a steady state will be reached (black line).

6.4 Where are the vulnerable areas to underwater released exhaust CO_2 from marine shipping geographically, based on environmental conditions?

Based on the results of Chapters 2 - 4, it was concluded that CO_2 was the main impactor on the studied planktonic community and also significantly affected other benthic calcifying and fouling invertebrates. The relative risk assessment that followed (Chapter 5) identified the ecoregions that would be vulnerable to acidification and algal blooms when exposed to underwater released exhaust CO_2. The ecoregions characterized as having a high vulnerability were located above 30° N latitude, but they were at a low risk when considering the limited volume of water that is expected to be impacted from shipping with underwater released exhaust gas. This is caused by the saturation level of the dissolved inorganic carbon in the ocean (2.07 mmol/l on average at ocean surface) and CO_2 exchange back to the atmosphere (Chapter 5 and Section 6.5).This study was a first – phase identification of the vulnerable areas, excluding some potentially essential criteria: change in alkalinity, biological composition and ice covered areas like the Arctic area.

Alkalinity was used as a vulnerability indicator of acidification in the study in Chapter 5, but the potential of its increase over time by decalcification (Chapter 2) was not considered. Therefore, an overestimation of the vulnerability in especially shallow coastal zones is to be expected. For example, the coastline of Malta was now identified as having a relatively high vulnerability (Figure 5.8, zone ID 228). Some water depths in the north-east of the coastline are between 6 to 57 meters only and around 80% of the studied 28 m^2 of the seabed composition was dominated by carbonate shells, carbonate fragments and coralline algae (Micallef et al., 2012). Underwater released CO_2 may quickly reach and decalcify those carbonate sources, after which the alkalinity will increase and weaken the OA impact, which would then reduce the vulnerability of this area to OA. Here, the physical composition of the local area is important. If a shallow area is characterized by carbonate poor bedrock, the carbonate source is finite and its vulnerability to OA remains.

The bedrock composition is not only crucial for predicting the change in alkalinity but also for selecting vulnerable areas to acidification in general. The presented GIS maps in Chapter

5 are based on the global ocean surface only, and do not include physical and biological composition of deeper water layers and the seabed. This may overestimate the vulnerability of the shallow coastal areas that are in relatively high risk, e.g. Strait of Dover and Strait of Gibraltar, although the calculated impacted relative water volume is small (Chapter 5). If the CO_2 enriched water could reach the seafloor, the acidified water could impact multiple sensitive biological communities that are located in deep water layers and on the seafloor (Micallef et al., 2012; Stevenson et al., 2020). In open oceans, the biological composition is likely to be less important than it is in the coastal areas. This is because the exposure level is relatively low from the strong dilution in the large volume of surrounding and moving water. This mechanism was not yet considered in the study in Chapter 5 and will probably dilute the exposure before it impacts deep water layers. Moreover, the availability of essential nutrients (e.g. N and P) for algae development is relatively low in the open ocean compared with the coastal areas. Therefore, the risk of inducing algal bloom from maritime underwater CO_2 emission is expected to be low in the open ocean.

The size of geographically vulnerable areas to underwater released exhaust CO_2 in the future may be underestimated by excluding a large part of the Arctic due to ice coverage. Increased shipping through the Arctic was reported in the past decade as a result of the rapid loss of sea ice (Pavlenko et al., 2020). Already an increase of 20% in number of ships was detected along the Northeast Passage in 2014 compared to 2011, and this increase was predicted to continue (Eguíluz et al., 2016). Therefore, a new assessment of the vulnerable areas to acidification impact from maritime shipping emissions in the Arctic is advisable in the short future.

The study in Chapter 5 completed the first phase of identifying vulnerable ecoregions to acidification and algal bloom from maritime emission and to set a method of global vulnerable ecoregion selection for other pollutants. Follow-up studies should refine the assessment for the identified highly vulnerable areas, including the potential of an increase in alkalinity to compensate for OA and the specific biological composition of these areas, and further assess the consequences of the increasingly available Arctic shipping lanes.

6.5 Could the underwater exhaust system be applied safely from an environmental perspective?

If we would avoid the ecoregions that were identified to be vulnerable to acidification and induction of algal blooms, can the underwater exhaust system then be safely applied from an environmental perspective?

In the light of the discussion in Section 6.3.1, several components in the exhaust gas are a hazard potential for the marine environment, but the main concern remains exposure to CO_2. The study described in Chapter 5 reveals that the amount of emitted CO_2 by ships passing through a 1 km^2 grid cell in the busiest shipping lane (134 ships/24 hours/km^2 grid cell) causes 228 m^2 of 5m deep water to reach the dissolved inorganic carbon (DIC) saturation level (Table 5.3). This is equivalent to 0.023% of the 1 km^2 grid cell, which seems negligible. On the other hand, the significant impact of elevated dissolved inorganic carbon on the marine organisms already occurs at DIC levels much lower than the maximum saturation (Chapter 2 – 4 and Section 6.2), and around this saturated area there will be a gradient of elevated DIC. Therefore, the impacted area was also calculated for lower DIC concentrations. To estimate the worst-case-scenario we simply assume that all emitted CO_2 is dissolved in water and is

only present in the top 10 cm of the water column. The background DIC level was set as the average ocean surface DIC level 2.07 mmol/l (Chapter 5), and the predicted ocean surface DIC level in 2100, 2.215 mmol/l, was used as impact level (Hartin et al., 2016). Then the GasDrive ships can impact a surface of 149,957 m^2 water, which is about 14.96% of the 1 km^2 grid cell (a volume of 14,958 m^3 of impacted water that is covered). In section 6.2.2, the NOEC level for pCO_2 derived from the pH 7.4 treated mesocosm was 3.01 mmol/l DIC level. If this level is used as the impact level, then the impacted water volume will be 2,301 m^3 and the impacted surface area will be 23,012 m^2 (about 2% of the 1 km^2 grid cell). Based on these findings, it is concluded that underwater emitted exhausted CO_2 from ships is likely to impact a very limited area. Nevertheless, its ecological impact on the longer run is yet to be established, especially considering the unknown factors, such as the depletion of buffering capacity and the toxicity of algal blooms.

One of the factors not yet included in the impact assessment is the temperature of the gas exhausted by the combustion engine. Generally, exhaust gas discharges at a temperature of approximately 420℃, and a temperature between 500 to 700℃ at full load and 200 to 300℃ without load (Nolan, 2017). These extremely high-temperature ranges are of course lethal for organisms that come into direct contact with it. Harvesting the heat via a heat exchanger could be applied as a cooling system to reduce the temperature of the exhausted gas, but this will pose additional technical and financial challenges. Of course the high temperature could support the anti-fouling potential of the GasDrive system as a ≤ 10 ℃ increase in temperature already interrupts the settlement and survival of marine fouling organisms like mussels and bryozoans (Sorte et al., 2010). Besides the temperature of the exhausted gas, the increased temperature of the surrounding water depends on factors such as the water currents and water volume as well. The impact of elevated water temperature for different species depends on the species specific acclimation temperature (de Vries et al., 2008). Here, the acute thermal impact was caused by the exhaust gas along the ship's hull, which is different from the gradual heating of the water column. Nevertheless, the well-known combined impact of elevated CO_2 concentration and high-temperature on marine organisms raises the concern of the effects from exhaust gas in busy shipping lanes and shallow water zones. Prada et al. (2017) and Harrington and Hamlin (2019) reported that acute thermal stress and acidification can synergistically impact the cardiac performance in lobsters and mortality in coral. Similar results were found on coastal and estuarine organisms as well, which are adapted to withstand thermal conditions, due to frequent exposure to varied water temperature caused by water movement along the coast. One of the most thermally tolerant species, the Sydney rock oyster *S. glomerate*, showed limited impact by 33 ℃ water condition in 380 µatm pCO_2 (Parker et al., 2017). However, their respiration rapidly depressed at 30 ℃ in 856 µatm pCO_2 treatment and 27 ℃ in 1,500 µatm pCO_2 treatment (Parker et al., 2017). It implies that, without considering the combined thermal and acidic effects, we may underestimate the overall environmental impact of the underwater exhaust system.

Like the discussed exhaust gas impacted area above, it is important to estimate the volume of heated water by the exhaust gas before judging its effects. It is known that in a 24-hour period, one ship passing through a 1 km^2 grid cell on average emits 0.71 kg CO_2 (Chapter 5). The exhausted CO_2 is approximately 5.8% of the total amount of exhaust gas (Chapter 4 S 4.1). Thus, in a 24 hour period, one ship passing through a 1 km^2 grid cell on average emits 12.24 kg of exhaust gas. It was assumed that the exhaust gas temperature was 700 ℃ (as full load exhaust gas temperature, the worst-case scenario) and the background seawater temperature was set as average global sea surface temperature, 16 ℃ (Cao et al., 2007). In

addition, we assumed that the seawater temperature will increase 10 °C by the heat of the exhausted gas before more seawater got impacted. Thus, the amount of heated water was calculated following the formula below:

$$C_{p_{water}} * \Delta K_{water} * W_{water} = C_{p_{exhaust\ gas}} * \Delta K_{gas} * W_{exhaust\ gas}$$

Where $C_{p_{water}}$ is the specific heat capacity of water, 4,200 J/kg/degree;
$Cp_{exhaust\ gas}$ is the specific heat capacity of the exhaust gas. This value is highly dependent on temperature and gas composition. Here, we assumed this value equal to standard dry air Cp, 1,005 J/kg/degree (Murphy et al., 2015);

ΔK_{water} is the increased water temperature by the exhausted gas, in this case, is 10 °C;
ΔK_{gas} is the decreased gas temperature by the surrounding water, in this case, is 700 °C – (16 °C + 10 °C) = 674 °C;
W_{water} is the amount of heated water, in kg;
$W_{exhaust\ gas}$ is the amount of exhaust gas, in this case, is 12.24 kg.

The calculated amount of heated water (increase of 10 °C) by a ship passing through a 1 km^2 grid cell emitted exhaust gas is 197.4 kg, which is approximately 197.4 liter. The thermal impact of such a small amount of heated water is expected to be negligible in open water. It may however impact the water temperature in busy canals.

The negative impact from the high temperature and acidic condition around the ship's hull on marine organisms may provide a potential of underwater released exhaust gas system in bio-fouling control. The most common anti-fouling techniques is coating the fouling surface with biocides to prohibit or kill microorganisms responsible for biofouling. After the most commonly used antifouling paint, tributyltin (TBT), being globally banned on all ships, organic booster biocides development started blooming (Terlizzi et al., 2001). However, most of these organic booster biocides are copper-based metal oxides based and very toxic to non-target organisms like fish, crustaceans and invertebrates as well (Amara et al., 2018). In comparison, the potential double function of underwater released exhaust CO_2 wouble be more environmental-friendly anti-fouling. Biofouling control with exhausted CO_2 and heat would works in two ways. Besides preventing the prevalence of microorganisms (like the antifouling paints do), it could also remove the already attached organisms, especially when boat is sailing. The study described in Chapter 3 showed the potential of elevated CO_2 concentrations via both ways in anti-fouling. Significant inhibition (at pH 7.6) on the development of biofilm biomass and weakening of the barnacles' attachment (at pH 6.3) were observed. Of course, the not yet specified biofilm species and the very low effect level (pH 6.3) and long exposure period (25 days) that were applied still hold uncertainties to this antifouling application in practice. The combination with elevated temperature was not tested in this study. Perhaps a more promising approach could be based on the assumption that free swimming larvae of fouling organisms are able to identify favourable and less favourable conditions for survival before they settle. Elevated CO_2 concentrations could very well be an indicator of less favourable conditions that might prevent the larvae from settling in that area. This principle could not be studied during this research project, but an inventory of this mechanism could be an interesting start of what might result in a new way to prevent and reduce biofouling.

Besides temperature impact, the underwater released exhaust gas-generated noise is another potential impactor to the ecosystem that requires attention. Although Matveev (2005) reported that the gaseous layer on the ship's hull can significantly reduce the acoustic signal of ships, their study was based on the available air lubrication system, which may be better than the yet underdeveloped underwater exhaust gas system. It needs to be studied how the differences in ship design can result in different frequencies of the generated sound and thus wavelengths of emitted noise. Furthermore, the location and the covered area of the released air layer on the ship's hull will impact noise levels as well. All these parameters can only be modelled after the GasDrive ships are further developed. Assuming the underwater exhaust gas is indeed reducing the shipping noise, it would be another eco-friendly attribution of the system. Numerous studies show the adverse impact of anthropogenic underwater noise pollution from shipping, oil drilling, sonar system and deep-sea mining on marine life. Especially the effects on marine mammals have been studied (e.g. navigation, hunting and communication) (Forney et al., 2017; Middel &Verones, 2017; K A Miller et al., 2018), and more recently also other marine organisms, including fish, have been shown to be adversely affected from noise pollution (Celi et al., 2016; Weilgart, 2018). Therefore, it is recommended that the influence of underwater release exhaust gas systems on the overall underwater noise produced by marine shipping should be included in the system's design as well as the impact on marine organisms such as marine mammals and fish.

In general, the underwater exhaust system **is likely to be safe** from an environmental perspective. But a concrete study is required on the generated noise level using an appropriate animal model (e.g. marine mammals in noise impact studies) and exposure conditions (acute, repeated and chronic exposure).

6.6 General conclusion and future perspectives for applying the GasDrive principle for ships

This thesis focuses on the impact of the underwater released exhaust gas from ships on the marine ecosystem. CO_2 in the exhausted gas was identified as the major driver of environmental impact. Injecting CO_2 into the water caused acidic conditions (low pH) which had a significant impact on multiple invertebrate communities and influenced the less sensitive species via the food chain. On the other hand, the overall fuel consumption and marine emission from GasDrive ships compared to regular ships will probably be lower, due to the highly efficient engine and reduced water resistance by air lubrication. In the worst-case-scenario, it was estimated that the amount of exhausted CO_2 from diesel vessels in the busiest shipping lanes only impacted a limited amount of water. Thus, the underwater released exhaust gas system is likely to be safe from an environmental perspective. However, there are still some future challenges and perspectives when applying the GasDrive ships worldwide.

Firstly, regulations of direct underwater marine emissions can be expected to be issued. Although GasDrive ships are likely to reduce the total amount of emissions **globally**, the significant increase of **locally** emitted exhaust gas, may be against the predicted underwater emission regulations and challenge the application. Regardless of other components in the exhaust gas, a significant increase of the CO_2 concentration in local waters by directly injecting, may challenge the existing regulations. In April 2018, IMO adopted a new strategy on greenhouse gas emission and aiming to reduce 50% by 2050 compared to 2008. This

strategy includes a specific reference to "a pathway of CO_2 emissions reduction consistent with the Paris Agreement temperature goals" (IMO, 2018). GasDrive ships have the potential to add to goals on a global scale, but the common thought pattern of "CO_2 induces ocean acidification and climate change" from societies and authorities may bring resistance of applying the underwater release of exhaust CO_2.

Secondly, the exposure of the exhaust gas from GasDrive ships on the crew is not yet assessed and the potential effects unknown. Shipping emission, e.g. the exhausted CO, NO_x, SO_x, and PMs, would be adverse for human health, especially for people that are chronically exposed when working onboard and in harbor cities (Van Fan et al., 2018). For regular ships, the exhausted gas is emitted via chimneys, which can be 50 m high above the working deck. While for GasDrive ships, the exhaust gas exchanges from water to the atmosphere. Therefore, people on board GasDrive ships are likely to be exposed differently, and possibly to a higher dose of different composition than to exhaust gas on regular ships. To reduce the risk for human exposure, the use of the underwater exhaust system could be restricted below a certain sailing speed. When the ships are laying still or sailing with a low speed, the exhaust gas can be directly released to the atmosphere like the regular ships. Such "underwater-atmosphere release" switching system may bring some technical challenges for the ships' design. However, it is probably necessary not only for human health but also to protect organisms in shallow, busy shipping lanes. To minimize the impact of exhaust gas on the organisms in shallow water with busy shipping lanes, issuing underwater Emission Control Areas (ECAs, Section 1.1.2) can be a solution. The study in Chapter 5 selected relatively high-risk areas, so not the entire ecoregion, that can be the potential underwater ECAs. In underwater ECAs, the exhaust gas may be released into the atmosphere instead of directly into the water, and after sailing out of the ECAs, it can be released underwater again.

To safely apply the underwater released exhaust gas system, its generated noise and occupational risk assessment must be studied when more technical information about the GasDrive ships becomes available. Overall, there is still some distance to releasing the GasDrive ships on the market due to both environmental and technical challenges and uncertainties. But the underwater released exhaust gas system also opens some perspectives in shipping efficiency, biofouling control, and marine emission regulation. This thesis paves the path to further guiding the application in an eco-friendly direction and sets an example of performing an environmental impact assessment on a novel designed technical product before releasing it to the market.

Summary

The high demand in maritime transportation for more and more strict regulations on its fuel and emission have motivated engineers to design innovative highly efficient ships, and 'GasDrive' is one of them. The GasDrive ships are powered by Liquid Natural Gas (LNG), which means less NO_x and SO_x are present in the exhaust gas. A new generation of fuel cells in combination with turbocharged gas engines are under development at this moment to lower the fuel consumption. In addition, this innovative ship would release exhaust gas under water along the ship's hull. The discharged gas bubbles will be "trapped" in a specially designed nanostructured hull surface and form an 'air lubricate' layer, thereby reducing the water resistance of the vessel. In this way, the total emission of GasDrive ships is expected to be significantly less compared to the current ships. However, the impact of this underwater emission on the local marine ecosystems is unknown. Especially, one of the dominant components in the exhaust gas, CO_2 (5 - 8% v/v), is well-known to cause ocean acidification and algal blooms. Besides CO_2, several components in the exhaust gas can impact marine ecosystems as well, such as SO_x, NO_x and PAHs. The research described in this thesis focuses first on the impact of underwater released CO_2 on marine algae and invertebrates and on the interaction between species in acidified conditions. After that, it investigated the effects of other components in the exhausted gas. Finally, a preliminary risk assessment of underwater released exhaust CO_2 was carried out from a global marine perspective based on the findings from these practical studies.

Chapter 2 describes the response of a marine community to a wide range of CO_2 concentrations. Fourteen mesocosms were used in this study and filled with about 8 cm natural sandy sediment and 600 l natural seawater. Marine worms (polychaetes), periwinkles (*Littorina littorea*), mud snails (*Peringia ulvae*), mud shrimps (C*orophium volutator*) and naturally introduced plankton and small benthic invertebrate species were exposed to pH 8.6 - 5.8 conditions as a result of CO_2 injection for 49 days. The studied benthic community shifted towards polychaete dominance between pH 6.6 and pH 7.1 and collapsed at pH 5.8. Due to the reduced grazing pressure and the flux of nutrients from decaying organic material, phytoplankton started blooming at the highest exposure level (pH 5.8). The periphyton (fouling microalgae) community, however, was not able to take advantage of these conditions as it reduced in biomass. This implies that periphyton is more sensitive to elevated CO_2 levels than phytoplankton or less grazed upon in the mesocosms. Periwinkles suffered directly from high CO_2 levels by shell damage and increased mortality. The growth of the surviving periwinkles was not directly related to pH but was positively correlated with the availability of periphyton and negatively correlated with the polychaete worm density that most likely also used the periphyton as food source. The results show the importance of testing species interactions in the response of an ecosystem to elevated CO_2 concentrations. Additionally, the alkalinity level increased along with the pH decrease, due to the decalcification of shell fragments present in the sediment. This implies that ocean acidification studies which exclude the increase of alkalinity may overestimate the effects of elevated CO_2 concentrations in some field conditions, such as shallow water with sediments containing shell fragments.

To further investigate the effects of underwater released CO_2 on marine organisms, microbial biofilms and barnacles were exposed in microcosms to high CO_2 concentrations (resulting in pH 7.8 to 6.3) (Chapter 3). With decreasing pH, the development of a microbial biofilm biomass was significantly reduced and a shift in taxonomic composition was observed. Barnacles tolerated acidic conditions up to pH 6.8 although their feeding activity and growth rate decreased, and high mortality occurred at pH 6.3. Over 50% of the barnacles pre-exposed

at pH 6.3 were removed from their growth plate by the water force during sailing with 12 km/h for 15 min. The effects on sessile organisms in this study suggest that CO_2-induced acidic conditions around the ship's hull may provide an the anti-fouling effect, which could be an additional benefit of using underwater exhaust systems.

The following experiments, described in Chapter 4, investigate the additional impact on marine organisms of the other components in diesel engine exhaust gas besides CO_2. The pure CO_2 enriched seawater was used as reference group in this study. CO_2 is an essential nutrient for photosynthetic organisms like microalgae, and induced algal growth. The combination of stimulated algal growth and negative effects on algal consumers could facilitate the development of algal blooms, which was studied with microalgae (*Isochrysis galbana*) alone or in combination with rotifers (*Brachionus plicatilis*) that feed on them. No significantly different effects were found between exhaust gas and elevated CO_2 treatments, suggesting that CO_2 is the main impact factor in the exhaust gas. Since CO_2 concentrations in exhaust gas can vary, a wider range of CO_2 concentrations (resulting in initial pH 5 to 8) were tested in separate experiments with the same species combination. An initial pH of 6 or lower had a negative impact on the previously used algal species, therefore, an algal species more resistant to low pH levels, *Dunaliella salina*, was used in the third experiment. The CO_2 in the culture was used up by the fast growing algae in the first 2 days, thereafter the growth of *D. salina* was low due to carbon shortage. Subsequently, the population of rotifers decreased as well, while they had survived the initial acidic condition (pH 6). The performed studies indicate that all observed effects were caused by CO_2 only. No additional impact of other compounds like NO_x and PAHs on the studied marine plankton was observed.

After identifying CO_2 as main impactor, the study described in Chapter 5 assessed the relative risk for distinct ecological areas with the highest potential impact of underwater released exhaust CO_2. Risk was characterized for 262 marine ecoregions by comparing the expected CO_2 emission to water, expressed as dissolved inorganic carbon (DIC) exposure, caused by the novel maritime shipping, with the estimated vulnerability to acidification and algal blooming. The DIC exposure in 1 km x 1 km grid cells was estimated based on the amount of emitted CO_2 from marine transportation in 2018, assuming all exhaust release would be underwater. The vulnerability of each ecoregion was assessed based on three indicators: background DIC level, chlorophyll-a and total alkalinity level. The results indicate that the areas with relatively high vulnerability are mainly located above 30° N latitude with limited seasonal impact. At the global relative risk assessment level, the Yellow Sea, Southern China Sea, and North Sea come out as relatively high-risk areas. At a more detailed level, zooming into European high-risk ecoregions, specifically areas with dense shipping lanes and maritime chokepoints, such as the Strait of Dover and the Strait of Gibraltar, appear at risk instead of the entire ecoregion. In this worst-case-scenario, it was estimated that the direct impact of exhausted CO_2 from vessels in the busiest shipping lane would be 0.023% of the 1 km^2 grid cell, so to a limited fraction of the marine system. This can be explained by the maximum dissolution of CO_2 in the upper water layers while the rest will exchange back to the air.

Overall, the underwater released exhaust gas system is likely to be safe from an environmental perspective, at least when compared with the environmental impact of traditional shipping. In addition to the perspective it provides, there are still some future challenges when applying the GasDrive ships worldwide. For instance, the common thought pattern of "CO_2 induces ocean acidification and climate change" from societies and authorities may bring resistance of applying the underwater release of exhaust CO_2.

Although, GasDrive ships will reduce maritime emission globally, the significant local increase of emitted exhaust gas, may challenge the application. To overcome this challenge, underwater emission control areas can be selected to exhaust gas sensitive areas, where exhausted gas must be emitted directly to the atmosphere. Further attention should be given to the occupational risk assessment for the crew and the generation of underwater noise and its effect on marine organisms.

The underwater released exhaust gas system in combination with the other GasDrive innovations, provides perspectives in enhanced shipping efficiency, biofouling control, and marine emission regulation. Regulating application of underwater marine emission would need to be developed, including regulating worker safety and health.

Reference

Ainsworth, T. D., Heron, S. F., Ortiz, J. C., Mumby, P. J., Grech, A., Ogawa, D., Eakin, C. M., & Leggat, W. (2016). Climate change disables coral bleaching protection on the Great Barrier Reef. *Science*, *352*(6283), 338-342.

Al-Anezi, K., Somerfield, C., Mee, D., & Hilal, N. (2008). Parameters affecting the solubility of carbon dioxide in seawater at the conditions encountered in MSF desalination plants. *Desalination*, *222*(1-3), 548-571.

Albright, R., Caldeira, L., Hosfelt, J., Kwiatkowski, L., Maclaren, J. K., Mason, B. M., Nebuchina, Y., Ninokawa, A., Pongratz, J., & Ricke, K. L. (2016). Reversal of ocean acidification enhances net coral reef calcification. *Nature*, *531*(7594), 362.

Algueró-Muñiz, M., Horn, H. G., Alvarez-Fernandez, S., Spisla, C., Aberle, N., Bach, L. T., Guan, W., Achterberg, E. P., Riebesell, U., & Boersma, M. (2019). Analyzing the impacts of elevated-CO_2 levels on the development of a subtropical zooplankton community during oligotrophic conditions and simulated upwelling. *Frontiers in Marine Science*, *6*, 61.

Ali, M. F., & Abbas, S. (2006). A review of methods for the demetallization of residual fuel oils. *Fuel Processing Technology*, *87*(7), 573-584.

Almeda, R., Wambaugh, Z., Wang, Z., Hyatt, C., Liu, Z., & Buskey, E. J. (2013). Interactions between zooplankton and crude oil: toxic effects and bioaccumulation of polycyclic aromatic hydrocarbons. *PLoS ONE*, *8*(6).

Amara, I., Miled, W., Slama, R. B., & Ladhari, N. (2018). Antifouling processes and toxicity effects of antifouling paints on marine environment. A review. *Environmental toxicology and pharmacology*, *57*, 115-130.

Anderson, M., Salo, K., & Fridell, E. (2015). Particle-and gaseous emissions from an LNG powered ship. *Environmental science & technology*, *49*(20), 12568-12575.

Anderson, M. J. (2014). Permutational multivariate analysis of variance (PERMANOVA). *Wiley statsref: statistics reference online*, 1-15.

Armstrong, E., Boyd, K. G., & Burgess, J. G. (2000). Prevention of marine biofouling using natural compounds from marine organisms.

Arnold, W., Diamond, R., & Smith, D. (2010). The effects of salinity, pH, and dissolved organic matter on acute copper toxicity to the rotifer, Brachionus plicatilis ("L" strain). *Archives of environmental contamination and toxicology*, *59*(2), 225-234.

Åström, S., Yaramenka, K., Winnes, H., Fridell, E., & Holland, M. (2018). The costs and benefits of a nitrogen emission control area in the Baltic and North Seas. *Transportation Research Part D: Transport and Environment*, *59*, 223-236.

Atlas, T. N. C. (2019). Marine Ecoregions Of the World (MEOW), edited, The Nature Conservantion Atlas.

Azim, M. E., & Likens, G. E. (2009). Photosynthetic Periphyton and Surfaces. in *Encyclopedia of Inland Waters*. pp. 184-191, Academic Press, Oxford, doi:https://doi.org/10.1016/B978-012370626-3.00144-7.

Azzara, A., Minjares, R., & Rutherford, D. (2015). Needs and opportunities to reduce black carbon emissions from maritime shipping. *assessment*, *118*, 5380-5552.

Bach, L. T., Alvarez-Fernandez, S., Hornick, T., Stuhr, A., & Riebesell, U. (2017). Simulated ocean acidification reveals winners and losers in coastal phytoplankton. *PLoS ONE*, *12*(11), e0188198.

Bamber, R. (1990). The effects of acidic seawater on three species of lamellibranch mollusc. *Journal of Experimental Marine Biology and Ecology*, *143*(3), 181-191.

Bamber, R. N. (1987). The effects of acidic sea water on young carpet-shell clams Venerupis decussata (L.)(Mollusca: Veneracea). *Journal of Experimental Marine Biology and Ecology*, *108*(3), 241-260.

Barcelos e Ramos, J., Biswas, H., Schulz, K. G., LaRoche, J., & Riebesell, U. (2007). Effect of rising atmospheric carbon dioxide on the marine nitrogen fixer Trichodesmium. *Global biogeochemical cycles*, *21*(2).

Bates, N. R., Best, M. H., & Hansell, D. A. (2005). Spatio-temporal distribution of dissolved inorganic carbon and net community production in the Chukchi and Beaufort Seas. *Deep Sea Research Part II: Topical Studies in Oceanography*, *52*(24-26), 3303-3323.

Bautista-Chamizo, E., Sendra, M., De Orte, M., & Riba, I. (2019). Comparative effects of seawater acidification on microalgae: Single and multispecies toxicity tests. *Science of the total environment*, *649*, 224-232.

Bellas, J., Saco-Álvarez, L., Nieto, Ó., & Beiras, R. (2008). Ecotoxicological evaluation of polycyclic aromatic hydrocarbons using marine invertebrate embryo–larval bioassays. *Marine Pollution Bulletin*, *57*(6-12), 493-502.

Benson, P., Brining, D., & Perrin, D. (1973). Marine fouling and its prevention. *Mar. Technol*, *10*(3), 37.

Bertucci, A., Moya, A., Tambutté, S., Allemand, D., Supuran, C. T., & Zoccola, D. (2013). Carbonic anhydrases in anthozoan corals—A review. *Bioorganic & medicinal chemistry*, *21*(6), 1437-1450.

Boßelmann, F., Romano, P., Fabritius, H., Raabe, D., & Epple, M. (2007). The composition of the exoskeleton of two crustacea: The American lobster Homarus americanus and the edible crab Cancer pagurus. *Thermochimica Acta*, *463*(1-2), 65-68.

Bots, P., Benning, L., Rickaby, R., & Shaw, S. (2011). The role of SO4 in the switch from calcite to aragonite seas. *Geology*, *39*(4), 331-334.

Bouchard, C., et al. (2014). Once upon a larva: revisiting the relationship between feeding success and growth in fish larvae. *ICES Journal of Marine Science*, *72*(2), 359-373, doi:10.1093/icesjms/fsu201.

Bourget, E. (1987). Barnacle shells: composition, structure and growth. *Barnacle biology*, *5*, 267-285.

Brandt, J., Silver, J. D., Christensen, J. H., Andersen, M. S., Bønløkke, J. H., Sigsgaard, T., Geels, C., Gross, A., Hansen, A. B., & Hansen, K. M. (2013). Assessment of past, present and future health-cost externalities of air pollution in Europe and the contribution from international ship traffic using the EVA model system. *Atmospheric Chemistry and Physics*, *13*(15), 7747-7764.

Bray, J. R., & Curtis, J. T. (1957). An ordination of the upland forest communities of southern Wisconsin. *Ecological monographs*, *27*(4), 325-349.

Bressy, C., & Lejars, M. (2014). Marine fouling: An overview. *The Journal of Ocean Technology*, *9*(4), 19-28.

Brockmann, D., & Janse, M. (2008). Calcium and carbonate in closed marine aquarium systems. *Advances in Coral Husbandry in Public Aquariums. Arnhem: Burgers' Zoo*, 133-142.

Buis, A., Lynch, P., Cook-Anderson, G., & Sullivant, R. (2011). Aquarius/SAC-D: Studying Earth's salty seas from space. *Jun*.

Burel, F., Taccani, R., & Zuliani, N. (2013). Improving sustainability of maritime transport through utilization of Liquefied Natural Gas (LNG) for propulsion. *Energy*, *57*, 412-420.

Callow, M. E., & Callow, J. A. (2002). Marine biofouling: a sticky problem. *Biologist*, *49*(1), 1-5.

Camiro-Vargas, T. K., Hernández-Ayón, J. M., Valenzuela-Espinoza, E., Delgadillo-Hinojosa, F., & Cajal-Medrano, R. (2005). Dissolved inorganic carbon uptake by Rhodomonas sp. and Isochrysis aff. galbana determined by a potentiometric technique. *Aquacultural engineering*, *33*(2), 83-95.

Campanati, C., Yip, S., Lane, A., & Thiyagarajan, V. (2015). Combined effects of low pH and low oxygen on the early-life stages of the barnacle Balanus amphitrite. *ICES Journal of Marine Science*, *73*(3), 791-802.

Campbell, A. H., Meritt, D. W., Franklin, R. B., Boone, E. L., Nicely, C. T., & Brown, B. L. (2011). Effects of age and composition of field-produced biofilms on oyster larval setting. *Biofouling*, *27*(3), 255-265.

Canesi, L., Ciacci, C., Betti, M., Fabbri, R., Canonico, B., Fantinati, A., Marcomini, A., & Pojana, G. (2008). Immunotoxicity of carbon black nanoparticles to blue mussel hemocytes. *Environment international*, *34*(8), 1114-1119.

Cao, L., Caldeira, K., & Jain, A. K. (2007). Effects of carbon dioxide and climate change on ocean acidification and carbonate mineral saturation. *Geophysical Research Letters*, *34*(5).

Casey, K. S., et al. (2011). AVHRR Pathfinder version 5.2 level 3 collated (L3C) global 4km sea surface temperature for 1981-2012. in *NOAA National Centers for Environmental Information*, edited, https://data.nodc.noaa.gov/cgi-bin/iso?id=gov.noaa.nodc:AVHRR_Pathfinder-NODC-L3C-v5.2;view=html, doi:https://doi.org/10.7289/v5wd3xhb.

Ceccio, S. L. (2010). Friction drag reduction of external flows with bubble and gas injection. *Annual Review of Fluid Mechanics*, *42*, 183-203.

Celi, M., Filiciotto, F., Maricchiolo, G., Genovese, L., Quinci, E. M., Maccarrone, V., Mazzola, S., Vazzana, M., & Buscaino, G. (2016). Vessel noise pollution as a human threat to fish: assessment of the stress response in gilthead sea bream (Sparus aurata, Linnaeus 1758). *Fish Physiology and biochemistry*, *42*(2), 631-641.
Chamberlain, S. A., & Szöcs, E. (2013). taxize: taxonomic search and retrieval in R. *F1000Research*, *2*.
Chambers, L. D., Stokes, K. R., Walsh, F. C., & Wood, R. J. (2006). Modern approaches to marine antifouling coatings. *Surface and Coatings Technology*, *201*(6), 3642-3652.
Champ, M. A. (2000). A review of organotin regulatory strategies, pending actions, related costs and benefits. *Science of the Total Environment*, *258*(1-2), 21-71.
Chen, J., Fei, Y., & Wan, Z. (2019). The relationship between the development of global maritime fleets and GHG emission from shipping. *Journal of Environmental Management*, *242*, 31-39.
Chen, W., Liu, H., Zhang, Q., & Dai, S. (2011). Effects of nitrite and toxic Microcystis aeruginosa PCC7806 on the growth of freshwater rotifer Brachionus calyciflorus. *Bulletin of Environmental Contamination and Toxicology*, *86*(3), 263-267.
Christiansen, M., Fagerholt, K., Nygreen, B., & Ronen, D. (2007). Maritime transportation. *Handbooks in operations research and management science*, *14*, 189-284.
Clements, J. C., & Darrow, E. S. (2018). Eating in an acidifying ocean: a quantitative review of elevated CO_2 effects on the feeding rates of calcifying marine invertebrates. *Hydrobiologia*, *820*(1), 1-21.
Cole, J. J. (2012). The carbon cycle: With a brief introduction to global biogeochemistry. *Fundamentals of Ecosystem Science*, 109-135.
Commission, E. (2011). Transport 2050: Commission outlines ambitious plan to increase mobility and reduce emissions, edited by E. Commission, Brussel.
Commission, E. (2016). Methane emissions from LNG-powered ships higher than current marine fuel oils. European Commission Environment News Alert Service, The University of the West of England, Bristol.
Conservancy, T. N. (2012). Marine Ecoregions and Pelagic Provinces of the World, Cambridge, UK.
Corbett, J. J., Winebrake, J. J., Green, E. H., Kasibhatla, P., Eyring, V., & Lauer, A. (2007). Mortality from Ship Emissions: A Global Assessment. *Environmental Science & Technology*, *41*(24), 8512-8518, doi:10.1021/es071686z.
Cornwall, C. E., & Hurd, C. L. (2016). Experimental design in ocean acidification research: problems and solutions. *ICES Journal of Marine Science*, *73*(3), 572-581.
Crain, C. M., Kroeker, K., & Halpern, B. S. (2008). Interactive and cumulative effects of multiple human stressors in marine systems. *Ecol Lett*, *11*(12), 1304-1315.
Currie, A. R., Tait, K., Parry, H., de Francisco-Mora, B., Hicks, N., Osborn, A. M., Widdicombe, S., & Stahl, H. (2017). Marine microbial gene abundance and community composition in response to ocean acidification and elevated temperature in two contrasting coastal marine sediments. *Frontiers in microbiology*, *8*, 1599.
Cyronak, T., Schulz, K. G., & Jokiel, P. L. (2015). The Omega myth: what really drives lower calcification rates in an acidifying ocean. *ICES Journal of Marine Science*, *73*(3), 558-562.
Dafforn, K. A., Lewis, J. A., & Johnston, E. L. (2011). Antifouling strategies: history and regulation, ecological impacts and mitigation. *Marine pollution bulletin*, *62*(3), 453-465.
Davenport, J., Hughes, R. N., Shorten, M., & Larsen, P. S. (2011). Drag reduction by air release promotes fast ascent in jumping emperor penguins—a novel hypothesis. *Marine Ecology Progress Series*, *430*, 171-182.
de Vries, P., Tamis, J. E., Foekema, E. M., Klok, C., & Murk, A. J. (2013). Towards quantitative ecological risk assessment of elevated carbon dioxide levels in the marine environment. *Marine pollution bulletin*, *73*(2), 516-523.
de Vries, P., Tamis, J. E., Murk, A. J., & Smit, M. G. (2008). Development and application of a species sensitivity distribution for temperature-induced mortality in the aquatic environment. *Environmental Toxicology and Chemistry: An International Journal*, *27*(12), 2591-2598.
Demarcq, H., Barlow, R., & Hutchings, L. (2007). Application of a chlorophyll index derived from satellite data to investigate the variability of phytoplankton in the Benguela ecosystem. *African Journal of Marine Science*, *29*(2), 271-282.

Diamond, S. A., Milroy, N. J., Mattson, V. R., Heinis, L. J., & Mount, D. R. (2003). Photoactivated toxicity in amphipods collected from polycyclic aromatic hydrocarbon–contaminated sites. *Environmental Toxicology and Chemistry: An International Journal*, *22*(11), 2752-2760.
Dolah, F. M. V., Roelke, D., & Greene, R. M. (2001). Health and ecological impacts of harmful algal blooms: risk assessment needs. *Human and Ecological Risk Assessment: An International Journal*, *7*(5), 1329-1345.
Doney, S. C., Fabry, V. J., Feely, R. A., & Kleypas, J. A. (2009). Ocean acidification: the other CO_2 problem. *Annual review of marine science*, *1*, 169-192.
Doney, S. C., Mahowald, N., Lima, I., Feely, R. A., Mackenzie, F. T., Lamarque, J.-F., & Rasch, P. J. (2007). Impact of anthropogenic atmospheric nitrogen and sulfur deposition on ocean acidification and the inorganic carbon system. *Proceedings of the National Academy of Sciences*, *104*(37), 14580-14585.
Duan, Z., & Sun, R. (2003). An improved model calculating CO_2 solubility in pure water and aqueous NaCl solutions from 273 to 533 K and from 0 to 2000 bar. *Chemical geology*, *193*(3-4), 257-271.
ECTA, C. a. (2011). Guidelines for measuring and managing CO2 emission from freight transport operations*Rep.*, https://www.ecta.com/resources/Documents/Best%20Practices%20Guidelines/guideline_for_measuring_and_managing_co2.pdf.
EEA (2013). The impact of international shipping on European air quality and climate forcing*Rep.*, 88 pp, European Environment Agenct, Copenhagen.
Eguíluz, V. M., Fernández-Gracia, J., Irigoien, X., & Duarte, C. M. (2016). A quantitative assessment of Arctic shipping in 2010–2014. *Scientific reports*, *6*(1), 1-6.
EIA (2018). Natural Gas Explained. U.S. Energy Information Administration, Washington DC, U.S.
EIA (2019). Residual fuel oil. U.S. Energy Information Administration, Washington, DC, USA.
Elbing, B. R., Winkel, E. S., Lay, K. A., Ceccio, S. L., Dowling, D. R., & Perlin, M. (2008). Bubble-induced skin-friction drag reduction and the abrupt transition to air-layer drag reduction. *Journal of Fluid Mechanics*, *612*, 201-236.
EPA (2000). Analysis of Commercial Marine Vessels Emissions and Fuel Consumption Data, edited by T. a. A. Quality, U.S. Environmental Protection Agency, USA.
Er, I. D. (2002). Overview of NO_x Emission Controls in Marine Diesel Engines. *Energy Sources*, *24*(4), 319-327.
Esters, L., Landwehr, S., Sutherland, G., Bell, T. G., Christensen, K. H., Saltzman, E. S., Miller, S. D., & Ward, B. (2017). Parameterizing air-sea gas transfer velocity with dissipation. *Journal of Geophysical Research: Oceans*, *122*(4), 3041-3056.
Fabry, V. J., Seibel, B. A., Feely, R. A., & Orr, J. C. (2008). Impacts of ocean acidification on marine fauna and ecosystem processes. *ICES Journal of Marine Science*, *65*(3), 414-432.
Fagerholt, K., Gausel, N. T., Rakke, J. G., & Psaraftis, H. N. (2015). Maritime routing and speed optimization with emission control areas. *Transportation Research Part C: Emerging Technologies*, *52*, 57-73.
Falkowski, P. G., & Raven, J. A. (2013). *Aquatic photosynthesis*, Princeton University Press.
Fassbender, A. J., Sabine, C. L., & Feifel, K. M. (2016). Consideration of coastal carbonate chemistry in understanding biological calcification. *Geophysical Research Letters*, *43*(9), 4467-4476.
Feng, E. Y., Keller, D. P., Koeve, W., & Oschlies, A. (2016). Could artificial ocean alkalinization protect tropical coral ecosystems from ocean acidification? *Environmental Research Letters*, *11*(7), 074008.
Ferrer-Gonzalez, M., & Ilyina, T. (2015). Mitigation potential, risks, and side-effects of ocean alkalinity enhancement. paper presented at Deglaciation Changes in Ocean Dynamics and Atmospheric CO2, Herausgegeben und redigiert im Namen der Kaiserlich Leopoldinisch ….
Findlay, H. S., Kendall, M. A., Spicer, J. I., & Widdicombe, S. (2009). Future high CO2 in the intertidal may compromise adult barnacle Semibalanus balanoides survival and embryonic development rate. *Marine Ecology Progress Series*, *389*, 193-202.
Findlay, H. S., Kendall, M. A., Spicer, J. I., & Widdicombe, S. (2010a). Post-larval development of two intertidal barnacles at elevated CO_2 and temperature. *Marine Biology*, *157*(4), 725-735.

Findlay, H. S., Kendall, M. A., Spicer, J. I., & Widdicombe, S. (2010b). Relative influences of ocean acidification and temperature on intertidal barnacle post-larvae at the northern edge of their geographic distribution. *Estuarine, Coastal and Shelf Science*, *86*(4), 675-682.
Fine, R. A., Willey, D., Thompson, C., & Jentoft-Nilsen, M. (2015). Ocean Alkalinity. NASA, USA.
Fine, R. A., Willey, D. A., & Millero, F. J. (2017). Global variability and changes in ocean total alkalinity from Aquarius satellite data. *Geophysical Research Letters*, *44*(1), 261-267.
Foekema, E. M., Fischer, A., Parron, M. L., Kwadijk, C., de Vries, P., & Murk, A. J. (2012). Toxic concentrations in fish early life stages peak at a critical moment. *Environmental Toxicology and Chemistry*, *31*(6), 1381-1390, doi:10.1002/etc.1836.
Forney, K. A., Southall, B. L., Slooten, E., Dawson, S., Read, A. J., Baird, R. W., & Brownell Jr, R. L. (2017). Nowhere to go: noise impact assessments for marine mammal populations with high site fidelity. *Endangered species research*, *32*, 391-413.
Fugiel, A., Burchart-Korol, D., Czaplicka-Kolarz, K., & Smoliński, A. (2017). Environmental impact and damage categories caused by air pollution emissions from mining and quarrying sectors of European countries. *Journal of cleaner production*, *143*, 159-168.
Fuglestvedt, J., Berntsen, T., Eyring, V., Isaksen, I., Lee, D. S., & Sausen, R. (2009). Shipping Emissions: From Cooling to Warming of Climate—and Reducing Impacts on Health. *Environmental Science & Technology*, *43*(24), 9057-9062, doi:10.1021/es901944r.
Fullenbaum, R., Fallon, J., & Flanagan, B. (2013). Oil & Natural Gas Transportation & Storage Infrastructure: Status, Trends, & Economic Benefits. *IHS Global Inc. and American Petroleum Institute (API), Report*.
Furtado, P. S., Gaona, C. A., Serra, F. P., Poersch, L. H., & Wasielesky Jr, W. (2017). Acute toxicity of carbon dioxide to juvenile marine shrimp Litopenaeus vannamei (Boone 1931). *Marine and Freshwater Behaviour and Physiology*, *50*(4), 293-301.
Glibert, P. M., Al-Azri, A., Allen, J. I., Bouwman, A. F., Beusen, A. H., Burford, M. A., Harrison, P. J., & Zhou, M. (2018). Key questions and recent research advances on harmful algal blooms in relation to nutrients and eutrophication. in *Global Ecology and Oceanography of Harmful Algal Blooms*. pp. 229-259, Springer.
Gobler, C., & Talmage, S. (2013). Short-and long-term consequences of larval stage exposure to constantly and ephemerally elevated carbon dioxide for marine bivalve populations. *Biogeosciences*, *10*(4).
Gore, S., Renforth, P., & Perkins, R. (2018). The potential environmental response to increasing ocean alkalinity for negative emissions. *Mitigation and Adaptation Strategies for Global Change*, 1-21.
Grosell, M., & Jensen, F. B. (2000). Uptake and effects of nitrite in the marine teleost fish Platichthys flesus. *Aquatic Toxicology*, *50*(1-2), 97-107.
Guo, Y., Wu, K., Huo, X., & Xu, X. (2011). INTERNATIONAL PERSPECTIVES: Sources, Distribution, and Toxicity of Polycyclic Aromatic Hydrocarbons. *Journal of environmental health*, *73*(9), 22-25.
Hadfield, M. G. (2011). Biofilms and marine invertebrate larvae: what bacteria produce that larvae use to choose settlement sites. *Annual review of marine science*, *3*, 453-470.
Halpern, B. S., Frazier, M., Potapenko, J., Casey, K. S., Koenig, K., Longo, C., Lowndes, J. S., Rockwood, R. C., Selig, E. R., & Selkoe, K. A. (2015). Spatial and temporal changes in cumulative human impacts on the world's ocean. *Nature communications*, *6*(1), 1-7.
Halpern, B. S., Walbridge, S., Selkoe, K. A., Kappel, C. V., Micheli, F., D'Agrosa, C., Bruno, J. F., Casey, K. S., Ebert, C., & Fox, H. E. (2008). A global map of human impact on marine ecosystems. *Science*, *319*(5865), 948-952.
Haris, V. (1990). *Sessile animals of the sea shore*, Springer Science & Business Media.
Harrington, A. M., & Hamlin, H. J. (2019). Ocean acidification alters thermal cardiac performance, hemocyte abundance, and hemolymph chemistry in subadult American lobsters Homarus americanus H. Milne Edwards, 1837 (Decapoda: Malcostraca: Nephropidae). *Journal of Crustacean Biology*, *39*(4), 468-476.
Hartin, C. A., Bond-Lamberty, B., Patel, P., & Mundra, A. (2016). Ocean acidification over the next three centuries using a simple global climate carbon-cycle model: projections and sensitivities. *Biogeosciences*, *13*(15).

Heil, C. A., Glibert, P. M., & Fan, C. (2005). Prorocentrum minimum (Pavillard) Schiller: a review of a harmful algal bloom species of growing worldwide importance. *Harmful Algae*, *4*(3), 449-470.
Herfort, L., Thake, B., & Taubner, I. (2008). Bicarbonate stimulation of calcification and photosynthesis in two hermatypic corals. *Journal of Phycology*, *44*(1), 91-98, doi:10.1111/j.1529-8817.2007.00445.x.
Hernroth, B., Sköld, H. N., Wiklander, K., Jutfelt, F., & Baden, S. (2012). Simulated climate change causes immune suppression and protein damage in the crustacean Nephrops norvegicus. *Fish & shellfish immunology*, *33*(5), 1095-1101.
Hofmann, G. E., Smith, J. E., Johnson, K. S., Send, U., Levin, L. A., Micheli, F., Paytan, A., Price, N. N., Peterson, B., & Takeshita, Y. (2011). High-frequency dynamics of ocean pH: a multi-ecosystem comparison. *PLoS ONE*, *6*(12), e28983.
Holmström, C., Rittschof, D., & Kjelleberg, S. (1992). Inhibition of settlement by larvae of Balanus amphitrite and Ciona intestinalis by a surface-colonizing marine bacterium. *Appl. Environ. Microbiol.*, *58*(7), 2111-2115.
Honda, M., & Suzuki, N. (2020). Toxicities of Polycyclic Aromatic Hydrocarbons for Aquatic Animals. *International Journal of Environmental Research and Public Health*, *17*(4), 1363.
Hunter, K. A., Liss, P. S., Surapipith, V., Dentener, F., Duce, R., Kanakidou, M., Kubilay, N., Mahowald, N., Okin, G., & Sarin, M. (2011). Impacts of anthropogenic SOx, NOx and NH_3 on acidification of coastal waters and shipping lanes. *Geophysical Research Letters*, *38*(13).
Hussner, A., Mettler-Altmann, T., Weber, A. P., & Sand-Jensen, K. (2016). Acclimation of photosynthesis to supersaturated CO 2 in aquatic plant bicarbonate users. *Freshwater Biology*, *61*(10), 1720-1732.
Hylland, K. (2006). Polycyclic aromatic hydrocarbon (PAH) ecotoxicology in marine ecosystems. *Journal of Toxicology and Environmental Health, Part A*, *69*(1-2), 109-123.
IMO (1997a). Nitrogen Oxides (NOx) - Regulation 13 International Maritime Organization, London, UK.
IMO (1997b). Sulphur oxides (SOx) – Regulation 14. International Maritime Organization, Lodon, UK.
IMO (2014). Third IMO Greenhouse Gas Study 2014. International Maritime Organization, London, UK.
IMO (2015). Third IMO GHG study 2014 executive summary and final report, edited by I. M. Organization, London.
IMO (2016a). IMO sets 2020 date for ships to comply with low sulphur fuel oil requirement. International Maritime Organization, London, UK.
IMO (2016b). New requirements for international shipping as UN body continues to address greenhouse gas emissions. International Maritime Organization, London,UK.
IMO (2018). Low carbon shipping and air pollution control. International Maritime Organization, London, UK.
IMO (2019). Brief History of IMO. International Maritime Organization, London, UK.
IPCC (2007). *Climate Change 2007: The physical science basis: Summary for policymakers*, IPCC.
Isari, S., Zervoudaki, S., Peters, J., Papantoniou, G., Pelejero, C., & Saiz, E. (2016). Lack of evidence for elevated CO_2-induced bottom-up effects on marine copepods: a dinoflagellate–calanoid prey–predator pair. *ICES Journal of Marine Science*, *73*(3), 650-658.
Ishimatsu, A., Hayashi, M., Lee, K. S., Kikkawa, T., & Kita, J. (2005). Physiological effects on fishes in a high-CO_2 world. *Journal of geophysical research: Oceans*, *110*(C9).
Ishimatsu, A., Kikkawa, T., Hayashi, M., Lee, K.-S., & Kita, J. (2004). Effects of CO_2 on marine fish: larvae and adults. *Journal of oceanography*, *60*(4), 731-741.
Jägerbrand, A. K., Brutemark, A., Svedén, J. B., & Gren, M. (2019). A review on the environmental impacts of shipping on aquatic and nearshore ecosystems. *Science of the Total Environment*, *695*, 133637.
Jensen, F. B. (2003). Nitrite disrupts multiple physiological functions in aquatic animals. *Comparative Biochemistry and Physiology Part A: Molecular & Integrative Physiology*, *135*(1), 9-24.
Jiang, L. Q., Feely, R. A., Carter, B. R., Greeley, D. J., Gledhill, D. K., & Arzayus, K. M. (2015). Climatological distribution of aragonite saturation state in the global oceans. *Global Biogeochemical Cycles*, *29*(10), 1656-1673.

Jiang, Z. P., Tyrrell, T., Hydes, D. J., Dai, M., & Hartman, S. E. (2014). Variability of alkalinity and the alkalinity-salinity relationship in the tropical and subtropical surface ocean. *Global Biogeochemical Cycles*, *28*(7), 729-742.
Kao, L. W., & Nanagas, K. A. (2006). Toxicity associated with carbon monoxide. *Clinics in laboratory medicine*, *26*(1), 99-125.
Karyab, H., Yunesian, M., Nasseri, S., Mahvi, A. H., Ahmadkhaniha, R., Rastkari, N., & Nabizadeh, R. (2013). Polycyclic aromatic hydrocarbons in drinking water of Tehran, Iran. *Journal of Environmental Health Science and Engineering*, *11*(1), 25.
Kocour Kroupová, H., Valentová, O., Svobodová, Z., Šauer, P., & Máchová, J. (2018). Toxic effects of nitrite on freshwater organisms: a review. *Reviews in Aquaculture*, *10*(3), 525-542.
Koehl, M. (1982). The interaction of moving water and sessile organisms. *Scientific American*, *247*(6), 124-135.
Kołwzan, K., & Narewski, M. (2012). Alternative fuels for marine applications. *Latvian Journal of Chemistry*, *51*(4), 398-406.
Kroupova, H., Machova, J., & Svobodova, Z. (2005). Nitrite influence on fish: a review. *Veterinarni medicina-praha-*, *50*(11), 461.
Kuiper, R. V., Canton, R. F., Leonards, P. E. G., Jenssen, B. M., Dubbeldam, M., Wester, P. W., van den Berg, M., Vos, J. G., & Vethaak, A. D. (2007). Long-term exposure of European flounder (Platichthys flesus) to the flame-retardants tetrabromobisphenol A (TBBPA) and hexabromocyclododecane (HBCD). *Ecotoxicology and Environmental Safety*, *67*(3), 349-360, doi:10.1016/j.ecoenv.2006.12.001.
Kumagai, I., Takahashi, Y., & Murai, Y. (2015). Power-saving device for air bubble generation using a hydrofoil to reduce ship drag: theory, experiments, and application to ships. *Ocean Engineering*, *95*, 183-194.
Kurihara, H. (2008). Effects of CO_2-driven ocean acidification on the early developmental stages of invertebrates. *Marine Ecology Progress Series*, *373*, 275-284.
Kurihara, H., Shimode, S., & Shirayama, Y. (2004). Effects of raised CO_2 concentration on the egg production rate and early development of two marine copepods (Acartia steueri and Acartia erythraea). *Marine Pollution Bulletin*, *49*(9), 721-727, doi:https://doi.org/10.1016/j.marpolbul.2004.05.005.
Lagadic, L., & Caquet, T. (1998). Invertebrates in testing of environmental chemicals: are they alternatives? *Environmental Health Perspectives*, *106*(suppl 2), 593-611.
Latarche, M. (2017). Explaining the types of fuel used on ships. ShipInsight.
Lau, S. C., & Qian, P. Y. (2000). Inhibitory effect of phenolic compounds and marine bacteria on larval settlement of the barnacle Balanus amphitrite amphitrite Darwin. *Biofouling*, *16*(1), 47-58.
Lauvset, S. K., Key, R. M., Olsen, A., van Heuven, S., Velo, A., Lin, X., Schirnick, C., Kozyr, A., Tanhua, T., & Hoppema, M. (2016). A new global interior ocean mapped climatology: The 1× 1 GLODAP version 2. *Earth System Science Data*, *8*, 325-340.
Lavigne, H., & Gattuso, J. (2010). Seacarb: seawater carbonate chemistry with R, edited, R package version.
Law, K. S., Roiger, A., Thomas, J. L., Marelle, L., Raut, J.-C., Dalsøren, S., Fuglestvedt, J., Tuccella, P., Weinzierl, B., & Schlager, H. (2017). Local Arctic air pollution: Sources and impacts. *Ambio*, *46*(3), 453-463.
Lee, K., Tong, L. T., Millero, F. J., Sabine, C. L., Dickson, A. G., Goyet, C., Park, G. H., Wanninkhof, R., Feely, R. A., & Key, R. M. (2006). Global relationships of total alkalinity with salinity and temperature in surface waters of the world's oceans. *Geophysical research letters*, *33*(19).
Levitan, O., Rosenberg, G., Setlik, I., Setlikova, E., Grigel, J., Klepetar, J., Prasil, O., & Berman-Frank, I. (2007). Elevated CO_2 enhances nitrogen fixation and growth in the marine cyanobacterium Trichodesmium. *Global Change Biology*, *13*(2), 531-538.
Lewis Jr, W. M., & Morris, D. P. (1986). Toxicity of nitrite to fish: a review. *Transactions of the American fisheries society*, *115*(2), 183-195.
Liu, D., Keesing, J. K., Xing, Q., & Shi, P. (2009). World's largest macroalgal bloom caused by expansion of seaweed aquaculture in China. *Marine Pollution Bulletin*, *58*(6), 888-895.
Liu, D., & Zhou, M. (2018). Green tides of the Yellow Sea: massive free-floating blooms of Ulva prolifera. in *Global Ecology and Oceanography of Harmful Algal Blooms*. pp. 317-326, Springer.

Liu, J., Wang, Y., Liu, Y., & Zhang, X.-H. (2016). Ahrensia marina sp. nov., a dimethylsulfoniopropionate-cleaving bacterium isolated from seawater, and emended descriptions of the genus Ahrensia and Ahrensia kielensis. *International journal of systematic and evolutionary microbiology*, *66*(2), 874-880.
Longmire, J. L., Maltbie, M., & Baker, R. J. (1997). *Use of" lysis buffer" in DNA isolation and its implication for museum collections*, Museum of Texas Tech University.
Love, M. I., Huber, W., & Anders, S. (2014). Moderated estimation of fold change and dispersion for RNA-seq data with DESeq2. *Genome biology*, *15*(12), 550.
Lozupone, C. A., Hamady, M., Kelley, S. T., & Knight, R. (2007). Quantitative and qualitative β diversity measures lead to different insights into factors that structure microbial communities. *Appl. Environ. Microbiol.*, *73*(5), 1576-1585.
Maki, J., Rittschof, D., Costlow, J., & Mitchell, R. (1988). Inhibition of attachment of larval barnacles, Balanus amphitrite, by bacterial surface films. *Marine Biology*, *97*(2), 199-206.
Malerba, M. E., Connolly, S. R., & Heimann, K. (2012). Nitrate–nitrite dynamics and phytoplankton growth: Formulation and experimental evaluation of a dynamic model. *Limnology and Oceanography*, *57*(5), 1555-1571.
Markou, G., Vandamme, D., & Muylaert, K. (2014). Microalgal and cyanobacterial cultivation: the supply of nutrients. *Water research*, *65*, 186-202.
Martinez, C. B., & Souza, M. M. (2002). Acute effects of nitrite on ion regulation in two neotropical fish species. *Comparative Biochemistry and Physiology Part A: Molecular & Integrative Physiology*, *133*(1), 151-160.
Mary, S. A., Mary, S. V., Rittschof, D., & Nagabhushanam, R. (1993). Bacterial-barnacle interaction: potential of using juncellins and antibiotics to alter structure of bacterial communities. *Journal of chemical ecology*, *19*(10), 2155-2167.
Mathesius, S., Hofmann, M., Caldeira, K., & Schellnhuber, H. J. (2015). Long-term response of oceans to CO 2 removal from the atmosphere. *Nature Climate Change*, *5*(12), 1107-1113.
Matveev, K. I. (2005). Effect of drag-reducing air lubrication on underwater noise radiation from ship hulls.
McCORMICK, M. E., & Bhattacharyya, R. (1973). Drag reduction of a submersible hull by electrolysis. *Naval Engineers Journal*, *85*(2), 11-16.
McCulloch, M., Falter, J., Trotter, J., & Montagna, P. (2012). Coral resilience to ocean acidification and global warming through pH up-regulation. *Nature Climate Change*, *2*(8), 623.
McDonald, M. R., McClintock, J. B., Amsler, C. D., Rittschof, D., Angus, R. A., Orihuela, B., & Lutostanski, K. (2009). Effects of ocean acidification over the life history of the barnacle Amphibalanus amphitrite. *Marine Ecology Progress Series*, *385*, 179-187.
McKinnon, A. C., & Piecyk, M. (2010). Measuring and managing CO_2 emissions in European chemical transport.
McLean, E. L., Katenka, N. V., & Seibel, B. A. (2018). Decreased growth and increased shell disease in early benthic phase Homarus americanus in response to elevated CO2. *Marine Ecology Progress Series*, *596*, 113-126.
McMurdie, P. J., & Holmes, S. (2013). phyloseq: an R package for reproducible interactive analysis and graphics of microbiome census data. *PLoS ONE*, *8*(4), e61217.
Micallef, A., Le Bas, T. P., Huvenne, V. A., Blondel, P., Hühnerbach, V., & Deidun, A. (2012). A multi-method approach for benthic habitat mapping of shallow coastal areas with high-resolution multibeam data. *Continental Shelf Research*, *39*, 14-26.
Middel, H., & Verones, F. (2017). Making marine noise pollution impacts heard: the case of cetaceans in the North sea within life cycle impact assessment. *Sustainability*, *9*(7), 1138.
Miller, C. E. (2018). Environmental influences on synthetic and biogenic calcium carbonate in aragonite-calcite sea conditions, University of Glasgow.
Miller, K. A., Thompson, K. F., Johnston, P., & Santillo, D. (2018). An overview of seabed mining including the current state of development, environmental impacts, and knowledge gaps. *Frontiers in Marine Science*, *4*, 418.
Millero, F. J., Zhang, J.-Z., Lee, K., & Campbell, D. M. (1993). Titration alkalinity of seawater. *Marine Chemistry*, *44*(2-4), 153-165.

Milliman, J. D. (1993). Production and accumulation of calcium carbonate in the ocean: Budget of a nonsteady state. *Global Biogeochemical Cycles*, *7*(4), 927-957, doi:doi:10.1029/93GB02524.
Moore, J. K., & Abbott, M. R. (2000). Chlorophyll distributions and primary production in the Southern Ocean. paper presented at Journal of Geophysical Research, Citeseer.
Moore, S. K., Trainer, V. L., Mantua, N. J., Parker, M. S., Laws, E. A., Backer, L. C., & Fleming, L. E. (2008). Impacts of climate variability and future climate change on harmful algal blooms and human health. paper presented at Environmental Health, Springer.
Morse, J. W., Arvidson, R. S., & Lüttge, A. (2007). Calcium carbonate formation and dissolution. *Chemical reviews*, *107*(2), 342-381.
Murphy, A., Norman, A., Pazouki, K., & Trodden, D. (2015). Thermodynamic simulation for the investigation of marine Diesel engines. *Ocean Engineering*, *102*, 117-128.
Nagata, T., Chang, K., & Hanazato, T. (2006). Impact of invertebrate predators on rotifer populations in lakes: field observation and experimental analysis. *Internationale Vereinigung für theoretische und angewandte Limnologie: Verhandlungen*, *29*(5), 2181-2186.
Nardone, J. A., Patel, S., Siegel, K. R., Tedesco, D., McNicholl, C. G., O'Malley, J., Herrick, J., Metzler, R. A., Orihuela, B., & Rittschof, D. (2018). Assessing the Impacts of Ocean Acidification on Adhesion and Shell Formation in the Barnacle Amphibalanus amphitrite. *Frontiers in Marine Science*, *5*, 369.
NASA Goddard Space Flight Center, O. E. L., Ocean Biology Processing Group (2018). Moderate-resolution Imaging Spectroradiometer (MODIS) Aqua Chlorophyll Data, edited by N. OB.DAAC, doi: data/10.5067/AQUA/MODIS/L3M/CHL/2018, Greenbelt, MD, USA.
Nasa/Jpl (2019). JPL SMAP Level 3 CAP Sea Surface Salinity Standard Mapped Image Monthly V4.3 Validated Dataset, edited, NASA Physical Oceanography DAAC, doi:10.5067/SMP43-3TMCS.
Navarro, J. M., Duarte, C., Manríquez, P. H., Lardies, M. A., Torres, R., Acuna, K., Vargas, C. A., & Lagos, N. A. (2016). Ocean warming and elevated carbon dioxide: multiple stressor impacts on juvenile mussels from southern Chile. *ICES Journal of Marine Science*, *73*(3), 764-771.
NEN (2007). Water Quality — Determination of Ammonium, Nitrate, Nitrite, Chloride, Ortho-phosphate, Sulphate and Silicate by Discrete Analyser System and Spectrophotometric Detection. The Netherlands Standardisation Institute (NEN), Delft, The Netherlands.
Nixon, S., & Thomas, A. (2001). On the size of the Peru upwelling ecosystem. *Deep Sea Research Part I: Oceanographic Research Papers*, *48*(11), 2521-2528.
Nolan, D. P. (2017). Chapter Twelve - Classified Area Pump Installations. in *Fire Pump Arrangements at Industrial Facilities (Third Edition)*. pp. 161-167, Gulf Professional Publishing, doi:https://doi.org/10.1016/B978-0-12-813043-8.00012-9.
Nørregaard, R. D., Gustavson, K., Møller, E. F., Strand, J., Tairova, Z., & Mosbech, A. (2015). Ecotoxicological investigation of the effect of accumulation of PAH and possible impact of dispersant in resting high arctic copepod Calanus hyperboreus. *Aquatic Toxicology*, *167*, 1-11.
Nunes, R., Alvim-Ferraz, M., Martins, F., & Sousa, S. (2017). The activity-based methodology to assess ship emissions-A review. *Environmental Pollution*, *231*, 87-103.
Okada, A. (2019). Benefit, cost, and size of an emission control area: a simulation approach for spatial relationships. *Maritime Policy & Management*, *46*(5), 565-584.
Oksanen, J., et al. (2018). vegan: community ecology package. R package version 2.5-2. R foundation for statistical computing, Vienna, Austria, edited.
Olivier, F., Tremblay, R., Bourget, E., & Rittschof, D. (2000). Barnacle settlement: field experiments on the influence of larval supply, tidal level, biofilm quality and age on Balanus amphitrite cyprids. *Marine Ecology Progress Series*, *199*, 185-204.
Olsen, A., Key, R. M., Van Heuven, S., Lauvset, S. K., Velo, A., Lin, X., Schirnick, C., Kozyr, A., Tanhua, T., & Hoppema, M. (2016). The Global Ocean Data Analysis Project version 2 (GLODAPv2)–an internally consistent data product for the world ocean. *Earth System Science Data (Online)*, *8*(2).
Omernik, J. M., & Powers, C. F. (1983). Total alkalinity of surface waters—a national map. *Annals of the Association of American Geographers*, *73*(1), 133-136.
Omstedt, A., Edman, M., Claremar, B., & Rutgersson, A. (2015). Modelling the contributions to marine acidification from deposited SOx, NOx, and NHx in the Baltic Sea: Past and present situations. *Continental Shelf Research*, *111*, 234-249.

Osinga, R., Redeker, D., De Beukelaer, P. B., & Wijffels, R. H. (1999). Measurement of Sponge growth by projected body area and underwater weight. *Memoirs of the Queensland Museum.*, *44*, 419-426.
Otten, M., Hoen, M. t., & Boer, E. d. (2017). STREAM Freight transport 2016*Rep.*, CE Delft, Delft, NL.
Park, M., Joo, H. S., Lee, K., Jang, M., Kim, S. D., Kim, I., Borlaza, L. J. S., Lim, H., Shin, H., & Chung, K. H. (2018). Differential toxicities of fine particulate matters from various sources. *Scientific reports*, *8*(1), 1-11.
Park, S. H., & Lee, I. (2018). Optimization of drag reduction effect of air lubrication for a tanker model. *International Journal of Naval Architecture and Ocean Engineering*, *10*(4), 427-438.
Parker, L. M., Scanes, E., O'Connor, W. A., Coleman, R. A., Byrne, M., Pörtner, H.-O., & Ross, P. M. (2017). Ocean acidification narrows the acute thermal and salinity tolerance of the Sydney rock oyster Saccostrea glomerata. *Marine pollution bulletin*, *122*(1-2), 263-271.
Pavlenko, N., Comer, B., Zhou, Y., Clark, N., & Rutherford, D. (2020). The climate implications of using LNG as a marine fuel.
Peteiro, L. G., Woodin, S. A., Wethey, D. S., Costas-Costas, D., Martínez-Casal, A., Olabarria, C., & Vázquez, E. (2018). Responses to salinity stress in bivalves: Evidence of ontogenetic changes in energetic physiology on Cerastoderma edule. *Scientific reports*, *8*(1), 8329.
Pierangelini, M., Stojkovic, S., Orr, P. T., & Beardall, J. (2014). Elevated CO_2 causes changes in the photosynthetic apparatus of a toxic cyanobacterium, Cylindrospermopsis raciborskii. *Journal of plant physiology*, *171*(12), 1091-1098.
Plaza-Bolaños, P., Frenich, A. G., & Vidal, J. L. M. (2010). Polycyclic aromatic hydrocarbons in food and beverages. Analytical methods and trends. *Journal of Chromatography A*, *1217*(41), 6303-6326.
Prada, F., Caroselli, E., Mengoli, S., Brizi, L., Fantazzini, P., Capaccioni, B., Pasquini, L., Fabricius, K., Dubinsky, Z., & Falini, G. (2017). Ocean warming and acidification synergistically increase coral mortality. *Scientific reports*, *7*(1), 1-10.
Preziosi, B. M., Runge, J. A., Christensen, J. P., & Jones, R. J. (2017). Effects of pH and temperature on egg hatching success of the marine planktonic copepod, Calanus finmarchicus. *Marine Biology*, *164*(11), 218.
Psaraftis, H. N., & Kontovas, C. A. (2013). Speed models for energy-efficient maritime transportation: A taxonomy and survey. *Transportation Research Part C: Emerging Technologies*, *26*, 331-351.
Qian, P.-Y., Thiyagarajan, V., Lau, S. C. K., & Cheung, S. C. K. (2003). Relationship between bacterial community profile in biofilm and attachment of the acorn barnacle Balanus amphitrite. *Aquatic microbial ecology*, *33*(3), 225-237.
Riebesell, U., Aberle-Malzahn, N., Achterberg, E. P., Algueró-Muñiz, M., Alvarez-Fernandez, S., Arístegui, J., Bach, L. T., Boersma, M., Boxhammer, T., & Guan, W. (2018). Toxic algal bloom induced by ocean acidification disrupts the pelagic food web. *Nature Climate Change*, *8*(12), 1082-1086.
Ries, J. B., Cohen, A. L., & McCorkle, D. C. (2009). Marine calcifiers exhibit mixed responses to CO_2-induced ocean acidification. *Geology*, *37*(12), 1131-1134.
Rost, B., Riebesell, U., Burkhardt, S., & Sültemeyer, D. (2003). Carbon acquisition of bloom-forming marine phytoplankton. *Limnology and Oceanography*, *48*(1), 55-67, doi:doi:10.4319/lo.2003.48.1.0055.
Sabine, C. L., Feely, R. A., Gruber, N., Key, R. M., Lee, K., Bullister, J. L., Wanninkhof, R., Wong, C., Wallace, D. W., & Tilbrook, B. (2004). The oceanic sink for anthropogenic CO2. *science*, *305*(5682), 367-371.
Sadler, D. E., Lemasson, A. J., & Knights, A. M. (2018). The effects of elevated CO2 on shell properties and susceptibility to predation in mussels Mytilus edulis. *Marine environmental research*, *139*, 162-168.
Sapra, H., Godjevac, M., Visser, K., Stapersma, D., & Dijkstra, C. (2017). Experimental and simulation-based investigations of marine diesel engine performance against static back pressure. *Applied Energy*, *204*, 78-92, doi:https://doi.org/10.1016/j.apenergy.2017.06.111.
Sapra, H. D., Linden, Y., van Sluijs, W., Godjevac, M., & Visser, K. (2019). Experimental Investigations of Hydrogen-Natural Gas Engines for Maritime Applications. paper presented at ASME 2018 Internal Combustion Engine Division Fall Technical Conference, American Society of Mechanical Engineers Digital Collection.

Saul, J., & Chestney, N. (2018). New fuel rules push shipowners to go green with LNG. Reuters, London.
Schaefer, J. K., Goodwin, K. D., McDonald, I. R., Murrell, J. C., & Oremland, R. S. (2002). Leisingera methylohalidivorans gen. nov., sp. nov., a marine methylotroph that grows on methyl bromide. *International journal of systematic and evolutionary microbiology*, *52*(3), 851-859.
Schinas, O., & Butler, M. (2016). Feasibility and commercial considerations of LNG-fueled ships. *Ocean Engineering*, *122*, 84-96.
Schultz, M. P. (2007). Effects of coating roughness and biofouling on ship resistance and powering. *Biofouling*, *23*(5), 331-341.
Schutter, M., Van Velthoven, B., Janse, M., Osinga, R., Janssen, M., Wijffels, R., & Verreth, J. (2008). The effect of irradiance on long-term skeletal growth and net photosynthesis in Galaxea fascicularis under four light conditions. *Journal of Experimental Marine Biology and Ecology*, *367*(2), 75-80.
Seddiek, I. S., & Elgohary, M. M. (2014). Eco-friendly selection of ship emissions reduction strategies with emphasis on SOx and NOx emissions. *International Journal of Naval Architecture and Ocean Engineering*, *6*(3), 737-748.
Semin, R. A. B. (2008). A technical review of compressed natural gas as an alternative fuel for internal combustion engines. *Am. J. Eng. Appl. Sci*, *1*(4), 302-311.
Seoane, M., Esperanza, M., Rioboo, C., Herrero, C., & Cid, Á. (2017). Flow cytometric assay to assess short-term effects of personal care products on the marine microalga Tetraselmis suecica. *Chemosphere*, *171*, 339-347.
Sharma, M., Paige, G. B., & Miller, S. N. (2010). DEM Development from Ground-Based LiDAR Data: A Method to Remove Non-Surface Objects. *Remote Sensing*, *2*(11), 2629-2642.
Sippula, O., Stengel, B., Sklorz, M., Streibel, T., Rabe, R., Orasche, J., Lintelmann, J., Michalke, B., Abbaszade, G., & Radischat, C. (2014). Particle emissions from a marine engine: chemical composition and aromatic emission profiles under various operating conditions. *Environmental science & technology*, *48*(19), 11721-11729.
Sofiev, M., Winebrake, J. J., Johansson, L., Carr, E. W., Prank, M., Soares, J., Vira, J., Kouznetsov, R., Jalkanen, J.-P., & Corbett, J. J. (2018). Cleaner fuels for ships provide public health benefits with climate tradeoffs. *Nature communications*, *9*(1), 1-12.
Song, S. (2014). Ship emissions inventory, social cost and eco-efficiency in Shanghai Yangshan port. *Atmospheric Environment*, *82*, 288-297.
Sorte, C. J., Williams, S. L., & Zerebecki, R. A. (2010). Ocean warming increases threat of invasive species in a marine fouling community. *Ecology*, *91*(8), 2198-2204.
Spalding, M. D., Agostini, V. N., Rice, J., & Grant, S. M. (2012). Pelagic provinces of the world: a biogeographic classification of the world's surface pelagic waters. *Ocean & Coastal Management*, *60*, 19-30.
Spalding, M. D., Fox, H. E., Allen, G. R., Davidson, N., Ferdaña, Z. A., Finlayson, M., Halpern, B. S., Jorge, M. A., Lombana, A., & Lourie, S. A. (2007). Marine ecoregions of the world: a bioregionalization of coastal and shelf areas. *BioScience*, *57*(7), 573-583.
Stevenson, A., Archer, S., Schultz, J., Dunham, A., Marliave, J., Martone, P., & Harley, C. (2020). Warming and acidification threaten glass sponge Aphrocallistes vastus pumping and reef formation. *Scientific Reports*, *10*(1), 1-11.
Sui, Y., Kong, H., Huang, X., Dupont, S., Hu, M., Storch, D., Pörtner, H.-O., Lu, W., & Wang, Y. (2016). Combined effects of short-term exposure to elevated CO2 and decreased O2 on the physiology and energy budget of the thick shell mussel Mytilus coruscus. *Chemosphere*, *155*, 207-216.
Sunday, J. M., Fabricius, K. E., Kroeker, K. J., Anderson, K. M., Brown, N. E., Barry, J. P., Connell, S. D., Dupont, S., Gaylord, B., & Hall-Spencer, J. M. (2017). Ocean acidification can mediate biodiversity shifts by changing biogenic habitat. *Nature Climate Change*, *7*(1), 81-85.
Tait, K., & Havenhand, J. (2013). Investigating a possible role for the bacterial signal molecules N-acylhomoserine lactones in Balanus improvisus cyprid settlement. *Molecular ecology*, *22*(9), 2588-2602.
Takahashi, T., Sutherland, S. C., Sweeney, C., Poisson, A., Metzl, N., Tilbrook, B., Bates, N., Wanninkhof, R., Feely, R. A., & Sabine, C. (2002). Global sea–air CO_2 flux based on climatological

surface ocean pCO_2, and seasonal biological and temperature effects. *Deep Sea Research Part II: Topical Studies in Oceanography*, *49*(9-10), 1601-1622.
Taucher, J., Haunost, M., Boxhammer, T., Bach, L. T., Algueró-Muñiz, M., & Riebesell, U. (2017). Influence of ocean acidification on plankton community structure during a winter-to-summer succession: An imaging approach indicates that copepods can benefit from elevated CO2 via indirect food web effects. *PLoS ONE*, *12*(2), e0169737.
Team, R. C. (2013). R: A language and environment for statistical computing.
Terlizzi, A., Fraschetti, S., Gianguzza, P., Faimali, M., & Boero, F. (2001). Environmental impact of antifouling technologies: state of the art and perspectives. *Aquatic Conservation: Marine and Freshwater Ecosystems*, *11*(4), 311-317, doi:10.1002/aqc.459.
Thiyagarajan, V., Lau, S. C., Cheung, S. C., & Qian, P.-Y. (2006). Cypris habitat selection facilitated by microbial films influences the vertical distribution of subtidal barnacle Balanus trigonus. *Microbial ecology*, *51*(4), 431-440.
Thomas, K., & Brooks, S. (2010). The environmental fate and effects of antifouling paint biocides. *Biofouling*, *26*(1), 73-88.
Thomas, M. K., Kremer, C. T., Klausmeier, C. A., & Litchman, E. (2012). A global pattern of thermal adaptation in marine phytoplankton. *Science*, *338*(6110), 1085-1088.
Thomsen, J., Gutowska, M., Saphörster, J., Heinemann, A., Trübenbach, K., Fietzke, J., Hiebenthal, C., Eisenhauer, A., Körtzinger, A., & Wahl, M. (2010). Calcifying invertebrates succeed in a naturally CO2 enriched coastal habitat but are threatened by high levels of future acidification. *Biogeosciences (BG)*, *7*(11), 3879-3891.
Tomlin, C. D. (2016). Cartographic modeling. *International Encyclopedia of Geography: People, the Earth, Environment and Technology: People, the Earth, Environment and Technology*, 1-6.
Toupoint, N., Mohit, V., Linossier, I., Bourgougnon, N., Myrand, B., Olivier, F., Lovejoy, C., & Tremblay, R. (2012). Effect of biofilm age on settlement of Mytilus edulis. *Biofouling*, *28*(9), 985-1001.
Tribollet, A., Chauvin, A., & Cuet, P. (2019). Carbonate dissolution by reef microbial borers: a biogeological process producing alkalinity under different pCO 2 conditions. *Facies*, *65*(2), 9.
UNCTAD (2018). Reivew of Maritime trasport 2018*Rep.*, United Nations Conference on Trade and Development, Geneva, Switzerland.
Van Biert, L., Godjevac, M., Visser, K., & Aravind, P. (2016). A review of fuel cell systems for maritime applications. *Journal of Power Sources*, *327*, 345-364.
Van Biert, L., Woudstra, T., Godjevac, M., Visser, K., & Aravind, P. (2018). A thermodynamic comparison of solid oxide fuel cell-combined cycles. *Journal of Power Sources*, *397*, 382-396.
Van Fan, Y., Perry, S., Klemeš, J. J., & Lee, C. T. (2018). A review on air emissions assessment: Transportation. *Journal of cleaner production*, *194*, 673-684.
Vaqué, D., Lara, E., Arrieta, J. M., Holding, J., Sa, E. L., Hendriks, I. E., Coello Camba, A., Alvarez, M., Agusti, S., & Wassmann, P. F. (2019). Warming and CO_2 enhance Arctic heterotrophic microbial activity. *Frontiers in Microbiology*, *10*, 494.
Verspagen, J. M., Van de Waal, D. B., Finke, J. F., Visser, P. M., Van Donk, E., & Huisman, J. (2014). Rising CO_2 levels will intensify phytoplankton blooms in eutrophic and hypertrophic lakes. *PLoS ONE*, *9*(8), e104325.
Wahl, M. (1989). Marine epibiosis. I. Fouling and antifouling: some basic aspects. *Marine Ecology progress series*, *58*, 175-189.
Waller, G. (1996). *Sealife: A complete guide to the marine environment*, Pica Press, Sussex.
Wang, Y., Wang, J., Mu, J., Wang, Z., Yao, Z., & Lin, Z. (2014). Aquatic predicted no-effect concentration for three polycyclic aromatic hydrocarbons and probabilistic ecological risk assessment in Liaodong Bay of the Bohai Sea, China. *Environmental Science and Pollution Research*, *21*(1), 148-158.
Ware, C. S., Smith-Palmer, T., Peppou-Chapman, S., Scarratt, L. R., Humphries, E. M., Balzer, D., & Neto, C. (2018). Marine Antifouling Behavior of Lubricant-Infused Nanowrinkled Polymeric Surfaces. *ACS applied materials & interfaces*, *10*(4), 4173-4182.
Watch, N. C. R. (2018, updated daily). NOAA Coral Reef Watch Version 3.1 Daily Global 5-km Satellite Coral Bleaching Degree Heating Week Product. in *Data set accessed 2018-09-01 at*

https://coralreefwatch.noaa.gov/satellite/hdf/index.php., edited, NOAA Coral Reef Watch, College Park, Maryland, USA.
Wei, Y., Plath, L., Penning, A., van der Linden, M., Murk, A. J., & Foekema, E. M. (2019). The Potential Impact of Underwater Exhausted CO_2 from Innovative Ships on Invertebrate Communities. *International Journal of Environmental Research*, *13*(4), 669-678.
Weilgart, L. (2018). The impact of ocean noise pollution on fish and invertebrates. *Ocean Care*.
Wells, M. L., Trainer, V. L., Smayda, T. J., Karlson, B. S., Trick, C. G., Kudela, R. M., Ishikawa, A., Bernard, S., Wulff, A., & Anderson, D. M. (2015). Harmful algal blooms and climate change: learning from the past and present to forecast the future. *Harmful algae*, *49*, 68-93.
Wells, P. G., Lee, K., & Blaise, C. (1997). *Microscale testing in aquatic toxicology: advances, techniques, and practice*, CRC Press.
Whiteley, N. (2011). Physiological and ecological responses of crustaceans to ocean acidification. *Marine Ecology Progress Series*, *430*, 257-271.
Wickham, H. (2016). *ggplot2: elegant graphics for data analysis*, Springer.
Wieczorek, S. K., Clare, A. S., & Todd, C. D. (1995). Inhibitory and facilitatory effects of microbial films on settlement of Balanus amphitrite amphitrite larvae. *Oceanographic Literature Review*, *11*(42), 999.
Wilbur, S., Williams, M., Williams, R., Scinicariello, F., Klotzbach, J., Diamond, G., & Citra, M. (2012). *Toxicoloigical profile for carbon monoxide*, Atlanta (GA): Agency for Toxic Substances and Disease Registry (US), US.
Williams, R., Wright, A. J., Ashe, E., Blight, L., Bruintjes, R., Canessa, R., Clark, C., Cullis-Suzuki, S., Dakin, D., & Erbe, C. (2015). Impacts of anthropogenic noise on marine life: publication patterns, new discoveries, and future directions in research and management. *Ocean & Coastal Management*, *115*, 17-24.
Winnes, H., & Fridell, E. (2009). Particle emissions from ships: dependence on fuel type. *Journal of the Air & Waste Management Association*, *59*(12), 1391-1398.
Wittmann, A. C., & Pörtner, H.-O. (2013). Sensitivities of extant animal taxa to ocean acidification. *Nature Climate Change*, *3*(11), 995.
Wood, H. L., Spicer, J. I., & Widdicombe, S. (2008). Ocean acidification may increase calcification rates, but at a cost. *Proceedings of the Royal Society B: Biological Sciences*, *275*(1644), 1767-1773.
Wood, S. N. (2006). *Generalized additive models: an introduction with R*, Chapman and Hall/CRC.
Wood, S. N. (2011). Fast stable restricted maximum likelihood and marginal likelihood estimation of semiparametric generalized linear models. *Journal of the Royal Statistical Society: Series B (Statistical Methodology)*, *73*(1), 3-36.
Wu, B., Zhang, R., Cheng, S.-P., Ford, T., Li, A.-M., & Zhang, X.-X. (2011). Risk assessment of polycyclic aromatic hydrocarbons in aquatic ecosystems. *Ecotoxicology*, *20*(5), 1124-1130.
Zeebe, R. E., & Wolf-Gladrow, D. (2001). *CO_2 in seawater: equilibrium, kinetics, isotopes*, Gulf Professional Publishing.
Zhao, H., Dilmore, R., Allen, D. E., Hedges, S. W., Soong, Y., & Lvov, S. N. (2015). Measurement and modeling of CO_2 solubility in natural and synthetic formation brines for CO_2 sequestration. *Environmental science & technology*, *49*(3), 1972-1980.
Zhen, L., Li, M., Hu, Z., Lv, W., & Zhao, X. (2018). The effects of emission control area regulations on cruise shipping. *Transportation Research Part D: Transport and Environment*, *62*, 47-63.

Acknowledgements

This thesis would have been impossible without help and support from many people.

First, I would like to acknowledge my promoter, Tinka Murk. You supervised both my Master thesis and internship in 2013. After that, you offered me my first job in life, as a research assistant. I am very thankful for this meaningful opportunity, which planted a seed in my mind about doing a PhD in the short future. In October 2016, you and Edwin (my co-promotor) transferred an original postdoc project, GasDrive, to a PhD project for me. I am very grateful for your trust and effort. During my PhD, besides the professional knowledge, the most important thing I learned from you is how to think independently and critically under pressure. You showed and taught me in challenging situations to stay creative and think of possibilities to break through. You encouraged me to transfer from an insecure girl to a confident lady. Those abilities are not only useful during my PhD, but also surely meaningful in the future of my life.

My big thanks to Edwin Foekema, my co-promotor and daily supervisor. I had a such great time working with you. Thanks to your trust and efforts, I was able to do my PhD on this original postdoc project. Thanks to your professional knowledge on Ecotoxicology and creative thinking, we carried out several great experiments during my PhD with limited budget. You are a very friendly and helpful supervisor. I felt comfortable to open my worries, feelings and stress about the project to you. In the past four years, I recognize that my emotions and performance have had "up and down" periods, especially in the first 2 years. I can imagine you experienced as much, probably even more, stress from the project as/than me. Sometimes, I probably brought some negative energy to you. My apologies about that. I am very much thankful that you always stayed patient and positive (I am still learning this part myself) when I was disappointed about the data. Without your encouragement in all the "down" moments, I was probably still busy with my PhD right now.

Thanks to all the staff members at MAE: Dolfi, Lisa, Luna, Martine, Maya, Pauline, Reindert, Rene, Ronald, Tim, Saskia and Susan. We shared great moments that will never be eliminated from my memory. Tim, thanks for all your help on my experimental set up. Thank you for your patience to handle all my "small questions" in the lab, which turned out caused you quite some time :).

Thanks to the colleagues at Wageningen Marine Research Den Helder who helped a lot on the experiments of this thesis: Cor, Babette, Lisabeth, Martijn, and Hans, and to Pepijn for helping out with the data analysis in R for the first publication. Thanks to the colleagues at aquatic research facility 'CARUS' of Wageningen University to support the experiment set-up: Emily, Menno, Robert-Jan, Sander and Wian. Thanks to the Dutch Royal Navy for generating exhaust gas and arranging and sailing the ship used in our experiment test. Thanks to all the students who did thesis on this project: Anne, Bodil, Csilla, Kees, Lara, Lennert, Maartje, Michel, Pao, Rik and Yuekai.

To my 'PhD band' mates at MAE: Alwin, Christiaan, Diede, Erik, Ewout, Joshua, Karlijn, Ludi, Mischa, Park, Mert, and Sahri. Thank you for making my 4 years of PhD life memorable! I love our "PhD band"! Although most of us had to go to field work every now and then, and the "band" is hard to be complete, all the dinners and game nights were so much fun and wonderful, especially the escape room night. You make the atmosphere at work 'gezellig'. Christiaan, thanks for all those 'lekkere' recipes! I love them all!

To my friends: Qianrui Wang, I enjoyed all the lunch and shopping with you. Thank you for helping me get Chinese food weekly after I moved out of Wageningen. Good luck for your own PhD! MingRuo, thanks for all the delicious food. I don't remember how many times I have had dinner in your house. The only thing that made me sad when I moved out from Wageningen is the fact that I will be far away from your kitchen. Justine, thanks for keeping in touch with me after your PhD. I enjoyed our Friday evening beer time very much, unfortunately we didn't do it very often, before we both moved out of Wageningen. Thanks for all the tips of "surviving" from PhD candidate life and job searching to be a regulatory Ecotoxicologist. I hope your work and new house in Den Bosch is going well and let's hang out again!

I would like to thank my Chinese and Dutch families. Expressing feelings is not the strong part of Chinese culture. So, my parents and I barely communicate about feelings. Mom and dad, thank you for all the updates about your life and listening to my nagging about my life during our video chats. That made me feel that you were around and saved me much homesickness. I know you are proud of me. But you probably don't know I am very proud of you too. It must be not easy to understand and support your only child to chase her dream that is about 8,000 km away and in a place you had never been. But you did it and thank you for that!

I'd also like to thank the Oogink family (Brenda, Marcel, Max and Lynne). We met in 2014 and you are the first Dutch family I ever met. The 6 months living with you was a great and happy period in my life that I will never forget. Thanks for always supporting me like a family since then. Thank you for making me feel that I'm accepted by a Dutch family. It was extremely important for an Asian girl who knew nobody in this Western world. This being accepted feeling also gave me more confidence later to fight for me staying in this country.

I am so lucky to have my Dutch Boter family (Carla, Eric, Lianne, Tim, Zoey and Feline). Thanks for always being there with me when I needed support. There were countless moments that you made me happy and feel loved: playing Catan (although sometimes it's more than a game), celebrating Christmas and New year's, helping with decorating and moving to our new house and celebrating my Dutch citizenship etc. You make me feel not alone and at home in the Netherlands.

Last words are to my love, Richard Boter. I am grateful to meet you and have you in my life. It is probably not easy to live with a PhD candidate, especially since she has a temper and a different cultural background. But you did a great job! You are such a great partner, so patient and caring. I appreciated that you always carefully listen to my complaints and try to cheer me up. Thank you for believing in me when I am doubting myself and for encouraging me to face all the challenges.

About the Author

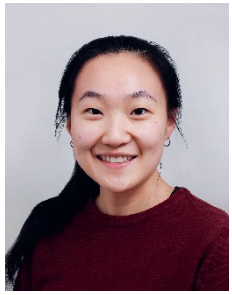

Yuzhu (Celia) Wei was born on November 11th, 1989, in Beijing, China. She studied Biomaterials in Beijing University of Chemical Technology from 2008. After completing her Bachelor in 2012, Celia continued her Master study abroad in the Master program Biotechnology at Wageningen University & Research (WUR).
On July 12th, 2012, Celia came to The Netherlands for the first time, which is also the first time that she stepped out of China. Before the Master program started in September, she went on a 1-month backpack travel in Europe by herself with her broken English and €2500 cash in pocket. This bit of silly and drama involved travel experience gave her the first taste of the completely different western culture compared to China. It also built her confidence to survive and keep developing in the western world.
Celia finished her Master thesis at the University of California, Davis in developing a one-week tadpoles (in vivo) assay for detecting thyroid hormone disruptors, which was followed by an internship at a Dutch algae company, Duplaco. B.V, in Hengelo. After finishing her Master program in 2014, Celia worked for 2 years as a research assistant in the Environmental Technology group at WUR, followed by a PhD study in the Marine Animal Ecology group in October 2016. During her PhD, she became a European registered Toxicologist candidate and followed the Postgraduate Education Toxicology program. Most proudly, she became a Dutch citizen in July 2019. Starting May 2020, Celia is employed as Regulatory Ecotoxicologist at Triskelion. B.V. in Utrecht.

Netherlands Research School for the
Socio-Economic and Natural Sciences of the Environment

D I P L O M A

for specialised PhD training

The Netherlands research school for the
Socio-Economic and Natural Sciences of the Environment
(SENSE) declares that

Yuzhu Wei

born on 11 November 1989 in Beijing, China

has successfully fulfilled all requirements of the
educational PhD programme of SENSE.

Wageningen, 20 January 2021

Chair of the SENSE board

Prof. dr. Martin Wassen

The SENSE Director

Prof. Philipp Pattberg

The SENSE Research School has been accredited by the Royal Netherlands Academy of Arts and Sciences (KNAW)

KONINKLIJKE NEDERLANDSE
AKADEMIE VAN WETENSCHAPPEN

The SENSE Research School declares that **Yuzhu Wei** has successfully fulfilled all requirements of the educational PhD programme of SENSE with a work load of 56.4 EC, including the following activities:

SENSE PhD Courses

- Environmental research in context (2017)
- Research in context activity: 'Applied and received travel funding for presenting in SETAC 2019 and reported on the event in NVT magazine' (2019)

Other PhD and Advanced MSc Courses

- Risk Assessment, Postgraduate Education in Toxicology (2016)
- Legal and regulatory toxicology, Postgraduate Education in Toxicology (2016)
- Laboratory Animal Science, Postgraduate Education in Toxicology (2017)
- Pathobiology, Postgraduate Education in Toxicology (2017)
- Environmental Toxicology, Wageningen University (2017)
- General Toxicology, Wageningen University (2017)
- Stress Identification & Management, Wageningen Graduate Schools (2017)
- Molecular Toxicology, Postgraduate Education in Toxicology (2017)
- Food Toxicology, Postgraduate Education in Toxicology (2018)
- Cell Toxicology, Postgraduate Education in Toxicology (2018)
- Epidemiology, Postgraduate Education in Toxicology (2018)
- Risk communication, Postgraduate Education in Toxicology (2018)
- Organ Toxicology, Postgraduate Education in Toxicology (2019)

Management and Didactic Skills Training

- Supervising two BSc students and four MSc students (2018-2020)
- Organising weekly thesis seminars for thesis students (2018-2020)
- Teaching in the MSc course ''Marine Animal Ecology' (2019)

Oral Presentations

- **Presentation award**: *Impact of underwater exhaust gas expulsion on marine ecosystem.* IMarEST Benelux, 4 April 2019, Delft, the Netherlands

SENSE coordinator PhD education

Dr. ir. Peter Vermeulen

Financial support

This research was made possible by a grant from the Netherlands Organization for Scientific Research, domain Applied and Engineering Sciences (TTW) (Granted project # 14504, project name 'GasDrive: Minimizing emissions and energy losses at sea with LNG combined prime movers, underwater exhausts and nano hull materials').

Financial support from the Marine Animal Ecology group for printing this thesis is gratefully acknowledged.

Cover designed and made by Jingxian Chang

Layout and Print by Digiforce